JOHANNES GUTENBERG UNIVERSITÄT MAINZ

Development of predictive tools for amorphous solid dosage forms

Dissertation
zur Erlangung des Grades
„Doktor der Naturwissenschaften"
im Promotionsfach Pharmazie

am Fachbereich Chemie, Pharmazie und Geowissenschaften
Institut für Pharmazie und Biochemie
Abteilung Biopharmazie und Pharmazeutische Technologie
der Johannes Gutenberg Universität Mainz

Matthias Manne Knopp
geboren in Glostrup, Dänemark

Mainz, 2016

D77 – Mainzer Dissertation

Dekan: Univ.-Prof. Dr. Dirk Schneider

1. Berichterstatter:

2. Berichterstatter:

Tag der mündlichen Prüfung: 4. November 2016

“The value of an education is not learning facts, but training the mind to think something that cannot be learned from textbooks” – Albert Einstein

Acknowledgements

Abbreviations list

ANOVA	Analysis of variance
AUC	Area under the curve
BCS	Biopharmaceutics classification system
BDDCS	Biopharmaceutics drug disposition classification system
$\boldsymbol{C}_{\mathbf{max}}$	Maximum concentration
CAP	Chloramphenicol
CCX	Celecoxib
COX	Cyclooxygenase
$\boldsymbol{C}_{\mathbf{p}}$	Heat capacity
DCS	Developability classification system
DSC	Differential scanning calorimetry
EDTA	Ethylenediaminetetraacetic acid
FaSSIF	Fasted state simulated intestinal fluid
FeSSIF	Fed state simulated intestinal fluid
FDA	Food and Drug Administration (USA)
FDP	Felodipine
FTIR	Fourier transform infrared
$\boldsymbol{H}_{\mathbf{m}}$	Melting enthalpy (enthalpy of fusion)
HPC	Hydroxypropyl cellulose
HPLC	High-performance liquid chromatography
HPMC	Hydroxypropyl methylcellulose
HPMCAS	Hydroxypropyl methylcellulose acetate succinate
IMC	Indomethacin
IVIVC	*In vitro–in vivo* correlation
LOD	Limit of detection
Log *P*	Partition coefficient
LOQ	Limit of quantification
MV	Molecular volume

M_w	Molecular weight
NSAID	Nonsteroidal anti-inflammatory drug
NVP	N-vinylpyrrolidone
PAA	Polyacrylic acid
PCM	Paracetamol (acetaminophen)
PEG	Polyethylene glycol
PVP	Polyvinylpyrrolidone
PVP/VA	Polyvinylpyrrolidone/vinyl acetate copolymer
PVA	Polyvinyl acetate
PTFE	Polytetrafluoroethylene (Teflon)
r^2	Coefficient of determination
RSD	Relative standard deviation
SD	Standard deviation
SEDDS	Self-emulsifying drug delivery system
SEM	Standard error of the mean
SOL	Soluplus® (polyvinyl caprolactam – PVA – PEG graft copolymer)
SSR	Sum of squared residuals
T_a	Annealing temperature
T_c	Crystallization temperature
T_{end}	Melting temperature (end point)
T_g	Glass transition temperature
T_m	Melting temperature (onset)
t_{max}	Time to reach maximum concentration (C_{max})
USP	United States Pharmacopoeia
UV	Ultraviolet
VA	Vinyl acetate
VP	Vinylpyrrolidone
XRPD	X-ray powder diffraction

Table of contents

Background

Since the introduction of modern medicine in the 19th century, oral delivery has remained the preferred route for drug administration due to increased patient safety and compliance, as well as reduced production costs compared to topical and parenteral drug delivery[1]. Upon ingestion of an oral dosage form, the drug must undergo disintegration and dissolution in the gastrointestinal fluid in order to reach the systemic circulation, as only molecules in solution are able to permeate the intestinal epithelial wall[2]. It is generally recognized that the rate and extent of drug absorption is controlled by two fundamental parameters: drug solubility and permeability[3]. An increasing number of new drug candidates have limited oral bioavailability due to poor water-solubility. Therefore, the development of strategies to improve the dissolution profile of these drugs constitutes one of the biggest challenges in pharmaceutical drug formulation[4-6].

The solubility and/or dissolution rate of a drug can either be increased through material engineering such as crystal modification, salt formation, amorphization, particle size reduction, or through different "enabling" formulation techniques such as solid dispersions, cyclodextrin complexations, and lipid-based formulations[7,8]. Of these, amorphous solid dosage forms are among the most promising strategies to overcome the poor oral bioavailability of poorly water-soluble drugs, and thus have become one of the most active areas of research within the pharmaceutical field[9-11]. The utilization of the amorphous form of a drug may increase the dissolution rate and apparent solubility compared to that of its crystalline counterpart as a result of higher internal free energy. However, as an amorphous material is thermodynamically unstable, it will eventually nucleate and crystallize upon storage with the subsequent loss of the solubility and dissolution advantages[12,13]. In order to avoid crystallization, the drug can be molecularly dispersed in an inert amorphous polymeric carrier – a formulation strategy formally known as an amorphous solid dispersion[11,14]. Besides stabilizing the amorphous drug in the solid state by forming intermolecular interactions and decreasing the molecular mobility, polymers have also shown to improve the dissolution rate and inhibit crystallization from the supersaturated solution generated upon dissolution of amorphous solid dispersions[15-17]. This generation of a supersaturated drug solution and subsequent inhibition of crystallization has been referred to as the "spring and parachute" effect and the magnitude of this effect is influenced by the physicochemical properties of the polymer[15,18,19].

Nevertheless, even though the number of marketed amorphous solid dispersions has increased during the last decade, the commercial application of this kind of dosage form is still limited[17,20]. This is mainly due to an insufficient understanding of the basic properties of amorphous solid dispersions, such as their physical stability and the lack of predictive *in vitro* models[7]. Therefore, the present work aimed at developing predictive tools for amorphous solid dosage form development, with emphasis on predicting the solubility of a drug in a polymer and supersaturation behavior upon dissolution, in order to enable a rational assessment of their stability and *in vitro* performance and avoid discrepancies with early *in vivo* studies.

Chapter 1

Poorly water-soluble drugs

With the introduction of combinatorial chemistry and high-throughput screening methods, the number of potent drug candidates is increasing. As these target-selective drugs often are lipophilic and exhibit poor solubility in water, it is estimated that up to 90% of all low-molecular-weight compounds in the drug discovery pipelines are practically insoluble in water[6]. However, in order for a drug to be absorbed and ultimately reach the systemic circulation upon oral delivery, the drug must be dissolved in the aqueous gastrointestinal fluids[5]. Consequently, as oral delivery remains the preferred route for drug administration, the development of methods to overcome the poor water-solubility of these drug candidates currently constitutes one of the biggest challenges for the pharmaceutical industry[4].

Following oral administration of a solid dosage form, the drug must undergo a series of processes in order to reach the systemic circulation. A schematic overview of these processes is shown in Figure 1.1. After ingestion of a tablet or capsule, it will begin to disintegrate into granules or primary particles upon contact with the gastrointestinal fluids. Disintegration is then followed by dissolution/solubilization of the drug from these particles, and the rate and extent of this process is highly dependent on the size of the particles and the solubility of the drug in the fluid[21]. As one potential formulation strategy, the solubility of the drug may be enhanced transiently above saturation solubility by using a metastable polymorphic or amorphous form of the drug; however, the induction of supersaturation will also create a thermodynamic driving force for precipitation or crystallization *in vivo*. Hence, for these systems there will be competing processes of precipitation/crystallization and resolubilization within the gastrointestinal tract and ultimately, only the dissolved drug will be able to permeate the intestinal epithelial wall[21].

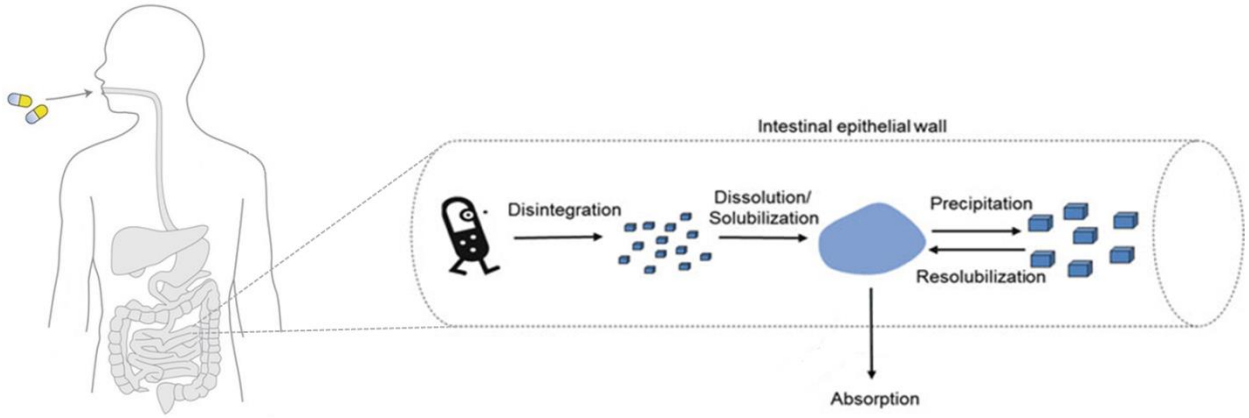

Figure 1.1: Schematic overview of the processes involved in oral drug administration.

1.1 Classification and definitions

To avoid discarding promising poorly water-soluble drug candidates, there is a desire to identify the rate-limiting step(s) for oral drug absorption early in the research and development process and enable rational drug development[22]. According to the biopharmaceutics classification system (BCS), developed in 1995, the dissolution process (in particular the solubility of the drug) along with the permeability across the intestinal membrane have been identified as the two main barriers to oral drug absorption[3]. On the basis of this simple two-variable model, drugs can be divided into four different classes according to their water solubility and intestinal permeability, as shown in Figure 1.2.

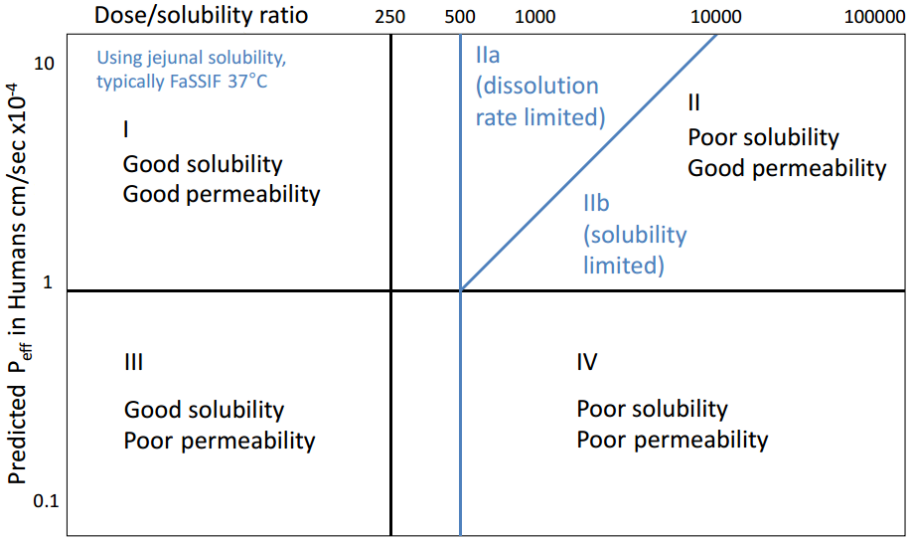

Figure 1.2: The biopharmaceutics classification system (BCS) is shown in black and the modifications from the BCS to the DCS are shown in blue. Modified from Butler and Dressman[23] with permission from Wiley-Liss© 2010.

In order to build higher efficiency into the drug development process, this information can be used to identify suitable *in vitro* methods that serve as prognostic tools to predict oral absorption. In fact, the information extracted from the BCS can serve as a platform in which bioequivalence may be assessed based on *in vitro* dissolution tests rather than costly empirical human *in vivo* studies[24]. The solubility classification is based on oral administration of an immediate release drug product to fasting humans together with a glass of water. Consequently, if the highest dose strength of a drug is soluble in 250 mL of water at 37 °C, over the entire physiologically relevant pH-range from 1.2 to 6.8, the drug is considered highly soluble[25]. On the other hand, if the highest dose is not soluble throughout this pH-range, the drug is considered poorly soluble. The permeability classification is based either directly on measurements of mass-transfer across a human intestinal membrane, or indirectly on the extent of absorption of a drug in humans. If the extent of absorption in humans is above 90% of the administered dose, based on mass-balance or in comparison to an intravenous reference dose, the drug is considered highly permeable.

Alternatively, if this information is unavailable, non-human *in vitro* models capable of predicting drug intestinal absorption in humans can also be applied[24,25].

Since the introduction of the BCS, several extensions to this drug classification system have been proposed[23]. In order to facilitate drug classification with respect to permeability, Wu and Benet proposed the biopharmaceutics drug disposition classification system (BDDCS) in which the metabolic clearance serves as an alternative to permeability[26]. In addition, Butler and Dressman introduced the developability classification system (DCS) with a revised solubility classification compared to the definition in the BCS that serve as a guidance to which formulation strategy should be employed when a new drug candidate is brought into development. This new solubility classification is more representative of the physiological conditions in the human gastrointestinal tract as it uses fasted state simulated intestinal fluid (FaSSIF) and a dose/solubility ratio to 500 mL instead of 250 mL as outlined in Figure 1.2[23]. In order to enable a prediction of the extent of oral absorption rather than the rate of absorption, Butler and Dressman proposed a division of the BCS class II compounds into class IIa and IIb depending on whether the drugs show dissolution rate-limited or solubility-limited absorption, respectively[23]. For DCS class IIb compounds, the bioavailability is likely to be limited by the poor solubility of the drug, and therefore focus should be on the enhancement of solubility.

1.2 Model compounds

To represent the increasing number of BCS class II compounds in drug discovery pipelines, a model compound should have low molecular weight (M_w, <600 g/mol), melting point (T_m, <200 °C), and glass transition temperature (T_g, <70 °C), good permeability, and poor aqueous solubility[27]. Several drugs were used as model compounds in the experimental framework of this dissertation, and an overview of the indications and physicochemical properties of the two main compounds are given below.

1.2.1 Indomethacin

Indomethacin (IMC) was discovered by Iroko Pharmaceuticals, LLC and approved by the FDA in 1965 under the brand name Indocin®. It is a non-selective cyclooxygenase (COX) inhibitor clinically used as a nonsteroidal anti-inflammatory drug (NSAID) for the treatment of pain and inflammation caused by rheumatoid arthritis, ankylosing spondylitis, gouty arthritis, osteoarthritis, and soft tissue injuries such as tendinitis and bursitis[28]. As can be seen in Figure 1.3a, the molecule is relatively small (M_w = 357.79 g/mol) and consists of four functional groups; anisole, chlorobenzene, formyl methylpyrrole, and a carboxylic acid of which the latter is both a hydrogen bond donor and acceptor. The stable γ crystal form of IMC has a T_m of 162 °C and a T_g of around 50 °C[29]. IMC is a hydrophobic (log P = 4.3) moderately weak acid with a pK_a value of 4.5, which means that it is ionized at intestinal but unionized at gastric pH levels, and the

solubility is significantly influenced by the changes of pH in the gastrointestinal tract. The normal maximum dose strength for adults is 50 mg and due to its poor water solubility of 2.5 µg/mL and good permeability, IMC is categorized as a BCS II compound[30]. However, with more than a 100-fold increase of solubility in FaSSIF to 320 µg/mL, it is categorized as a DCS IIa compound, indicating that the bioavailability of IMC is dissolution rate-limited[31].

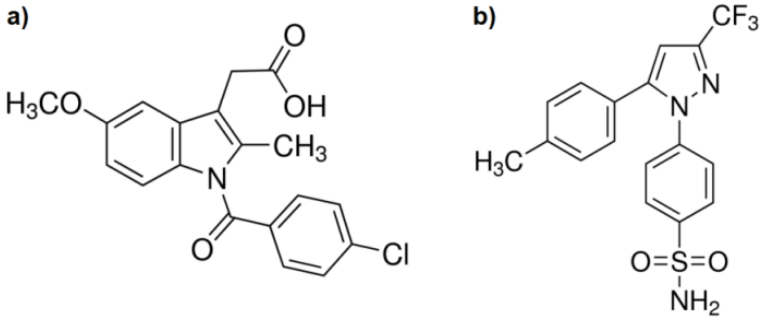

Figure 1.3: Chemical structures of the two main model compounds used in the present dissertation: a) indomethacin and b) celecoxib.

1.2.2 Celecoxib

Celecoxib (CCX) was discovered by G. D. Searle and Company and approved by the FDA in 1998 under the brand name Celebrex®. It is a selective COX-2 inhibitor and clinically used as a NSAID for the treatment of pain and inflammation caused by osteoarthritis, juvenile arthritis, rheumatoid arthritis, and ankylosing spondylitis, and the relief of acute pain and menstrual cramps[32]. As can be seen in Figure 1.3b, the molecule is relatively small (M_w = 381.37 g/mol) and consists of four functional groups: phenylpyrazole, trifluoromethyl, toluene, and phenyl sulfonamide of which the latter is a hydrogen bond donor. The stable crystal form III of CCX has a T_m of 162 °C and a T_g of around 50 °C[29]. CCX is a hydrophobic (log P = 3.9) weak acid with a pK_a value of 10.7, which means that it is unionized at both gastric and intestinal pH levels and that the solubility is not influenced by the changes of pH in the gastrointestinal tract. The normal maximum dose strength for adults is 200 mg and due to its poor water solubility of 5 µg/mL and good permeability, CCX can be categorized as a BCS II compound[30]. Even though the solubility is increased approximately 10-fold in FaSSIF to 46 µg/mL, it is categorized as a DCS IIb compound, indicating that the absorption of CCX is solubility-limited[33].

Chapter 2

Amorphous solid dispersions

One of the most promising strategies to overcome the poor oral bioavailability associated with BCS class II compounds is the utilization of the amorphous form of the drug. The amorphous form of a drug has a higher free energy than its crystalline counterpart, which will increase the apparent solubility and dissolution rate. However, it is also thermodynamically unstable and tends to crystallize over time with a subsequent loss of these advantages. Thus, in order to avoid crystallization during storage, the drug can be dispersed in a hydrophilic carrier, also known as a solid dispersion[11]. The basic principle behind solid dispersions (i.e. continuous dispersion of one solid material in another) has been applied in the industry for several purposes for centuries. For instance in metallurgy to produce alloys that have superior properties compared to the pure metals, ceramics and glassmaking to produce colored or porous glass, and plastic production to increase the flexibility and durability of plastics[34]. In comparison, the application of solid dispersions as an oral drug delivery strategy has only recently gained interest in pharmaceutical research and industry[35].

The most popular solid dispersion for pharmaceutical use is the so-called amorphous solid dispersion, in which the drug is molecularly dispersed in a hydrophilic amorphous polymeric carrier such as polyvinylpyrrolidone (PVP), polyvinylpyrrolidone/vinyl acetate copolymer (PVP/VA), polyethylene glycol (PEG), hydroxypropyl methylcellulose (HPMC), or hydroxypropyl methylcellulose acetate succinate (HPMCAS)[36]. This formulation strategy is attractive for several reasons; besides stabilizing the amorphous drug in the solid state, the hydrophilic polymer may also further increase the dissolution rate and maintain the supersaturation generated upon dissolution through improved wettability and inhibition of drug precipitation, respectively[17,37]. As the advantage of polymers to improve the stability and biopharmaceutical performance of amorphous drugs is discussed in detail in Chapter 3, the following sections will introduce (amorphous) solid dispersions as a formulation strategy.

2.1 Thermodynamics of amorphous materials

To illustrate the differences in the thermodynamic properties of crystalline and amorphous materials, changes in the enthalpy and volume as a function of temperature for a typical glass-forming material are shown in Figure 2.1. In this context, it should be noted that other thermodynamic properties, such as the entropy, also could be depicted on the y-axis. Upon cooling of a liquid below its melting point (T_m), the material may solidify into a crystal if the cooling rate is slow enough to allow for the molecules to nucleate and grow into a crystal lattice with three-dimensional long-range order. This results in a discontinuity of enthalpy and volume and is therefore considered a first-order phase transition[38]. In contrast, if cooling through T_m is fast enough to avoid nucleation and crystal growth, a material with no long-range order but with

the structural properties of a liquid, albeit with higher viscosity, can be obtained. As the enthalpy and volume of this viscous material can be extrapolated from the properties of the liquid, it is considered to be in a supercooled liquid state that is in equilibrium with the liquid phase also known as the rubbery state[39]. Cooling this supercooled liquid even further will decrease the molecular mobility of the material to a point where it is unable to relax in accordance with the cooling rate, resulting in a dramatic increase in the viscosity of the material and a change in the temperature dependence of the enthalpy and volume (vitrification). The temperature at which this event occurs is known as the glass transition temperature (T_g). As the change in enthalpy and volume over the glass transition is not discontinuous, this is not a first-order phase transition in a thermodynamic sense but rather a kinetic event (a so-called second-order transition), and therefore the glass transition and the properties of the glass are not well-defined, but will depend on the thermal history of the material[12].

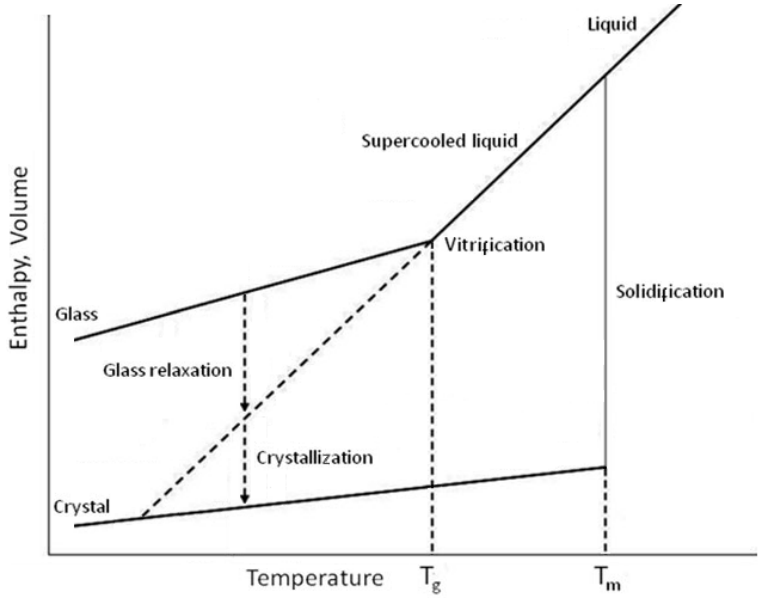

Figure 2.1: Schematic depiction of the change in volume and enthalpy as a function of temperature during glass formation and structural relaxation. Modified from Hancock and Zografi[12] with permission from Wiley-Liss© 1997.

Below the T_g, the material is kinetically locked in a glassy non-equilibrium state that has a higher entropy, enthalpy and free energy relative to the crystalline state, which is responsible for its higher apparent solubility and dissolution rate[40]. For the same reason, the amorphous form is also thermodynamically unstable and even though the glass exhibits solid-like properties, the molecular mobility is increased compared to the crystalline state due to the higher free volume, which allows for molecular rearrangements. Consequently, by annealing (i.e. maintaining a temperature to allow for thermal equilibrium) the material below the T_g, the configurational enthalpy and volume of the glass will move towards that of the supercooled liquid as the molecules rearrange, in a process referred to as structural relaxation. Over time these molecular

rearrangements will eventually also lead to devitrification of the glass to the thermodynamically stable crystalline state (also known as crystallization), with a subsequent loss of the solubility and dissolution rate advantages[38].

The ability of materials to form glasses varies widely. Materials that tend to display high viscosity at their melting points readily form glasses, while materials with high melting enthalpies (including many drugs) generally prefer the thermodynamically favorable process of crystallization. Nevertheless, if cooled fast enough, most substances can be successfully amorphized[41]. Besides supercooling of the melt, there are several other means by which amorphous solids can be prepared including mechanical activation of the crystal, vapor condensation, and precipitation or evaporation from a solution[12]. However, as mentioned previously, the properties of a glass depend on the thermal history of the material, and therefore the preparation method utilized to induce amorphicity will affect the properties and quality of the final product.

2.2 Classification and definitions

The term *solid dispersion* for pharmaceutical applications was introduced in 1971 by Chiou and Riegelman[35] and was defined as a "dispersion of one or more active ingredients in an inert carrier or matrix at solid state". The term covers a range of different systems and based on their molecular arrangement and physicochemical properties, solid dispersions can be classified into four different types, as described in Table 2.1. Even though the number of components in a solid dispersion in theory is unlimited, the different types and subtypes will here be defined based on a binary system of a drug and a carrier for the sake of simplicity.

Table 2.1: Classification of solid dispersions.

	1 phase	**2 phases**
Crystalline	Solid solution	Eutectic mixture
Amorphous	Amorphous solid dispersion or glass solution	Amorphous solid suspension

Crystalline solid dispersions, in which both drug and carrier are present in the crystalline state, can be divided into eutectic mixtures and solid solutions. A simple eutectic mixture is a mixture of two crystalline components that are miscible in the liquid state but completely immiscible in the solid state. Eutectic mixtures exhibit two distinct melting points of which one is lower than the melting point of either of the pure components. At a specific compound-dependent mixing ratio, referred to as the eutectic point, the mixture only exhibits one single melting point and forms a homogenous liquid mixture that will phase separate simultaneously upon cooling[35,42,43]. However, if the two crystalline components have a degree of miscibility in the solid state, a fraction of the drug may be molecularly dispersed in the carrier to form a solid solution.

Depending on the miscibility and size difference between the drug and carrier, solid solutions can be divided into four subtypes. If the interactions between the two different components are stronger than the interactions between the individual components, the two components are miscible in all proportions and a *continuous* solid solution is formed. However, for pharmaceutically relevant molecules this kind of solid solution is uncommon. A *discontinuous* solid solution is formed when the components are only miscible over a specific (temperature dependent) composition range in the solid state. As it is expected that there is some degree of miscibility in the majority of binary systems, this subtype is probably the most prevalent crystalline solid dispersion[10,35,44]. If the size and chemical structures of both components are similar, one of the components can take the place of the other in the crystal lattice to form a single-phase mixed crystal. This subtype is referred to as a *substitutional* solid solution and can also be *continuous* or *discontinuous*. In contrast, if the size of one of the components is considerably smaller than that of the other, *interstitial* solid solutions can be formed when the smaller component is able to occupy the interstitial space in the crystalline lattice of the larger component, and thus by nature *interstitial* solid solutions can only be *discontinuous*[37,45].

Amorphous suspensions are comparable to eutectic mixtures, but consist of two amorphous phases that are immiscible in the solid state. Therefore, amorphous suspensions are heterogeneous on a molecular level. Due to the inherent unstable nature of the amorphous form, these systems will almost inevitably crystallize over time. In order to overcome crystallization, the drug can be molecularly dispersed in a carrier in which it is miscible to form a homogenous single-phase amorphous solid dispersion. However, even though the molecular mobility in an amorphous solid dispersion is often reduced by the carrier, these systems may also be unstable and phase separate into an amorphous suspension and eventually crystallize[43,46,47]. Physical stability can only be ensured if the drug is solubilized in the amorphous carrier below its equilibrium solubility in the carrier, a system known as a glass solution. Consequently, glass solutions are thermodynamically stable (as long as the carrier does not crystallize), which means that the drug will not crystallize during storage, at least under dry conditions. In this context, it is important to emphasize that in glass solutions, the drug is not forming an amorphous phase but it still has the solubility and dissolution advantages of the amorphous drug[17]. However, currently there are no established standardized methods to determine the solubility of a drug in a carrier (which usually is an amorphous hydrophilic, non-crystallizing polymer). This situation is mainly due to the fact that the majority of pharmaceutically relevant drugs and polymers are solid, and therefore measuring the drug–polymer solubility at room temperature is very time-consuming, if not impossible. Consequently, in practice it may be difficult to distinguish between an amorphous solid dispersion and a glass solution[48,49].

2.3 Historical overview

A list of marketed products formulated as solid dispersions is given in Table 2.2 of which the majority is amorphous solid dispersions or glass solutions. The first product approved by the FDA was Gris-PEG®; a solid dispersion of griseofulvin in PEG prepared by a fusion method[9]. However, the solid dispersion concept was introduced more than a decade earlier and since then several generations of solid dispersions have emerged, as illustrated in Figure 2.2. The first generation of solid dispersions for pharmaceutical application was prepared using crystalline carriers. In the early 1960's eutectic mixtures of drugs in the water-soluble crystalline carrier urea were reported in the literature[11,50]. As urea is a normal physiological metabolite it was considered non-toxic and pharmacologically inert. Furthermore, it increased the aqueous solubility of many drugs and compared to previous formulations, eutectic mixtures with urea increased the bioavailability both in human and animals[44]. Later in that decade, solid solutions, i.e. molecular dispersions of drugs in water-soluble crystalline carriers such as the sugar alcohols mannitol and sorbitol were introduced. The advantage of these solid solutions over the eutectic mixtures was an improved dissolution rate due to increased wettability and the initial release of microcrystals, i.e. particles with a high specific surface area[51-53]. Even though the dissolution rate and bioavailability of the first generation of (crystalline) solid dispersions was improved compared to the crystalline drug alone, they were thermodynamically more stable than amorphous solid dispersions. Therefore there was potential to further improve dissolution rate and apparent solubility of poorly water-soluble drugs by using higher energy solid forms.

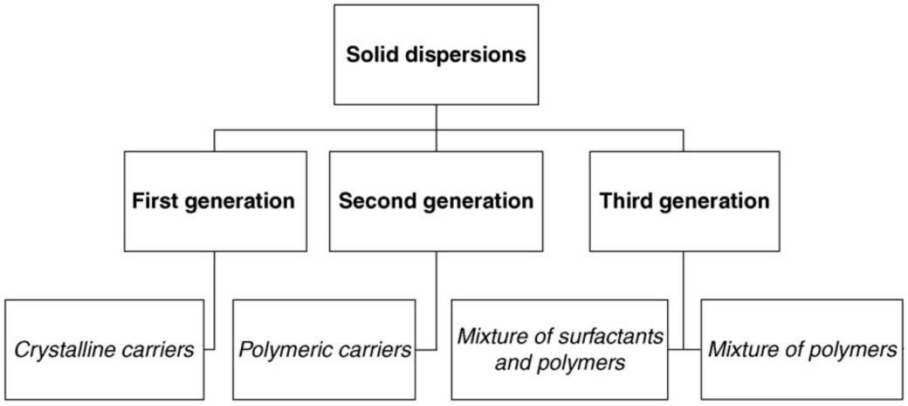

Figure 2.2: Schematic diagram of the different generations of solid dispersions. Adapted and modified from Vasconcelos et al.[11] with permission from Elsevier© 2007.

The second generation of solid dispersions emerged in the late 1960's and was prepared using amorphous water-soluble polymeric carriers such as PVP, PEG, and HPMC[11]. Depending on their molecular arrangement, the second generation solid dispersions can be divided into amorphous solid suspensions and amorphous solid dispersions (or glass solutions), as described above. The advantage of amorphous solid dispersions is that the particle size of the drug in these

systems can be reduced to a near molecular level, and thus the drug can reach supersaturating concentrations as a result of forced solubilization when the polymer is dissolved. Furthermore, the amorphous polymer can also increase the wettability and inhibit crystallization of the supersaturated drug[11,53].

As the supersaturation generated from the second generation of solid dispersions may cause rapid crystallization, thus negatively influencing the bioavailability, a third generation of solid dispersions was introduced in the 1990's. In this generation of solid dispersions, a combination of polymers or a mixture of polymer and a carrier that has surface active or self-emulsifying properties, are intended to ensure an optimal dissolution profile in order to achieve the highest bioavailability[11,54,55]. Polymers such as poloxamer and Soluplus® but also low-molecular-weight compounds such as sodium lauryl sulfate or sucrose laurate have been used in this generation of solid dispersions[53]. Besides improving the wettability of the drug, these additives can also solubilize the supersaturated drug and prevent crystallization upon dissolution. Furthermore, surfactants with amphiphilic structures have also shown to enhance the drug–polymer miscibility, thereby increasing the physical stability of the formulation[56].

Table 2.2: List of marketed solid dispersions[8,17,20,53].

Drug(s)	Brand name	Carrier(s)[a]	Manufacturer	Year of approval[b]
Griseofulvin	Gris-PEG®	PEG	Pedinol Pharmaceutical	1975
Verapamil	Isoptin®	HPMC/PVP/PEG	Abbott Laboratories	1982
Nabilone	Casamet®	PVP	Meda Pharmaceuticals	1985
Nimopidine*	Nimotop®	PEG	Bayer	1988
Nivaldipine	Nivadil®	HPMC	Astellas Pharma	1989
Itraconazole	Sporanox®	HPMC	Janssen Pharmaceutica	1992
Tacrolimus	Prograf®	HPMC	Astellas Pharma	1994
Troglitazone*	Rezulin®	PVP/HPMC	Pfizer	1997
Nifedipin	Afeditab®	PVP/Poloxamer	Actavis	2001
Rosuvastatin	Crestor®	HPMC	Astra Zeneca	2003
Lopinavir/ritonavir	Kaletra®	PVP/VA	Abbott Laboratories	2005
Fenofibrate	Fenoglide®	Poloxamer/PEG	Santarus	2007
Etravirine	Intelence®	HPMC	Janssen Therapeutics	2008
Tolvaptan	Samsca®	HPMC	Otsuka Pharma	2009
Ritonavir	Norvir®	PVP/VA	Abbott Laboratories	2010
Everolimus	Zortress®	HPMC	Novartis	2010
Telaprevir	Incivek®	HPMCAS	Vertex Pharmaceuticals	2011
Vermurafenib	Zelboraf®	HPMCAS	Roche	2011
Ivacaftor	Kalydeco®	HPMCAS	Vertex Pharmaceuticals	2012
Posaconazole	Nofaxil®	HPMCAS/HPC	Merck	2013
Tacrolimus	Astagraf XL®	HPMC	Astellas Pharma	2013
Suvorexant	Belsomra®	PVP/VA	Merck	2014
Ombitasavir etc.	Viekira™	PVP/VA	AbbVie	2014
Ledipasvir/sofosbuvir	Harvoni®	PVP/VA	Gilead Sciences	2014
Tacrolimus	Envarsus®	Poloxamer/HPMC	Veloxis Pharmaceuticals	2015
Lumacaftor/Ivacaftor	Orkambi®	HPMCAS	Vertex Pharmaceuticals	2015

* Discontinued product in USA

[a] Based on the inactive ingredients list and other literature information

[b] Information based on FDA approval history on www.drugs.com

2.4 Methods of preparation

As illustrated in Figure 2.3, amorphous materials including amorphous solid dispersions can generally be induced in a solid in two fundamentally different ways: the thermodynamic and the kinetic path. The kinetic path is a "top-down" amorphization approach where particle size reduction and loss of molecular order in a bulk powder is introduced over time. This approach requires high energy or pressure input and includes technologies such as high-pressure homogenization and different milling methods[57]. In contrast, the thermodynamic path is a "bottom-up" vitrification approach and basically a solidification process where the final particles are obtained from individual molecules[58]. The thermodynamic path is the more popular of the two paths to prepare amorphous solid dispersions and is commonly divided into solvent-based and melt-based technologies. The solvent-based technologies include spray drying, co-precipitation, supercritical fluid extraction, electrospinning, and freeze drying; and the melt-based technologies include melt agglomeration, spray congealing and melt extrusion[53]. The selection of a suitable processing technology for the preparation of amorphous solid dispersions depends on the desired outcome and the physicochemical properties of both the drug and polymer such as their T_m or T_g, thermal stability, and solubility/stability in organic solvents. Therefore, the principles and advantages of the most common preparation techniques are presented in detail in the following sections.

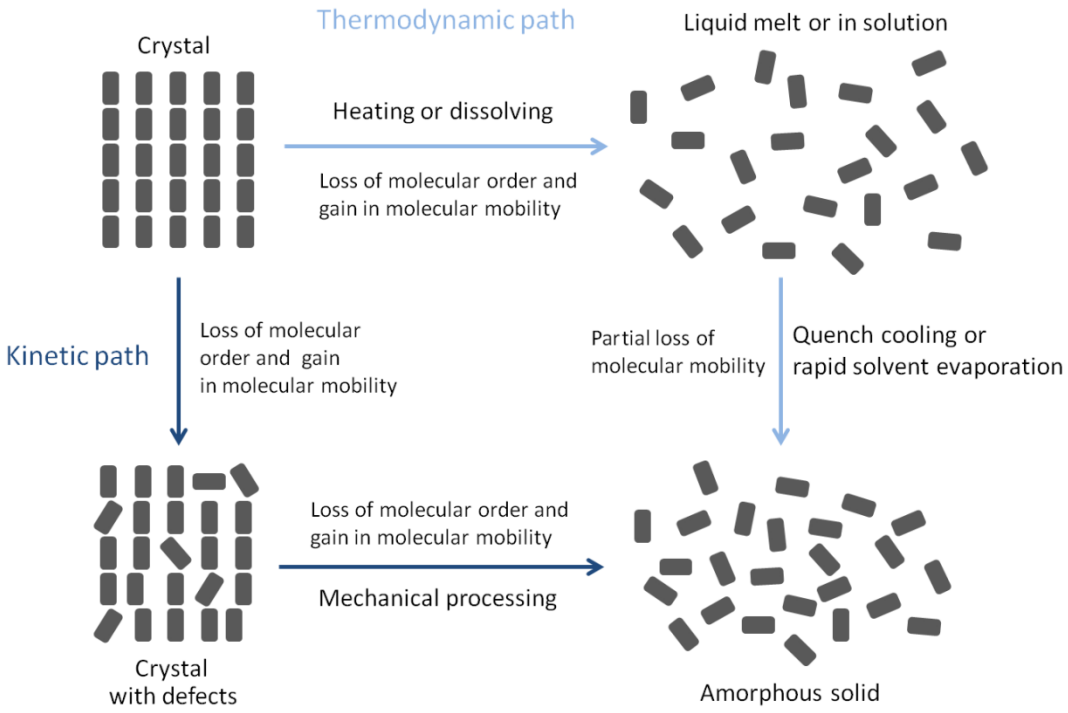

Figure 2.3: Simplified schematic presentation of the conversion from the crystalline state to the amorphous form via the thermodynamic and kinetic path. Modified from Allen[57] with permission from Pharmaceutical Press© 2012.

2.4.1 Melting/fusion

The simplest way to produce an amorphous solid dispersion is using the melting or fusion method, where a drug and polymer are heated to a combined melt and rapidly solidified by cooling. If cooling of the melt through the supercooled liquid state exceeds the rate of crystallization (a process known as quenching), the drug and polymer may be "frozen" in the glassy state as outlined in Section 2.1. Therefore, adequate mixing of the drug and polymer in the melt and rapid cooling are essential to form homogenous amorphous solid dispersions[58]. Several different methods have been proposed based on fusion and they differ by the way the compounds are mixed and cooled. In the original procedures, the melt was mixed by stirring and simply poured onto a stainless steel plate to cool, pulverized and sieved to obtain an amorphous solid dispersion at the desired particle size. Later, the use of ice-baths or liquid nitrogen was applied to speed up the cooling process[35]. Alternatively, powders can be readily produced if the melt is spray cooled (a process also known as spray congealing). In this method, that is conceptually similar to spray drying, the melt is sprayed into a chamber that is continuously perfused with chilled air, causing the droplets to solidify almost instantly into spherical particles with good flow properties[59].

However, the current melt-based method of choice in the pharmaceutical industry is hot melt extrusion as it overcomes some of the practical limitations of the simpler fusion methods. In a normal hot melt extrusion operation, a physical mixture of crystalline drug and polymer is introduced via a hopper into an extruder, containing a heated barrel and one or two rotating screws that transport the material down the barrel. The mixture is then subjected to mechanical forces as well as being heating to yield a well-mixed melt, forced through a die and formed or cut into the desired shape and size. The combination of a rotating screw and a heated barrel results in a high shear stress, which allows for intimate mixing of the components, and the short residence times reduce the chance of thermal degradation[60]. Compared to the traditional fusion methods, hot melt extrusion enables continuous manufacturing, which makes it suitable for large-scale production. Nevertheless, application of the fusion method requires that the drug and polymer are completely miscible and thermally/chemically stable in the liquid state, and therefore it is only applicable to drugs with relatively low melting points[40]. Despite these limitations, the application of the hot melt extrusion technology for commercial manufacturing of amorphous solid dispersions is well documented and includes marketed products such as Casemet® (nabilone) and Kaletra® (lopinavir/ritonavir)[61].

2.4.2 Solvent evaporation

In a solvent evaporation method, drug and polymer are dissolved in a common solvent (or a mixture of solvents), which is then rapidly evaporated to avoid crystallization of the drug from the supersaturated solvent. If the solvent evaporation is fast enough and the drug and polymer are miscible in the solid state, the drug will become kinetically trapped in the polymeric matrix in a solution-like solid state due to a rapid viscosity increase. This situation is comparable to cooling

from a melt, only here the components are molecularly/homogenously dispersed in a solvent, and thus compared to the fusion method, mixing is not as critical[62]. Several different solvent evaporation methods have been proposed and they differ by the type of solvent used and the conditions under which the solvent is evaporated. The most simple lab-scale solvent evaporation method is film casting, where an organic solution is spread onto a glass and evaporated under normal pressure either at room temperature or on a hot plate. Alternatively, the film can be obtained by rotary evaporation under reduced pressure to allow for lower processing temperatures[63]. If the drug is thermosensitive the heating process can (and should) be avoided by using a freeze drying process, where the solution is frozen at low temperatures and the solvent removed by reducing the pressure to allow for a solid-gas transition (sublimation). However, as the use of organic solvents in freeze drying is limited and these are often necessary to dissolve the poorly water-soluble drugs, the technique is not commonly used to prepare amorphous solid dispersions[64].

Another possibility to prepare amorphous solid dispersions with thermosensitive drugs is using supercritical CO_2 as a solvent. Above a critical temperature (31.4 °C) and pressure (74 bar), CO_2 is present in a supercritical state, possessing both gaseous and liquid state properties, such as the ability to dissolve materials. Consequently, a drug and polymer can be dissolved in supercritical CO_2, which can then be removed as gaseous CO_2 through rapid expansion caused by a sudden decompression. Furthermore, supercritical CO_2 can also be used as an anti-solvent in a co-precipitation procedure, which is described in further detail in Section 2.4.3[65].

Due to the very fast solvent evaporation, spray drying is the most successful solvent-based method to prepare amorphous solid dispersions. In this rather complex process, a solution of drug and polymer in a volatile organic solvent is atomized into fine droplets by applying a force (pneumatic, centrifugal or vibrational) in a drying chamber that is continuously perfused with conditioned drying gas (often inert nitrogen gas). This causes the solvent to evaporate and the droplets to solidify into spherical particles, which are then separated from the gas using a cyclone and/or a filter bag. Even though the processing temperature in a normal spray drying operation is relatively high, the product rarely reaches temperatures above 50 °C because the heat transfer associated with evaporation causes the temperature of the surrounding gas to drop[62]. Hence, compared to the fusion method, the thermal decomposition of thermosensitive drugs and polymers may be prevented as evaporation of organic solvents can be performed at comparatively low temperatures. However, there are also disadvantages associated with solvent evaporation methods such as incomplete solvent evaporation of potentially toxic solvents and difficulties in finding a common volatile solvent for both the drug and the polymer due to differences in hydrophilicity[58]. Nevertheless, along with hot melt extrusion, spray drying is the method of choice for large-scale production of amorphous solid dispersions, and commercially available products such as Incivek® (telaprevir) and Intelence® (etravirine) have been produced using the spray drying technology[8].

2.4.3 Co-precipitation

In a co-precipitation method, drug and polymer are dissolved in a common organic solvent and slowly added to a large volume of anti-solvent (often water), causing simultaneous precipitation of drug and polymer. The resulting suspension is then filtered and washed to remove residual solvents before it is dried to yield a fine powder referred to as a microprecipitated bulk powder[53]. The rate of precipitation is dependent on the solubility of the drug and polymer in the anti-solvent. If the precipitation is fast enough, the microprecipitate will become amorphous. Thus, the selection of a suitable solvent and anti-solvent is crucial for the quality of the amorphous solid dispersion. As they are washed out, the solvents can be less volatile than those used for solvent evaporation methods, and therefore polar "super solvents" such as dimethylacetamide, dimethylformamide and N-methyl pyrrolidone are used due to their ability to solubilize even high-molecular-weight polymers. The precipitation method is particularly effective for polymers with pH dependent solubility as these can be precipitated using an aqueous solution as the anti-solvent (acidic or basic depending on the polymer properties), but can also be applied for other polymers[66]. Consequently, the co-precipitation method is advantageous compared to techniques such as melt extrusion and spray drying for compounds that have high melting points and low solubility in conventional volatile organic solvents. These features are characteristic for vemurafenib that has a melting point of 272 °C and is poorly soluble (<5 mg/mL) in most organic solvents. The marketed amorphous solid dispersion of vemurafenib (Zelboraf®) is thus manufactured using a precipitation method[61,67].

2.4.4 Mechanical force

Mechanical treatment in a mill is a widespread technique to reduce the particle size of a material. However, besides reducing the particle size, milling can also result in significant changes in the structure of a material including polymorphic transformation and amorphization. The milling process is then often termed mechanical activation or grinding. During a milling operation, the particles will reduce in size until a certain threshold is reached, beyond which no further particle size reduction is possible even if the milling time is increased. The continued transfer of mechanical force from the mill will induce defects in the crystal structure, which eventually may manifest throughout the entire crystal with the subsequent loss of the long-range order, resulting in partial or full amorphization (kinetic path)[57]. Furthermore, co-milling of a drug with a polymer has also been shown to induce intimate mixing between the two components at the molecular level[68]. The temperature of milling is important for the properties of the final product and, as a rule of thumb, grinding a crystal below the T_g of its respective amorphous form, favors amorphization and grinding above the T_g favors transformation to other crystal polymorphs (due to higher molecular mobility, which allows for restoration of crystallographic order)[69]. Therefore, depending on the physicochemical properties of the starting materials and the desired outcome, grinding can be carried out using either a traditional ball mill at room temperature or in a cryogenic impact mill immersed in liquid nitrogen (cryomilling). However, studies have shown

that the physical stability of amorphous solids prepared by grinding often is lower compared to other preparation methods such as melt extrusion and spray drying. This is probably because during milling, although the material will lose its long-range order, it retains the molecules in similar positions to those seen in the crystalline form, whereas in a spray dried or melt extruded material the molecules are more randomly distributed, similar to a the situation in a melt[70].

Due to the nature of the milling operation it is a difficult method to scale up and none of the marketed amorphous solid dispersions have been produced using mechanical activation. Nevertheless, grinding serves as an excellent lab-scale alternative to the melting/fusion and solvent evaporation methods, especially if the compounds are susceptible to thermal or solvent-induced degradation[71]. As a concluding remark, it is important to note that even though materials can be amorphized using different preparation methods, they are not necessarily identical on the molecular level, and thus their physical properties may differ[72,73].

Chapter 3

Development considerations

Despite the relatively low number of commercially available amorphous solid dispersions, recent research has provided evidence that physically stable amorphous solid dispersions can increase the biopharmaceutical performance of poorly soluble drugs[58]. When developing amorphous solid dispersions, there are a number of factors that need to be considered, which can be categorized into physical attributes of drug and polymer, *in vitro* dissolution testing, and biological *in vivo* evaluation, as shown in Table 3.1[36].

As the performance of amorphous solid dispersions is mainly governed by the choice of polymer, a suitable polymer candidate is preferably identified in the beginning of the development process[11,74]. A suitable manufacturing process can then be selected based on the physicochemical properties of the drug and polymer, such as their T_g, T_m, thermal stability, and solubility in volatile solvents, as explained in Section 2.4[36]. To ensure the physical stability of amorphous solid dispersions at storage conditions, it is first and foremost important that a single-phase amorphous system (preferably a glass solution) can be produced, which will depend on the miscibility/solubility of the drug in the polymer. As a change in conditions (e.g. an increase in humidity) may cause phase separation or crystallization of the drug, the effect of water uptake on the physical stability of the formulation will also have to be evaluated[40].

When a stable amorphous solid dispersion has been produced, the *in vitro* performance should be assessed. In this context, it is important that the method (apparatus, media, pH, etc.) mimics the physiological conditions in the gastrointestinal tract. For amorphous solid dispersions, non-sink *in vitro* conditions are essential in order to evaluate their supersaturation behavior and enable a prediction of *in vivo* performance. This is because predictions based on non-physiological sink condition may result in false assumptions and discrepancies with early *in vivo* studies. Finally, as drug candidates often fail Phase I clinical trials due to poor oral bioavailability, the performance of amorphous solid dispersions should be evaluated using appropriate animal models relevant to humans, including aspects such as food effects and dose linearity/proportionality of the formulation[36].

Even though several factors will affect the performance and quality of the final dosage form, maintaining a molecularly dispersed homogenous system over the entire product shelf-life and ensuring the highest possible oral bioavailability is essential. Consequently, different methods to predict the maximum drug–polymer ratio (to prepare stable amorphous solid dispersions) and the assessment of the *in vitro* dissolution supersaturation behavior of these systems (with respect to their *in vivo* performance) are introduced in the following sections.

Table 3.1: Pharmaceutical considerations for the development of amorphous solid dispersions. The two most important considerations that will be elaborated upon in detail in this chapter are highlighted in bold. Adapted and modified from Newman et al.[36] with permission from Wiley Periodicals© 2012.

Area	Considerations	Recommendations
Physical	Choice of polymer(s)	Select based on physicochemical properties such as melting point/glass transition temperature, drug–polymer miscibility/solubility, solubility in solvents, wettability, hygroscopicity, dissolution rate, etc.
	Drug–polymer ratio	Determine/estimate the highest drug load that will provide acceptable biopharmaceutical performance (dissolution rate and crystallization inhibition in solution) and long-term stability in the solid state.
	Manufacturing process	Chose a suitable process depending on the thermal stability and solubility of the drug and polymer in solvents. Ensure that amorphous solid dispersions produced at elevated temperatures do not phase separate/crystallize upon cooling.
	Miscibility	Confirm that the manufacturing process is able to produce an amorphous single-phase, miscible system using DSC and XRPD.
	Hygroscopicity	Evaluate the effect of water uptake on the glass transition temperature, physical stability and crystallization kinetics.
Dissolution	Dissolution method	Focus on dissolution methods and media that mimic the conditions in the GI tract (biorelevant media, pH, volume, stirring rate, dose, etc.).
	pH effects	Assess the effect of pH (1−7.5) on the dissolution behavior, especially for pH-responsive polymers.
	Sink vs. non-sink conditions	Investigate the dissolution performance in both sink and non-sink conditions and compare with *in vivo* data. For poorly soluble drugs (dose insoluble in 250 mL aqueous media), non-sink conditions are essential.
	Polymer controlled dissolution/wettability	As the drug release is driven by the dissolution of the polymer, the polymer properties needs to be taken into consideration during dissolution method development.
	Supersaturation behavior	Test the supersaturation behavior (degree and duration of supersaturation and crystallization inhibition) over biologically relevant time frames.
Biological	Fed/fasted	Evaluate food effects on the plasma concentration–time profile.
	Dose dependency	Establish the dose dependency of the formulation. As poorly soluble drugs are likely to crystallize *in vivo*, dose-linearity or proportionality should not be expected.
	Species differences	Investigate the use of appropriate animal models relevant to humans.
	Absorption and metabolism	Determine if the drug is a substrate for human transporters, efflux pumps and/or metabolizing isoforms and the effect this will have on absorption.

3.1 Methods to predict maximum drug–polymer ratio

An important aspect to consider when developing an amorphous solid dispersion is that the formulation remains amorphous over its entire shelf-life. This is referred to as kinetic or physical stability and it is crucial to ensure that the biopharmaceutical performance of the formulation does not change over time. As the amorphous drug alone is thermodynamically unstable, the realization of the full potential of amorphous solid dispersions relies on the stabilizing ability of the polymer to prevent crystallization[36]. Even though the exact mechanisms are not yet fully understood, polymers are thought to improve the physical stability of an amorphous drug through intermolecular interactions[75] and increasing the T_g of the system, which ultimately leads to decreased molecular mobility[76,77]. In fact, it is generally accepted that if the storage temperature is >50 °C below the T_g, the molecular mobility is so low that the system is stable enough to avoid crystallization for years[78]. Consequently, it appears that for a polymer to be an efficient stabilizer it must have a high T_g and similar properties to the drug molecule, according to the solvent rule (like dissolves like). This has also led to the use of solubility parameter calculations to identify suitable polymer candidates for a given drug[79,80]. Therefore, careful selection of polymers and prediction of the drug–polymer ratio that will provide acceptable long-term stability are probably the most important factors in the development of homogenous amorphous solid dispersions.

Despite their apparent simplicity, amorphous solid dispersions can form several different structures depending on their composition. In order to achieve a homogenous single-phase amorphous solid dispersion, the drug can be dissolved in the polymer below the equilibrium solubility of the drug in the polymer or it must be miscible with the polymer at the given storage conditions[14]. However, the difference between drug–polymer solubility and miscibility has led to some confusion in the literature and the two different terms have been used indiscriminately to describe the same thermodynamic situation. Therefore, to illustrate this difference a typical phase diagram of a small drug molecule–polymer system is shown in Figure 3.1, including the solubility curve, the miscibility curve and the T_g curve.

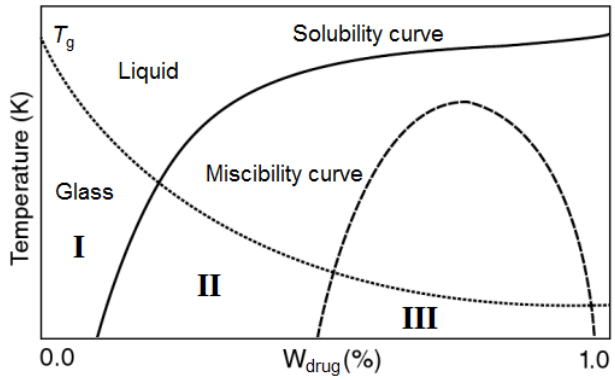

Figure 3.1: Phase diagram of a drug–polymer mixture including the solubility curve (solid line), miscibility curve (dashed line) and the T_g curve (dotted line). Area **I** represents a thermodynamically stable amorphous solid dispersion (glass solution), area **II** represents a metastable amorphous solid dispersion where the mixture is kinetically stabilized due to low molecular mobility, area **III** represents an unstable amorphous solid dispersion in which phase separation occurs spontaneously.

The T_g curve in Figure 3.1 represents the composition dependence of the T_g of a homogenous drug–polymer amorphous solid dispersion. *Per se* this curve does not represent a true phase transition but it is important as it indicates a kinetic boundary of molecular mobility. Above the T_g curve, the mixture is a supercooled liquid with high molecular mobility, and thus structural relaxation is fast and solubility and miscibility can be measured at equilibrium. Below the T_g curve, the mixture is a non-equilibrium glass with low molecular mobility and slow structural relaxation. Therefore, the equilibrium solubility or miscibility in this region can neither be strictly defined in a thermodynamic sense nor measured experimentally[49]. The solubility curve in Figure 3.1 represents the thermodynamic solubility of the crystalline drug and the miscibility curve represents the kinetic miscibility of the amorphous drug in the polymer. As the amorphous form has a higher free energy than the crystalline state of the drug, the miscibility curve will always be below the solubility curve[37].

Above the solubility curve, the drug is soluble in the polymer and the system is a thermodynamically stable homogenous solution, also referred to as a glass solution if the temperature is below the T_g curve (area **I** in Figure 3.1). In this context it should be noted that the drug in a glass solution is not forming an amorphous phase, but is rather dissolved in the polymer, and therefore the solubility curve defines the drug–polymer ratio at which there is no risk of crystallization[81]. Below the solubility curve the system is thermodynamically unstable and will crystallize over time. This will result in an inhomogeneous dispersion of crystalline drug in a glass solution, in which the drug concentration corresponds to the equilibrium solubility at that temperature[14]. In this region, amorphous–amorphous phase separation may occur prior to crystallization, represented by the miscibility curve.

Below the miscibility curve, there is no thermodynamic barrier to prevent the mixture from destabilization and phase separation will occur spontaneously even if the temperature is below T_g curve (area **III** in Figure 3.1) whereas above the miscibility curve, an energy barrier has to be overcome in order to cause destabilization[14,82]. The area in between the solubility and miscibility curves, and below the T_g curve (area **II** in Figure 3.1), thus, represents a metastable state from which the drug does not necessarily crystallize or phase separate immediately. In fact, even though the mixture is thermodynamically unstable, a homogenous molecular dispersion can be preserved for months or even years if it is stored in this area[78]. Miscibility is thus an apparent property of the system involving the kinetics of structural relaxation and phase separation, and may experimentally only be defined from long-term stability studies[49].

Hence, although the concept of drug–polymer miscibility is still controversially debated, from an industrial perspective it might be an important attribute in the stabilization of an amorphous solid dispersion, especially if the drug–polymer solubility is very low and thermodynamic stability cannot be guaranteed[14,49,82]. However, as there are currently no standardized methods to predict drug–polymer miscibility, it seems that at present the stability of an amorphous solid dispersion can only be fully ensured by dissolving the drug in the polymer below its equilibrium solubility

(i.e. a glass solution). Therefore, the prediction of drug–polymer solubility at room temperature is of great academic and industrial interest[83].

The equilibrium solubility of a drug in a polymer can be measured in at least four different, but thermodynamically equivalent pathways, as illustrated in Figure 3.2[80]. In the pharmaceutical industry, when determining the solubility of a solute in a *liquid* solvent, the most commonly used approach is the shake-flask method, where the dissolution of the solute in an undersaturated solution is measured at constant temperature until equilibrium solubility has been reached (*a*→*e* in Figure 3.2). Even though solubility studies are normally conducted with a solid solute (drug) in a liquid solvent, it is also possible to reach equilibrium through this pathway using a solid (or highly viscous) solvent such as a polymer. In contrast to dissolution, the crystallization of a solute from a supersaturated solvent can also be measured at constant temperature (*b*→*e* in Figure 3.2).

Alternatively, the equilibrium solubility can be measured using constant concentration rather than temperature[80]. Of these pathways, freezing point depression is perhaps the most familiar as this is applied in practice to lower the freezing point of water with sodium chloride to avoid icy roads[84]. Using freezing point depression, the crystallization temperature (depressed freezing point) is measured at constant concentration from decreasing temperature (*d*→*e* in Figure 3.2). However, due to the low chemical stability of drugs and polymers at temperatures above the melting point, combined with slow crystallization kinetics, this pathway is not feasible for drug–polymer systems. Hence, melting point depression is an alternative pathway, where the dissolution temperature (depressed melting point) is measured at constant concentration from increasing temperature (*c*→*e* in Figure 3.2)[80].

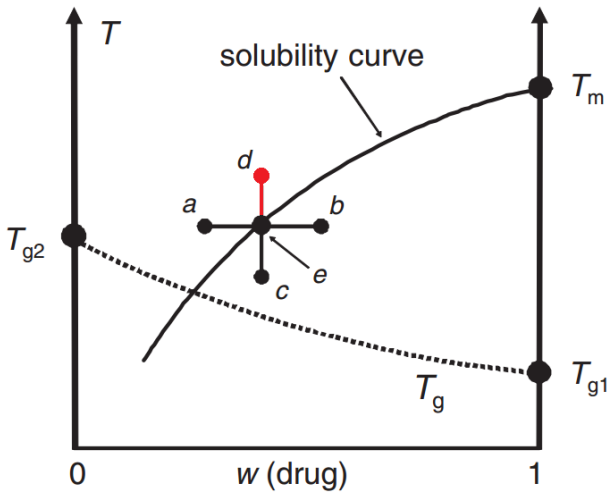

Figure 3.2: Phase diagram of a drug–polymer mixture. The solid line represents the solubility curve and the lines leading to *e* represent different pathways to reach equilibrium solubility. *d*→*e* is colored in red as this pathway is not feasible for drug–polymer mixtures. Modified from Sun et al.[80] with permission from Wiley-Liss© 2010.

As mentioned above, the drug–polymer solubility as a thermodynamic property is only properly defined above the T_g, where the system is in an equilibrium supercooled liquid state. However, due to the (infinitely) slow relaxation kinetics of most polymers it is possible to predict the apparent solubility below the T_g based on data obtained in the supercooled liquid state[39,49]. Furthermore, as most pharmaceutically relevant drugs and polymers are solid or highly viscous at room temperature, measuring the solubility below the T_g is not feasible as reaching equilibrium would be very time-consuming[48]. Therefore, the majority of the methods proposed to predict drug–polymer solubility are based on equilibrium thermodynamics at elevated temperature using a differential scanning calorimeter (DSC).

The solubility of a drug in a polymer can be described using the Flory-Huggins model[85]. This model is derived from statistical thermodynamics and based on the lattice theory of a binary solution of a solvent and a solute under the assumption that the solute is much larger than the solvent. By considering that a drug molecule behaves like a solvent for a polymer, the lattice theory can be extended to describe the drug–polymer systems[83]. Thus, the drug–polymer solubility measurements obtained at elevated temperatures can be fitted to the Flory-Huggins model to determine the fitting parameter χ (for more details see Chapter 8 and Appendix A) and by assuming that χ is independent of temperature, the drug-polymer solubility at any given temperature (e.g. room temperature) can be predicted through extrapolation[86]:

$$\frac{\Delta H_m}{R}\cdot\left(\frac{1}{T_m}-\frac{1}{T}\right)=\ln\left(v_{drug}\right)+\left(1-\frac{1}{\lambda}\right)\cdot\left(1-v_{drug}\right)+\chi\cdot\left(1-v_{drug}\right)^2 \qquad (3.1)$$

where ΔH_m and T_m are the enthalpy of fusion and melting temperature for the pure drug, respectively, R is the gas constant, λ is the molar volume ratio of the polymer to the drug, χ is the Flory-Huggins interaction parameter, T is the temperature at which the measurement is made and v_{drug} is the volume fraction of the drug in the polymer.

In addition, several different *in silico* approaches have been reported to predict the maximum drug–polymer ratio such as solubility parameter calculation[79], molecular dynamics simulation[87], and perturbed chain statistical associating fluid theory (PC-SAFT)[81]. However, as these methods are based on simplified theories, their predictability is still limited and hence, they may only serve as an indicative screening tool. Therefore, in the following sections, different *experimental* methods proposed to predict drug–polymer solubility are presented, as they appeared in the literature.

3.1.1 Melting point depression method

Even though the principle of measuring solubility in microsamples using DSC was proposed in 2002[88], it was not until 2006 that the first experimental protocol was developed to predict drug–polymer solubility at room temperature[83]. The method was inspired by the melting point depression of crystalline solvent–amorphous polymer mixtures suggested by Hoei et al. in 1992 and since the introduction of the first melting point depression method, several optimizations and variations have been suggested[48,86,89-93]. In brief, if the dissolution of a crystalline drug into a polymer is favored by the thermodynamics of mixing, the chemical potential is reduced compared to that of the pure crystalline drug, which can be observed using DSC through detection of a depressed melting point (*c*→*e* in Figure 3.2). As this event can be regarded as a dissolution process, the degree of melting point depression is related to the drug–polymer solubility[83,86]. In the original method, physical mixtures of crystalline drug and polymer of known composition (75−95% w/w drug) are prepared by geometric mixing. The resulting powders are then scanned at a heating rate of 1 °C/min to determine the onset temperatures of melting (T_{onset}) of the drug in the presence of polymer, as illustrated in Figure 3.3. By considering the melting point as the equilibrium solubility temperature, several points on the solubility curve can be obtained, fitted to the Flory-Huggins model (Equation 3.1) and extrapolated to predict the solubility at room temperature[83].

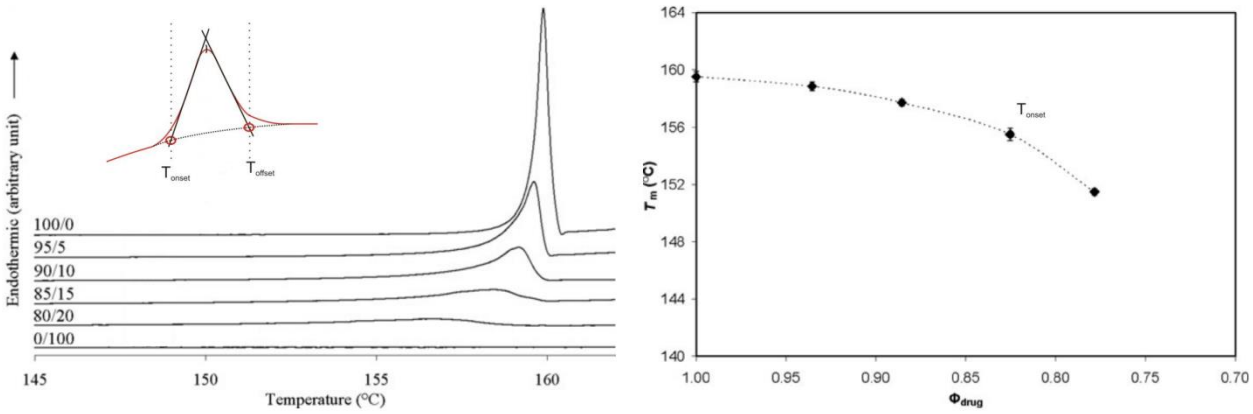

Figure 3.3: Graphical illustration of the melting point depression method. DSC scans of IMC:PVP/VA physical mixtures (80−95% w/w IMC) are shown on the left and the onset temperatures of melting (T_{onset}) are plotted as a function of composition on the right. As can be seen, the melting point decreased with increasing polymer concentration, indicating that the thermodynamics of mixing between the drug and polymer is favored. Adapted and modified from Zhao et al.[93] with permission from Wiley-Liss© 2011.

Using this method, the drug must be chemically stable at temperatures around the melting point and the melting temperature should be high enough for the polymer to be in the supercooled liquid state and able to interact and mix with the melting drug. Therefore, the method is most appropriate for polymers with a T_g that is significantly lower than the melting point of the drug[89].

In order to enable measurements at temperatures closer to the T_g, Tao et al. introduced cryomilling of the samples prior to the DSC measurements to reduce the particle size and facilitate mixing of the components[48]. Furthermore, as the melting point is ideally recorded at a state of phase equilibrium, the authors determined the melting point of the mixtures at different heating rates (0.1−2 °C/min) and extrapolated the melting point to zero heating rate. In this method, the offset of melting (T_{offset}) rather than the onset of melting was considered as the equilibrium solubility temperature of the given composition as this temperature represents the melting point of the final composition, assuming complete mixing has occurred[48]. Even though the use of onset or offset of melting is still being debated, variations of the melting point depression method are currently the most commonly used methods to predict drug–polymer solubility at room temperature in the literature[82,90-94].

3.1.2 Liquid analogue solubility method

In order to avoid extrapolations over long temperature ranges, Marsac et al. proposed a method that could calculate the Flory-Huggins interaction parameter from solubility measurements in a liquid low-molecular-weight analogue (or monomer) of the polymer[83]. The basic principle behind the liquid analogue solubility method was proposed along with the melting point depression method in 2006 and was later refined by the same group in 2009[89]. In this method, an excess of crystalline drug is added to a vessel containing a liquid, low-molecular-weight analogue of a polymer and maintained at 25 °C for at least 24 h under stirring using the simple shake-flask method (*a*→*e* in Figure 3.2). Samples are then withdrawn, filtered and diluted with ethanol and compared to a standard concentration curve using HPLC[89]. By assuming that the analogue constitutes the lattice of the polymer and that the interactions and combinatorial entropy of mixing of the drug–analogue and drug–polymer are equal, the activity coefficient of the drug in the analogue ($\gamma_{analogue}$) can be derived from the ratio of ideal mole fraction solubility (X_{id}) and the experimental mole fraction solubility (X_{exp})[91]:

$$\gamma_{analogue} = \frac{X_{id}}{X_{exp}}, \quad \ln(X_{id}) = -\frac{\Delta H_m (T_m - T)}{R(T_m T)} + \frac{\Delta C_p (T_m - T)}{RT} - \frac{\Delta C_p}{R} \ln\left(\frac{T_m}{T}\right) \tag{3.2}$$

where ΔH_m and T_m are the enthalpy of fusion and melting temperature for the drug, respectively, ΔC_p is the heat capacity change at the glass transition of the amorphous drug, R is the gas constant, and T is the temperature at which the measurement was made. The $\gamma_{analogue}$ can now be used to calculate the activity coefficient of the drug in the polymer ($\gamma_{polymer}$)[89]:

$$\ln(\gamma_{\text{polymer}}) = \ln(\gamma_{\text{analogue}}) + \frac{MV_{\text{drug}}}{MV_{\text{analogue}}}\left[\frac{1}{m_{\text{drug}}}\ln\left(\frac{v_{\text{drug}}}{X_{\text{drug}}}\right) + \frac{1}{m_{\text{drug}}} - \frac{1}{m_{\text{polymer}}}v_{\text{polymer}}\right] \quad (3.3)$$

where MV_{drug} and MV_{analogue} are the molar volume of drug and analogue, respectively, m_{drug} and m_{polymer} are the ratio of the volume of drug and polymer to the analogue, respectively, and v_{drug} and v_{polymer} are the volume fraction of drug and polymer, respectively. Finally, the mole fraction solubility of crystalline drug in the polymer can be derived from the ratio of X_{id} to γ_{polymer} and converted to mass fraction (w/w). In this context, it is important to note that even though the method enables a calculation of the solubility at room temperature, it provides an estimate of the solubility in the liquid state rather than in the solid glass and, therefore, should be evaluated with caution. Nevertheless, it still provides valuable indications on the solubility of a drug in a polymer if a liquid analogue of the polymer is available[83,89,91].

3.1.3 Dissolution method

The dissolution method (also known as the annealing method) was introduced by Sun et al. in 2010 to improve the likelihood of reaching equilibrium solubility compared to the melting point depression method[80]. In this method, a physical mixture of crystalline drug and polymer of known composition (30−80% w/w drug) is prepared by grind milling at 400 rpm for 12−16 min in periods of 2 min with breaks of 2 min to prevent overheating of the sample. After preparation, it is confirmed that the polymorphic form of the drug and crystallinity is intact using XRPD. The resulting powder is then annealed at a constant temperature above the T_g in a DSC for 4−10 h in order to allow for drug to dissolve into the polymer (*a*→*e* in Figure 3.2). This mixture (still in the DSC) is then cooled and scanned at a heating rate of 10 °C/min to determine whether residual crystals remain after annealing. If the annealing temperature is below the solubility equilibrium temperature, crystals will remain after annealing and the scan will show a melting event, as shown in Figure 3.4[80].

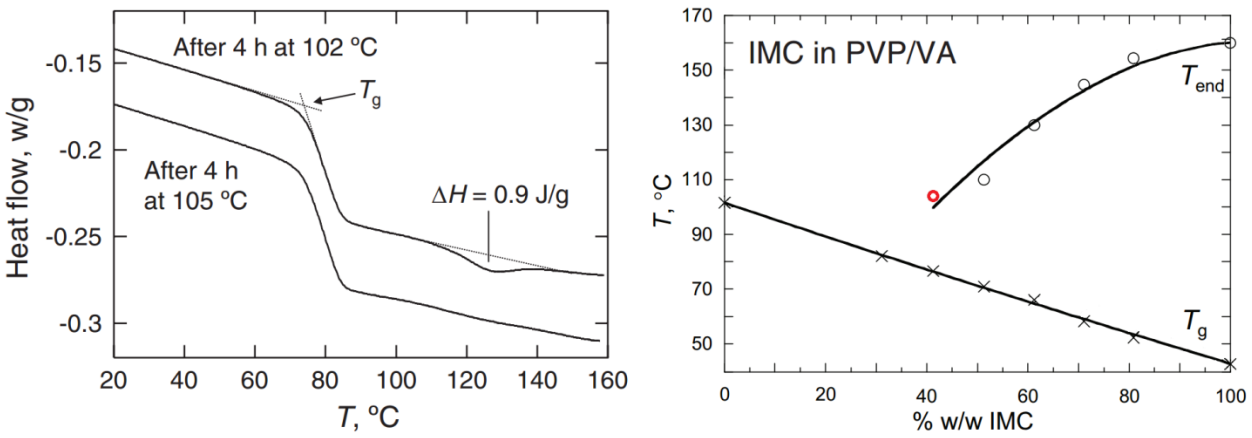

Figure 3.4: Graphical illustration of the dissolution method. DSC scans after annealing of a physical mixture of IMC:PVP/VA (40% w/w IMC) at 102 °C and 105 °C are shown on the left. As can be seen, a melting event is observed after annealing at 102 °C, but no melting event is seen after annealing at 105 °C, indicating that the solubility equilibrium temperature of the 40% w/w drug–polymer is located between 102 °C and 105 °C. On the right, the average equilibrium solubility temperatures from different compositions (40−80% w/w IMC) are plotted and the solubility curve is fitted with the Flory-Huggins model. The red circle (**o**) represents the data point obtained from the annealing on the left. Adapted and modified from Sun et al.[80] with permission from Wiley-Liss© 2010.

Consequently, by systematically varying the annealing temperature, the lower and upper boundaries of the equilibrium solubility temperature can be determined. Repeating this protocol using different compositions, several points (realistically it is more an interval than a point) on the solubility curve can be obtained, fitted to the Flory-Huggins model (Equation 3.1) and extrapolated to predict the solubility at room temperature. Alternatively, rather than annealing the same mixture at different temperatures; mixtures of different compositions can also be annealed at the same temperature to give the same result. Here the upper and lower boundaries of the equilibrium solubility concentration at a given annealing temperature can be determined. However, for both approaches, longer annealing times must also be performed in order to confirm that the residual crystals remaining after annealing are not a result of an incomplete dissolution process due to slow dissolution kinetics at the annealing temperature[80] (Sun, 2010). Thus, although the method has the potential to provide more accurate solubility data at lower temperatures, it requires a great number of DSC scans with long annealing times, which makes it even longer to implement than the melting point depression method[95].

3.1.4 Recrystallization method

The recrystallization method was proposed by Mahieu et al. in 2013 and is similar to the dissolution method, but instead of dissolution into an undersaturated solution, the equilibrium solubility is reached by recrystallization from a supersaturated solution[95]. In this method, a supersaturated amorphous solid dispersion of drug and polymer is prepared by ball milling at 400 rpm for 8 h in periods of 10 min with breaks of 5 min to prevent overheating, and thus

crystallization of the sample. The composition of the amorphous solid dispersion is 85% w/w drug, which in most cases will correspond to a situation of strong supersaturation. After preparation, it is confirmed that the sample is fully amorphous and homogenously mixed before proceeding using DSC and XRPD. The resulting powder is then annealed at a constant temperature between the onset of crystallization and melting in a DSC for 2 h in order to allow for the excess drug to recrystallize out of the polymer (*b*→*e* in Figure 3.2). At this stage, a mixture of amorphous polymer saturated with dissolved drug and crystallized drug is obtained. This mixture (still in the DSC) is then cooled and scanned at a heating rate of 5 °C/min to determine the T_g of the remaining amorphous phase. The equilibrium solubility concentration of the drug in the polymer for that given annealing temperature is then derived from this T_g using the Gordon-Taylor relationship, which describes the composition dependence of the T_g of two-component mixtures[96]:

$$X_{\text{drug}} = \frac{K \cdot \left(T_{\text{g(polymer)}} - T_{\text{g}}(X_{\text{drug}})\right)}{K \cdot \left(T_{\text{g(polymer)}} - T_{\text{g}}(X_{\text{drug}})\right) - T_{\text{g(drug)}} + T_{\text{g}}\left(X_{\text{drug}}\right)} \tag{3.4}$$

where X_{drug} is the mass fraction of the drug in the mixture, $T_g(X_{\text{drug}})$ is the glass transition temperature of the remaining amorphous phase after annealing, $T_{\text{g(drug)}}$ and $T_{\text{g(polymer)}}$ are the glass transition temperatures of pure drug and polymer, respectively, and K is ratio of the heat capacity change over the glass transition ΔC_p of the polymer to the drug.

By repeating this protocol at different annealing temperatures, several points on the solubility curve can be obtained, fitted to the Flory-Huggins model (Equation 3.1) and extrapolated to predict the solubility at room temperature as illustrated in Figure 3.5. According to Mahieu et al., the high drug load in the amorphous phase (which often has a low T_g compared to most polymers) will increase the molecular mobility of the system, and therefore the crystallization kinetics from a supersaturated polymer are expected to be faster compared to the dissolution kinetics into an undersaturated polymer[95]. Furthermore, as one experiment gives direct access to one point on the solubility curve, the time required to establish the solubility curve using the recrystallization method can be reduced by a factor of 10 compared to the dissolution method. However, the author also acknowledge that although the method is faster, it does not give access to a more extended part of the solubility curve compared to the previous methods[95].

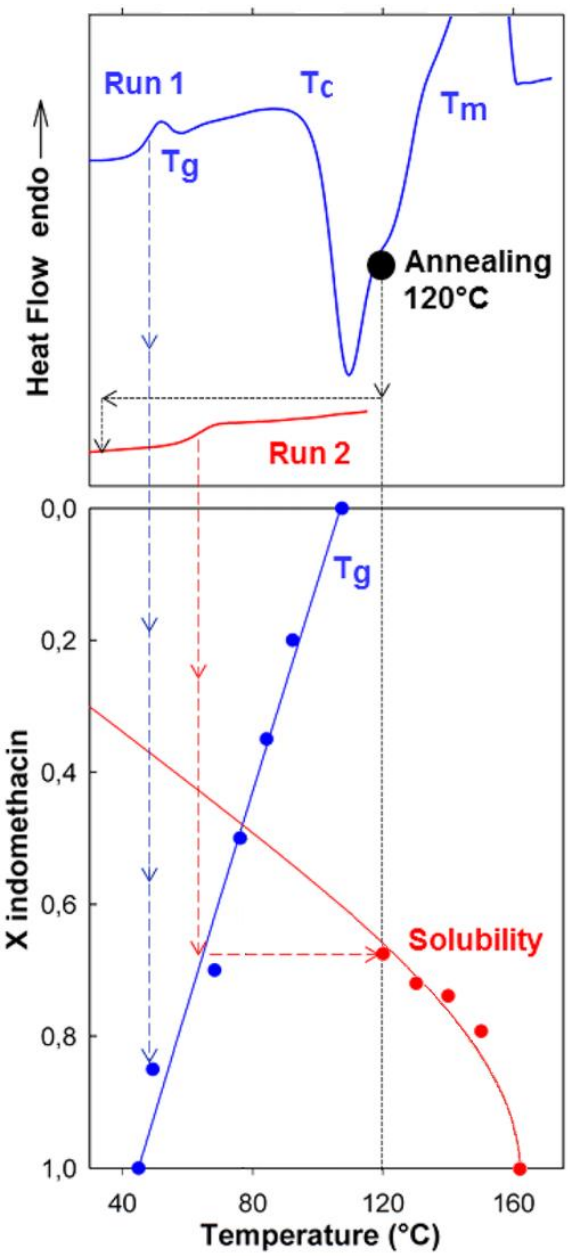

Figure 3.5: Graphical illustration of the recrystallization method. DSC curves of a supersaturated IMC:PVP amorphous solid dispersion (85% w/w IMC) obtained by ball milling are shown on top. In Run 1, the T_g of the supersaturated amorphous solid dispersion is followed by a recrystallization exotherm (T_c) and a melting endotherm of the recently recrystallized drug (T_m). By annealing the supersaturated amorphous dispersion at 120 °C (●), the supersaturated drug will (partially) recrystallize until solubility equilibrium is reached. On the subsequent scan of the annealed material (Run 2), the T_g of the remaining amorphous phase is increased compared to the supersaturated amorphous solid dispersion as a result of the decreased drug content. As the T_g is composition dependent, the composition (equilibrium solubility) at the annealing temperature can be derived from the Gordon-Taylor relationship. Consequently, a phase diagram including the experimental composition dependence of the T_g (●) and the solubility of IMC in PVP at different annealing temperatures (●) are shown in the bottom; the evolution of the T_g is fitted with the Gordon-Taylor relationship and the solubility curve is fitted with the Flory-Huggins model and extrapolated to room temperature. Adapted and modified from Mahieu et al.[95] with permission from American Chemical Society© 2013.

3.1.5 Zero enthalpy extrapolation method

The zero enthalpy extrapolation method was proposed by Amharar et al. in 2014[39] and is inspired by the work of Theeuwes et al. from 1974[97]. In this method, physical mixtures of crystalline drug and polymer of known composition (60−90% w/w drug) are prepared by ball milling at 400 rpm for 10 min. The resulting powders are then annealed at a constant temperature above the T_g in a DSC for 10 h in order to allow for the drug to dissolve into the polymer (*a*→*e* in Figure 3.2). At this stage, mixtures of crystalline drug and amorphous polymer saturated with dissolved drug are obtained. These mixtures (still in the DSC) are then cooled and scanned at a heating rate of 20 °C/min to determine the melting enthalpy (ΔH_m) of the remaining undissolved crystalline phase. The melting enthalpies of the different compositions are then plotted as a function of drug mass fraction (% w/w) to yield a linear correlation, as shown in Figure 3.6[39].

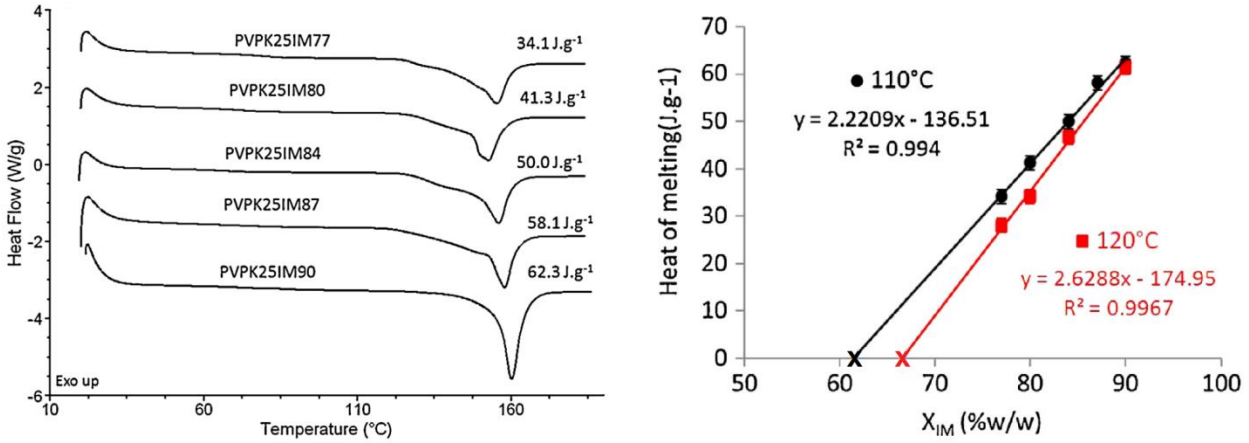

Figure 3.6: Graphical illustration of the zero enthalpy extrapolation method. DSC curves after annealing at 110 °C of IMC-PVP physical mixtures of different compositions (77−90% w/w IMC) are shown on the left. On the right, the melting enthalpies of the different compositions obtained after annealing for 10 h at 110 °C (●) and 120 °C (■) are plotted as a function of drug mass fraction and fitted to a linear regression. Through extrapolation of the regression to zero enthalpy (intersection with the 1st axis), the solubility of IMC in PVP at 110 °C (**X**) and 120 °C (**X**) can be determined. Adapted and modified from Amharar et al.[39] with permission from Elsevier© 2014.

Through extrapolation of this trend to zero enthalpy, the drug mass fraction where all drug is theoretically dissolved in the polymer during annealing can be obtained, and thus the equilibrium solubility for the given annealing temperature. By repeating this protocol at different annealing temperatures above the T_g, several points on the solubility curve can be obtained, fitted to the Flory-Huggins model (Equation 3.1) and extrapolated to predict the solubility at room temperature[39]. The use of "low" heating rates for solubility predictions of this kind has been criticized by other researchers, as the remaining undissolved crystalline drug may dissolve into the polymer before the melting event, giving rise to an underestimation of the melting enthalpy[98]. However, even though the authors are aware that this might lead to an overestimation of the solubility prediction, a previous study showed that increasing the heating rate from 20 °C/min to

400 °C/min did not significantly affect the melting enthalpy[98]. Therefore, it seems that despite the method requiring a great number of experiments involving long annealing stages (10 h) to obtain just one point on the solubility curve, it enables determination of the solubility at lower temperatures compared to the other methods, which increases the confidence of the temperature extrapolation, and thus the solubility prediction at room temperature[39].

3.2 Assessing *in vitro* supersaturation behavior

In modern pharmaceutical drug development, traditional dissolution testing is one of the most important tools to evaluate the biopharmaceutical performance of a formulation. Dissolution testing is a dynamic measurement of drug release from a formulation as a function of time. Whilst mostly used in quality control of dosage forms, the ultimate goal of dissolution testing is perhaps to establish a direct link between the *in vitro* and *in vivo* behavior also known as *in vitro–in vivo* correlation (IVIVC). Since the introduction of the BCS, *in vitro* dissolution data has even been able to act as a surrogate to *in vivo* human data for establishing bioequivalence of BCS class I and III compounds[3,25]. However, for amorphous solid dispersions that often contain BCS class II compounds, using dissolution data as a biowaiver is still not possible due to the lack of predictive *in vitro* methods. This situation is mainly due to the complexity associated with the physiology of the gastrointestinal tract. Therefore, in an attempt to mimic the *in vivo* gastrointestinal conditions better, physiologically based biorelevant media such as FaSSIF and FeSSIF[99] and more sophisticated *in vitro* methods such multi-compartment dissolution, dissolution-permeation and dynamic dialysis have been proposed[100-102]. However, even though this development has advanced the understanding of enabling drug formulations such as amorphous solid dispersions, predicting the *in vivo* biopharmaceutical performance of these formulations remains challenging due to the complex intraluminal processes that they undergo in the gastrointestinal tract upon ingestion such as solubilization, supersaturation and precipitation/crystallization[22]. Consequently, rather than optimizing the existing *in vitro* techniques and protocols, it seems that a deeper understanding of the supersaturation behavior of amorphous solid dispersions is needed in order to identify the most important *in vitro* parameters that are predictive of *in vivo* performance. By doing so, the performance of different amorphous solid dispersions can be assessed and compared, which will enable a more rational drug design.

According to Guzmán et al., the performance of supersaturating drug delivery systems such as amorphous solid dispersions depends mainly on their ability to generate and maintain a superstaturated solution. This concept has been described as the “spring and parachute” approach and is illustrated in Figure 3.7[18,103]. The “spring” refers to the initial dissolution of the drug from the dosage form. Upon dissolution of an amorphous drug, the dissolution rate and apparent solubility will be higher than that of the crystalline drug due to higher free energy of the amorphous form (see Figure 2.1). The apparent solubility in this context is a supersaturated condition and should not be confused with the thermodynamic equilibrium solubility of the drug[18]. As this supersaturation is thermodynamically unstable, the molecules have a

thermodynamic driving force for precipitation or crystallization and, thus, without a precipitation inhibitor, the supersaturation generated is short-lived and will rapidly decrease to reach the equilibrium solubility of the crystalline drug (Figure 3.7B).

The "parachute" refers to a temporary maintenance of supersaturation. By co-administering a precipitation inhibitor e.g. a polymer in an amorphous solid dispersion, the supersaturation generated upon dissolution of the amorphous drug can be maintained. Depending on the efficiency of the polymer, the supersaturation may be maintained for a short period of time (though longer than for the amorphous drug alone) if the polymer is a weak precipitation inhibitor (Figure 3.7C). In contrast, if the polymer is a strong precipitator the supersaturation generated may also be maintained for longer (Figure 3.7D). As the area under the supersaturation dissolution-time curve (AUC) represents the amount of drug available for absorption, a strong precipitation inhibitor may ensure that the supersaturation is maintained for long enough for the entire dose to be absorbed and thereby achieve the highest possible oral bioavailability[104].

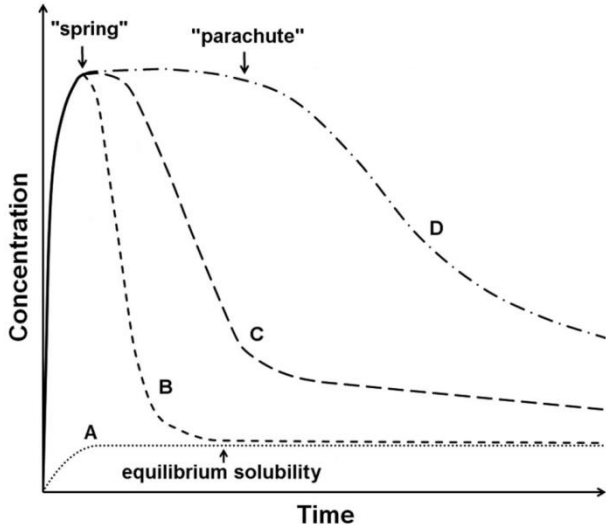

Figure 3.7: Schematic concentration-time profile illustrating the "spring and parachute" approach. Curve A represents the dissolution profile of crystalline drug reaching thermodynamic equilibrium solubility; curve B shows the dissolution profile of amorphous drug without precipitation inhibitors; curve C shows the dissolution profile of the amorphous drug in presence of a weak precipitation inhibitor, and; curve D shows the dissolution profile of the amorphous drug in presence of a strong precipitation inhibitor. Adapted and modified from He and Ho[104] with permission from Wiley Periodicals and the American Pharmacists Association© 2015.

Based on the "spring and parachute" approach, the performance of enabling formulations depends mainly on the supersaturation behavior. Consequently, in order to assess the *in vitro* dissolution behavior of amorphous solid dispersions, the selection of appropriate dissolution conditions is crucial. As the formulation most likely also generates supersaturation *in vivo*, data based on non-physiological sink condition may result in false predictions. Nevertheless, it is generally recommended that, when selecting a supersaturating formulation during early

development, the decision is based on sink conditioned *in vitro* dissolution testing in compendial methodologies such as the United States Pharmacopoeia (USP) dissolution apparatus II – paddle method[105]. For BCS class II drugs it has been proposed that IVIVC can be expected if the *in vitro* dissolution rate is similar to the *in vivo* dissolution rate[25,36]. Although there is a general awareness that IVIVCs generated this way are far from being perfect, enabling formulations are often ranked according to their dissolution rate in early development[105]. However, as the thermodynamic driving force for crystallization is increased with increasing degree of supersaturation, a fast dissolution rate may lead to rapid precipitation/crystallization. Therefore, the fastest dissolving system will not necessarily show the best overall performance and the dissolution rate itself is probably not predictive of *in vivo* performance[105]. This indicates that non-sink conditions are essential when evaluating the performance of amorphous solid dispersions. The key challenge in designing and developing amorphous solid dispersions is thus to identify the optimal combination of a "spring" and "parachute".

Amorphous solid dispersions using hydrophilic water-soluble polymers such as PVP, PEG and HPMC are by far the most widely used carriers to improve the bioavailability of BCS class II compounds. Through solubilization and enhancing the wettability and surface area, hydrophilic carriers can increase the rate and extent of the dissolution ("spring") compared to the pure amorphous drug[10,106]. Besides inducing supersaturation, these polymers can also inhibit precipitation of the supersaturation generated ("parachute"). The exact mechanisms for the precipitation/crystallization inhibition remains unknown but it is speculated that intermolecular interactions, such as hydrogen bonding, between the drug and polymer[107], polymer hydrophobicity[108], steric hindrance and solution viscosity (polymer molecular weight)[109] contribute positively to precipitation inhibition[106]. This emphasizes that the choice of polymer will have great impact on the *in vitro* and *in vivo* supersaturation behavior of the drug, and thus the biopharmaceutical performance of an amorphous solid dispersion.

Aims of the dissertation

In accordance with the aspects introduced in Chapters 1-3, the overall aim of this dissertation was to develop predictive tools for amorphous solid dosage forms with emphasis on the prediction of the physical stability and *in vivo* performance of amorphous solid dispersions. In this context, estimating the solid solubility of a drug in a polymer at room temperature and assessing the supersaturation behavior upon dissolution is essential. Thus, in order to achieve the overall aim, the dissertation was divided into six different objectives:

- Statistical evaluation of the confidence of drug-polymer solubility predictions at room temperature based on extrapolations using the Flory-Huggins model

- Identification of polymer properties important for the physical or thermodynamic stabilization of amorphous solid dispersions/glass solutions (miscibility/solubility)

- Providing a guidance for the selection of the most suitable method(s) for predicting drug-polymer solubility at room temperature based on the physicochemical properties of the drug and polymer

- Development of a new method to estimate drug-polymer solubility at room temperature that do not rely on temperature extrapolations using the Flory-Huggins model

- Development of an *in vitro* model to assess the performance of amorphous solid dispersions and identify *in vitro* parameters predictive of *in vivo* performance

- Identification of polymer properties important for the induction of supersaturation ("spring") and crystallization inhibition ("parachute") upon dissolution

Chapter 4

Evaluation of drug–polymer solubility curves through formal statistical analysis: Comparison of preparation techniques

4.1 Abstract

In this study, the influence of the preparation technique (ball milling, spray drying, and film casting) of a supersaturated amorphous dispersion on the quality of solubility determinations of indomethacin in polyvinylpyrrolidone was investigated by means of statistical analysis. After annealing of the amorphous dispersions above the recrystallization temperature for 2 h, the solubility curve was derived from the glass transition temperature of the demixed material using the Gordon-Taylor relationship and fitting with the Flory-Huggins model. The study showed that the predicted solubility from the ball-milled mixtures was not consistent with those from spray drying and film casting, indicating fundamental differences between the preparation techniques. Through formal statistical analysis, the best combination of fit to the Flory-Huggins model and reproducibility of the measurements was analyzed. Ball milling provided the best reproducibility of the three preparation techniques; however, an analysis of residuals revealed a systematic error. In contrast, film casting demonstrated a good fit to the model but poor reproducibility of the measurements. Therefore, this study recommends that techniques such as spray drying or potentially film casting (if experimental reproducibility can be improved) should be used to prepare the amorphous dispersions when performing solubility measurements of this kind.

4.2 Introduction

An increasing number of new drug candidates have a low oral bioavailability because of poor aqueous solubility and obtaining a formulation that ensures high and consistent absorption of these compounds constitutes a great challenge to pharmaceutical scientists[11]. In order to address this challenge, several formulation strategies have been described, including the utilization of the amorphous form[5]. As the free energy of the amorphous form of a drug is higher than that of the corresponding crystalline state, the apparent solubility and dissolution rate is increased[110]. However, the amorphous form is thermodynamically unstable causing the drug to nucleate and recrystallize over time[12,13]. Hence, the stabilization of the amorphous form is critical for this formulation approach to succeed. One way of stabilizing an amorphous drug against crystallization is to molecularly disperse it in amorphous polymers[111] and therefore, the successful development of such dispersions is dependent on the drug–polymer miscibility and solubility. If the drug is miscible and molecularly dispersed in the polymer below solubility

equilibrium, it will most likely remain stable[10,83]. Thus, determination of the drug–polymer solubility at typical storage temperatures is of great interest.

Different experimental approaches have been proposed to determine the solubility of crystalline drugs in polymers. However, as most pharmaceutically relevant drugs and polymers are solid at ambient temperature the solubility equilibrium is difficult to reach[48]. Until recently, the solubility of crystalline drugs in polymers has mainly been determined by variations of the "melting point depression" method[48,80,83,89]. Common for these methods is that differential scanning calorimetry (DSC) is used to detect the completion of a dissolution endotherm for a physical mixture of crystalline drug and polymer. Sun et al.[80] suggested a protocol where a drug–polymer mixture, at a given concentration of the drug, is milled and annealed at different temperatures until equilibrium is reached and subsequently scanned for a residual dissolution endotherm. The absence of a dissolution endotherm indicates that the dissolution is completed and that the dissolution temperature is located below the annealing temperature. This procedure is then repeated at different temperatures in order to determine the equilibrium solubility temperature corresponding to the initial concentration[80]. Even though this method provides accurate solubility curves, the long annealing stages and numerous DSC scans make it very time-consuming.

As a consequence thereof, Mahieu et al.[95] suggested an optimization of the scanning protocol developed by Sun et al.[80], taking advantage of the fact that recrystallization is generally faster than dissolution. In this method, a supersaturated amorphous dispersion is annealed at different temperatures above the recrystallization temperature until equilibrium is reached. The equilibrium solubility concentration is then derived directly from the glass transition temperature (T_g) of the demixed material using the Gordon-Taylor relationship[96]. By repeating this at different temperatures, a part of the solubility curve is obtained, and by fitting to the Flory-Huggins model[85], the solubility at ambient temperature can be obtained by extrapolation[95]. Results from both of the aforementioned methods are in general agreement demonstrating that, although the new method does not give access to an extended part of the solubility curve, it can be used to determine drug solubility in polymers up to ten times faster than the previously proposed methods[95]. Mahieu et al.[95] prepared the supersaturated amorphous dispersion by co-milling a physical mixture of polymer and crystalline drug. However, previous work has shown that milling may yield a higher T_g of amorphous dispersions compared with spray drying[70]. As the equilibrium solubility concentration is derived directly from the T_g of the demixed material, even a small deviation in T_g will have great influence on the solubility curve, according to the Gordon-Taylor relationship[96]. Thus, if refined, this method is of great practical relevance for the screening of drug–polymer systems as the solubility curve can be obtained in less than 24 h.

Spray drying is an important process for preparing amorphous dispersions, but it requires a comparatively large quantity of drug, making it difficult to implement early in the development process where most drug candidates are made in small quantities. In order to overcome this limitation, preparation techniques such as film casting and ball milling have been suggested for screening of amorphous dispersion formulations at smaller scales[71,112,113]. Film casting and spray

drying are “bottom-up” techniques that rely on the same fundamental process principles (rapid solvent evaporation), and therefore it is expected that film casting can provide early information on drug–polymer solubility in spray-dried solid dispersions. However, to our knowledge no methodical comparison of preparation techniques has been reported defining the most suitable for drug–polymer solubility measurements of this kind. Therefore, the current study aim to investigate whether the preparation technique (ball milling, spray drying, or film casting) of a supersaturated amorphous dispersion has an influence on the solubility curve using the indomethacin:polyvinylpyrrolidone (IMC:PVP) binary system previously investigated by several authors including Sun et al.[80] and Mahieu et al.[95]. As the predictive power of such solubility curves has not previously been studied, the preparation techniques and the confidence of the solubility curves in this study will be compared and evaluated through formal statistical analysis by considering both the intra- and intervariability of the measurements. The ultimate aim is to provide an extension of the work of Mahieu et al.[95] by refining the experimental protocol and propose a mathematical tool to evaluate the confidence of the data in relation to the Flory-Huggins model[85].

4.3 Experimental

4.3.1 Materials

IMC was purchased from Hawkins, Inc. Pharmaceutical Group (Minneapolis, MN, USA). Amorphous Kollidon® 12 PF (PVP K12, M_w = 2000–3000 g/mol) was kindly supplied by BASF (Ludwigshafen, Germany).

4.3.2 Ball milling

IMC and PVP K12 (85:15, w/w, 1000 mg) were ball-milled in a Mixer Mill MM400 from Retsch GmbH (Haan, Germany). Samples were placed into a 25 mL milling jar containing two 12 mm stainless steel ball bearings and milled at 20 Hz for a total of 8 h at 5 °C. Alternating milling periods (75 min) with pauses (5 min) were used to prevent overheating of the sample. Amorphous IMC was prepared using the same protocol.

4.3.3 Spray drying

IMC and PVP K12 (85:15, w/w, 1000 mg) were dissolved in 10 mL of acetone-ethanol (80:20, v/v) and spray-dried using a 4M8-TriX spray drier from ProCepT (Zelzate, Belgium). Solutions were fed at a rate of 3 g min^{-1} (addition rate <10% of lower explosion limit = 3.7 g min^{-1}) and atomized with a 0.5 mm two-fluid nozzle at a pressure of 1.3 bar (20 L min^{-1}). Heated air was drawn through the open loop drying system at 500 L min^{-1} with a temperature of 100 °C.

4.3.4 Film casting

IMC and PVP K12 (85:15, w/w, 100 mg) were dissolved in 1 mL of acetone-ethanol (80:20, v/v) and casted on a Teflon-coated 76 × 26 mm Menzel-glass placed on a Jenway 1100 Hotplate from Bibby Scientific Ltd. (Staffordshire, UK). Samples were prepared using a plate temperature of 200 °C and a total solution volume of 500 µL was pipetted onto the hot glass yielding 50 mg of film. After solvent evaporation, the film was scraped of the glass plate and gently grounded using a mortar and pestle.

4.3.5 Differential scanning calorimetry

The DSC thermograms were acquired using a Q2000 from TA Instruments Inc. (New Castle, DE, USA). Sample powders (2–4 mg) were analyzed in Tzero Aluminium Hermetic pans with a perforated lid and scanned from – 10–200 °C at a heating rate of 5 °C min^{-1} with a modulation of ± 0.21 °C amplitude and 40 s period of modulation and purged with 50 mL min^{-1} pure nitrogen gas. Temperature and enthalpy of the DSC instrument was calibrated using indium as a standard. The melting temperature (T_m, peak) and glass transition temperatures (T_g, midpoint) were determined using the Universal Analysis 2000 (version 4.5A) software.

4.3.6 X-ray powder diffraction

X-ray powder diffraction (XRPD) measurements were performed on an X'Pert PRO MRD diffractometer from PANalytical (Almelo, The Netherlands) equipped with a TCU 100 temperature control unit and an X'Celerator detector using nickel-filtered CuKα radiation (λ = 1.5406 Å) at 45 kV and 40 mA. Samples were placed on zero background (0-BG) Si-plates and measured over the angular range 3–40 °2θ at a scanning rate of 1.20 °2θ min^{-1}. Results were analyzed using X'Pert Data Viewer (version 1.2) software.

4.3.7 Density

The true densities of the powders were determined using an AccuPyc 1330 helium pycnometer from Micromeritics Instruments Corporation (Norcross, GA, USA). Prior to the measurements, samples were stored for 24 h at 60 °C to remove any sorbed moisture. During measurements, the powders were purged with 19.5 psig dry helium in the instrument test chamber. The reported values were averages of 10 consecutive measurements.

4.3.8 Determination of solubility

The method used to determine the solubility of crystalline drug in a polymer was based on the method developed by Mahieu et al.[95] with minor modifications. In brief, a supersaturated amorphous dispersion of IMC and PVP K12 (85:15, w/w) was prepared by ball milling, spray

drying, or film casting as described above. The amorphous dispersion was then annealed above its recrystallization temperature for 2 h in a DSC, cooled to room temperature and ramped at 5 °C min^{-1} to determine the T_g of the demixed material by DSC. The equilibrium solubility concentration was then derived directly from this T_g using the Gordon-Taylor relationship. Experimental points were obtained in triplicates in 5 °C intervals within the measureable range. For a more detailed description of the analytical protocol, the interested readers are referred to Mahieu et al.[95].

4.4 Results

4.4.1 Solid state characterization

Figure 4.1 shows the XRPD patterns of IMC, PVP K12, and IMC:PVP K12 (85:15, w/w) mixtures before and after processing. The diffraction pattern recorded from crystalline IMC (Figure 4.1a) showed sharp and well-defined Bragg peaks, characteristic of the stable γ-form of IMC[114]. In contrast, the diffraction pattern recorded after processing (Figure 4.1c) showed a diffuse halo with no Bragg peaks, characteristic of an amorphous material. The diffractogram recorded for unprocessed PVP K12 (Figure 4.1b) was also free of Bragg peaks with a diffuse halo identical to the pattern for the processed PVP K12 (data not shown), demonstrating that PVP K12 was not structurally modified during processing. The diffractograms of IMC:PVP K12 (85:15 w/w) obtained after milling (Figure 4.1d), spray drying (Figure 4.1e), and film casting (Figure 4.1f) were free of Bragg peaks, suggesting that all three preparation techniques successfully produced a supersaturated amorphous dispersion.

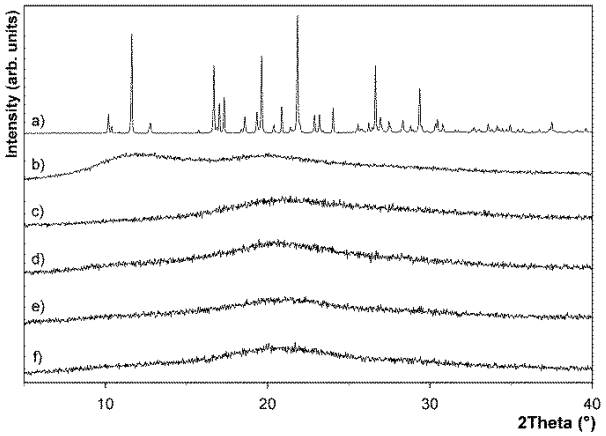

Figure 4.1: X-ray powder diffraction patterns obtained at room temperature: crystalline IMC (a), unprocessed PVP K12 (b), amorphous IMC (c), and processed IMC:PVP K12 (85:15, w/w) prepared by ball milling (d), spray drying (e), and film casting (f).

As the mixtures are highly supersaturated and therefore thermodynamically unstable, the drug could recrystallize over time. It was therefore initially examined whether the processed amorphous mixtures recrystallized during the course of the experiments. All processed materials remained amorphous; however, the mixtures prepared by ball milling tended to partially recrystallize over the course of 2–3 months when stored in a closed container at 5 °C. The supersaturated mixtures prepared by spray drying and film casting remained amorphous after 4 months at room temperature (data not shown). This is in agreement with an observation by Ke et al.[115] and suggests that even though the components are the same, the technique used for preparation can greatly affect the dispersibility (degree of homogeneity), and hence the stability of the final product. After annealing of the samples, IMC recrystallized to the initial γ form of IMC (data not shown). There was no apparent visual difference between the diffractograms obtained from the three different preparation techniques (Figures 4.1d–4.1f). However, in order to determine whether the processes produced a simple mixture of amorphous IMC and amorphous PVP K12 or a homogenous glass solution, DSC scans were performed.

4.4.2 Thermal analysis

DSC thermograms of crystalline and amorphous IMC, PVP K12, and processed IMC:PVP K12 (85:15 w/w) mixtures are presented in Figure 4.2. Prior to the DSC scan of PVP K12 the sample was annealed for 5 min at 100 °C to prevent the evaporation of absorbed water from obscuring the weaker glass transition signal. The subsequent scan showed a change in heat capacity (ΔC_p), distinctive of a glass transition with a midpoint around 107 °C (Figure 4.2e). The DSC scan of crystalline IMC presented only one endothermic event with a peak around 161 °C attributed to melting (Figure 4.2a). This T_m and the enthalpy of fusion (ΔH_m) were close to previously published values for the γ form of IMC[116] and in accordance with the results from XRPD (Figure 4.1a). The scan of the amorphous IMC (Figure 4.2b) presented three thermal events – a glass transition with a midpoint around 45 °C, an exothermic recrystallization event from 80–110 °C, and an endothermic event with a peak at 161 °C corresponding to the melting of the crystallized material. The T_m of (recrystallized) amorphous and crystalline IMC was similar, indicating that the amorphous IMC recrystallized into the initial γ form of IMC (also confirmed by XRPD). Prior to the DSC scan of the processed IMC:PVP K12 (85:15, w/w) mixtures (Figures 4.2c and 4.2d), a short annealing step was introduced to prevent any water evaporation endotherm from obscuring the glass transition signal.

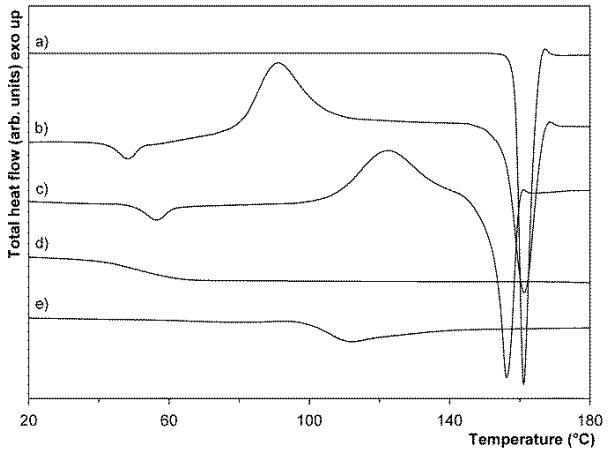

Figure 4.2: DSC thermograms of crystalline IMC (a), amorphous IMC (b), ball-milled IMC:PVP K12 (85:15, w/w) (c), spray-dried/film-casted IMC:PVP K12 (85:15, w/w) (d) and PVP K12 (e).

The T_g in all the processed mixtures was located between that of amorphous IMC and PVP K12and there was no sign of other glass transition signals in the temperature range studied. This indicates that all three preparation techniques produced a homogenous amorphous mixture where IMC and PVP K12 were mixed at the molecular level[117] at least within the sensitivity limit of the DSC method. In the ball-milled mixture (Figure 4.2c), an exothermic event from 100–140 °C represented the recrystallization of IMC from the PVP K12 matrix, demonstrating that the amorphous dispersion was supersaturated with IMC. The broad endotherm around 140–160 °C could potentially represent the melting of the α form of IMC. However, as XRPR revealed that IMC recrystallized into the γ form, this endotherm most likely represented the dissolution of IMC in PVP K12. There was no melting endotherm for IMC present at 161 °C, probably because of the increasing solubility of IMC in PVP K12 with increasing temperature. When the temperature reached the melting point of IMC, the crystals were most likely already completely dissolved in the polymeric matrix[70]. The mixtures prepared by spray drying and film casting (Figure 4.2, d) had similar DSC patterns. However, unlike ball milling, they did not display a recrystallization exotherm during the DSC analysis and consequently also did not exhibit melting. This was a consequence of the heating rate and does not mean that these mixtures did not recrystallize in practice. During the annealing stage a clear exothermic recrystallization signal was present. These deviations in the DSC pattern indicate physical differences between the mixtures prepared by the three techniques. In Table 4.1, the data obtained from the DSC scans are summarized, including the particle density of IMC and PVP K12 determined using helium pycnometry.

4.4.3 Solubility of IMC in PVP K12

The method developed by Mahieu et al.[95], with minor modifications, was used to determine the solubility of crystalline IMC in PVP K12. In theory, it is possible to determine the equilibrium

solubility of IMC in PVP K12 from the recrystallization temperature to the T_m of IMC. However, reaching equilibrium becomes increasingly more time-consuming at temperatures closer to the recrystallization temperature. This is because of decreased molecular mobility as a result of the lower temperature, which is slowing the nucleation and crystallization processes[118]. In addition, at temperatures closer to the melting point there is a possibility that the IMC concentration (85:15 w/w) is not sufficient to saturate the mixture. The equilibrium solubility of IMC (X_{IMC}) in PVP K12 at a given temperature can be derived directly from the T_g of the demixed material after annealing. In order to determine X_{IMC}, the composition dependence on T_g was established. The theoretical relationship between T_g and X_{IMC} can be calculated using the Gordon-Taylor relationship[96]:

$$X_{IMC} = \frac{K \cdot \left(T_{g(PVP)} - T_g(X_{IMC})\right)}{K \cdot \left(T_{g(PVP)} - T_g(X_{IMC})\right) - T_{g(IMC)} + T_g\left(X_{IMC}\right)} \quad (4.1)$$

where X_{IMC} is the mass fraction of amorphous IMC in the mixture, $T_g(X_{IMC})$ is the T_g of the demixed material as a function of X_{IMC}, $T_{g(IMC)}$, and $T_{g(PVP)}$ are the T_gs of amorphous IMC and PVP K12, respectively, and K is the interaction parameter controlling the curvature, given by Equation 4.2:

$$K = \frac{\Delta C_{p(PVP)}}{\Delta C_{p(IMC)}} \quad (4.2)$$

where $\Delta C_{p(IMC)}$ and $\Delta C_{p(PVP)}$ are the heat capacity changes in the glass transition of amorphous IMC and PVP K12, respectively. Table 4.1 provides all parameters necessary to determine the predicted relationship between X_{IMC} and T_g using Equations 4.1 and 4.2.

Table 4.1: Experimental physical and thermodynamic values of PVP K12 and IMC measured by DSC and density measured by helium pycnometry (values are mean ± SD, *n* = 3).

Material	M_w (g·mol^{-1})	Density (g·cm^{-3})	T_g (°C)	ΔC_p (J·g^{-1}·K^{-1})	ΔH_m (J·g^{-1})	T_m (°C)
PVP K12	2,500[a]	1.19 ± 0.00	107.1 ± 0.6	0.36 ± 0.6	-	-
IMC	357.8	1.38 ± 0.00	45.5 ± 0.2	0.38 ± 0.4	113.4 ± 2.6	161.0 ± 0.1

[a]Average M_w according to the supplier.

In order to ensure that the Gordon-Taylor relationship was applicable, amorphous dispersions with different IMC concentrations were prepared by film casting and measured in the DSC to determine T_g. The experimental relationship between T_g and X_{IMC} is presented in Table 4.2 and illustrated along with the theoretical curve from the Gordon-Taylor relationship in Figure 4.3. The experimental values were well predicted by the Gordon-Taylor relationship, indicating ideal mixing behavior of the two components.

Table 4.2: Glass transition temperatures (T_g) of IMC:PVP K12 glass solutions with different mass fractions of IMC (X_{IMC}) measured by DSC (values are mean ± SD, n = 3).

X_{IMC} (w/w)	T_g (°C)
1.00	45.5 ± 0.2
0.80	59.4 ± 0.4
0.60	71.2 ± 0.1
0.40	77.5 ± 0.3
0.20	88.3 ± 0.4
0.00	107.1 ± 0.6

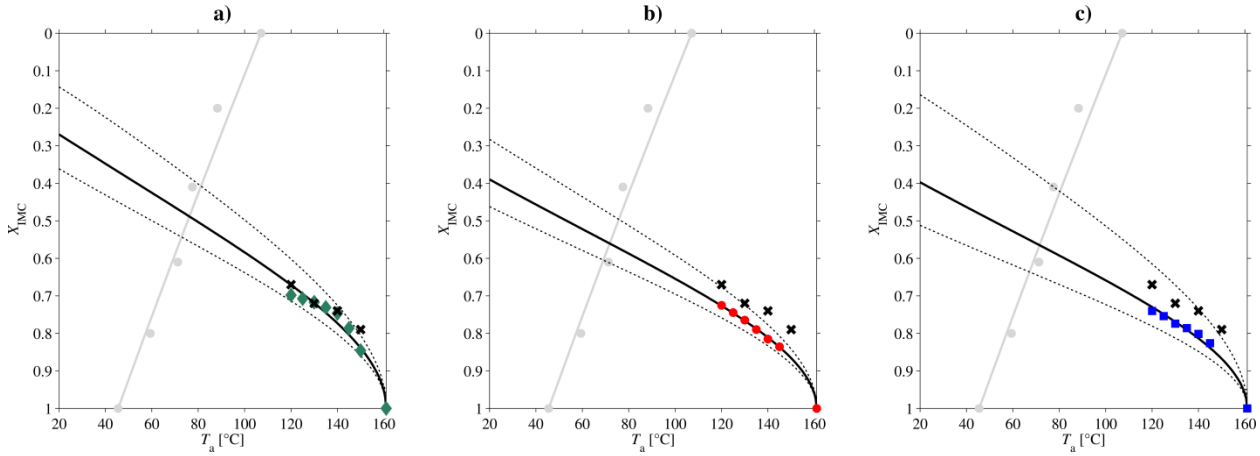

Figure 4.3: Equilibrium solubility of IMC (X_{IMC}) in PVP K12 as a function of annealing temperature (T_a). Green diamonds (♦) represent the data from ball milling (a), red circles (●) represent the data from spray drying (b), and blue squares (■) represent the data from film casting (c). The data previously reported by Mahieu et al.[95] is presented as black crosses (×). The evolution of solubility of the three data sets has been fitted with the Flory-Huggins model (black curves) including the 95% prediction interval (dotted curves). The grey circles (●) represent the experimental relationship between T_g and X_{IMC} and the gray curve is the Gordon-Taylor relationship.

Having established the relationship between X_{IMC} and T_g, it was possible to obtain data points on the solubility curve. As mentioned earlier, it is theoretically possible to determine the equilibrium solubility of IMC from the recrystallization temperature to the T_m (100–161 °C); however, parameters including drug solubility, viscosity, degree of supersaturation, and annealing temperature affect the nucleation and crystallization rate of drugs in amorphous dispersions[119]. In this case, the degree of supersaturation or drug–polymer ratio was chosen as a compromise between annealing time, T_g signal strength, and the number of data points possible to obtain. Increasing the IMC concentration (to e.g. 90:10, w/w) could potentially provide a data point closer to the T_m, however, with the risk of losing valuable data points closer to ambient temperature as a result of increased recrystallization/annealing time and a weaker T_g signal because of the lower polymer content. It is therefore important to evaluate the drug–polymer ratio and annealing time needed to reach crystallization equilibrium every time a new drug–polymer mixture is studied. The exothermic crystallization event can be monitored from the heat flow during the isothermal annealing of the mixture and the process is considered to be at equilibrium when the signal reaches a baseline. Using the parameters listed in Section 4.3, it was only possible to obtain data from 120–150 °C. At temperatures below 120 °C, the equilibration time exceeds the 2 h of annealing, and above 150 °C, the concentration of IMC (85:15 w/w) was not sufficient to saturate the mixture. Consequently, experimental points from 120–150 °C were obtained in 5 °C intervals and the equilibrium solubility of IMC in PVP K12 at each temperature was derived from the T_g of the demixed material using Equations 4.1 and 4.2. The T_g of the demixed materials and the corresponding equilibrium solubility of IMC, using the three different preparation techniques, are listed in Table 4.3.

Table 4.3: Glass transition temperature (T_g) of the demixed material and the corresponding equilibrium solubility of IMC in PVP K12 (X_{IMC}) obtained at different annealing temperatures (T_a) using the three preparation techniques (values are mean ± SD, n = 3).

	Ball milling		Film casting		Spray drying	
T_a (°C)	T_g (°C)	X_{IMC} (w/w)	T_g (°C)	X_{IMC} (w/w)	T_g (°C)	X_{IMC} (w/w)
150	54.6 ± 0.2	0.846 ± 0.004	[a]	[a]	[a]	[a]
145	58.1 ± 0.5	0.786 ± 0.008	55.7 ± 0.1	0.826 ± 0.002	55.2 ± 0.4	0.835 ± 0.005
140	60.5 ± 0.4	0.746 ± 0.008	57.2 ± 0.7	0.802 ± 0.012	56.4 ± 1.0	0.815 ± 0.013
135	61.4 ± 0.6	0.730 ± 0.010	58.1 ± 1.6	0.786 ± 0.027	57.9 ± 1.6	0.789 ± 0.022
130	62.3 ± 0.2	0.716 ± 0.004	58.8 ± 1.7	0.774 ± 0.028	59.4 ± 1.1	0.764 ± 0.015
125	62.8 ± 0.5	0.707 ± 0.009	60.0 ± 1.9	0.754 ± 0.031	60.6 ± 1.1	0.744 ± 0.015
120	63.4 ± 0.5	0.698 ± 0.008	60.9 ± 1.9	0.740 ± 0.031	61.8 ± 0.7	0.725 ± 0.010

[a]Data excluded as concentration of IMC in PVP K12 (85:15 w/w) is below the equilibrium saturated state.

As anticipated, the solubility increased with increasing annealing temperature. Using ball milling, it was possible to obtain solubility data in the entire measured temperature interval. However, as the T_g of the demixed material did not change after annealing from the spray-dried and film-casted mixtures at 150 °C, the concentration of IMC in PVP K12 (85:15, w/w) was considered below the equilibrium solubility and the results were omitted. As the solubility at typical storage temperatures is of practical interest, a solubility curve was established on the basis of these results. According to the Flory-Huggins model[85], the solubility data from Table 4.3 was expected to obey the following equation:

$$\frac{\Delta H_m}{R}\cdot\left(\frac{1}{T_m}-\frac{1}{T_a}\right)=\ln\left(v_{IMC}\right)+\left(1-\frac{1}{\lambda}\right)\cdot v_{PVP}+\chi\cdot\left(v_{PVP}\right)^2 \tag{4.3}$$

where ΔH_m and T_m are the enthalpy of fusion and melting temperature for IMC respectively, R is the gas constant, T_a is the annealing temperature, λ is the molar volume ratio of the polymer and drug, χ is the Flory-Huggins interaction parameter, and v_{IMC} and v_{PVP} are the volume fractions of IMC and PVP K12 respectively, derived from Equation 4.4:

$$v_{IMC}=\frac{\frac{X_{IMC}}{\rho_{IMC}}}{\frac{X_{IMC}}{\rho_{IMC}}+\frac{1-X_{IMC}}{\rho_{PVP}}},\quad v_{PVP}=1-v_{IMC} \tag{4.4}$$

where ρ_{IMC} and ρ_{PVP} are the densities of IMC and PVP K12 respectively, and X_{IMC} is the mass fraction of IMC. Table 4.1 and 4.3 provide the data needed to obtain a solubility curve from the three preparation techniques using Equations 4.3 and 4.4.

The optimal estimate for χ was found by minimizing the sum of squares of the residuals between the observed and predicted volume fractions of the drug according to the Flory-Huggins model. The residuals were defined as the variability associated with the T_g measurements, and hence v_{IMC}, whereas the annealing temperatures were considered practically free of error. This definition of the residuals requires the regression problem to be treated as an error-in-variable model (see Appendix A). For instance, if the least-square estimate of χ is calculated from the difference between observed and predicted annealing temperatures, the estimate will be biased. Additionally, in order to account for the variability, the fit was calculated from all the data simultaneously. The solubility at 20 °C can be predicted by extrapolating the fitted model. This of course requires that the fitted model is valid over the extrapolated temperature range. In order to express confidence of the point estimate, a 95% prediction interval was calculated (see

Appendix A). This expresses the interval in which 95% of future measurements, at a given annealing temperature, will be.

Figure 4.3 shows the average experimental solubilities of IMC in PVP K12 from Table 4.3 and the solubility curves when fitted with Flory-Huggins model including the 95% prediction interval. As χ is influenced by all factors in the Flory-Huggins model, it is generally not comparable between studies. For example, a higher T_m or ΔH_m measurement of IMC will result in a higher numerical value of χ. Therefore, the evolution of the solubility curve rather than χ should be used for comparison. In this study, however, because the χ values wewre based on the same thermal data, they were directly comparable. In general, a negative χ value indicates that the two compounds are miscible[120]. The average Flory-Huggins interaction parameter χ and the expected solubility of IMC in PVP K12 at 20 °C, including the 95% prediction interval at 20 °C, for the three preparation techniques are listed in Table 4.4.

Table 4.4: Flory-Huggins interaction parameter χ, predicted solubility of IMC in PVP K12 (X_{IMC}) at 20 °C and the 95% prediction interval at 20 °C.

Preparation technique	χ	X_{IMC} at 20 °C	Prediction interval
Ball milling	-8.3	0.27	0.14-0.36
Spray drying	-12.1	0.39	0.28-0.46
Film casting	-12.4	0.40	0.16-0.51

The prediction interval was determined by the size of the residuals and the two contributions to the residuals can be identified as the inter-replicate variance (reproducibility) and the intra-replicate variance (fit to the Flory-Huggins model). The reproducibility of the three preparation techniques can be derived from the standard deviations of the measurements given in Table 4.3. The most narrow prediction interval was found for spray drying (Figure 4.3b), indicating a combination of good intra- and inter-replicate variance. The prediction interval for ball milling (Figure 4.3a) was wider than that of spray drying, but still relatively narrow. As ball milling provided the best reproducibility of the three techniques (Table 4.3), the broader prediction interval was probably a result of large intra-replicate residuals (poor fit to the model). In case of a bad fit, the prediction interval has no practical relevance. Contrarily, the broad prediction interval for film casting (Figure 4.3c) was most likely a consequence of poorer reproducibility compared with the other two techniques. However, in order to support these assumptions, an analysis of the residuals was necessary (see below).

4.5 Discussion

In this study, the original co-milling method using a high-energy planetary mill[95] was substituted by a ball-milling method. From Figure 4.3 it is evident that the ball milling data obtained in this study was similar to the data reported by Mahieu et al.[95], suggesting that the two milling methods are comparable and that the proposed analytical protocol is reliable and reproducible. However, the predicted solubility from the ball-milled mixture was not consistent with those predicted for mixtures prepared by spray drying and film casting, indicating fundamental differences between the three preparation techniques. Through formal statistical analysis, it was possible to compare and evaluate the preparation techniques with respect to their suitability as preparation techniques for this kind of solubility measurements. As the solubility curve is very sensitive even to small deviations in T_g, several factors can influence the outcome. The long annealing periods at elevated temperatures used in this method may potentially lead to chemical degradation. However, data from the literature have shown that IMC:PVP K12 mixtures do not decompose significantly even at temperatures up to 170 °C[121], but generally this is important to consider when new compounds are evaluated. Furthermore, there is a risk that the ball-milled mixture was not in equilibrium after sample preparation. However, increasing the milling time did not influence the T_g significantly (data not shown). Besides the inconsistency of the predicted solubility at 20 °C (Table 4.4), the three preparation techniques also exhibited differences in relation to the fit to the Flory-Huggins model. These differences can be studied by evaluating the pattern of the residuals shown in Figure 4.4. In this case, the residuals denote the difference between the average experimental solubility of IMC at a given temperature and the value fitted by the Flory-Huggins model.

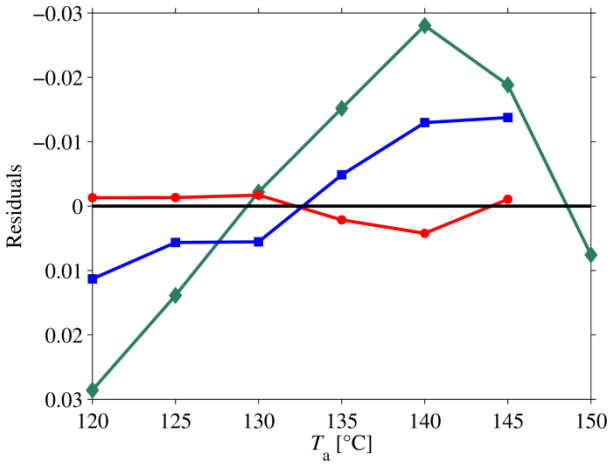

Figure 4.4: Residual plot of the three different data sets fitted to the Flory-Huggins model. Green diamonds (♦) represent the data from ball-milled mixtures, red circles (●) represent the data from the spray-dried mixtures, and blue squares (■) represent the data from film-casted mixtures.

The residual plot for the ball milling data showed a non-random inverted U-shaped pattern suggesting a bad fit to the Flory-Huggins model. A similar systematic error, albeit not as pronounced, was found when fitting the data reported by Mahieu et al.[95] (data not shown). In contrast, the residual plot for the spray drying data showed a fairly random pattern with small residuals, indicating a good fit to the model. The residual plot for the film casting data did not show completely random behavior. However, considering the standard deviations in the measurements given in Table 4.3, it was difficult to determine whether the pattern of residuals was systematic because of bad fit to the model or a result of the poor reproducibility of the film casting technique. The difference in reproducibility between the techniques is somewhat expected as ball milling is the simplest technique, whereas the processes involved in the two solvent evaporation techniques are more complex. Furthermore, the film casting technique used in this study is operator dependent and very sensitive to small changes in the process, such as temperature and evaporation time. The processes involved in ball milling are fundamentally different from the solvent evaporation techniques (spray drying and film casting), which is likely to account for some of the differences observed in the solubility curves and the (lack of) fit to the Flory-Huggins model. In the solvent evaporation methods the amorphous dispersion is formed almost instantly from a highly disordered state ("bottom-up" method), whereas the crystal lattice is interrupted over time by strong mechanical forces during ball milling ("top-down" method). This means that even though the final mixtures may look alike with respect to their XRPD and DSC patterns, the difference in preparation technique can result in a different degree of dispersion at the molecular level. In all measurements, the T_g of the demixed material after annealing period was consistently higher for the ball-milled mixture than the spray-dried and film-casted mixtures. This gives rise to an underestimation of the solubility when using ball milling as a preparation technique compared with film casting and spray drying.

These observations are in accordance with previous studies reporting that the physical properties of an amorphous material can be affected by the preparation technique[70,73,92,115,122]. Patterson et al.[70] studied the solid-state properties of amorphous dispersions prepared by spray drying and ball milling. DSC scans showed that both techniques resulted in amorphous drug, which was well dispersed as shown by single T_g values. However, a higher T_g of the ball-milled mixtures was observed when compared with the spray-dried mixtures, indicating that the degree of dispersion was different. A subsequent Raman mapping of the spray-dried mixtures showed that the spray drying technique resulted in a completely homogeneous mixture. In contrast, the ball-milled mixture revealed the presence of small clusters of drug and polymer-rich areas, indicating an incomplete glass solution formation. These findings lead Patterson et al.[70] to conclude that spray drying facilitated better mixing at the molecular level than ball milling. This was further supported by Ke et al.[115], who reported that the preparation technique significantly affected the solid state of amorphous dispersions and that mixtures produced by ball milling were heterogeneous at the molecular level. Furthermore, Qian et al.[123] demonstrated that a distinctive single T_g measured by DSC can be misleading in the indication of mixing homogeneity of

amorphous dispersions and even phase separation of an amorphous mixture, at the scale of tens of microns, can be undetectable in the DSC.

The essential prerequisite for the evaluated method to be applicable is that drug and polymer are homogenously mixed at the molecular level before annealing. If the drug and polymer are not mixed at the molecular level, the process involved in reaching the equilibrium is most likely driven by dissolution of the drug rather than the intentional demixing. Reaching the solubility equilibrium via dissolution is more time-consuming than from demixing and the dissolution endotherm can be difficult to monitor on the DSC, particularly if competing with a crystallization exotherm. This gives reason to suspect that the ball-milled sample was not in equilibrium after 2 h of annealing, even though the DSC signal appeared to have reached a baseline. However, this does not mean that ball milling should be avoided at any time when determining drug solubility in polymers, but rather used for the dissolution protocols where molecular level mixing is not required, for example, the "melting point depression" method[48,80,83]. Further, in a study by Caron et al.[92], it was demonstrated that spray drying allowed amorphous dispersions to be obtained over a wider concentration range than ball milling. This means that there is a greater chance of achieving a supersaturated amorphous dispersion when using spray drying compared with ball milling, and this attribute is important when testing other drug–polymer systems, thus, supporting the recommendations in the present study. Even though film casting did not provide as good reproducibility and fit to the Flory-Huggins model as spray drying, it is believed that application of a more automated/controlled film casting method could increase its precision. As the solubility curves of spray drying and film casting were almost identical, the two techniques are believed to be monotonic and thus, spray drying and potentially film casting (if preparative conditions are improved), can be used as a screening technique for drug–polymer solubility measurements.

4.6 Conclusion

In this study, we compared and evaluated ball milling, film casting, and spray drying as preparation techniques for supersaturated amorphous dispersions used for determination of drug solubility in polymers through formal statistical analysis. All techniques successfully produced amorphous dispersions of IMC:PVP K12 with a single T_g and no sign of crystallinity. The method proposed by Mahieu et al.[95] to determine drug–polymer solubility generated (relatively) fast data with good reproducibility when using the amorphous dispersions produced by the three preparation techniques. However, the solubility curve obtained from ball milling was different from those obtained by spray drying and film casting. As the ball milling technique and the solvent evaporation techniques (spray drying and film casting) are very different in nature, this is likely to account for the differences observed in the solubility curves. Previous studies suggested that the physical properties of an amorphous material can be affected by the preparation technique and that mixtures produced by ball milling are heterogeneous at the molecular level. Therefore, the process involved in reaching the equilibrium solubility was most likely driven by

dissolution of the drug rather than the intentional demixing. As the dissolution process is more time-consuming than demixing, it is expected that equilibrium of the ball-milled mixture was not reached within the 2 h annealing time. The most narrow prediction interval was found for spray drying, indicating a combination of a good fit to the Flory-Huggins model and reproducibility of the measurements. The prediction interval for ball milling was wider than that for spray drying, but still relatively narrow. However, as ball milling provided the best reproducibility of the three techniques, the broader prediction interval was a result of a poor fit to the model. In contrast, the broad prediction interval for film casting was a consequence of a poorer reproducibility than for the other two techniques. Therefore, this study recommends that techniques such as spray drying or potentially film casting (if experimental reproducibility can be improved) should be used to prepare the amorphous dispersions when performing solubility measurements using the method proposed by Mahieu et al.[95].

Chapter 5

Influence of polymer molecular weight on drug–polymer solubility: A comparison between experimentally determined solubility in PVP and prediction derived from solubility in monomer

5.1 Abstract

In this study, the influence of polymer molecular weight on drug–polymer solubility was investigated using binary systems containing indomethacin (IMC) and polyvinylpyrrolidone (PVP) of different molecular weights. The experimental solubility in PVP, measured using a differential scanning calorimetry annealing method, was compared with the solubility calculated from the solubility of the drug in the liquid analogue N-vinylpyrrolidone (NVP). The experimental solubility of IMC in the low-molecular-weight PVP K12 was not significantly different from that in the higher molecular weight PVPs (K25, K30 and K90). The calculated solubilities derived from the solubility in NVP (0.31–0.32 g/g) were found to be lower than those experimentally determined in PVP (0.38–0.40 g/g). Nevertheless, the similarity between the values indicates that the analogue solubility approach can provide valuable indications on the solubility in the polymer. Hence, if a drug is soluble in an analogue of the polymer, it is most likely also soluble in the polymer. In conclusion, the solubility of a given drug–polymer system is determined by the strength of the drug–polymer interactions rather than the molecular weight of the polymer. Therefore, during the first screenings for drug solubility in polymers, only one representative molecular weight per polymer is needed.

5.2 Introduction

The development of amorphous drug delivery systems is getting increased attention in the pharmaceutical industry because of the potential of these systems to enhance the oral bioavailability of poorly water soluble drugs[49]. The free energy of the amorphous form is higher than that of the corresponding crystalline state, which will increase the apparent drug solubility and dissolution rate, compared with the crystalline form of the drug[12]. However, as the amorphous form is thermodynamically unstable, the drug will nucleate and recrystallize over time[13]. Therefore, stabilization of the amorphous form is critical for this formulation approach to succeed. Currently, the preferred method to stabilize amorphous drugs against crystallization is solid molecular dispersion in a polymer (glass solution)[10,11,124]. The mechanisms responsible for the stabilization are still not fully understood however, it is generally accepted that the high glass transition temperatures (T_g) of polymers and drug–polymer intermolecular interactions play an

important role[125,126]. Incorporation of the drug in a polymer with a high T_g elevates the T_g of the drug–polymer system, compared with the T_g of the pure amorphous drug, and reduces the molecular mobility and hence crystallization rate of the drug during storage. Molecular non-covalent interactions, such as hydrogen- and ionic bonds, van der Waals forces and hydrophobic interactions are also considered to be responsible for improving and maintaining a supersaturated drug concentration during dissolution in aqueous media[107]. In order to fully stabilize the molecularly dispersed drug in the polymer against recrystallization, it is essential that the drug is present below its saturation solubility in the polymeric matrix at typical storage temperature[127] and therefore, determination of drug–polymer solubility is of great interest.

For a polymer to be useful in a commercial pharmaceutical drug application it must have a T_g well above room temperature. It is well known that the T_g and other properties such as viscosity, free volume and tensile strength are dependent on the average molecular weight of the polymer[128,129]. Water-soluble polymers such as polyvinylpyrrolidone (PVP) and high-molecular-weight polyethylene glycol are amongst the most commonly used carriers for solid dispersions[130]. This is because of their high molecular weight and universal solubility in both hydrophobic and hydrophilic solvents, making them particularly suitable for solvent evaporation techniques such as spray drying[10]. PVP is a synthetic linear chain homopolymer with no branching obtained by polymerization of the monomer *N*-vinylpyrrolidone (NVP). It is available in several viscosity grades, ranging from low to high mean molecular weight (2,500–3,000,000 g/mol), characterized by the K value in the pharmacopeias[131]. As the molecular weight of PVP increases, so does the viscosity, whereas the aqueous solubility of the polymer decreases[132]. The influence of molecular weight of PVP on drug dissolution from solid dispersions has been studied widely[133-138]. These studies, across compounds, generally conclude that solid dispersions with PVP exhibit increased dissolution rate and higher apparent drug solubility in aqueous solution compared to the solid parent compound[137,138]. Furthermore, the drug dissolution rate decreases with increasing PVP molecular weight[133,135], which is probably due to an increased viscosity of the stagnant diffusion layer[134]. However, even though the aqueous drug solubility increases with polymer concentration, it does not seem to be significantly affected by the molecular weight of PVP[130].

The positive effects of PVP on drug solubility and dissolution rate are generally obtained from dispersions with the drug molecularly dispersed in the polymer (glass solutions) and hence, the solubility of the drug in the polymer is of particular importance[44]. If the drug is molecularly dispersed in the polymer below the equilibrium solubility, it will remain physically stable during storage[10,83] at least as long as significant water sorption into the glass solution can be avoided. Therefore, different methods to measure the solubility of drugs in polymers have been developed based on differential scanning calorimetry (DSC) and several studies have already determined the solubility of different drugs in PVP[48,80,83,92,95,139]. Furthermore, according to Marsac et al.[83], the solubility of a drug in PVP can be predicted from the solubility in a low-molecular-weight analogue of PVP by assuming that the monomer/analogue constitutes the lattice of the polymer.

However, despite the widespread use of PVP, the influence of polymer molecular weight (chain length) on drug–polymer solubility has not been sufficiently elucidated. Only a few studies have addressed this issue and none have, to the best of our knowledge, supported the theoretical considerations and predictions with relevant experimental data[83,89,91]. Therefore, the aim of the present study was to investigate the influence of polymer molecular weight on the drug–polymer solubility of indomethacin:PVP (IMC:PVP) binary system prepared by spray drying using a recently proposed DSC protocol[95,139] and comparing this with the prediction derived from the solubility in NVP.

5.3 Experimental section

5.3.1 Materials

IMC (M_w = 357.79 g/mol) was purchased from Hawkins, Inc. Pharmaceutical Group (Minneapolis, Minnesota). Kollidon® 12 PF (PVP K12, M_w = 2000–3000 g/mol), Kollidon® 17 PF (PVP K17, M_w = 7000–11,000 g/mol), Kollidon® 30 (PVP K30, M_w = 44,000–54,000 g/mol), and Kollidon 90® F (PVP K90, M_w = 1,000,000–1,500,000 g/mol) were kindly supplied by BASF (Ludwigshafen, Germany). NVP (M_w = 111.14 g/mol) was purchased from Sigma-Aldrich Company (St. Louis, Missouri). All materials were used as received.

5.3.2 Spray drying

IMC and PVP (85:15, w/w, 2000 mg) were dissolved in 20 mL of acetone:ethanol (80:20, v/v) and spray dried using a 4M8-TriX spray drier from ProCepT (Zelzate, Belgium). The spray dryer was pre-conditioned using pure solvent and, when in thermal equilibrium, the solutions were fed at a rate of 3 g/min (addition rate < 10% of lower explosion limit = 3.7 g/min) and atomized with a 0.5 mm two-fluid nozzle with at a pressure of 1.3 bar (20 L/min). Heated air was drawn through the open loop drying system at 500 L/min with a temperature of 100 °C.

5.3.3 Film casting

In order to reduce the time- and drug consumption, film casting was used to prepare the drug–polymer mixtures for the Gordon-Taylor relationship. IMC and PVP (20, 40, 60, 80, w/w, 100 mg) were dissolved in 1 mL of acetone:ethanol (80:20 v/v) and cast onto a Teflon coated 76 × 26 mm Menzel-glass. The solvent was evaporated on a Jenway 1100 Hotplate from Bibby Scientific Ltd. (Staffordshire, UK) using a plate temperature of 150 °C. The dried samples were scraped of the Teflon-coated glass plate and gently grounded using a mortar and pestle.

5.3.4 Differential scanning calorimetry

The spray dried powders, cast films and pure compounds were analyzed using a DSC Q2000 from TA Instruments Inc. (New Castle, Delaware). Sample powders (2–3 mg) were scanned from – 10–200 °C and purged with 50 mL/min pure nitrogen gas using Tzero aluminum hermetic pans with a perforated lid. The temperature and enthalpy of the DSC instrument were calibrated using indium as a standard. The thermograms were analyzed using the Universal Analysis 2000 (version 4.5A) software.

5.3.5 X-ray powder diffraction

X-ray powder diffraction (XRPD) analysis was performed using an X'Pert PRO MRD diffractometer from PANalytical (Almelo, The Netherlands) equipped with a TCU 100 temperature control unit and an X'Celerator detector using nickel-filtered CuKα radiation (λ = 1.5406 Å) at 45 kV and 40 mA. Approximately 1 mg of sample powder was placed on zero background (0-BG) Si-plates and measured over the angular range 3–40 °2θ at a scanning rate of 1.20 °2θ/min. The diffractograms were analyzed using the X'Pert Data Viewer (version 1.2) software.

5.3.6 Particle density

The particle densities of the raw materials were determined using an AccuPyc 1330 helium pycnometer from Micromeritics Instruments Corporation (Norcross, Georgia). Prior to the measurements, approximately 1 g of the samples was annealed in an oven just above the melting point and quench cooled to remove any sorbed moisture and yield the amorphous form. The samples were weighed before analysis and purged with 19.5 psig dry helium. The reported results are averages of 10 consecutive measurements.

5.3.7 Solubility determination in analogue

The solubility of IMC in NVP was assayed using a HPLC system comprised of an L-7110 pump, an L-7200 auto sampler, an L-7300 column oven, and a D-7000 interface, all from Merck (Darmstadt, Germany). An X-Bridge C-18 column (4.6 × 150 mm, 3.5 μm) from Waters (Milford, Massachusetts) was used for the separation and the mobile phase consisted of methanol and 0.0025 M potassium dihydrogen phosphate aqueous buffer (72:28, v/v) adjusted to pH 3 with phosphoric acid. An excess of crystalline IMC was added to a capped glass tube containing NVP and shaken for 72 h using a mechanical rotor from Heto Lab Equipment (Birkerod, Denmark). A sample was withdrawn, filtered using a 0.2 μm PTFE syringe filter from Merck Millipore Ltd. (Darmstadt, Germany) and properly diluted with mobile phase. The diluted sample was then injected in the HPLC and analyzed using the aforementioned method.

5.3.8 Solubility determination in polymers

The method used to determine the solubility of IMC in PVP was a DSC scanning protocol based on recrystallization of a supersaturated amorphous dispersion[95,139]: A supersaturated amorphous dispersion of IMC:PVP (85:15, w/w), prepared by spray drying, was loaded into the DSC and annealed at different temperatures (120–145 °C) for 3 h to crystallize the excess drug in the mixture and reach equilibrium solubility. After annealing, the sample was cooled to – 10 °C and ramped at a rate of 5 °C/min to 100 °C to determine the T_g of the demixed material. The concentration of drug remaining in the polymer matrix was then derived directly from the T_g of the demixed material using the Gordon-Taylor model[96]. By repeating this protocol at different annealing temperatures, a part of the solubility curve was obtained and by fitting to the Flory-Huggins model[85], the solubility at ambient temperature was obtained by extrapolation. For a more detailed description of the method, the interested reader is referred to Mahieu et al.[95] and Knopp et al.[139].

5.4 Theoretical considerations

5.4.1 Statistical analysis

The Flory-Huggins model[85] was used to model the measurements of the T_g for various values of the annealing temperature (T_a) by adjusting the interaction parameter χ. In order to find the least-square estimate of χ, it is important to understand which variable is subject to experimental noise. The T_a is the variable under control and will be regarded as free of error whereas the v_{IMC} is subject to error as it is derived from the T_g. The least-squares estimate $\hat{\chi}$ is therefore found by minimizing the residuals sum-of-square given by $SSR(\chi) = \sum_{i=1}^{N} \left(v_{IMC}^{measurement}(i) - v_{IMC}^{fitted}(i;\chi) \right)^2$, where N is the number of measurements. The standard deviation of is given by $s_{\hat{\chi}} = \sqrt{\frac{SSR(\hat{\chi})}{J^T J}}$, where J denotes the Jacobian matrix at $\hat{\chi}$. The 1 – α prediction interval for a future observation of χ is given by:

$$\hat{\chi} \pm t_{\alpha/2,N-1} \cdot s_{\hat{\chi}} \cdot \sqrt{1 + \frac{1}{N}} \qquad (5.1)$$

where $t_{\alpha/2,N-1}$ is the α/2 quantile in the t distribution with N – 1 degrees of freedom.

5.4.2 Prediction of drug–polymer solubility from drug-monomer solubility

It is possible to estimate the solubility in the polymer from the solubility in a low-molecular-weight analogue using the Flory-Huggins model[85], by assuming that the analogue constitutes the lattice of the polymer, and that the activity coefficient and solubility limit of the drug in the polymer is equal to that of the analogue[89,91]. In this study, NVP (the monomeric precursor to PVP) was used as the analogue and considered as the lattice in the model. The activity coefficient in NVP (γ_{NVP}) is the ratio of ideal mole fraction solubility (X_{id}) and the experimental mole fraction solubility of IMC in NVP (X_{exp}). The X_{exp} was obtained from HPLC analysis as described previously and X_{id} was calculated using[91]:

$$\ln(X_{id}) = -\frac{\Delta H_m(T_m - T)}{R(T_m T)} + \frac{\Delta C_p(T_m - T)}{RT} - \frac{\Delta C_p}{R}\ln\left(\frac{T_m}{T}\right) \quad (5.2)$$

where ΔH_m and T_m are the enthalpy of fusion and melting temperature for IMC, respectively, ΔC_p is the heat capacity change at the glass transition of amorphous IMC, R is the gas constant, and T is the temperature where the solubility estimate is desired. The activity coefficient in NVP (γ_{NVP}) can now be used to calculate the activity coefficient in PVP (γ_{PVP}) at the solubility limit using[89]:

$$\ln(\gamma_{PVP}) = \ln(\gamma_{NVP}) + \frac{MV_{IMC}}{MV_{NVP}}\left[\frac{1}{m_{IMC}}\ln\left(\frac{v_{IMC}}{X_{IMC}}\right) + \frac{1}{m_{IMC}} - \frac{1}{m_{PVP}}v_{PVP}\right] \quad (5.3)$$

where MV_{IMC} and MV_{NVP} are the molar volume of IMC and NVP, m_{IMC} and m_{PVP} are the ratio of the volume of IMC and PVP to the NVP, and v_{IMC} and v_{PVP} are the volume fraction of IMC and PVP, respectively. Finally, the mole fraction solubility of crystalline IMC in PVP can be derived from the ratio of X_{id} to γ_{PVP} and converted to mass fraction (w/w) for comparison with the experimentally determined solubility. It must be noted that this approach provides an estimate of the solubility in a liquid rather than a glass and therefore, should be evaluated with caution[89].

5.5 Results

5.5.1 Solid state characterization

Figure 5.1 presents the XRPD patterns for unprocessed IMC and PVP, amorphous IMC, and spray dried IMC:PVP (85:15 w/w) systems before and after annealing. The diffraction patterns for all the PVP grades (K 12, 25, 30, 90) and spray dried IMC:PVP (85:15 w/w) systems were

identical, and therefore only representative diffractograms with PVP K12 are shown. The diffraction pattern of crystalline IMC (Figure 5.1, a) shows Bragg peaks at 11.6, 19.6, 21.8, and 26.6 °2θ, characteristic for the stable γ-form of IMC[140]. After spray drying (Figure 5.1, c), the characteristic peaks for γ-IMC were absent and replaced by a diffuse halo with no Bragg peaks, indicating that IMC was amorphous. The diffraction patterns of pure PVP (Figure 5.1, d) and spray dried IMC:PVP (85:15 w/w) (Figure 5.1, e) also revealed a diffuse halo, indicating that spray drying successfully produced a supersaturated amorphous dispersion. Further studies revealed that the IMC:PVP (85:15 w/w) systems remained amorphous during the course of investigation. As can be identified from the Braggs peaks, the IMC recrystallized into the initial γ-form of the drug after annealing of the IMC:PVP (85:15 w/w) systems (Figure 5.1, b). Increasing the annealing time from 3–12 h did not cause any polymorphic conversion (data not shown).

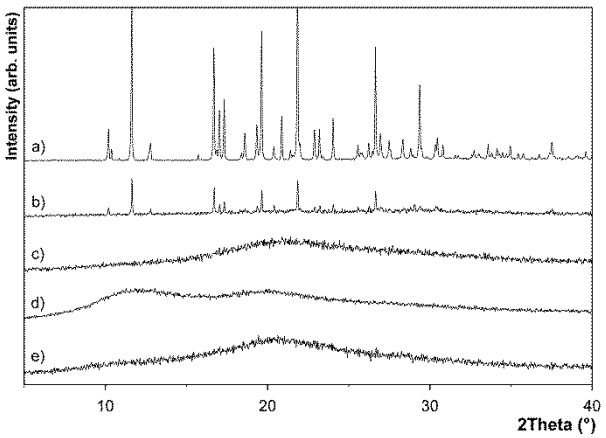

Figure 5.1: X-ray powder diffraction patterns of crystalline IMC (a), IMC:PVP (85:15 w/w) after annealing (b), amorphous IMC (c), PVP (d), and spray dried IMC:PVP (85:15 w/w) (e).

5.5.2 Thermal analysis

In Figure 5.2, the DSC scans of crystalline and amorphous IMC, PVP K12 and processed IMC:PVP K12 (85:15 w/w) mixture are shown. The thermograms for all the PVP grades provided similar DSC patterns (apart from increasing T_g as a function of molecular weight) and therefore only representative scans with PVP K12 are included in the figure. The DSC scan for crystalline IMC (Figure 5.2, a) showed a melting with a peak around 160 °C as the only thermal event. The temperature of melting and the enthalpy of melting were close to those expected for the γ-form of IMC[116] previously identified on XRPD. After amorphization of pure IMC, through film casting (see Section 5.3.3), the DSC scan showed a clear T_g around 45 °C followed by a strong recrystallization event ranging from 80–110 °C and a melting peak around 160 °C (Figure 5.2, b). Prior to the DSC scan of PVP K12 the sample was annealed for 5 min at 100 °C to evaporate any sorbed water from the hygroscopic polymer. The subsequent scan showed a

change in the T_g with a midpoint around 107 °C (Figure 5.2, c). The thermogram for the spray dried IMC:PVP K12 (85:15 w/w) (Figure 5.2, d) mixtures revealed a single T_g located between that of pure amorphous IMC and PVP K12, indicating that spray drying produced a homogenous amorphous mixture where IMC and PVP were mixed at a molecular level[117]. The scan did not display recrystallization and consequently also did not exhibit melting, however, during the annealing stage a clear exothermic recrystallization signal was present, which indicates that IMC was supersaturated in PVP. The data obtained from the DSC scans are summarized in Table 5.1.

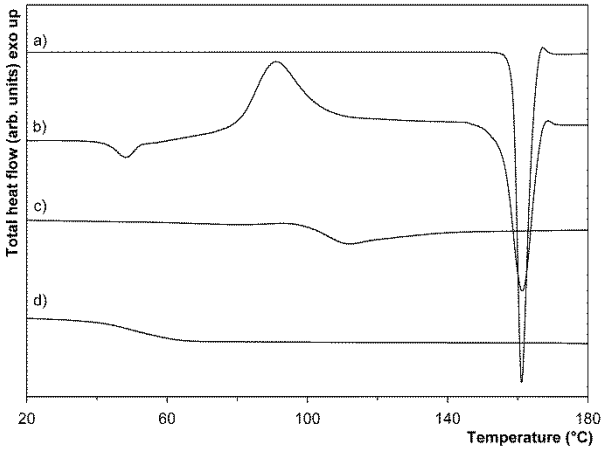

Figure 5.2: DSC thermograms of crystalline IMC (a), amorphous IMC (b), PVP K12 (c) and spray dried IMC:PVP K12 (85:15 w/w) (d).

Table 5.1: Experimental physical and thermodynamic values measured by DSC and density measured by helium pycnometry (values are mean ± s.d., *n* = 3).

Material	M_w (g·mol^{-1})[a]	Density (g·cm^{-3})	T_g (°C)	ΔC_p (J·g^{-1}·K^{-1})	ΔH_m (J·g^{-1})	T_m (°C)
IMC	357.79	1.38 ± 0.00	45.5 ± 0.2	0.38 ± 0.02	113.4 ± 2.6	161.0 ± 0.1
N-vinylpyrrolidone	111.14	1.04 ± 0.00	-	-	-	-
PVP K12	2,500	1.19 ± 0.00	107.1 ± 0.5	0.37 ± 0.02	-	-
PVP K25	25,000	1.18 ± 0.00	152.4 ± 0.3	0.30 ± 0.01	-	-
PVP K30	40,000	1.12 ± 0.00	159.3 ± 0.1	0.28 ± 0.02	-	-
PVP K90	1,100,000	1.21 ± 0.00	173.3 ± 0.3	0.29 ± 0.05	-	-

[a]Average M_w according to the supplier.

5.5.3 Prediction of drug–polymer solubility

The experimental solubility of IMC in the polymer PVP was determined using the analytical protocol described in Section 5.3.7. The equilibrium solubility of IMC in PVP at a given temperature can be derived directly from the T_g of the demixed material after annealing using the Gordon-Taylor relationship[96]:

$$X_{\mathrm{IMC}} = \frac{K \cdot \left(T_{\mathrm{g(PVP)}} - T_{\mathrm{g}}(X_{\mathrm{IMC}})\right)}{K \cdot \left(T_{\mathrm{g(PVP)}} - T_{\mathrm{g}}(X_{\mathrm{IMC}})\right) - T_{\mathrm{g(IMC)}} + T_{\mathrm{g}}\left(X_{\mathrm{IMC}}\right)} \tag{5.4}$$

where X_{IMC} is the mass fraction of amorphous IMC in the mixture, $T_g(X_{\mathrm{IMC}})$ is the glass transition temperature of the demixed material as a function of X_{IMC}, $T_{g(\mathrm{IMC})}$ and $T_{g(\mathrm{PVP})}$ are the glass transition temperatures of IMC and PVP respectively, and K is ratio of the heat capacity change over the glass transition ($\Delta C_{p)}$ of the polymer to the drug.

Table 5.1 gives all parameters necessary to determine the Gordon-Taylor relationship using Equation 5.4. The Gordon-Taylor relationship and experimentally determined data points are illustrated along with the solubility curves in Figure 5.3. Having established the Gordon-Taylor relationship it was possible to obtain data points on the solubility curve. Experimental points were obtained in 5 °C intervals and the equilibrium solubility of IMC in PVP at each temperature was derived from the T_g of the demixed material after annealing using Equation 5.4. The T_g of the demixed materials, after annealing, and the corresponding equilibrium solubility of IMC in PVP are listed in Table 5.2. As can be seen, the solubility increases with increasing annealing temperature.

The solubility at ambient temperature was predicted by extrapolation from the solubility data from Table 5.2 using the Flory-Huggins model[85]:

$$\frac{\Delta H_{\mathrm{m}}}{R} \cdot \left(\frac{1}{T_{\mathrm{m}}} - \frac{1}{T_{\mathrm{a}}}\right) = \ln\left(v_{\mathrm{IMC}}\right) + \left(1 - \frac{1}{\lambda}\right) \cdot \left(1 - v_{\mathrm{IMC}}\right) + \chi \cdot \left(1 - v_{\mathrm{IMC}}\right)^2 \tag{5.5}$$

where ΔH_{m} and T_{m} are the enthalpy of fusion and melting temperature for IMC, respectively, R is the gas constant, T_{a} is the annealing temperature, λ is the molar volume ratio of the polymer and drug, χ is the Flory-Huggins interaction parameter and v_{IMC} is the volume fraction of IMC.

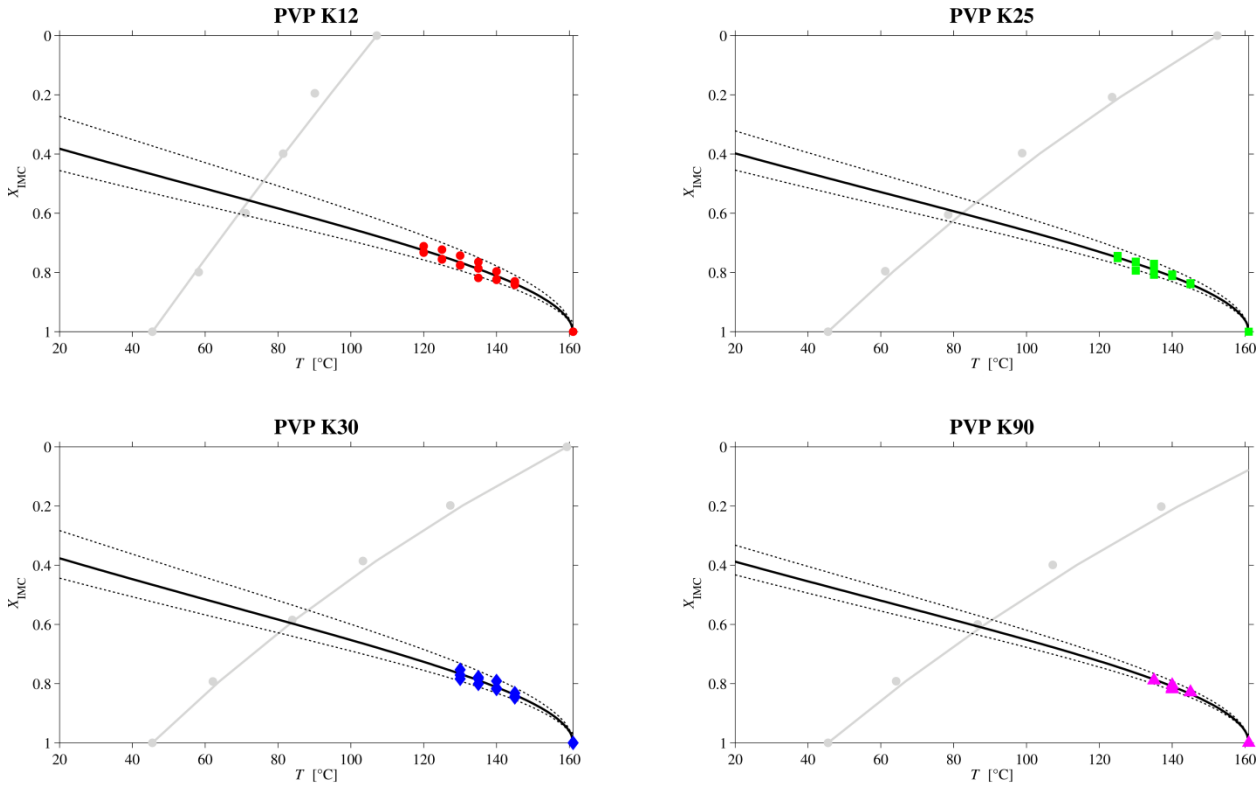

Figure 5.3: Equilibrium solubility of IMC (X_{IMC}) in PVP of different molecular weight as a function of annealing temperature (T_a). Red circles (●) represent the data from PVP K12, green squares (■) represent the data from PVP K25, blue diamonds (♦) represent the data from PVP K30, and purple triangles (▲) represent the data for PVP K90. The evolution of solubility of the four data sets has been fitted with the Flory-Huggins model (black curves) including the 95% prediction interval (dotted curves). The grey circles (●) represent the experimental relationship between T_g and X_{IMC} and the grey curve is the Gordon-Taylor relationship.

Table 5.2: Glass transition temperatures (T_g) of the demixed material and the corresponding equilibrium solubilities of IMC (X_{IMC}) obtained at different annealing temperatures (T_a) (values are mean ± SD, n = 3).

	IMC:PVP K12		IMC:PVP K25		IMC:PVP K30		IMC:PVP K90	
T_a (°C)	T_g (°C)	X_{IMC} (w/w)	T_g (°C)	X_{IMC} (w/w)	T_g (°C)	X_{IMC} (w/w)	T_g (°C)	X_{IMC} (w/w)
145	55.2 ± 0.3	0.836	59.7 ± 0.2	0.834	59.4 ± 0.6	0.841	62.9 ± 0.1	0.824
140	56.4 ± 0.8	0.815	62.2 ± 0.2	0.805	62.4 ± 1.1	0.808	64.6 ± 0.7	0.807
135	57.9 ± 1.3	0.790	63.9 ± 1.4	0.786	64.3 ± 0.9	0.787	67.2 ± 0.1	0.783
130	59.4 ± 0.9	0.765	65.5 ± 1.3	0.768	66.1 ± 1.2	0.770	[a]	-
125	60.6 ± 0.9	0.745	67.9 ± 0.3	0.741	[a]	-	[a]	-
120	61.8 ± 0.6	0.725	[a]	-	[a]	-	[a]	-

[a]Data not obtained as system did not reach equilibrium solubility within the annealing period.

Tables 5.1 and 5.2 provide the data needed to obtain the solubility curves of IMC in PVP using Equations 5.4 and 5.5 and the resulting solubility curves can be found in Figure 5.3. The solubility at 20 °C is predicted by extrapolation and can be found in Table 5.3. This extrapolation of course requires that the model assumptions are valid in the entire extrapolated temperature range. The greatest difference in the experimental solubility was seen between NVP and PVP K12. In contrast, the difference between the solubility in the low molecular weight PVP K12 and that of the high molecular weight PVP K90 was negligible.

Table 3: Predicted solubilities of IMC in PVP of different molecular weight obtained from calculations and experimental solubility along with the corresponding Flory-Huggins interaction parameter χ, activity coefficient γ and the 95% prediction interval.

	IMC:NVP	IMC:PVP K12	IMC:PVP K25	IMC:PVP K30	IMC:PVP K90
Values calculated from solubility in NVP					
Activity coefficient γ	0.076	0.120	0.126	0.128	0.126
Solubility at 20 °C (g/g)	0.52	0.33	0.31	0.31	0.31
Interaction parameter χ	-	-9.7	-9.3	-8.9	-9.5
Values obtained from experimental solubility in PVP					
Interaction parameter χ	-	-11.6	-12.4	-11.0	-12.2
Solubility at 20 °C (g/g)	-	0.38	0.40	0.38	0.39
95% prediction interval at 20 °C	-	0.27-0.46	0.32-0.45	0.28-0.44	0.33-0.43

The importance of including statistical analysis in the assessment of solubility measurements of this kind have previously been emphasized[139]. This is because the solubility curve fit is very sensitive even to small variations in the inter-replicate variance (reproducibility) and intra-replicate variance (fit to the Flory-Huggins model). Consequently, in order to evaluate the goodness-of-fit, a statistical analysis was performed and expressed as a prediction interval using Equation 1 as described in the Section 5.4.1. The prediction intervals from the four different IMC:PVP systems are given in Table 5.3 and illustrated in Figure 5.3. All the intervals were relatively narrow, indicating a combination of good fit to the Flory-Huggins model and good reproducibility of the measurements. The solubility of IMC in the monomer N-vinylpyrrolidone at 20 °C was determined using the analytical protocol described in Section 5.3.7 and measured to be 0.539 g/cm^3. From this value, the predicted solubility in the polymers was calculated using Equations 5.2 and 5.3. The predicted solubilities of IMC in the different PVPs can be found in Table 5.3.

5.6 Discussion

The relatively high solubility predicted in this study is to some extent contradicted by the proximity of the *K* values (in the Gordon-Taylor relationship) to 1, which may indicate that the interactions between the two compounds are weak. However, as identified by Taylor and Zografi[125] there is strong hydrogen bonding between the carbonyl group of PVP and the hydroxyl group of IMC. The pure amorphous IMC is mainly composed of carboxylic acid dimers involving two hydrogen bonds. Consequently, the formation of the IMC:PVP hydrogen bond requires the disruption of a hydrogen bond in the IMC dimer and, as these two kinds of hydrogen bonds are similar in terms of energy; this explains the seemingly "weak" interactions between the compounds suggested by the *K* value. Although the solubility data at elevated temperature is in accordance with values reported in literature based on DSC[80,95,139], there seems to be some discrepancy between the predicted solubility at 20 °C and predictions based on molecular dynamics[141]. However, as this is out of scope of this study it needs to be addressed in detail in future work.

In order to correlate the experimentally determined solubility with the calculated solubility, the solubility of IMC in the liquid NVP was determined. The solubility of IMC in NVP at room temperature was higher than the values extrapolated from the solubility in the PVP polymers at elevated temperatures (see Table 5.3). This difference was most likely due to the reduced entropic contribution to the mixing free energy in the PVP system compared to the NVP solution. As described previously by Marsac et al.[83], the entropy of mixing for a solid drug–polymer system is less favorable than for a liquid drug–monomer system due to reduced configurational entropy of the polymer compared to the monomer – a consequence of the connectivity of the repeat units in the polymer chain. However, the effect of polymer molecular weight on mixing thermodynamics is less pronounced and in fact, the entropy contribution has been found to be relatively constant regardless of molecular weight[83]. Consequently, it is presumed that the mixing thermodynamics of a drug–polymer system is governed by the relative strength of the enthalpic interactions between the drug and polymer rather than the entropy of mixing. In other words, the solubility of a given drug–polymer system is essentially determined by the drug–polymer interactions and not the anti-plasticizing effect, and thus molecular weight, of the polymer. This means that if a drug is immiscible in a polymer, a change to a chemically different polymer is more likely to induce solubility than to switch to a different molecular weight of the same polymer[83]. Furthermore, any observed difference of solubility in relation to molecular weight of the polymer is only expected with polymers consisting of a few monomers. This is in accordance with the observations made in this study where the greatest difference in the experimental solubility was seen between NVP and PVP K12. In contrast, the experimental solubility in the low molecular weight PVP K12 was not significantly different from that of the high molecular weight PVP K90 (see Table 5.3). Furthermore, after correcting for the reduced entropic contribution to the mixing free energy in the PVP systems using Equations 5.2 and 5.3, the calculated solubilities (0.31–0.33 g/g) were lower than the experimentally determined values (0.38–0.40 g/g). This could imply that either Equation 5.3 underestimates solubility or that the

annealing method overestimates the solubility of IMC in PVP. Nonetheless, the close similarity between the values indicates that the analogue solubility approach can provide valuable indications on the solubility of a drug in a polymer where a liquid analogue is available. Thus, if a drug is poorly soluble in an analogue of the polymer it is most likely also poorly soluble in the polymer, particularly if the molecular structure of the analogue is not altered significantly during polymerization.

PVP is obtained by radical polymerization, which involves the breaking of the carbon-carbon double bond in NVP. The product is mainly polymerized in aqueous solution using hydrogen peroxide as initiator and therefore, the polymers have hydroxyl and carbonyl end groups[142]. Consequently, these end groups have more and different functional groups than the repeat units in the polymer chain, which can interact non-covalently with the drug and potentially influence solubility due to additional intermolecular interactions. However, even for the lowest molecular weight polymer in this study, PVP K12, the end groups constitute less than 10% of the total molecular weight and therefore, the relative influence of the end groups on drug solubility in the larger polymers is presumed to be minor. These theoretical considerations all support the hypothesis that molecular weight of a polymer does not influence the solubility of a drug significantly. This is in accordance with the findings reported by Marsac et al.[89] and Paudel et al.[91], who investigated the solubility of a number of poorly water soluble drugs in a low molecular weight analogue to PVP and used this to calculate the solubility in different molecular weight grades of PVP. Although these calculations were not verified with experimental data, and thus no definite conclusion about the influence of molecular weight of the polymer could be drawn, they support the hypothesis of the present study. Consequently, when a new solid glass solution is to be formulated, only one representative molecular weight per polymer seems needed during the initial screening of drug–polymer solubility. However, it is important to emphasize that this does not mean that the influence of polymer molecular weight on other important factors such as dissolution rate, physical stability, degree of supersaturation, apparent drug solubility and crystallization inhibition should not be considered in the polymer selection process.

Whilst the solubility of a drug in a polymer is mainly governed by drug–polymer interactions, previous studies have shown that the physical stabilization of the drug is associated with the anti-plasticizing effect of the polymer, i.e. increased viscosity and decreased molecular mobility of the binary system will decrease the nucleation rate of the drug molecule[43,143]. Therefore, even though the solubility of IMC in PVP may not be influenced by the molecular weight of the polymer, the kinetic stability of a supersaturated system might. The molecular mobility and T_g are correlated to the molecular weight of the polymer and increasing the chain length will generally increase viscosity and T_g and hence, decrease the molecular mobility[118,128,129]. If the molecular mobility is decreased, the crystallization kinetics may become slower than the time scale of the annealing period in this study. Due to the slow crystallization kinetics, the T_g of the demixed material remains the same after a given annealing temperature, which may be seen as a *plateau effect*.

The effect of polymer molecular weight on the kinetic stability of the supersaturated drug–polymer systems is directly reflected in the results of this study, more particularly the onset temperature of this *plateau effect*. For example, after annealing of the IMC:PVP K90 mixture for 3 h at 120–130 °C, the T_g was not different from that measured after annealing at 135 °C (data not shown). In practice, this means that the system did not reach equilibrium solubility within the 3 h of annealing at these lower temperatures. Hence, depending on the molecular weight of the polymer and the associated annealing time, this *plateau effect* will set in at different temperatures. Increasing the annealing time will generally allow for more data points to be obtained, but as the crystallization kinetics are slow, even doubling the annealing time might not provide additional data points. In fact, the crystallization kinetics at this point can be so slow that it is not observable as an exotherm in the DSC and therefore, the system can falsely be considered in equilibrium. However, a single-point determination at 140 °C revealed that increasing the annealing time from 3–12 h did not influence the T_g (and thus solubility) significantly (data not shown), indicating that the system was in equilibrium after 3 h. Accordingly, from a cost-benefit point of view, the annealing time was fixed at 3h and consequently, the onset temperature of the *plateau effect* increased with increasing molecular weight of the polymer (see Table 5.2), indicating that kinetic stabilization is directly proportional to molecular weight of the polymer. These considerations and observations are in accordance with Paudel et al.[91], who showed a correlation between recrystallization temperature and polymer molecular weight in the order PVP K90 ≥ PVP K25 > PVP K12. However, other parameters including glass stability, miscibility and degree of supersaturation also affect the nucleation and crystallization rate of drugs in amorphous dispersions[119]. It is therefore important to establish the annealing time needed to reach crystallization equilibrium every time a new drug–polymer mixture is studied. The exothermic crystallization event can be monitored from the heat flow during the isothermal annealing of the mixtures and the process is considered to be in equilibrium after the signal reaches a baseline. However, as the crystallization rate decrease rapidly when the concentration approaches solubility equilibrium[116], the "true equilibrium" may not be reached. Consequently, it is rational to assume that the annealing method might overestimate the true saturation solubility of the drug in the polymer, but this assumption has not been verified in this study.

It is likely that the findings reported in the present study are applicable for most amorphous homopolymers, alternating copolymers, and block copolymers if the subunit ratio can be controlled. If any, the biggest difference in solubility was expected for low molecular weight polymers as the end groups potentially have different functional groups than the repeat units in the polymer chain and because the relative difference in the entropic contribution becomes larger with decreasing molecular weight. Further studies are needed in order to confirm these findings, which could include a validation with different drug–polymer systems and long term stability to confirm the solubility at room temperature.

5.7 Conclusion

In the present study, the influence of molecular weight of a polymer on drug–polymer solubility was investigated. It was found that the experimentally determined solubility of IMC in PVP was independent of the molecular weight of the polymer. Even though the calculated solubilities in the PVPs, based on the solubility in NVP, were found to be slightly lower than the experimental solubilities, their proximity indicates that the analogue solubility approach can provide valuable indications on the solubility of a drug in a polymer in an early development process. Hence, if a drug is poorly soluble in an analogue of the polymer it is presumably also poorly soluble in the polymer and thus, a change to a chemically different polymer is more likely to induce solubility than to switch to a different molecular weight of the same polymer. Therefore, during the first screenings for drug solubility, only one representative molecular weight per polymer is needed.

Chapter 6

A comparative study of different methods for the prediction of drug–polymer solubility

6.1 Abstract

In this study, a comparison of different methods to predict drug–polymer solubility was carried out on binary systems consisting of five model drugs (paracetamol, chloramphenicol, celecoxib, indomethacin, and felodipine) and polyvinylpyrrolidone/vinyl acetate copolymers (PVP/VA) of different monomer weight ratios. The drug–polymer solubility at 25 °C was predicted using the Flory-Huggins model, from data obtained at elevated temperature using thermal analysis methods based on the recrystallization of a supersaturated amorphous solid dispersion and two variations of the melting point depression method. These predictions were compared with the solubility in the low molecular weight liquid analogues of the PVP/VA copolymer (N-vinylpyrrolidone and vinyl acetate). The predicted solubilities at 25 °C varied considerably depending on the method used. However, the three thermal analysis methods ranked the predicted solubilities in the same order, except for the felodipine:PVP system. Furthermore, the magnitude of the predicted solubilities from the recrystallization method and melting point depression method correlated well with the estimates based on the solubility in the liquid analogues, which suggests that this method can be used as an initial screening tool if a liquid analogue is available. The learnings of this important comparative study provided general guidance for the selection of the most suitable method(s) for the screening of drug–polymer solubility.

6.2 Introduction

The development of amorphous drug formulations has attracted a lot of attention, both in the pharmaceutical industry and in academic research, owing to the potential enhancement of solubility and dissolution rate of poorly water-soluble drug candidates[10,12,41]. However, the number of formulations containing drug in the amorphous form that have made it through to the market is limited due to the generally poor physical stability of the amorphous form[9,74,144]. The high internal free energy of amorphous compounds often results in fast recrystallization with the subsequent loss of the dissolution rate and solubility advantage[80]. Therefore, a key requirement for any amorphous formulation to succeed is that it be stable against crystallization during the shelf-life of the formulation. Incorporation of the amorphous drug into a polymer with a higher glass transition temperature (T_g) will generally increase the T_g of the resulting mixture, reducing the molecular mobility and thus nucleation and crystal growth of the drug and therefore improving the kinetic stability[78]. This is commonly known as an amorphous solid dispersion and

can be defined as a molecular dispersion of the drug in an amorphous polymer matrix. Even though this is a promising approach, it does not ensure physical stability during storage, as the drug can still crystallize at temperatures well below the T_g[116]. Consequently, in order to stabilize the system thermodynamically it is essential that the drug be molecularly dispersed in the polymer below its saturation solubility, and therefore, determination of drug–polymer solubility is of great importance for the rational development of amorphous systems[10,145]. However, as the majority of pharmaceutically relevant drugs and polymers are solid (or highly viscous) at ambient temperature, measuring the drug–polymer solubility constitutes a major challenge[48]. Therefore, several differential scanning calorimetry (DSC) protocols have been proposed based on determination of equilibrium thermodynamics at elevated temperature and extrapolation to room temperature[39,48,83,89,95].

The initial protocols exploited the melting point depression of a drug in the presence of a polymer[83,88,146]. The concept of melting point depression to describe the interaction between a crystalline polymer and an amorphous polymer can be derived from the Flory-Huggins model of chemical potential of mixing and the condition of phase equilibrium[85,86]. In theory, melting of a crystal occurs at the temperature when the chemical potential of the crystal is equal to the chemical potential of the melt. Addition of an amorphous polymer to the crystal may (if miscible) reduce the chemical potential of the crystalline material, leading to melting point depression[85,86]. Consequently, by extending the equations presented by Flory-Huggins to fit crystalline drug–polymer systems and assuming that amorphous drug behaves as a solvent, it is possible to relate the solubility of a drug in a polymer to the melting point depression of the drug[83,147]. In a protocol developed by Marsac et al.[95], physical drug–polymer mixtures of known composition were prepared by geometric mixing and analyzed by DSC. The onset of the bulk melting endotherm (T_m) was considered the equilibrium solubility temperature of the given composition. The onset of the melting was chosen to eliminate the impact of sample preparation on the T_m[93,148]. This protocol was further developed by Tao et al.[48] who introduced cryomilling of the physical mixtures before DSC analysis in order to compensate for the slow dissolution kinetics by reducing particle size to allow for diffusive mixing[80]. In this case the end point of the dissolution endotherm (T_{end}) was considered the equilibrium solubility temperature of the given composition. The end point (offset) value was chosen because this value represents the melting point of the final composition, assuming complete mixing has occurred[48,89,149]. This approach is currently the most commonly used in the literature to determine drug polymer solubility[48,82,89,91,92,94,145].

As a result of the high viscosity of polymers, the dissolution kinetics are slow and can potentially (depending on heating rate) exceed the time scale of the DSC scan[48]. This may result in a higher dissolution end point and ultimately lead to an underestimation of the drug–polymer solubility[7]. Therefore, Mahieu et al.[95] proposed a protocol that takes advantage of the fact that recrystallization is generally faster than dissolution. In this method, a supersaturated amorphous solid dispersion was annealed at different temperatures above the recrystallization temperature until the equilibrium solubility was reached[95,139,150]. The equilibrium solubility concentration was

then derived directly from the T_g of the annealed material using the Gordon-Taylor relationship[96].

Even though they vary in detail, the different approaches used to determine the drug–polymer solubility reported in the literature can be divided into three general thermal analysis methods: (i) the recrystallization method[95], (ii) the dissolution end point method[48,145], and (iii) the melting point depression method[83]. Despite the increased interest in determination of drug solubility in polymers, to the best of our knowledge, no comparative study across methods has been conducted. The aim of this study was therefore to compare the three aforementioned thermal analysis methods, through formal statistical analysis, for the prediction of drug–polymer solubility using binary systems consisting of five model drugs (paracetamol, chloramphenicol, celecoxib, indomethacin, and felodipine) and polyvinylpyrrolidone/vinyl acetate copolymers (PVP/VA) of different vinylpyrrolidone/vinyl acetate weight ratios (30/70, 50/50, 60/40, 70/30, and 100/0). The model drugs were selected in order to cover a range of general physicochemical properties of low molecular weight drugs; i.e., T_m (140−175 °C), T_g (20−60 °C), and molecular weight (M_w, 150−400 g/mol). In addition to the three thermal analysis methods described above, it is possible to estimate the solubility of a drug in a polymer from the solubility of the drug in a liquid low molecular weight analogue of the polymer using the Flory-Huggins lattice model[89,91]. Therefore, drug–polymer solubilities obtained using the three thermal analysis methods were compared with a prediction based on the solubility of the drugs in the liquid monomeric precursors to the copolymer (N-vinylpyrrolidone and vinylacetate). The ultimate aim of this comparative study was to provide a general guidance for the screening of polymers suitable for glass solutions.

6.3 Experimental section

6.3.1 Materials

Paracetamol (PCM, M_w = 151.17 g/mol) and chloramphenicol (CAP, M_w = 323.13 g/mol) were purchased from Sigma-Aldrich Co. (St. Louis, MO, USA). Celecoxib (CCX, M_w = 381.37 g/mol) was purchased from AK Scientific, Inc. (Union City, CA, USA). Indomethacin (IMC, M_w = 357.79 g/mol) was purchased from Hawkins Pharmaceutical Group (Minneapolis, MN, USA). Felodipine (FDP, M_w = 384.26 g/mol) was purchased from Combi-Blocks, Inc. (San Diego, CA, USA). N-Vinylpyrrolidone (NVP, M_w = 111.14 g/mol) and vinyl acetate (VA, M_w = 86.09 g/mol) were purchased from Sigma-Aldrich Co. (St. Louis, MO, USA). Plasone^{TM} K-17 (PVP K17, M_w = 10,000 g/mol), PVP/VA copolymer E-335 (PVP/VA 335, M_w = 28,000 g/mol), PVP/VA copolymer E-535 (PVP/VA 535, M_w = 36,700 g/mol), PVP/VA copolymer E-635 (PVP/VA 635, M_w = 38,200 g/mol), and PVP/VA copolymer E-735 (PVP/VA 735, M_w = 56,700 g/mol) were kindly supplied by Ashland Chemical Co. (Columbus, OH, USA). Since the PVP/VA copolymers were sourced as solutions, they were converted to the solid forms by spray drying. The supplied liquids were diluted with ethanol to form 5% (w/w) solutions and

processed, using the Mini Spray Dryer B-290 from Büchi (Flawil, Switzerland) in the open pressure mode with air as drying gas, applying the following conditions: inlet temperature 140 ºC, aspirator rate 100% and pump speed 30%. These parameters resulted in an outlet temperature of around 80 ºC.

6.3.2 Liquid analogue solubility approach

The solubility of the different drugs in the liquid analogues NVP and VA was determined using the shake-flask method. An excess of crystalline drug was added to a capped glass tube containing 1 mL of the liquid analogue and shaken for 72 h using a mechanical rotor from Heto Lab Equipment (Birkerod, Denmark). Samples were withdrawn, filtered using a 0.2 μm PTFE hydrophobic syringe filter from Merck Millipore Ltd. (Darmstadt, Germany), and diluted with mobile phase to appropriate concentrations. The diluted samples were assayed using a HPLC system composed of an L-7100 pump, an L-7200 auto sampler, a T-6000 column oven, and a D-7000 interface, all from Merck-Hitachi LaChrom (Tokyo, Japan). A reverse phase X-Bridge C-18 column (4.6 x 150 mm, 3.5 μm) from Waters (Milford, MA, USA) was used for the separation, and the mobile phase consisted of methanol and 0.0025 M potassium dihydrogen phosphate aqueous buffer (72:28 v/v) adjusted to pH 3 with phosphoric acid. A variable wavelength ultraviolet L-7450A diode array detector from Merck-Hitachi LaChrom (Tokyo, Japan) was used to detect signals at wavelengths 280, 280, 250, 270, and 230 nm and retention times 1.62, 2.03, 8.06, 4.04, and 11.95 min for PCM, CAP, CCX, IMC, and FDP, respectively.

6.3.3 Recrystallization method

6.3.3.1 Sample preparation

Supersaturated amorphous solid dispersions were prepared by a film casting method. The drug and polymer (80:20 or 85:15 w/w, 500 mg) were dissolved in 5 mL of acetone:ethanol (80:20 v/v) and cast onto a Teflon coated 76 x 26 mm Menzel glass. The solvent was evaporated on a Jenway 1100 hot plate from Bibby Scientific Ltd. (Staffordshire, U.K.) using a plate temperature of 150 °C. The dried samples were scraped of the Teflon coated glass plate and gently ground using a mortar and pestle.

6.3.3.2 Thermal analysis

The cast film powders and pure compounds were analyzed using a Q2000 DSC from TA Instruments Inc. (New Castle, DE, USA). Sample powders (2−3 mg) were scanned under 50 mL/min pure nitrogen gas purge using Tzero aluminum hermetic pans with a perforated lid. The temperature and enthalpy of the DSC instrument were calibrated using indium. The melting temperature (T_m, onset), melting enthalpy (ΔH_m), glass transition temperature (T_g, inflection),

and heat capacity change (ΔC_p) were determined using the Universal Analysis 2000 (version 4.5A) software.

6.3.3.3 Solubility determination

The supersaturated amorphous solid dispersions were loaded into the DSC and annealed at different temperatures below the T_m of the particular drug under investigation for 3 h to crystallize the excess drug in the mixture and to reach equilibrium solubility. After annealing, the sample was cooled to −10 °C and ramped at a rate of 5 °C/min to determine the T_g of the annealed material. The concentration of drug remaining in the polymer matrix was then derived directly from the T_g of the annealed material. In order to determine the composition dependence of the T_g, physical mixtures of drug–polymer of known composition were prepared using a mortar and pestle. The samples were then heated above the T_m of the pure drug, quench cooled to −10 °C *in situ* in the DSC and ramped at a rate of 5 °C/min to determine the T_g. For a detailed description of the method, please refer to Mahieu et al.[95] and Knopp et al.[139].

6.3.3.4 Solid state characterization

X-ray powder diffraction (XRPD) analysis was performed using an X'Pert PRO MRD diffractometer from PANalytical (Almelo, The Netherlands) equipped with a TCU 100 temperature control unit and an X'Celerator detector using nickel-filtered Cu Kα radiation (λ = 1.5406 Å) at 45 kV and 40 mA. Approximately 1 mg of sample powder was placed on zero background Si plates and measured over the angular range 3−40 °2θ at a scan rate of 1.20 °2θ/min. The diffractograms were analyzed using the X'Pert Data Viewer (version 1.2) software.

6.3.4 Dissolution end point method

6.3.4.1 Sample preparation

Drug and polymer mixtures with different compositions were first mixed using a mortar and pestle followed by mixing in a MM 200 ball mill mixer from Retsch GmbH (Haan, Germany). The individual materials were kept in a drying chamber for at least 24 h at 50 °C before sample preparation. In a typical milling procedure, pure drug or drug–polymer powder samples of 500 mg were loaded in 25 mL stainless steel milling containers with two stainless steel balls (15 mm in diameter) and milled at 20 Hz. A pre-defined milling time of 2 min was chosen, which was subsequently followed by a 2 min cooling time. The number of milling-cooling cycles to be used for each drug–polymer combination was determined by measuring the melting end point of the mixture, where no further decrease in the melting end point was observed with increased number of milling-cooling cycles. Longer milling time enhanced the dissolution rate of the crystalline drug into the polymer but decreased the sensitivity of the DSC measurement due to increased

amorphous content (observed by XRPD). Thus, fewer milling-cooling cycles were used for mixtures containing lower drug loadings.

6.3.4.2 Thermal analysis

Samples were analyzed using the power compensation DSC8000 from PerkinElmer (Waltham, MA, USA). Nitrogen was used as the purge gas for low speed scanning. Approximately 8−10 mg of freshly ball-milled sample was packed into an aluminum pan with a perforated lid. Melting point end point determination was conducted at a heating rate of 1 °C/min from 20−200 °C. The end point of the melting endotherm (T_{end}) was calculated from the intercept point of the endothermic trace and the post melting baseline.

6.3.4.3 Solid state characterization

The solid state properties of the ball-milled samples were determined using a MiniFlex II X-ray powder diffractometer from Rigaku Corp. (Tokyo, Japan). Radiation was generated from a copper source operating at a voltage of 30 kV and a current of 15 mA. The test samples were packed into a glass sample holder and scanned from 0−40 °2θ, using a step width of 0.01 °2θ and a scan rate of 1 °2θ/min; continuous mode was used. There were certain levels of increased amorphous halo background in the XRPD pattern of ball-milled samples in comparison to crystalline drug and amorphous polymer physical mixtures, but the polymorphic form of all crystalline drugs was determined to be the same as that of the starting drug materials.

6.3.5 Melting point depression method

6.3.5.1 Sample preparation

Physical mixtures (w/w) of drug and polymer were prepared by ball milling at 400 rpm for 10 min with a PM 100 planetary ball mill from Retsch GmbH (Haan, Germany) at room temperature. A total amount of 500 mg was loaded to the stainless steel milling container with a volume of 25 mL and two stainless steel balls (15 mm in diameter) were used. Care was taken to ensure that no polymorphic transition occurred and crystalline API was still present at the end of milling (confirmed by XRPD)[92]. Collected samples were stored in a desiccator over silica gel at 5 °C until use.

6.3.5.2 Thermal analysis

The melting events of the physical mixtures were measured using a Diamond DSC from PerkinElmer (Waltham, MA, USA) with HyperDSC and an ULSP-130 cooling system from ULSP BV (Ede, The Netherlands) operated under a nitrogen flow of 40 mL/min. The gas flow was controlled using a Thermal Analysis Gas Station (TAGS) from PerkinElmer (Waltham, MA,

USA). The instrument was calibrated for both melting onset and enthalpy with indium. Before the measurement, samples (5−8 mg) in standard aluminum DSC pans were first annealed for 2 h in an oven from Memmert GmbH (Schwabach, Germany) at a temperature 10 °C above the glass transition temperature of the polymer. The 2 h annealing time was chosen based on a comparison of the heat of fusion values obtained for the 90:10 w/w drug–polymer physical mixtures of non-annealed sample and samples annealed for 2, 4, and 6 h. Samples were then cooled down to room temperature, and the final sample weight was determined. The DSC program used was as follows: samples were first heated to 100−120 °C at a heating rate of 10 °C/min, and then a heating rate of 1 °C/min was applied to obtain the melting temperature value as close to the equilibrium as possible. All curves were evaluated, and the values of melting point (T_m, onset) and melting enthalpies (ΔH_m) were determined. In order to determine the T_g of the drug–polymer mixtures, the samples were preheated in the DSC pans from 100 °C to a temperature above the T_m of drug at a 10 °C/min heating rate and then cooled to 30−40 °C below the expected T_g at a cooling rate of 300 °C/min and then a step scan method was applied to determine the T_g. For the step scan, the samples were heated to 30−40 °C above the expected T_g at 5 °C/min in 2 °C steps. A 1 min isothermal step was applied between each of the dynamic steps.

6.3.5.3 Solid state characterization

XRPD analysis on all physical mixtures was conducted using a Rigaku MiniflexII Desktop X-ray diffractometer (Tokyo, Japan) with a Haskris cooling unit (Grove Village, IL, USA). The tube output voltage used was 30 kV, and tube output current was 15 mA. A Cu tube with Ni filter suppressing Kβ radiation was used. Measurements were taken from 5 to 40 °2θ at a scan rate of 0.05 °2θ/s. A zero background Si plate was used during measurements to support the sample.

6.3.6 Density determination

The amorphous densities of the materials were determined using an AccuPyc 1330 helium pycnometer from Micromeritics Instruments Corp. (Norcross, GA, USA). Prior to the measurements, approximately 1 g of the samples was melt quenched to remove any sorbed moisture and to obtain the amorphous form. The samples were weighed before analysis and purged with 19.5 psig dry helium. The reported results are averages of 10 consecutive measurements.

6.4 Theoretical considerations

6.4.1 Prediction of drug–polymer solubility from drug-analogue solubility

Considering that a low molecular weight liquid analogue constitutes the lattice of a polymer, the molecular volume, activity coefficient and experimental solubility in the analogue can be used to estimate the solubility of the drug in the polymer[91]. The activity coefficient in an analogue

($\gamma_{analogue}$) is the ratio of ideal mole fraction solubility (X_{id}) and the experimental mole fraction solubility of drug in the analogue (X_{drug}). The X_{drug} in the analogue is obtained experimentally from HPLC analysis as described above, and X_{id} is calculated using[91]:

$$\ln(X_{id}) = -\frac{\Delta H_m (T_m - T)}{R(T_m T)} + \frac{\Delta C_p (T_m - T)}{RT} - \frac{\Delta C_p}{R}\ln\left(\frac{T_m}{T}\right) \quad (6.1)$$

where ΔH_m and T_m are the enthalpy of fusion and melting temperature for the drug, respectively, ΔC_p is the heat capacity change at the glass transition of the amorphous drug, R is the gas constant, and T is the temperature for which the solubility estimate is desired. The $\gamma_{analogue}$ can now be used to calculate the activity coefficient in the polymer ($\gamma_{polymer}$) at the solubility limit using[89]:

$$\ln(\gamma_{polymer}) = \ln(\gamma_{analogue}) + \frac{MV_{drug}}{MV_{analogue}}\left[\frac{1}{m_{drug}}\ln\left(\frac{v_{drug}}{X_{drug}}\right) + \frac{1}{m_{drug}} - \frac{1}{m_{polymer}}v_{polymer}\right] \quad (6.2)$$

where MV_{drug} and $MV_{analogue}$ are the molar volume of drug and analogue, respectively, m_{drug} and $m_{polymer}$ are the ratio of the volume of drug and polymer to the analogue, respectively, and v_{drug} and $v_{polymer}$ are the volume fraction of drug and polymer, respectively. Finally, the mole fraction solubility of crystalline drug in the polymer can be derived from the ratio of X_{id} to $\gamma_{polymer}$ and converted to mass fraction (w/w) for comparison with the experimentally determined solubility.

6.4.2 Prediction of drug–polymer solubility from DSC data

The experimental solubility of drug in the polymer at elevated temperature was determined using the analytical protocols described in Section 6.3. The data sets were fitted with the Flory-Huggins model in order to predict the solubility at ambient temperature by extrapolation[85]:

$$\frac{\Delta H_m}{R}\cdot\left(\frac{1}{T_m} - \frac{1}{T}\right) = \ln(v_{drug}) + \left(1 - \frac{1}{\lambda}\right)\cdot(1 - v_{drug}) + \chi\cdot(1 - v_{drug})^2 \quad (6.3)$$

where ΔH_m and T_m are the enthalpy of fusion and melting temperature for the pure drug respectively, R is the gas constant, λ is the molar volume ratio of the polymer and drug, χ is the Flory-Huggins interaction parameter. T is the annealing temperature, onset temperature of

melting, or dissolution end point temperature, depending on the method in question, and v_{drug} is the volume fraction of drug derived from:

$$v_{drug} = \frac{\frac{X_{drug}}{\rho_{drug}}}{\frac{X_{drug}}{\rho_{drug}} + \frac{1 - X_{drug}}{\rho_{polymer}}} \tag{6.4}$$

where ρ_{drug} and $\rho_{polymer}$ are the densities of drug and polymer, respectively, and X_{drug} is the mass fraction of drug.

6.4.3 Statistical analysis

The aim of the statistical analysis was to provide a prediction of the drug–polymer solubility at storage temperature (25 °C). As measurements at such low temperatures are infeasible (or even impossible), one has to rely on extrapolations of data obtained at elevated temperatures from the Flory-Huggins model[85]. The predictions of the drug solubility at room temperature were reported as a central estimate (the least-squares estimate) and a 95% prediction interval in the present study. The predicted solubility was derived from Equations 6.3 and 6.4 by inserting the 1 − α prediction interval for a future observation of χ given by $\hat{\chi} \pm t_{\alpha/2,N-1} \cdot s_{\hat{\chi}} \cdot \sqrt{1 + \frac{1}{N}}$, where $\hat{\chi}$ is the least-squares estimate of the interaction parameter, $s_{\hat{\chi}}$ is the standard deviation of $\hat{\chi}$ and $t_{\alpha/2,N-1}$ is the $\alpha/2$ quantile in the t-distribution with $N - 1$ degrees of freedom. In order to make a proper statistical analysis it is important to realize which variable that is subject to experimental noise.

6.4.3.1 The recrystallization method

In the recrystallization method, v_{drug} was subject to error as it was derived from the glass transition temperature of the annealed material. However, as v_{drug} cannot be expressed analytically by rearranging the Flory-Huggins model, the statistical analysis was characterized as an implicit regression problem. The least-squares estimate $\hat{\chi}$ was found by minimizing the residual sum-of-square given by $SSR(\chi) = \sum_{i=1}^{N} \left(v_{drug}^{measurement}(i) - v_{drug}^{fit}(i;\chi) \right)^2$, where N is the number of measurements. Due to the implicit nature of the problem, the implementation of the analysis requires numerical software, such as MatLab from MathWorks (Natick, MA, USA), which was

used in the current work. The standard deviation of χ is given by $s_{\hat{\chi}} = \sqrt{\frac{SSR(\hat{\chi})}{J^T(\hat{\chi})J(\hat{\chi})}}$, where $J(\hat{\chi})$ is the Jacobian matrix at $\hat{\chi}$ which was directly obtainable from the nonlinear least-squares routine in MatLab.

6.4.3.2 The dissolution end point method and the melting point depression method

For the dissolution end point and melting point depression methods, the experimentally uncertain variable was the melting point, and therefore, the regression problem can be formulated explicitly and can be implemented in most standard software. The residual sums-of-squares were, for these two methods, given by: $SSR(\chi) = \sum_{i=1}^{N} \left(T^{measurement}(i) - T^{fitted}(i;\chi)\right)^2$, where N is the number of measurements. However, it was observed that when the dependent variable was the melting point, the leverage of the fitted values $h_{ii} = \frac{\partial T^{fitted}(i)}{\partial T^{measurement}(i)}$ was highly variable. Points with high leverages have a larger influence on the fit, which was undesirable as all data points should contribute equally. In order to correct for this, the residuals sum-of-squares was studentized: $SSR(\chi) = \sum_{i=1}^{N} \frac{1}{\sqrt{1-h_{ii}}} \left(T^{measurement}(i) - T^{fitted}(i;\chi)\right)^2$. Due to the simpler structure of the regression problem for these two experimental methods, most software will be able to calculate studentized residuals and the standard deviation of $\hat{\chi}$ directly. For consistency, however, MatLab was also used for this regression problem.

6.4.3.3 Outlier detection

Data points that did not follow the pattern described by the Flory-Huggins model can be described as outliers. Removal of outliers from the sample can improve the power of the predictions radically. Therefore, outlier detection was done by calculating Cook's distance of the data points[151]. Points with Cook's distance larger than three times the mean Cook's distance were removed from the particular sample analysis. Upon removal, the model was refitted on the new outlier-reduced sample and the Cook's distance was recalculated. This procedure was iterated until no outliers were detected.

6.5 Results and discussion

6.5.1 Liquid analogue solubility approach

The drug–polymer solubility can be estimated from the drug solubility in a liquid low molecular weight analogue using the Flory-Huggins lattice model by assuming that the analogue constitutes the lattice of a polymer and that the interactions and combinatorial entropy of mixing in the drug–polymer systems are similar[89,91]. In this study NVP and VA were used as the analogues because they are the monomeric precursors of the PVP/VA copolymer investigated in this study and structurally identical with the repeat units after polymerization. The solubility of the different drugs in NVP and VA was obtained experimentally from HPLC analysis as described above, and the thermodynamic values used to calculate the activity coefficient in the analogues and polymers were obtained from DSC analysis. The solubility of the five different drugs in the respective PVP/VA copolymers was calculated from the solubility in the liquid NVP and VA monomers and the thermodynamic values given in Table 6.1 using Equations 6.1 and 6.2. The results are given in Table 6.2.

Table 6.1: Experimental physical and thermodynamic values of the materials measured by DSC and density measured by helium pycnometry (values are mean ± SD, n = 3).

Material	M_w (g·mol^{-1})[a]	Density (g·cm^{-3})[b]	T_g (°C)	ΔC_p (J·g^{-1}·K^{-1})	ΔH_m (J·g^{-1})
PCM	151.17	1.22 ± 0.01	23.3 ± 0.2	0.64 ± 0.04	193.5 ± 1.7
CAP	323.13	1.47 ± 0.00	29.5 ± 0.3	0.54 ± 0.02	115.1 ± 0.3
CCX	381.37	1.35 ± 0.01	56.8 ± 0.0	0.38 ± 0.02	99.4 ± 0.8
IMC	357.79	1.31 ± 0.01	45.4 ± 0.1	0.39 ± 0.01	116.7 ± 0.4
FDP	384.26	1.29 ± 0.00	45.2 ± 0.1	0.36 ± 0.01	82.6 ± 0.4
Vinylacetate	86.09	0.93 ± 0.00	-	-	-
N-vinylpyrrolidone	111.14	1.04 ± 0.00	-	-	-
PVP/VA 335	28,000	1.18 ± 0.00	68.5 ± 0.3	0.34 ± 0.01	-
PVP/VA 535	36,700	1.19 ± 0.01	91.3 ± 0.1	0.34 ± 0.02	-
PVP/VA 635	38,200	1.18 ± 0.01	105.3 ± 0.2	0.33 ± 0.02	-
PVP/VA 735	56,700	1.18 ± 0.01	117.2 ± 0.1	0.33 ± 0.02	-
PVP K17	10,000	1.20 ± 0.00	125.2 ± 0.4	0.31 ± 0.01	-

[a]Average M_w according to the supplier. [b]Amorphous density measured by helium pycnometry.

Table 6.2: Solubility of the drugs in NVP and VA and predicted solubilities in the pure polymers and the five drug-copolymer systems.

	PCM:PVP/VA 335	CAP:PVP/VA 535	CCX:PVP/VA 635	IMC:PVP/VA 735	FDP:PVP K17
Solubility in NVP at 25°C (g/g)	0.34	0.71	0.61	0.52	0.12
Predicted solubility in PVP at 25°C (g/g)	0.18	0.52	0.41	0.31	0.05
Solubility in VA at 25°C (g/g)	0.00	0.01	0.09	0.01	0.09
Predicted solubility in PVA at 25°C (g/g)	0.00	0.00	0.03	0.01	0.04
PVP/PVA ratio (w/w)[a]	30/70	50/50	60/40	70/30	100/0
Predicted solubility in PVP/VA copolymer at 25°C (g/g)	0.05	0.26	0.26	0.22	0.05

[a]Weight ratios according to supplier information.

The solubility (g/g) ranged from 0.00 for PCM in VA to 0.71 for CAP in NVP, and the solubility for all the different drugs was higher in NVP than in VA. After correcting for the reduced entropy of mixing, the predicted solubilities in the pure homopolymers (PVP and PVA) were reduced drastically compared to those in the analogues. In order to predict the solubility in the copolymer, the solubility in each of the two homopolymers was determined and multiplied by the weight fraction in the copolymer. The influence of molecular weight on the predicted solubility is negligible for high molecular weight polymers as the term that compensates for molecular weight in Equation 6.2, $\frac{1}{m_{polymer}}$ approaches zero[91].

Therefore, the solubility of the drugs in the copolymers can be compared without accounting for the difference in molecular weight of the copolymers. It is important to note that this approach provides an estimate of the solubility in the liquid state rather than in the solid glass, and therefore, should be evaluated with caution[89]. Nevertheless, this approach might still provide valuable indications on the solubility of a drug in a polymer if a liquid analogue of the polymer is available[150]. A review of the Sigma-Aldrich (St. Louis, MO, USA) product range revealed that, in addition to PVP and PVA, liquid analogues of pharmaceutically relevant polymers are available for polymethacrylates (Eudragit), poly(vinyl alcohol), poly(acrylic acid) (Carbomer), polyethylene glycol (PEG), poly(ethylene oxide), but not for cellulose ethers (e.g., hydroxypropylmethylcellulose, HPMC) and polysaccharides (e.g.. chitosan).

6.5.2 Recrystallization method

Thermodynamically, the equilibrium solubility can be measured in at least four different ways, of which the shake-flask method (applied in the liquid analogue solubility approach) is probably the most commonly used. Here the increase of solution concentration is measured from an undersaturated solution at constant temperature[80]. However, this method is impracticable for solid drug–polymer systems due to the solid nature or high viscosity of polymers. The recrystallization method approaches the equilibrium in a different but thermodynamically equal way, by measuring the *decrease* of solution concentration from a supersaturated solution at constant temperature. As this method relies on the recrystallization of the supersaturated drug from the polymer matrix, it is only feasible to determine the equilibrium solubility above the recrystallization temperature of the supersaturated system[95]. This is because reaching the equilibrium becomes increasingly more time-consuming at temperatures close to the recrystallization temperature due to decreased molecular mobility, which inhibits nucleation and crystallization[139].

Parameters including drug solubility, polymer T_g and viscosity, degree of supersaturation, and annealing temperature as well as time affect the nucleation and crystallization rate of drugs in supersaturated amorphous solid dispersions. Therefore, it is important to evaluate the drug–polymer ratio and annealing time/temperatures every time a new drug–polymer system is investigated[139]. Finding the right drug–polymer ratio is a balance between having a too unstable system that recrystallizes before the annealing temperature is reached and a too stable system that will not recrystallize during annealing. The annealing time can be established by monitoring the exothermic recrystallization event during the annealing step, and the process is considered to be in equilibrium after the signal reaches a baseline. However, as the crystallization rate decreases rapidly when the concentration approaches equilibrium solubility[116], the true equilibrium may not be reached. Nevertheless, in this study, a 3 h annealing time and 80:20 w/w ratios of drug–polymer were found to be suitable for the PCM, CAP, CCX, and FDP systems and 85:15 w/w for the IMC system.

In the original method proposed by Mahieu et al.[95], the equilibrium solubility concentration after annealing is derived from the T_g of the annealed material using the Gordon-Taylor relationship. However, in this study the composition dependence of the T_g did not correlate with the Gordon-Taylor relationship (data not shown), and therefore, this could not be used to determine the equilibrium solubility after annealing. As an alternative, the experimental composition dependence of the T_g in all systems was used to derive the equilibrium solubility concentration after annealing. Using the annealing temperature and drug fraction, the interaction parameter χ was determined from Equations 6.3 and 6.4. The T_g of the annealed materials and the corresponding equilibrium solubilities of the various drugs in the polymers are listed in Table 6.3.

Table 6.3: Summary of raw data (values are mean ± SD, *n* = 3).

	Recrystallization method									
	PCM:PVP/VA 335		**CAP:PVP/VA 535**		**CCX:PVP/VA 635**		**IMC:PVP/VA 735**		**FDP:PVP K17**	
T_a (°C)	T_g (°C)	X_{drug} (w/w)	T_g (°C)	X_{drug} (w/w)	T_g (°C)	X_{drug} (w/w)	T_g (°C)	X_{drug} (w/w)	T_g (°C)	X_{drug} (w/w)
150	-	-	-	-	72.0 ± 0.2	0.779	56.2 ± 0.1	0.834	-	-
145	-	-	-	-	74.3 ± 0.1	0.744	60.2 ± 0.4	0.765	-	-
140	-	-	-	-	76.5 ± 0.2	0.710	62.3 ± 0.7	0.726	-	-
135	45.6 ± 0.3	0.414	40.2 ± 0.3	0.772	78.0 ± 0.3	0.688	64.1 ± 0.7	0.693	55.5 ± 0.4	0.743
130	47.2 ± 0.1	0.385	44.8 ± 0.2	0.709	79.4 ± 0.1	0.666	65.5 ± 0.5	0.667	63.6 ± 0.2	0.644
125	48.0 ± 0.1	0.370	48.4 ± 0.5	0.660	-	-	67.2 ± 0.9	0.634	67.1 ± 0.1	0.601
120	49.4 ± 0.5	0.343	51.4 ± 0.5	0.619	-	-	-	-	70.2 ± 0.3	0.563
115	-	-	53.1 ± 0.1	0.595	-	-	-	-	-	-
	Dissolution end point method									
X_{drug} (w/w)	T_{end} (°C)		T_{end} (°C)		T_{end} (°C)		T_{end} (°C)		T_{end} (°C)	
0.95	172.0 ± 0.04		151.2 ± 0.03[a]		163.8 ± 0.3[a]		161.8 ± 0.02[a]		141.5 ± 0.2[a]	
0.90	171.5 ± 0.3		150.5 ± 0.1		162.8 ± 0.8		160.8 ± 0.02		140.5 ± 0.3	
0.85	169.7 ± 0.03		149.1 ± 0.1		161.1 ± 0.8		159.4 ± 0.1		139.2 ± 0.1	
0.8	168.8 ± 0.1		146.7 ± 0.1		158.3 ± 0.6		156.9 ± 0.1		137.3 ± 0.2	
0.75	168.6 ± 0.4		143.9 ± 0.04		154.5 ± 0.6		152.3 ± 0.2		134.9 ± 0.2	
0.70	167.4 ± 0.3		140.2 ± 0.5		150.1 ± 0.3		147.3 ± 0.3		132.0 ± 0.1	
0.65	165.1 ± 0.6		-		148.3 ± 0.2[a]		140.5 ± 1.2		-	
0.60	163.5 ± 0.6		-		-		132.4 ± 1.0		-	
	Melting point depression method									
X_{drug} (w/w)	T_m (°C)		T_m (°C)		T_m (°C)		T_m (°C)		T_m (°C)	
0.95	168.5 ± 0.01		148.4 ± 0.1		160.1 ± 0.04		158.3 ± 0.1		140.8 ± 0.1[a]	
0.90	167.5 ± 0.2		145.9 ± 0.1		157.6 ± 0.03		154.8 ± 0.1		139.9 ± 0.02	
0.85	166.4 ± 0.3		141.9 ± 0.4		152.2 ± 0.4		145.0 ± 0.3		138.6 ± 0.01	
0.8	164.8 ± 0.3		139.2 ± 0.3		145.5 ± 0.2		144.6 ± 0.1		138.1 ± 0.01	
0.75	159.8 ± 0.5		-		-		-		-	
0.70	156.1 ± 0.3		-		-		-		137.3 ± 0.3	
0.65	151.1 ± 0.1		-		-		-		-	
0.60	142.5 ± 0.1		-		-		-		136.9 ± 0.01	

[a]Data detected as outlier by calculation of Cook's distance and excluded[151].

After annealing, it was confirmed that only one T_g was detectable in DSC thermograms for all systems. It was possible to obtain data at annealing temperatures from 115−150 °C. At temperatures below 115 °C the time to reach equilibration exceeded the 3 h of annealing, and above 150 °C the drug concentration was not sufficient to saturate the mixture. As anticipated from the liquid analogue solubility approach, the CAP, CCX, and IMC systems exhibited the lowest degree of recrystallization and the PCM and FDP systems the highest.

6.5.3 Dissolution end point and melting point depression methods

As described in Section 6.2, it is possible to relate the magnitude of melting point depression (chemical potential reduction) to the solubility of a drug–polymer system using the Flory-Huggins model[85,86]. Pure crystalline materials melt at a temperature when the chemical potential of the crystalline and liquid states is equal. If an "impurity", such as a polymer, is added to the crystalline material, the chemical potential can be reduced compared to that of the pure crystalline material[85]. This reduction in chemical potential can be observed using DSC through detection of a depressed melting point[48,83]. For drug–polymer systems this phenomenon is observed when the dissolution of the crystalline drug into the amorphous polymer is favored by the thermodynamics of mixing due to solid state interactions between the drug and polymer[83]. Consequently, it is expected that the depression of the melting point is greater if mixing is exothermic compared to athermal or endothermic mixing and not present for immiscible systems[89].

The level of mixing of the components as well as the particle size will affect the accuracy of the DSC measurements as the dissolution requires transport of molecules into the polymer matrix. If the components are poorly mixed and contain large particles, mixing requires transport over long distances, which will result in a thermal lag. This can be accounted for by decreasing the heating rate or introducing milling of the sample to reduce the particle size and increase the level of mixing. Intensive low-temperature milling of physical mixtures can increase the drug–polymer surface interactions and reduce diffusive mixing to a point where dissolution of the crystalline drug is completed during the thermal analysis; however, milling is also known to potentially render the drug (partially) amorphous[111]. Consequently, for the dissolution end point method, a degree of amorphization is promoted, but complete amorphization should be avoided. In contrast, for the melting point depression method, as the drug–polymer solubility is derived from the chemical potential difference in the Flory-Huggins model, it is important that the drug fraction be 100% crystalline. The determination of the melting point of the crystalline drug represents the ideal case assuming that it can be obtained in an equilibrium transition state[93]. Therefore, the melting point is ideally recorded at zero heating rate[48]; however, as this is not possible in practice, the heating rate should be slow enough to induce molecular mixing. Conversely, from a practical point of view, it is also desirable to reduce the duration of the DSC run, and thus, the optimal heating rate depends on the molecular mobility of the system and, hence, the viscosity and T_g of the polymer. If the T_g of the polymer is above the temperature of

equilibrium, the molecular mobility in the polymer might be so low that mixing of the components becomes slower than the time scale of the DSC measurement[48]. Therefore, these methods to predict drug–polymer solubility are limited to polymers with a relatively low T_g. In this study, data was only recorded at temperatures above the T_g of the polymer, and a heating rate of 1 °C/min was applied as this rate was believed to be sufficiently low to induce molecular mixing while providing data relatively fast.

Finally, it is still debated whether to use the onset or end point values of melting to determine the Flory-Huggins interaction parameter. While both methods are still being applied, the end point is currently most commonly used to determine the solubility of drugs in polymers in the literature[48,82,89,91,94,145]. The underlying argument is that this value represents the melting point of the final composition, assuming that complete mixing has occurred[48,83,149]. Nevertheless, more research is needed in order to ultimately determine what the most appropriate method is. Therefore, in this study both the onset and end point values were obtained from the two different methods and compared. The data obtained from the two different methods can be found in Table 6.3, and the interaction parameter χ from the dissolution end point and melting point depression was derived directly from the data by applying Equations 6.3 and 6.4. From Table 6.3 it can be seen that both methods demonstrated some degree of melting point depression, suggesting that all systems were miscible. As expected, the onset values were lower than the end point values using the two different methods. However, for the FDP:PVP K17 system the onset values were higher than the end point values, indicating a discrepancy. As both methods use the same heating rate, this discrepancy could be due to the intimate milling (and perhaps partial amorphization) applied in the dissolution end point method.

6.5.4 Comparison of the different methods

The predicted solubility at 25 °C of the five drug-copolymer systems using the four different methods can be found in Figure 6.1 and Table 6.4 along with χ values and 95% prediction intervals. Note that the estimates from the liquid analogue solubility approach do not include a 95% prediction interval. This is because the estimates were based on a single-point determination obtained at 25 °C and thus not obtained from extrapolation. Representative equilibrium solubility curves of the IMC:PVP/VA 735 system using the data obtained from the three different thermal analysis methods are shown in Figure 6.2. As the value of χ is influenced by all factors in the Flory-Huggins model, it is not comparable between the different systems or methods. Therefore, the evolution of the solubility curve or the predicted solubility at 25 °C rather than χ should be used for comparison. The predicted solubilities at 25 °C vary considerably depending on whether (dissolution) end point or (melting point depression) onset values are used. Defining which of the methods is better requires more effort to understand the difference in detail and is beyond the scope of the current work; however, this is certainly something which should be considered when selecting experimental method.

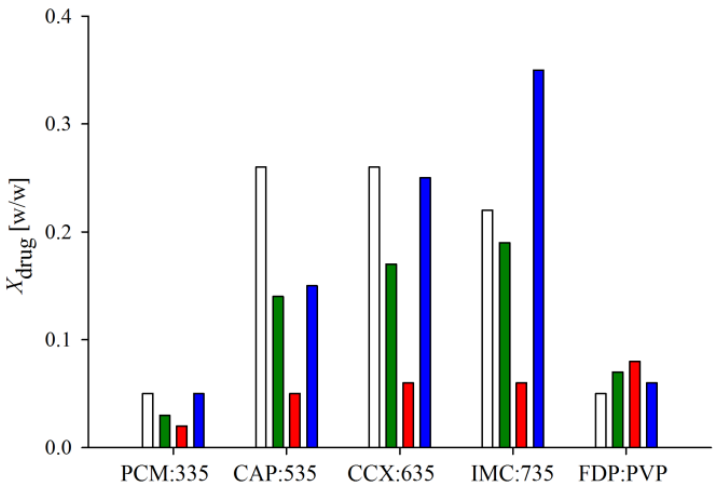

Figure 6.1: Graphical illustration of the drug–polymer solubilities of the five systems predicted from the four different methods presented in Table 6.4. The white bars represent the liquid analogue solubility approach, the green bars represent the recrystallization method, the red bars represent the dissolution end point method, and the blue bars represent the melting point depression method.

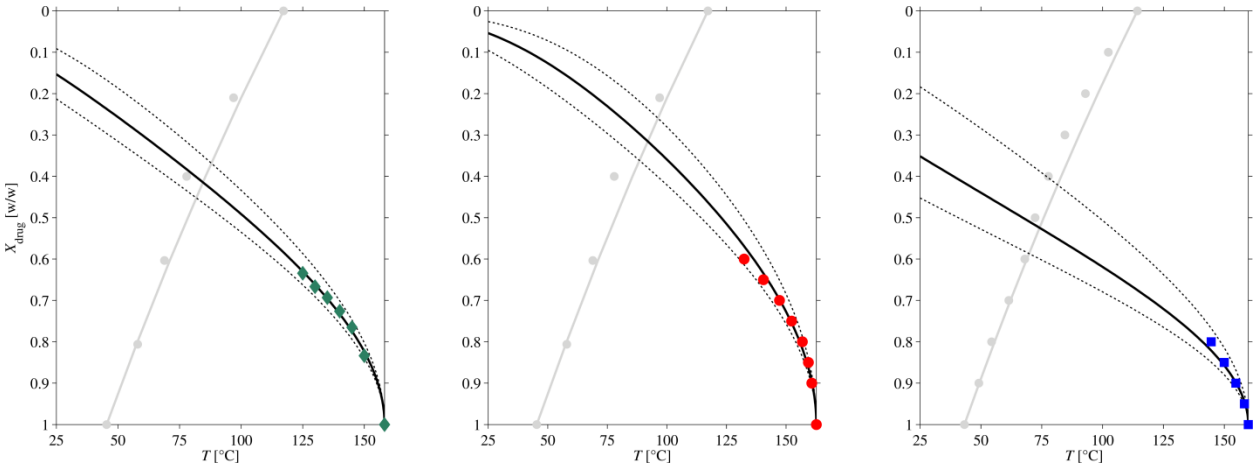

Figure 6.2: Representative equilibrium solubility curves of IMC (X_{drug}) in PVP/VA 735 as a function of temperature (T) from the three different thermal analysis methods. Green diamonds (♦) represent the data from the recrystallization method, red circles (●) represent the data from the dissolution end point method, and blue squares (■) represent the data from the melting point depression method. All data points are illustrated as averages (n = 3). The evolution of solubility of the three data sets has been fitted with the Flory-Huggins model (black curves) including the 95% prediction interval (dotted curves). The gray circles (●) represent the experimental relationship between T_g and X_{drug} and the gray curve is the theoretical Gordon-Taylor relationship.

Table 6.4: Drug–polymer solubilities of the five systems predicted from the four different methods along with the Flory-Huggins interaction parameter χ and the 95% prediction interval.

	PCM:PVP/VA 335	CAP:PVP/VA 535	CCX:PVP/VA 635	IMC:PVP/VA 735	FDP:PVP K17
Values predicted from the liquid analogue solubility approach					
Predicted solubility in PVP/VA copolymer at 25 °C (g/g)	0.05	0.26	0.26	0.22	0.05
Values predicted from the recrystallization method					
Interaction parameter χ	-1.2 ± 0.3	-4.1 ± 1.0	-5.2 ± 0.9	-6.3 ± 1.6	-2.2 ± 0.6
Solubility at 25 °C (g/g)	0.03	0.14	0.17	0.19	0.07
95% prediction interval at 25 °C	0.02-0.04	0.08-0.20	0.12-0.21	0.11-0.25	0.04-0.10
Values predicted from the dissolution end point method					
Interaction parameter χ	-0.6 ± 0.9	-1.9 ± 0.8	-2.9 ± 1.6	-2.9 ± 0.9	-1.4 ± 0.6
Solubility at 25 °C (g/g)	0.02	0.05	0.06	0.06	0.08
95% prediction interval at 25 °C	0.01-0.04	0.03-0.09	0.01-0.14	0.03-0.10	0.05-0.12
Values predicted from the melting point depression method					
Interaction parameter χ	-1.3 ± 0.8	-3.9 ± 1.8	-5.7 ± 1.1	-8.8 ± 3.7	-1.5 ± 3.0
Solubility at 25 °C (g/g)	0.05	0.15	0.25	0.35	0.06
95% prediction interval at 25 °C	0.02-0.09	0.05-0.26	0.19-0.31	0.18-0.45	0.00-0.25

From Figure 6.1 and Table 6.4 it is evident that the recrystallization and melting point depression methods rank the predicted solubility in the same order, IMC:PVP/VA 735 > CCX:PVP/VA 635 > CAP:PVP/VA 535 > FDP:PVP K17 > PCM:PVP/VA 335. Except for the FDP:PVP K17 system, this ranking is identical to the predicted solubility obtained from the dissolution end point method, but different from that predicted by the liquid analogue solubility approach. However, the magnitude of the predicted solubilities from the recrystallization method and melting point depression methods correlated well with the predictions from the liquid analogue

solubility approach. This suggests that this method can be used to screen for drug solubility in polymers if a liquid analogue is available. The solubility predictions at 25 °C based on the recrystallization method were consistently higher than the predictions based on dissolution end point method (except for FDP:PVP K17). This difference was to some extent expected, as the thermodynamics behind the two methods are fundamentally different. The recrystallization method approaches equilibrium solubility from the supersaturated state, and the equilibrium thermodynamics are driven by recrystallization kinetics. In contrast, the dissolution end point method approaches equilibrium solubility from an undersaturated state and the equilibrium thermodynamics are thus driven by dissolution kinetics.

In addition to being dependent on temperature and viscosity[91], the recrystallization and dissolution kinetics slow down when the concentration approaches equilibrium solubility. In fact, the recrystallization kinetics may be so slow that it is not detectable in the DSC, and therefore, the system can falsely be considered in equilibrium[139]. This could give a reason to believe that the recrystallization method might be overestimating the solubility. Furthermore, as the dissolution end point method relies on dissolution kinetics that are expected to be slower than recrystallization kinetics[95], an underestimation of the solubility is expected. It is therefore rational to assume that the true solubility is somewhere between that predicted by the recrystallization and dissolution end point methods. Even though this is a hypothesis left unverified in this study, it could explain why the predicted solubility was consistently higher when using the recrystallization method compared to the dissolution end point method. A way of limiting the predicted error is to increase the annealing time and lower the heating rate to allow for equilibrium to be reached for the recrystallization method and dissolution end point method, respectively. However, due to the previously mentioned slow kinetics, this would drastically increase the duration of the experiments and probably not impact the solubility prediction significantly.

In the case of the melting point depression method, the evaluation of the prediction is more complex. As the method is not based on equilibrium thermodynamics, it is difficult to say whether the method is under- or overestimating the solubility. However, this could be investigated by annealing the sample at the determined T_m until equilibrium has been reached and subsequent scanning for a residual dissolution endotherm, as proposed by Sun et al.[80]. The presence of a dissolution endotherm after annealing indicates that the dissolution is not completed and that the "true" T_m is located above the annealing temperature. This approach is very time-consuming and is therefore laborious compared to the methods used in this study. Due to the nature of the method and as the solubility data from the melting point depression method was not significantly different from that of the recrystallization method, it is expected that the melting point depression method is also likely to overestimate solubility. The advantages and disadvantages of the four different methods are summarized in Table 6.5.

Table 6.5: Advantages and disadvantages of the four different methods.

	Advantages	**Disadvantages**
Liquid analogue solubility approach	Simple shake-flask method Measures at room temperature Enables multiple screening	Requires liquid analogue Predicts the solubility in a liquid rather than a solid
Recrystallization method	Heating rate independent Applicable for most polymers with $T_g \gtrsim 90$ °C[a]	Time-consuming May overestimate solubility
Dissolution end point method	Applicable for most polymers with $T_g \lesssim 120$ °C[a] Relatively fast	Heating rate and milling condition dependent May underestimate solubility Not applicable if drug is thermally decomposed at T_m
Melting point depression method	Applicable for most polymers with $T_g \lesssim 120$ °C[a] Relatively fast	Heating rate dependent May overestimate solubility Requires 100% crystallinity Not applicable if drug is thermally decomposed at T_m

[a]Estimation based on a general assumption of the T_m (>140 °C) and T_g (<70 °C) of low molecular weight drugs[27].

The negative χ value, signifying miscibility predicted for all systems in this study, is, to some extent, also supported by the experimental deviation from the theoretical Gordon-Taylor relationship as mentioned previously (data not shown). The Gordon-Taylor relationship is based on ideal mixing behavior (additivity) of the two components. Deviations from the ideal behavior are the result of entropy effects beyond combinatorial mixing such as strong intermolecular interactions[152]. As cohesive intermolecular interactions (e.g. hydrogen bonds) favor miscibility[83], it is rational to assume that strong/numerous interactions indicate good miscibility between the components. As can be derived from the data presented in Table 6.4, the predictions based on the recrystallization method were more precise (relatively) than the predictions based on the melting point depression and dissolution end point methods. This is probably a result of the nature of these methods as the interaction parameter is more sensitive to experimental uncertainty, at temperatures closer to the melting point of the pure drug. Even a small change in the melting temperature will have a large impact on χ and thus also the curve fitting and predicted solubility at 25 °C. Therefore, it is recommended that data points are only obtained for compositions lower than 90% drug. Conversely, at lower drug contents the dissolution kinetics can potentially exceed the time scale of the experiment depending on heating rate. In order to account for thermal lag and the influence of the heating rate on the phase equilibrium temperature, Tao et al.[48] proposed an extrapolation of the temperature to zero heating rate. However, the validity and

linearity of these extrapolations has still not been confirmed. Generally for a glass solution to be pharmaceutically relevant, the drug–polymer solubility should ideally be higher than 20% w/w at typical storage temperatures[14]. Consequently, based on the findings of this study, a decision tree for the screening of polymers suitable for glass solutions has been proposed in Figure 6.3. It is important to emphasize that the decision tree is designed for the selection of polymers suitable for glass solutions only and thus do not regard considerations of kinetic stability. This means that polymers classified as unsuitable for glass solutions according to the decision tree are not necessarily also unsuitable for (kinetically stabilized) solid dispersions.

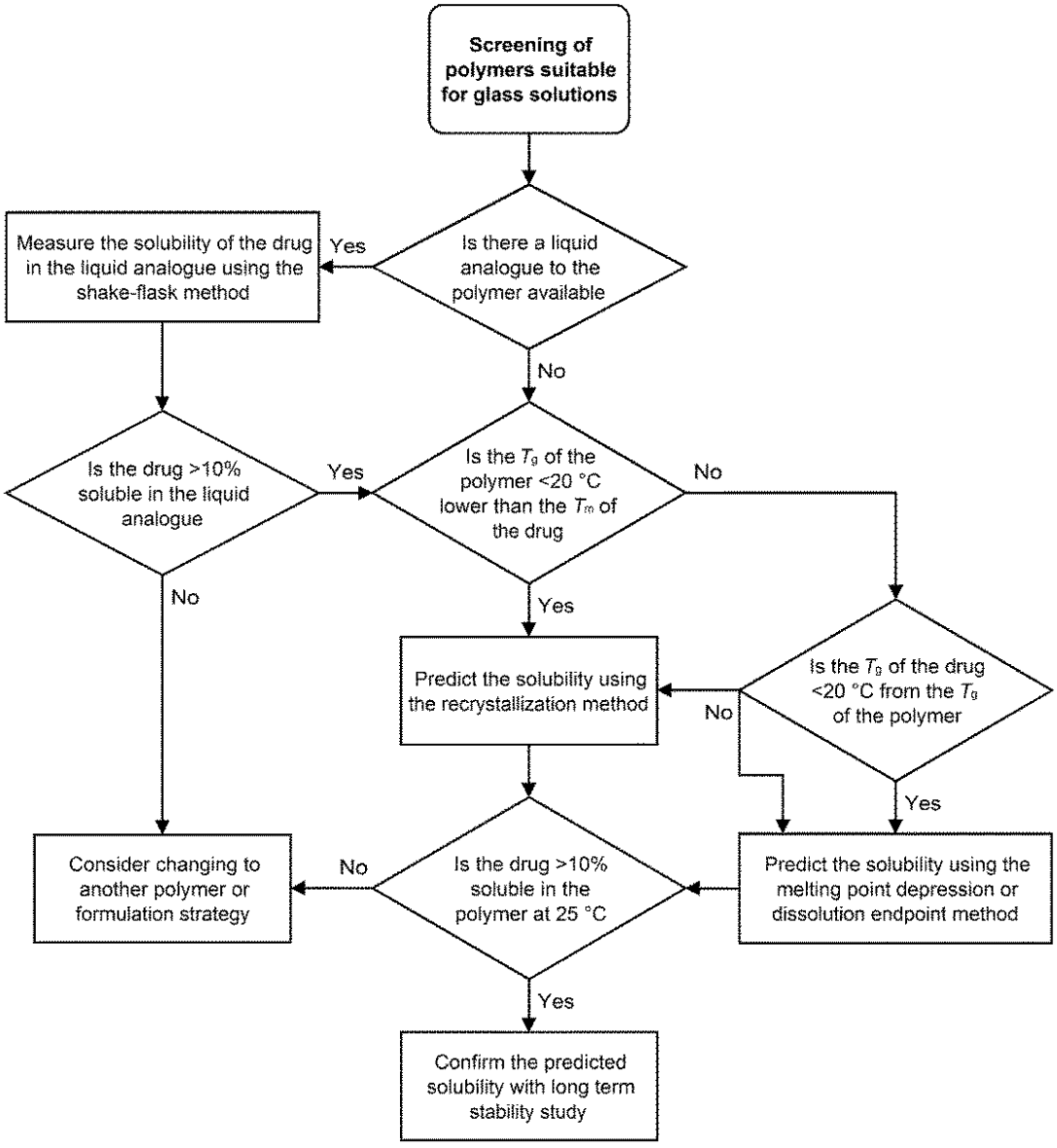

Figure 6.3: Decision tree for the screening of polymers suitable for glass solutions including the selection of the most optimal methods to predict drug–polymer solubility. Please note that this does not regard considerations of kinetic stability.

The proximity of the Hildebrand solubility parameter of the drug to that of the copolymer (±7.5 $MPa^{1/2}$) has been proposed to indicate miscibility between the compounds[153]. This could potentially give valuable indications on the drug–polymer solubility and speed up the screening process (by excluding unpromising polymers early in the screening). However, no direct correlation between the proximity of the Hildebrand solubility parameter and drug–polymer or drug–analogue solubility was found in this study (data not shown). Therefore, it is recommended that the screening be initiated by determining the solubility in liquid analogues of pharmaceutically relevant polymers if available. If the drug is not freely soluble (<10% w/w) in an analogue of the polymer, it is most likely also not soluble in the polymer, and therefore, a change to a structurally different polymer should be considered. Having established the most promising polymer candidates from the liquid analogue solubility approach, the solubility of the drug in the polymers can now be predicted from one or more of the three thermal analysis methods. Which of these three different thermal analysis methods are optimal for the prediction of drug–polymer solubility is dependent on the thermal properties of both the drug and polymer. If the T_g of the polymer is higher than the T_m of the drug or the difference between the T_m of the drug and T_g of the polymer is less than 20 °C, the mixing of the components might be slower than the time scale of the DSC measurement, and therefore, the recrystallization method should be used. On the other hand, if the difference between T_g of the polymer and the T_g of the drug is less than 20 °C, the experimental composition dependence of the T_g might not be sufficient to derive the equilibrium solubility concentration with satisfactory precision after annealing. In this case, it is recommended that drug–polymer solubility be predicted from the dissolution end point or melting point depression method. If none of the above restrictions apply, all three thermal analysis methods can be used to predict the drug–polymer solubility. As mentioned previously an overestimation of the solubility should be expected when using the recrystallization and melting point depression methods and an underestimation should be expected when using the dissolution end point method. The data obtained at elevated temperature from the thermal analysis method(s) is then fitted with the Flory-Huggins model and extrapolated in order to predict the solubility at ambient temperature. If the drug is not freely soluble (>10% w/w) in the polymer, then a change to another polymer or formulation strategy should be considered. Finally, for the most promising polymer(s), the drug–polymer solubility can be confirmed with long-term stability at dry conditions at room temperature.

6.6 Conclusions

In this work, a comparative study of different methods to predict drug–polymer solubility was carried out. The drug–polymer solubility at 25 °C was predicted by extrapolation of data obtained at elevated temperature using the Flory-Huggins model. The predictions from the recrystallization and melting point depression methods provided similar predictions that were consistently higher than the predictions made from the dissolution end point method. Furthermore, the recrystallization method provided smaller confidence intervals of the

predictions (relatively) compared to the dissolution end point and melting point depression methods due to a better fit of the obtained data to the Flory-Huggins model. All methods could successfully produce data with satisfactory reproducibility that fitted relatively well with the Flory-Huggins model, and thus, no limitations to the methods were discovered. The learnings of this comparative study provided a general guidance for the selection of the most suitable thermal analysis method for the screening of drug–polymer solubility. However, defining which of the thermal analysis methods is superior requires more effort to understand in detail and will have to be investigated in future work.

Chapter 7

Influence of PVP/VA copolymer composition on drug–polymer solubility

7.1 Abstract

In this study, the influence of copolymer composition on drug–polymer solubility was investigated. The solubility of the model drug celecoxib (CCX) in various polyvinylpyrrolidone/vinyl acetate (PVP/VA) copolymer compositions (70/30, 60/40, 50/50 and 30/70 w/w) and the pure homopolymers polyvinylpyrrolidone (PVP) and polyvinyl acetate (PVA) was predicted at 25 °C using a thermal analysis method based on the recrystallization of a supersaturated amorphous dispersion (recrystallization method). These solubilities were compared with a prediction based on the solubility of CCX in the liquid monomeric precursors of PVP/VA, N-vinylpyrrolidone (NVP) and vinyl acetate (VA), using the Flory-Huggins lattice theory (liquid monomer solubility approach). The solubilities predicted from the liquid monomer solubility approach increased linearly with increasing VP/VA ratio from 0.03–0.60 w/w. Even though the solubilities predicted from the recrystallization method also increased with increasing VP/VA ratio from 0.02–0.40 w/w, the predicted solubility seemed to approach a plateau at high VP/VA ratios. Increasing positive deviations from the Gordon-Taylor equation with increasing VP/VA ratio indicated strong interactions between CCX and the VP repeat unit, which was in accordance with the relatively high solubilities predicted using both methods. As the solubility plateau may be a consequence of steric hindrance caused by the size differences between CCX and the VP repeat units, it is likely that a CCX molecule interacting with a VP repeat unit hinders another CCX molecule from binding to the neighboring repeat units in the polymer chain. Therefore, it is possible that replacing these neighboring hygroscopic VP repeat units with hydrophobic VA repeat units, could increase the physical stability of an amorphous solid dispersion without compromising the drug–polymer solubility. This knowledge could be used advantageously in future development of amorphous drug delivery systems as copolymers could be customized to provide optimal drug–polymer solubility and physical stability.

7.2 Introduction

An increasing number of new drug candidates have poor aqueous solubility, which makes them unsuitable for oral administration in conventional formulations hence, strategies that overcome this challenge are strongly needed[7,39]. A well-known approach is to utilize the amorphous form of the drug, which is advantageous compared to its crystalline counterpart due to a higher apparent solubility, faster dissolution rate, and enhanced oral bioavailability[10,12,41]. However, amorphous solids are thermodynamically unstable and tend to convert to a more stable

crystalline state during preparation and storage, which will neutralize the aforementioned advantages[9,144,154]. This crystallization process can to some extent be inhibited by incorporation of a polymer into the formulation (amorphous solid dispersion)[78,111] but the thermodynamic stability of such a formulation can only be ensured if the drug is soluble in the polymer and the drug concentration is below its equilibrium solubility (glass solution)[139]. Thus, determining the solubility of the drug in the polymer is critical for the development of stable amorphous drug delivery systems.

The high viscosity of polymers makes it practically difficult to obtain solubility equilibria of drugs at room temperature[48]. Therefore, several methods based on differential scanning calorimetry (DSC) have been proposed to predict drug–polymer solubility at room temperature from solubility determination at elevated temperatures[48,83,89]. In a recently proposed protocol[95], referred to as the recrystallization method[155], a supersaturated amorphous solid dispersion is annealed at temperatures above its glass transition temperature (T_g) to recrystallize excess drug and reach equilibrium solubility. The solubility after annealing is then derived from the T_g of the annealed material using the Gordon-Taylor equation[156] and extrapolated to ambient temperature using the Flory-Huggins model[85]. However, previous studies have shown that the experimental composition dependence of the T_g is not always consistent with the prediction from the Gordon-Taylor equation[154,157,158]. Consequently, in order to avoid erroneous solubility predictions, the experimental composition dependence of the T_g should be established before applying the Gordon-Taylor equation in the recrystallization method[155]. As the confidence of the prediction in these DSC methods may be compromised by the large temperature extrapolation, another approach has been proposed, which can estimate the drug–polymer solubility based on measurements at ambient temperature. In this approach, the drug–polymer solubility is estimated from the drug solubility in a liquid monomeric precursor of the polymer at room temperature from the Flory-Huggins lattice theory, assuming that the interactions and combinatorial entropy of mixing in the drug-monomer and drug–polymer systems are identical[89,91]. Consequently, this method can give valuable indications on the drug–polymer solubility and enable a screening of polymers suitable for amorphous solid dosage forms.

The properties of an amorphous solid dispersion are defined by the polymer matrix. Besides stabilizing the drug in the solid state, polymers have also been shown to enhance the solubility and dissolution rate, and inhibit crystallization of the supersaturated drug upon dissolution. Therefore, the choice of polymer will have a major influence on the dissolution behavior and physical stability of amorphous solid dispersions[11,19]. The polymer, polyvinylpyrrolidone (PVP), is one of the most commonly used polymers for amorphous solid dispersion formulations due to its ability to stabilize amorphous drugs and inhibit recrystallization upon dissolution[159]. However, as the repeat unit vinylpyrrolidone (VP) in PVP is highly hygroscopic it will absorb water vapor from the air, which will compromise the kinetic stability of the amorphous solid dispersions during storage due to the plasticizing nature of water[160-162]. Therefore, it is possible that the physical stability can be increased by replacing some of the hygroscopic VP repeat units with hydrophobic repeat units e.g. vinyl acetate (VA) as is the case in polyvinylpyrrolidone/vinyl

acetate copolymers (PVP/VA) (Prudic et al., 2014). Even though this in theory would increase the physical stability, the pure homopolymer of VA, polyvinyl acetate (PVA), has been shown to be a very ineffective crystallization inhibitor upon dissolution[159]. However, according to Matsumoto and Zografi[118] the crystallization inhibition of PVP is not decreased when some of the VP repeat units are replaced by VA; rather it seems that a minimum number of VP repeat units needs to be accessible to the drug molecules in order to ensure crystallization inhibition[118]. Thus, partial replacement of VP with hydrophobic VA repeat units may likely increase the physical stability of an amorphous solid dispersion without the loss of the crystallization inhibitory effect of VP[163]. Previous studies have shown that the drug–polymer solubility of indomethacin, naproxen and nifedipine in polyvinyl acetate (PVA) is lower than in PVP indicating that the introduction of the VA repeat units in PVP may influence the drug solubility negatively[80,81]. As the desirable drug loadings for amorphous solid dispersions should be above 20%[14] to maintain a cost efficient drug delivery system, this could severely limit the usability of these copolymers for pharmaceutical purposes. Therefore, the aim of this study was to investigate the influence of copolymer composition on drug–polymer solubility. The solubility of the model drug celecoxib (CCX) in PVP, PVA and PVP/VA copolymers of different compositions (70/30, 60/40, 50/50 and 30/70 w/w) was predicted using the recrystallization method and compared with an estimation based on the solubility of CCX in the liquid monomeric precursors to the copolymer (NVP and VA).

7.3 Experimental section

7.3.1 Materials

Celecoxib (CCX, M_w = 381.37 g/mol) was purchased from Astatech, Inc. (Bristol, PA, USA). N-vinylpyrrolidone (NVP, M_w = 111.14 g/mol) and vinyl acetate (VA, M_w = 86.09 g/mol) were purchased from Sigma-Aldrich Co. (St. Louis, MO, USA). PVP/VA copolymer E-335 (PVP/VA 335, M_w = 28,000 g/mol), PVP/VA copolymer E-535 (PVP/VA 535, M_w = 36,700 g/mol), PVP/VA copolymer E-635 (PVP/VA 635, M_w = 38,200 g/mol), and PVP/VA copolymer E-735 (PVP/VA 735, M_w = 56,700 g/mol) were kindly supplied by Ashland Chemical Co. (Columbus, OH, USA). Kollidon® 12 PF (PVP, M_w = 2500 g/mol) was kindly supplied from BASF (Ludwigshafen, Germany) and polyvinyl acetate (PVA, M_w = 40,000 g/mol) was purchased from VWR Chemicals (Leuven, Belgium). The PVP/VA copolymers were received as 50% (w/w) solutions in ethanol and were therefore dried to powders by spray drying before use. Before spray drying, the solutions were diluted with ethanol to 5% (w/w) polymer concentration and processed using the B-290 Mini Spray Dryer from Büchi (Flawil, Switzerland). Air was drawn through the open-loop system with an aspirator rate at 100%, a temperature of 140 °C and the pump speed set to 30%, which resulted in an outlet temperature of approximately 80 °C. PVA was received as beads and was therefore powdered using a Tube Mill control (at 10,000 rpm) from IKA® (Staufen, Germany) and sieved through a 0.4 mm sieve. The resulting powders were stored in air-tight vials until use.

7.3.2 Particle density

The amorphous densities of CCX and all polymers were determined using an AccuPyc 1330 helium pycnometer from Micromeritics Instruments Corp. (Norcross, GA, USA). Samples of approximately 1 g were melt-quenched in an APT.line model ED 53 electrical furnace from Binder GmbH (Tuttlingen, Germany) at 150 °C for 15 min in order to remove any sorbed water and yield the amorphous form. Before density measurements, the samples were weighed and then transferred to the sample holder in the pycnometer and purged with 19.5 psig dry helium to measure the powder volumes. The reported results were averages of 10 consecutive measurements.

7.3.3 X-ray powder diffraction (XRPD)

The solid-state properties of the pure materials and amorphous solid dispersions were analyzed using X-ray powder diffraction (XRPD). The analyses were performed using an X'Pert PRO MRD diffractometer from PANalytical (Almelo, The Netherlands) equipped with a TCU 100 temperature control unit and an X'Celerator detector using nickel-filtered CuKα radiation (λ = 1.5406 Å) at 45 kV and 40 mA. Approximately 1 mg of sample powder was placed on zero background (0-BG) Si-plates and measured over the angular range 3–40 °2θ at a scanning rate of 1.20 °2θ/min. The diffractograms were analyzed using the X'Pert Data Viewer (version 1.2) software.

7.3.4 Differential scanning calorimetry (DSC)

The pure components and amorphous solid dispersions were analyzed using a Q2000 DSC from TA Instruments Inc. (New Castle, DE, USA). Samples of 2–4 mg were weighed into Tzero aluminum hermetic pans with a perforated lid and scanned at a rate of 5 °C/min from − 10–200 °C under 50 mL/min nitrogen gas purge. Calibration of temperature and enthalpy were performed by using an indium standard and the heat capacity was calibrated using a sapphire standard. The melting temperature (T_m, onset), melting enthalpy (ΔH_m), glass transition temperatures (T_g, inflection point), and the heat capacity change over the glass transition (ΔC_p) were determined using the automated tools in the Universal Analysis 2000 (version 4.5 A) software.

7.3.5 Solubility in the liquid monomers

The solubility of CCX in the liquid monomers and mixtures of NVP and VA (70/30, 60/40, 50/50, 30/70 w/w) was determined using the shake-flask method. Approximately 750 mg crystalline CCX was added to a 4 mL (14.7 x 45 mm) capped glass tube and 1 mL of the pure monomers or mixtures were added and shaken for 72 h at 25 °C using a mechanical rotor from Heto Lab Equipment (Birkerød, Denmark). The sample was then filtered using a 0.20 μm PTFE

hydrophobic syringe filter from Millipore (Carrigtwohill, Co. Cork, Ireland) and diluted 1:2000 with mobile phase (see below):acetonitrile (50:50 v/v). The diluted sample was assayed using a HPLC system comprised of a L-7100 pump, a L-7200 auto sampler, a T-6000 column oven, and a D-7000 interface, all from Merck-Hitachi LaChrom (Tokyo, Japan). A reverse phase X-Bridge C-18 column (4.6 x 150 mm, 3.5 µm) from Waters (Milford, MA, USA) was used for the separation and the mobile phase consisted of methanol:0.0025 M potassium dihydrogen phosphate aqueous buffer pH 6.0 (65:35 v/v). A variable wavelength ultraviolet L-7450A diode array detector from Merck-Hitachi LaChrom (Tokyo, Japan) was used to detect signals at 250 nm after 8.50 min retention time.

7.3.6 Composition dependence of the glass transition temperature

Physical mixtures of 100 mg were prepared in concentrations ranging from 10–90% w/w CCX and milled with a mortar and pestle to uniformity. The mixtures and the pure components were then analyzed for their T_g by DSC. Samples of 2–4 mg were *in situ* melt-quenched by heating to 170 °C, kept isothermal for 2 min and subsequently rapidly cooled to − 10 °C. The samples were then scanned at a rate of 5 °C/min from − 10–200 °C to determine the T_g of the amorphous mixture. The relationship between T_g and composition within a given T_g interval was then found by linear regression between the two experimental data points and used to determine the composition of the annealed material from the measured T_g.

7.3.7 Recrystallization method

Supersaturated amorphous solid dispersions were prepared by melt-quenching. Physical mixtures of crystalline CCX in the copolymers (75–85% w/w CCX) were prepared and placed on aluminum foil covered with PTFE extruded film tape (50.8 mm) from 3M (Saint Paul, NM, USA) and melted in an APT.line model ED 53 electrical furnace from Binder GmbH (Tuttlingen, Germany) at 168 °C for 2 min. The mixture was then removed from the furnace, cooled and pulverized using a mortar and pestle. The resulting powders were sieved through a 0.4 mm sieve and stored in air-tight vials until use. The supersaturated amorphous solid dispersions were then annealed at different temperatures (120–150 °C) for 3 h in the DSC, cooled to – 10 °C at a cooling rate of 50 °C/min and subsequently ramped at a heating rate of 5 °C/min to 200 °C to determine the T_g of the demixed material. Experimental data points were obtained in triplicate at 5 °C intervals within the measureable range.

7.3.8 Statistical analysis

The Flory-Huggins model (Equation 7.4) was used to model the measurements of the T_g for various annealing temperatures (T_a). The optimal fit with χ as an adjustable parameter was found by regression analysis as previously described by Knopp et al.[139]. The predicted solubilities at 25

°C were subsequently compared by a multiple comparison test using the Bonferroni correction to control the simultaneous familywise error rate and a *p*-value below 0.05 was considered statistically significant.

7.4 Theoretical considerations

7.4.1 Estimation of drug–polymer solubility from liquid monomer solubility

A polymer is synthesized from monomeric precursors and the properties of these monomeric precursors (e.g. solubility) can be translated into properties of the repeat units in the polymer lattice by assuming that the interactions and combinatorial entropy of mixing are similar in the drug–monomer and the drug–polymer system[91]. It is possible to estimate the drug–polymer solubility from the drug–monomer solubility using the expressions derived from the Flory-Huggins lattice theory[85,164]. The activity coefficient in a monomer (γ_{monomer}) is the ratio of ideal mole fraction solubility (X_{id}) and the experimental mole fraction solubility of drug in the monomer (X_{drug}). The X_{drug} in the monomer is obtained experimentally from HPLC analysis as described previously and X_{id} is calculated using[91]:

$$\ln(X_{\text{id}}) = -\frac{\Delta H_m \cdot (T_m - T)}{R \cdot T_m \cdot T} + \frac{\Delta C_p \cdot (T_m - T)}{R \cdot T} - \frac{\Delta C_p}{R} \cdot \ln\left(\frac{T_m}{T}\right) \qquad (7.1)$$

where ΔH_{m} is the melting enthalpy of the drug, T_{m} is the melting point of the drug, ΔC_{p} is the heat capacity change over the glass transition of the amorphous drug, R is the gas constant, and T is the temperature at which the solubility estimate is desired. The γ_{monomer} can now be used to calculate the activity coefficient in the polymer (γ_{polymer}) at the solubility limit using[89]:

$$\ln(\gamma_{polymer}) = \ln(\gamma_{monomer}) + \frac{MV_{drug}}{MV_{monomer}}\left[\frac{1}{m_{drug}}\ln\left(\frac{v_{drug}}{X_{drug}}\right) + \left(\frac{1}{m_{drug}} - \frac{1}{m_{polymer}}\right) \cdot v_{polymer}\right] \qquad (7.2)$$

where MV_{drug} and $MV_{monomer}$ are the molar volume of drug and monomer, respectively, m_{drug} and m_{polymer} are the ratio of the volume of drug and polymer to the monomer, respectively, and v_{drug} and v_{polymer} are the volume fraction of drug and polymer, respectively. Finally, the mole fraction solubility of crystalline drug in the polymer can be derived from the ratio of X_{id} to γ_{polymer} and converted to mass fraction (w/w) for comparison with the experimentally determined solubility.

7.4.2 Composition dependence of the glass transitions temperature

The Gordon-Taylor equation can be used to predict the T_g of a drug–polymer mixture as a function of the composition:

$$T_g(X_{drug}) = \frac{X_{drug} \cdot T_{g(drug)} + K \cdot (1 - X_{drug}) \cdot T_{g(polymer)}}{X_{drug} + K \cdot (1 - X_{drug})} \tag{7.3}$$

where $T_{g\ (drug)}$ and $T_{g\ (polymer)}$ are the T_g for the pure drug and polymer, respectively, X_{drug} is the weight fraction of the drug in the mixture and K is ratio of the heat capacity change over the glass transition (ΔC_p) of the polymer to the drug[165].

7.4.3 Prediction of drug–polymer solubility from recrystallization method

Drug–polymer solubility was measured at elevated temperatures using the protocols described in the Section 7.2.7. The data sets were fitted with the Flory-Huggins model in order to predict the solubility at ambient temperature by extrapolation[85]:

$$\frac{\Delta H_m}{R} \cdot \left(\frac{1}{T_m} - \frac{1}{T_a} \right) = \ln\left(v_{drug}\right) + \left(1 - \frac{1}{\lambda}\right) \cdot (1 - v_{drug}) + \chi \cdot \left(1 - v_{drug}\right)^2 \tag{7.4}$$

where ΔH_m is the melting enthalpy of the drug, T_m is the melting point for the drug, R is the gas constant, λ is the molar volume ratio of the polymer to the drug, and χ is the Flory-Huggins interaction parameter. T_a is the annealing temperature, and v_{drug} is the volume fraction of drug derived from:

$$v_{drug} = \frac{\dfrac{X_{drug}}{\rho_{drug}}}{\dfrac{X_{drug}}{\rho_{drug}} + \dfrac{1 - X_{drug}}{\rho_{polymer}}} \tag{7.5}$$

where ρ_{drug} and $\rho_{polymer}$ are the densities of drug and polymer respectively, and X_{drug} is the weight fraction of drug.

7.5 Results

7.5.1 X-ray powder diffraction (XRPD)

Figure 7.1 shows the XRPD powder diffraction patterns of crystalline and amorphous CCX, PVP/VA 335 and the CCX:PVP/VA 335 (75:25 w/w) amorphous solid dispersions before and after annealing. The diffractograms for all the pure polymers and amorphous solid dispersions had similar patterns, and therefore only representative scans of PVP/VA 335 and CCX:PVP/VA 335 (75:25 w/w) are presented in the figures. The pattern from crystalline CCX (Figure 7.1a) consists of sharp and well-defined Bragg peaks at 5.4, 10.7, 16.1, 21.5 and 27.0 °2θ, characteristic for the stable crystal form III of CCX[166]. In contrast, the patterns obtained from amorphous CCX (Figure 7.1b) and PVP/VA 335 (Figure 7.1c) showed no Bragg peaks, but a diffuse halo characteristic for an amorphous substance. After preparation, the CCX:PVP/VA 335 (75:25 w/w) system (Figure 7.1d) was completely amorphous, which suggests that the melt-quenching process was capable of producing supersaturated amorphous solid dispersions with no detectable crystalline content. In order to determine whether the CCX:PVP/VA 335 (75:25 w/w) systems were homogenous, DSC scans were performed (see below). After annealing of the CCX:PVP/VA 335 (75:25 w/w) for 3 h at 135 °C (Figure 7.1e) the diffractogram showed that the sample was still mostly amorphous, but Bragg peaks observed at 13.9 16.1, 20.7, 21.5 and 25.8 °2θ indicated that during annealing CCX crystallizes into a mixture of form II and III[166]. A previous study has shown that the presence of crystallites, regardless of the polymorphic form, can cause segregation in the amorphous phase of semi-crystalline polymers. This could affect the T_g measurements and would be reflected in a T_g-distribution or two separate T_gs rather than a single T_g[167]. However, as the polymers used in this study (PVP, PVP/VA and PVA) were fully amorphous and only a single T_g was observed after annealing, it appears that the crystalline CCX did not affect the T_g measurements.

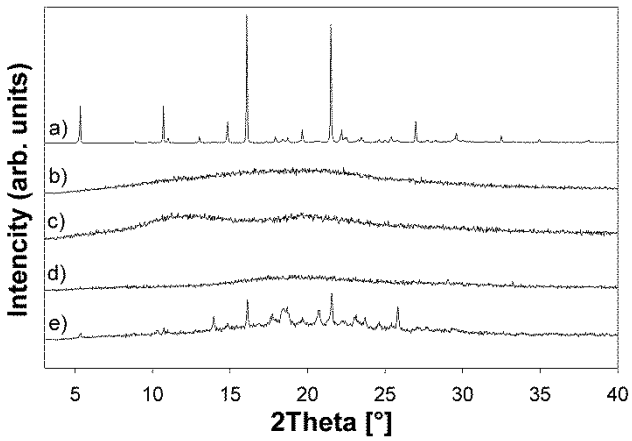

Figure 7.1: XRPD patterns of a) crystalline CCX, b) amorphous CCX, c) PVP/VA 335, d) CCX:PVP/VA 335 (75:25 w/w) after melt-quenching and e) CCX:PVP/VA 335 (75:25 w/w) after 3 h annealing at 135 °C.

7.5.2 Differential scanning calorimetry (DSC)

Figure 7.2 shows the DSC thermograms of crystalline and amorphous CCX, CCX:PVP/VA 335 (80:20 w/w), CCX:PVP/VA 335 (75:25 w/w) before and after annealing and PVP/VA 335. The thermograms for all the pure polymers used and amorphous solid dispersions prepared in this study had similar patterns except for different T_gs (data not show) and therefore, only representative scans with PVP/VA 335 are included in the figure. Prior to the scans of the pure polymers, the samples were annealed for 2 min at 140 °C to evaporate the sorbed water in order to measured T_g at dry conditions. The DSC scan of crystalline CCX (Figure 7.2a) showed an endothermic melting peak around 162 °C with a melting enthalpy (ΔH_m) of approximately 95 J/g, in accordance with the previously identified crystal form III of CCX[166,168]. A heat capacity change characteristic of a glass transition was observed for the amorphous CCX (Figure 7.2b) and PVP/VA 335 (Figure 7.2f) around 57 °C and 69 °C, respectively. Furthermore, the amorphous CCX showed an exothermal crystallization peak between 120–140 °C with a subsequent endothermic melting peak, indicating that CCX is unstable in the amorphous form.

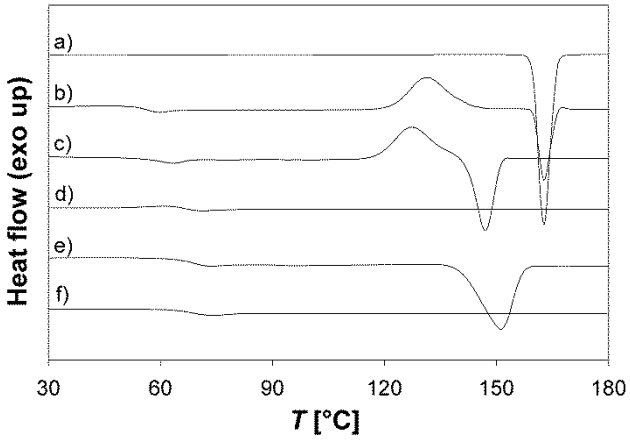

Figure 7.2: DSC thermograms of: a) crystalline CCX, b) amorphous CCX, c) CCX:PVP/VA 335 (80:20 w/w), d) CCX:PVP/VA 335 (75:25 w/w), e) CCX:PVP/VA 335 (75:25 w/w) after 3 h annealing and f) PVP/VA 335.

In the recrystallization method, it is essential that the supersaturated amorphous solid dispersion does not crystallize upon heating towards the annealing temperature. A premature crystallization would require redissolution of the crystalline material in the polymer with the risk of underestimating the solubility as the dissolution process in general is slower than the recrystallization process[95]. Before the annealing of all drug–polymer systems, the highest drug load, for which no crystallization occurred during a normal temperature scan, was selected for annealing. As can be seen in Figure 7.2c, CCX:PVP/VA 335 (80:20 w/w) showed an exothermic crystallization peak between 110 and 135 °C whereas CCX:PVP/VA 335 (75:25 w/w) (Figure 7.2d) did not show any sign of crystallization and was therefore considered suitable for annealing. Similarly, suitable concentrations were found to be 65, 80, 80, 80, and 85% w/w CCX

for CCX:PVP/VA, CCX:PVP/VA 535, CCX:PVP/VA 635, CCX:PVP/VA 735 and CCX:PVP, respectively. The scan of CCX:PVP/VA 335 (75:25 w/w) after 3 h annealing at 135 °C (figure 7.2e) showed a glass transition at a higher temperature than the starting material along with a melting event (close to the melting point of crystalline CCX), confirming that annealing caused some crystallization of CCX. The thermodynamic values for all the pure components measured by DSC along with other physical data used for the solubility predictions are listed in Table 7.1.

Table 7.1: Experimental physical and thermodynamic values measured by DSC and density measured by helium pycnometry (values are mean ± SD, n = 3).

Material	M_w ($g \cdot mol^{-1}$)[a]	Density ($g \cdot cm^{-3}$)[b]	T_g (°C)	ΔC_p ($J \cdot g^{-1} \cdot K^{-1}$)	T_m (°C)	ΔH_m ($J \cdot g^{-1}$)
CCX	381.37	1.35 ± 0.01	56.8 ± 0.4	0.40 ± 0.01	162.0 ± 0.1	94.9 ± 1.1
Vinylacetate	86.09	0.93 ± 0.00	-	-	-	-
N-vinylpyrrolidone	111.14	1.04 ± 0.00	-	-	-	-
PVA	40,000	1.20 ± 0.00	36.4 ± 0.2	0.41 ± 0.01	-	-
PVP/VA 335	28,000	1.18 ± 0.00	68.7 ± 0.3	0.38 ± 0.01	-	-
PVP/VA 535	36,700	1.19 ± 0.01	92.5 ± 0.3	0.33 ± 0.01	-	-
PVP/VA 635	38,200	1.18 ± 0.01	106.6 ± 0.6	0.32 ± 0.01	-	-
PVP/VA 735	56,700	1.18 ± 0.01	116.6 ± 0.8	0.30 ± 0.01	-	-
PVP	2,500	1.18 ± 0.00	108.9 ± 1.4	0.28 ± 0.01	-	-

[a]Average M_w according to the supplier. [b]Amorphous density measured by helium pycnometry.

7.5.3 Prediction of drug–polymer solubility

The Flory-Huggins lattice theory can be used to estimate the drug–polymer solubility from the solubility in a liquid monomer[89,91]. For the PVP/VA copolymer, the two liquid monomeric precursors to the copolymer (NVP and VA) are structurally identical with the repeat units after polymerization[155]. Therefore, the solubility of CCX in NVP:VA mixtures corresponding to the ratio of the repeat units in the copolymer (30, 50, 60 and 70% w/w VP) and the pure liquid monomers were measured. The solubility (w/w) ranged from 0.09 in VA to 0.75 in NVP, linearly increasing with increasing NVP/VA ratio. This linear correlation indicates that the solubility of CCX in PVP/VA may also be predicted simply by the solubility in the two homopolymers. The solubility data from the liquid monomer solutions is presented in Table 7.2 along with the estimates of the solubility in the copolymers based on Equations 7.1 and 7.2.

Table 7.2: Drug–polymer solubilities (w/w) at 25 °C of the six drug–polymer systems predicted from the liquid monomer solubility approach.

	CCX:PVA	CCX:PVP/VA 335	CCX:PVP/VA 535	CCX:PVP/VA 635	CCX:PVP/VA 735	CCX:PVP
Solubility in monomer solutions corresponding to copolymer ratio	0.09 ± 0.00	0.36 ± 0.02	0.46 ± 0.01	0.58 ± 0.04	0.62 ± 0.01	0.75 ± 0.01
Predicted solubility in PVP/VA copolymer	0.03 ± 0.00	0.18 ± 0.02	0.26 ± 0.01	0.38 ± 0.05	0.42 ± 0.02	0.60 ± 0.02

In the original recrystallization method proposed by Mahieu et al.[95], the solubility after annealing is derived from the T_g of the annealed material using the Gordon-Taylor equation. However, previous studies have shown that the experimental composition dependence of the T_g for CCX:PVP systems are not consistent with the prediction from the Gordon-Taylor equation[154,155]. Therefore, a comparison between the experimental composition dependence of the T_g and the prediction from the Gordon-Taylor equation on all the systems was carried out. The experimental T_g data were obtained by *in situ* melt-quenching physical mixtures of known compositions in the DSC. The predicted composition dependence of T_g was calculated using Eq. 3 with the physical and thermodynamic values of CCX and the polymers listed in Table 7.1. In Figure 7.3, the experimental composition dependence of the T_g for the CCX:PVP/VA 335 system is illustrated along with the predictions based on the Gordon-Taylor equation.

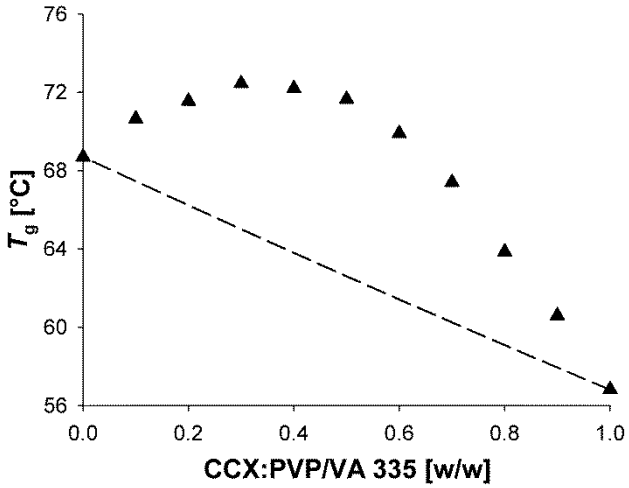

Figure 7.3: Composition dependence of the T_g for the CCX:PVP/VA 335 system. Represented with a filled triangle (▲) is the experimental data (values are mean, n = 3) and the dashed black line is the predictions based on the Gordon-Taylor equation.

As can be seen, all drug–polymer compositions show a higher T_g than the T_g predicted by the Gordon-Taylor equation. Furthermore, the compositions ranging from 0.10–0.60 w/w CCX exhibit a higher T_g than any of the pure components. Consequently, there were two compositions for a given T_g in this composition range and therefore, measurements from the recrystallization method in this range should be evaluated with caution. It should be emphasized that this issue was only relevant for the CCX: PVP/VA 335 system even though all the other systems (PVA, 535, 635, 735, and PVP) also demonstrated positive deviations from the Gordon-Taylor as shown in Figure 7.4. Therefore, the Gordon-Taylor equation could not be used to determine the drug concentration after annealing in this case and the experimental composition dependence of the T_g was applied instead.

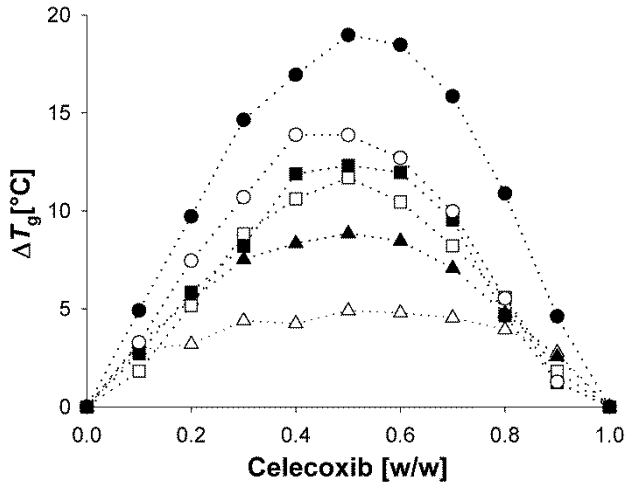

Figure 7.4: Deviations of T_g from the Gordon-Taylor equation as a function of composition for CCX:PVA (Δ), CCX:PVP/VA 335 (▲), CCX:PVP/VA 535 (□), CCX:PVP/VA 635 (■), CCX:PVP/VA 735 (○) and CCX:PVP (●).

For the drug–polymer systems investigated in this study, annealing was possible between 120 and 150 °C. Below 120 °C, the equilibrium solubility was not reached within 3 h, and for temperatures above 150 °C, the solubility was higher than the initial concentration of the drug in the polymer. As can be seen in Table 7.3, it was possible to obtain more data points for some drug–polymer systems than for others. This is because the time to reach equilibrium solubility is influenced by different factors including T_g and viscosity of the polymer, drug loading and annealing temperature[155]. The feasible annealing temperatures for all the drug–polymer systems along with T_g after annealing and corresponding CCX concentrations determined using the experimental composition dependence of the T_g are presented in Table 7.3. Using these values along with the data from Table 7.1, the solubility at 25 °C was predicted by extrapolation using Equation 7.4. The solubility (w/w) ranged from 0.02 in PVA to 0.40 in PVP, increasing with increasing VP/VA ratio. All the predicted solubilities at 25 °C from the recrystallization method are listed in Table 7.4 and the evolution of the solubility curves is illustrated in Figure 7.5.

Table 7.3: Summary of raw data obtained from the recrystallization method. The glass transition temperatures of the annealed material (T_g) and the corresponding drug fraction (X_{drug}) were measured at different annealing temperatures (T_a) (Values are mean ± SD, n = 3).

	CCX:PVA (65:35 w/w)		CCX:PVP/VA 335 (75:25 w/w)		CCX:PVP/VA 535 (80:20 w/w)		CCX:PVP/VA 635 (80:20 w/w)		CCX:PVP/VA 735 (80:20 w/w)		CCX:PVP (85:15 w/w)	
T_a (°C)	T_g (°C)	X_{drug} (w/w)	T_g (°C)	X_{drug} (w/w)	T_g (°C)	X_{drug} (w/w)	T_g (°C)	X_{drug} (w/w)	T_g (°C)	X_{drug} (w/w)	T_g (°C)	X_{drug} (w/w)
150	-	-	65.9 ± 0.1	0.739	-	-	-	-	-	-	-	-
145	53.6 ± 0.3	0.615	66.6 ± 0.2	0.718	70.1 ± 0.3	0.775	70.4 ± 0.1	0.800	-	-	73.5 ± 0.2	0.821
140	52.8 ± 0.1	0.574	68.3 ± 0.4	0.658	73.1 ± 0.4	0.721	73.2± 0.2	0.769	74.3 ± 0.4	0.786	74.9 ± 0.5	0.807
135	51.5 ± 0.3	0.502	69.2 ± 0.1	0.623	74.7 ± 0.3	0.691	74.2 ± 0.1	0.757	76.9 ± 0.5	0.760	76.5 ± 0.4	0.790
130	50.4 ± 0.3	0.462	69.7 ± 0.5	0.604	76.1 ± 0.2	0.667	76.8 ± 0.2	0.729	79.0 ± 0.3	0.738	-	-
125	49.6 ± 0.2	0.434	-	-	77.2 ± 0.3	0.648	78.0 ± 0.2	0.716	80.5 ± 0.2	0.723	-	-
120	48.9 ± 0.2	0.408	-	-	-	-	-	-	81.6 ± 0.2	0.712	-	-

Table 7.4: Drug–polymer solubilities of the six drug–polymer systems predicted from the recrystallization method along with the Flory-Huggins interaction parameter χ and the 95% prediction interval.

	CCX:PVA	CCX:PVP/VA 335	CCX:PVP/VA 535	CCX:PVP/VA 635	CCX:PVP/VA 735	CCX:PVP
Interaction parameter χ	-1.7 ± 0.3	-3.3 ± 0.8	-5.4 ± 0.8	-8.3 ± 1.2	-9.2 ± 1.2	-10.2 ± 2.3
Solubility at 25 °C (w/w)	0.02	0.08	0.20	0.33	0.36	0.40
95% prediction interval at 25 °C	0.02 - 0.03	0.04 - 0.12	0.15 - 0.24	0.28 - 0.37	0.32 - 0.39	0.32 - 0.45

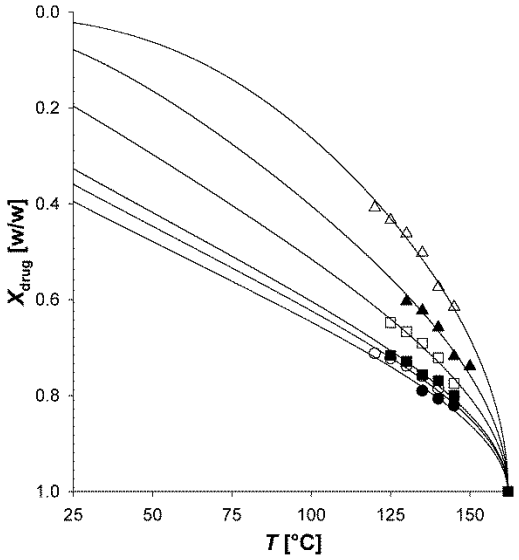

Figure 7.5: Equilibrium solubility of CCX as a function of annealing temperature for CCX:PVA (Δ), CCX:PVP/VA 335 (▲), CCX:PVP/VA 535 (□), CCX:PVP/VA 635 (■), CCX:PVP/VA 735 (○) and CCX:PVP (●) fitted with the Flory-Huggins model to enable an extrapolation of the solubility curves to 25 °C (values are mean, n = 3).

7.6 Discussion

As mentioned above, all investigated drug–polymer systems demonstrated positive deviations from the Gordon-Taylor equation, which could be due to thermal decomposition of the components. The thermal decomposition of CCX and the polymers does not occur until after 185 °C, which was below the melt-quenching temperature of 170 °C. Thermal decomposition was therefore not the reason for the large deviations[109,169-171]. As can be seen in Figure 7.4, the largest deviations were observed for the CCX:PVP system and the deviations decreased with decreasing VP/VA ratio. As the Gordon-Taylor equation is based on an idealized (athermal) system and hence, on the entropy of mixing in relation to the T_g of the pure materials, deviations from this idealized behavior are the result of effects beyond combinatorial mixing. Accordingly, strongly interacting mixtures that exhibit large negative enthalpic effects will result in large positive deviations from the composition dependence of T_g predicted from the theoretical Gordon-Taylor model[152]. Consequently, it is highly probable that the large positive deviations from the Gordon-Taylor equation in this study were due to solid state interactions between CCX and the VP repeat unit. This is supported by the work of Gupta et al.[154], who investigated the interactions between CCX and PVP using Fourier transform infrared (FTIR) spectroscopy and computational molecular modelling and reported strong specific H-bonds between the $–NH_2$ group of CCX and the –C=O group of PVP. Since PVA also contains a –C=O group, it seems reasonable that CCX will also form strong specific interactions with PVA. However, this is in conflict with the findings of the current study cf. the deviations from the Gordon-Taylor equation and a study by Taylor et al.[163], who investigated the intermolecular interactions between water and PVP, PVP/VA, and PVA using Raman spectroscopy. This study found that the hygroscopicity of PVP

is higher than that of PVA due to increased hydrogen bond donor capability of the –C=O group in PVP compared to that of the PVA group, as the pyrrolidone group in PVP is considerably more basic than the acetate group in PVA. Consequently, it is rational to assume that the hydrogen bond between CCX and PVP is stronger than between CCX and PVA, which is reflected in relative deviations from the Gordon-Taylor equation and explains why the deviation increased with increasing VP/VA ratio. Furthermore, it seems that the predicted solubilities from both the liquid monomer solubility approach and the recrystallization method were proportional with the relative deviations of the T_g from the Gordon-Taylor equation (increasing solubility/deviations with increasing VP/VA ratio). Therefore, it is reasonable to assume that these strong interactions were also responsible for inducing solubility of CCX in the polymers. However, as can be seen in Figure 7.6, contrary to the solubility predicted by the liquid monomer solubility approach, there is not a linear relationship between the monomer ratio and the solubility predicted by the recrystallization method. Rather it is an S-shaped curve where the solubility seems to approach a plateau. A multiple comparison test could not reject that the predicted solubilities of CCX at 25 °C in PVP/VA 635, PVP/VA 735, and PVP was identical. However, the predicted solubilities in PVP/VA 635, PVP/VA 735, and PVP were all significantly different from the predicted solubilities in PVA, PVP/VA 335, and PVP/VA 535. Furthermore, the predicted solubilities in PVA, PVP/VA 335, and PVP/VA 535, respectively, were all significantly different from the other five systems. This multiple comparison test confirmed that the solubility plateaued with increasing VP/VA ratio.

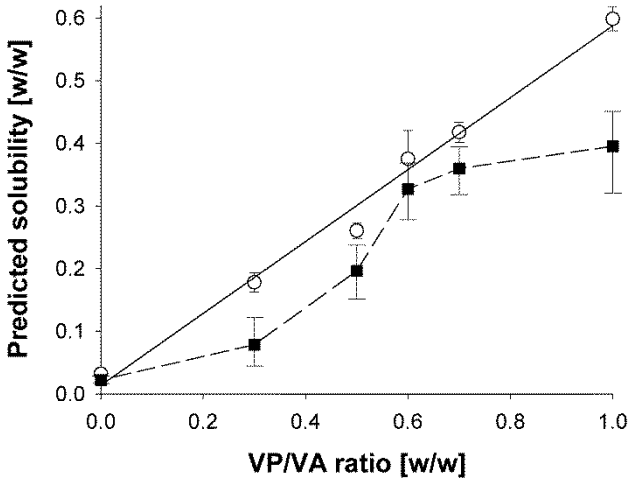

Figure 7.6: Predicted CCX solubilities at 25 °C as a function of copolymer composition (w/w). Represented with (○) is data from the liquid monomer solubility approach and represented with (■) is data from the recrystallization method (values are mean ± prediction interval, $n = 3$).

The discrepancy between the solubility predictions between the two methods (especially for PVP) is likely to be a consequence of the fundamental physical differences between monomers and polymers. In a monomer liquid, the molecules do not have any long-range order, which

allows for relatively unrestricted intermolecular movement. Therefore, it is theoretically possible for the drug molecules to form molecular interactions with all the monomer molecules, which explain the linear correlation between NVP/VA monomer ratio and CCX solubility (see Table 7.2). In a solid polymer, however, the repeat units are covalently bound in the polymer chain and thus, if the molecular volume of the drug is larger than that of the repeat units, it may not be possible for the drug to interact with every repeat unit in the polymer due to steric hindrance caused by already interacting drug molecules. This could be the reason for the S-shaped curve observed for the solubilites predicted from the recrystallization method. Since the theory behind the liquid monomer solubility approach does not take this aspect into account it will overestimate the predicted drug–polymer solubility in situations where interactions between repeat units and drug molecules are responsible for inducing solubility. Nonetheless, if a drug is soluble in the liquid monomeric precursor to the polymer it is most likely also soluble in the polymer (if the molecular structure of the monomer is not altered significantly during polymerization) and therefore, the liquid monomer approach can still provide a valuable indication of the solubility of a drug in a polymer[150]. Based on the hypothesis of steric hindrance (due to differences in molecular volume of the drug and the repeat units), the previously described solubility plateau illustrated in Figure 7.6 can be explained by considering the intramolecular chain structure of the copolymer. PVP/VA is a random copolymer, which means that the two different repeat units (VP and VA) are randomly distributed in the polymer and thus, the probability of finding a given repeat unit in the polymeric chain is equal to the mole fraction of the repeat unit[172]. Thus, if the mol fraction of the VP repeat units is increased in the PVP/VA copolymer, the average distance between the VP repeat units in the polymer chain decreases. Therefore, as the molecular volume of CCX (299.28 $Å^3$) is larger than that of VP (108.42 $Å^3$) and VA (83.03 $Å^3$) (calculated using the MarvinSketch software from ChemAxon (Budapest, Hungary)), respectively, the solubility of CCX will increase with increasing VP/VA ratio until a critical minimal average distance between the VP repeat units is reached. Below this critical minimal average distance, the molecular volume of the CCX molecules will be larger than the distance between the VP repeat units, making it impossible for another CCX molecule to bind to the neighboring VP repeat unit. However, these VP repeat units are still accessible to smaller molecules (such as water that has a molecular volume of 19.51 $Å^3$), and would thus still contribute for example to the overall hygroscopicity of the polymer. Given that this hypothesis is true, the plateau effect may be expected to arise at higher VP/VA ratios for smaller drug molecules and at lower VP/VA ratios for larger drug molecules. However, this still needs to be confirmed through additional investigations using substantially larger and smaller molecules than CCX, respectively. This means that replacing the accessible hygroscopic VP repeat units with hydrophobic VA repeat units will increase the physical stability of an amorphous solid dispersion[81,163], without compromising the drug–polymer solubility. Consequently, knowledge of the plateau effect may be used advantageously in future development of amorphous drug delivery systems as copolymers can theoretically be customized to fit any given drug with a ratio and sequence of repeat units that provide the optimal drug–polymer solubility and physical stability.

7.7 Conclusions

In this study, the influence of PVP/VA copolymer composition on CCX–polymer solubility was investigated. Both the predicted solubilities at 25 °C and the relative deviations of the T_g from the Gordon-Taylor equation increased with increasing VP/VA ratio. This indicates that that the strong interactions responsible for the deviation from the Gordon-Taylor equation are also responsible for inducing solubility of CCX in the polymer. In contrast to the predictions from the liquid monomer solubility approach, the relationship between the monomer ratio and the solubility predicted by the recrystallization method approached a plateau where the solubility of CCX did not further increase significantly with increasing VP/VA ratio. This is likely caused by steric hindrance as a consequence of the size difference between the CCX and the VP repeat unit. Consequently, replacing the (hygroscopic) VP repeat units that are not interacting with CCX with (hydrophobic) VA repeat units could increase the physical stability of an amorphous solid dispersion without compromising the drug–polymer solubility.

Chapter 8

Statistical analysis of a method to predict drug−polymer miscibility

8.1 Abstract

In this study, a method proposed to predict drug−polymer miscibility from differential scanning calorimetry measurements was subjected to statistical analysis. The method is relatively fast and inexpensive and has gained popularity as a result of the increasing interest in the formulation of drugs as amorphous solid dispersions. However, it does not include a standard statistical assessment of the experimental uncertainty by means of a confidence interval. In addition, it applies a routine mathematical operation known as "transformation to linearity", which previously has been shown to be subject to a substantial bias. The statistical analysis performed in this present study revealed that the mathematical procedure associated with the method is not only biased, but also too uncertain to predict drug−polymer miscibility at room temperature. Consequently, the statistical inference based on the mathematical procedure is problematic and may foster uncritical and misguiding interpretations. From a statistical perspective, the drug−polymer miscibility prediction should instead be examined by deriving an objective function, which results in the unbiased, minimum variance properties of the least-square estimator as provided in this study.

8.2 Introduction

Amorphous drug formulations have gained increasing interest in both academic and industrial research because of their potential to overcome the limited and variable bioavailability often associated with poorly water-soluble drugs[11]. On its own, the amorphous drug is thermodynamically unstable and will eventually crystallize, which will neutralize the benefits. In the amorphous solid dispersion approach, this is counteracted by molecularly incorporating the amorphous drug in a polymeric matrix[10,49]. The thermodynamic stability of such a formulation can be ensured if the drug is soluble in the polymer (glass solution). However, at normal storage conditions, the solubility of most drugs in pharmaceutically relevant polymers is low unless favorable cohesive drug−polymer interactions are formed[14,89]. If this is not fulfilled, the drug will likely be supersaturated in the polymer with the risk of crystallizing during storage[36].

The realization of the full potential of amorphous solid dispersions therefore often relies on the kinetic/physical stability provided by the polymer to prevent crystallization. Polymers are thought to improve the physical stability by increasing the glass transition temperature (T_g), thereby reducing the molecular mobility and thermodynamic driving force for

crystallization[78,126,173]. Thus, for a polymer to be an effective crystallization inhibitor, it needs to have a high T_g and be molecularly miscible with the drug, which requires intermolecular interactions between the two components. Generally, stronger interactions will lead to increased drug−polymer miscibility and thus, physical stability of the amorphous solid dispersion[11,43]. For an amorphous polymer−polymer mixture, miscibility is defined as a stable single-phase system with only one T_g[174]. However, as low-molecular-weight drugs are unstable in the amorphous form, the measurable miscibility in the case of amorphous drug–polymer mixtures is associated with a metastable state from which the drug does not crystallize within an experimental time frame. Hence, miscibility is usually only apparent and involves the kinetics of phase separation and structural relaxation, and may practically only be predicted from extrapolation and modeling or by performing long-term stability studies[49].

From an industrial perspective, it is desirable to have an accurate prediction of the drug−polymer miscibility (maximum drug loading) to formulate an amorphous solid dispersion with sufficient kinetic stability to prevent crystallization during shelf-life. In order to circumvent the practical and temporal issues associated with long term stability studies, Lin and Huang[82] proposed a method to predict a complete drug−polymer phase diagram, including the miscibility curve, from experimental differential scanning calorimetry (DSC) data, in order to circumvent the practical and temporal issues associated with long term stability studies. The method is based on melting point depression data obtained at elevated temperatures and extrapolated to room temperature using the Flory−Huggins expression for the free energy of mixing. In order to perform this extrapolation, it is assumed that the Flory−Huggins interaction parameter χ is temperature dependent[43,82]. In the original work, Lin and Huang emphasized that the mathematical procedure associated with the method relies heavily on the validity of the underlying assumptions and the precision of the melting point depression data and therefore, should only be considered as a rough draft. This statement is underlined by the fact that the miscibility (or more specifically the interaction parameter χ) prediction is very sensitive to experimental uncertainty[139,150]. Consequently, even small variations in the measured melting temperatures will have great impact on the predicted miscibility and therefore, a statistical analysis is required to ensure reliability of the method.

Nevertheless, since the method was introduced, several studies have used the method without a reflection on the requirements to provide viable predictions of the drug−polymer miscibility[82,90,93,94,127,145,148,175]. Because of the increasing popularity of the method, we felt obligated to stimulate critical thinking on interpretation of DSC measurements. Therefore, the aim of the current study is to assess the statistical assumptions of the mathematical procedure associated with the method proposed by Lin and Huang to predict the drug−polymer miscibility. The intention is not to cover all assumptions necessary for regression analysis but rather to address the assumptions, which we believe results in uncertain or even misleading predictions.

8.3 Theoretical considerations

The physical basis underlying the prediction of drug−polymer miscibility was proposed by Lin and Huang and is based on the Flory−Huggins solution theory for polymers[85] and a frequently applied empirical relation for the interaction parameter, χ. According to the Flory−Huggins model, the Gibbs free energy of mixing for a drug−polymer mixture is given by[82,93]:

$$\Delta G_{\text{mix}} = RT\left[\phi_{\text{drug}} \ln \phi_{\text{drug}} + \frac{1-\phi_{\text{drug}}}{m} \ln\left(1-\phi_{\text{drug}}\right) + \chi \cdot \phi_{\text{drug}} \cdot \left(1-\phi_{\text{drug}}\right)\right] \tag{8.1}$$

where ϕ_{drug} is the volume fraction of the drug, m is the molar volume ratio of the polymer to the drug, χ is the interaction parameter, R is the gas constant, and T is the absolute temperature. In order to apply this expression to measureable thermodynamic values, the Gibbs free energy of mixing can be related to the melting point depression of a drug−polymer mixture using DSC[83,93]. Crystalline materials melt at a temperature when the chemical potential of the solid and liquid state are equal. Addition of an impurity such as an amorphous polymer to the crystal may reduce the chemical potential of the material in the liquid state, leading to melting point depression[85,86]. Consequently, it is possible to extend Flory−Huggins solution theory to predict the interaction parameter, χ, from melting point depression data by assuming that the melting enthalpy of melting is temperature independent[83]:

$$\frac{1}{T_{\text{m}}^{0}} - \frac{1}{T_{\text{m}}^{\text{mix}}} = \frac{R}{\Delta H_{\text{m}}}\left[\ln \phi_{\text{drug}} + \left(1-\frac{1}{m}\right)\left(1-\phi_{\text{drug}}\right) + \chi \cdot \left(1-\phi_{\text{drug}}\right)^{2}\right] \tag{8.2}$$

where T_{m}^{0} is the melting temperature of the pure drug in absence of polymer, $T_{\text{m}}^{\text{mix}}$ is the melting temperature of the drug in the presence of a polymer and ΔH_{m} is the melting enthalpy of the pure drug. In order to enable extrapolation to other temperatures, Lin and Huang assumed that the temperature dependence of χ can be described by:

$$\chi = A + \frac{B}{T_{\text{m}}^{\text{mix}}} \tag{8.3}$$

where A and B are constants and A is referred to as the non-combinatorial contribution to χ and $B/T_{\text{m}}^{\text{mix}}$ is the enthalpic contribution[43].

From the physicochemical assumptions in Equations 8.2 and 8.3, Lin and Huang constructed a complete drug−polymer phase diagram, including the solubility and miscibility curves. The drug−polymer miscibility can be derived from the lever rule; when the composition dependence of the free energy of mixing is convex, any mixed state has lower free energy than any state the mixtures could phase separate into[176]. The criterion for the boundary between unstable and metastable regions (the spinodal curve) is thus given by $\frac{\partial^2 \Delta G_{\text{mix}}}{\partial \phi_{\text{drug}}^{\ 2}} = 0$ and applying this criterion to Equation 8.1 yields:

$$\phi_{\text{drug}} = \frac{1}{4} \frac{2\chi \cdot m + m - 1 \pm \sqrt{1 + 4\left(\chi - \frac{1}{2}\right)^2 m^2 - (4\chi + 2) \cdot m}}{\chi \cdot m}, \ \chi \geq \frac{1}{2} + \frac{1}{2m} + \frac{1}{\sqrt{m}} \qquad (8.4)$$

In summary, the mathematical procedure suggested by Lin and Huang to obtain the complete phase diagram is given by the following three steps: (i) determine the melting point depression of drug−polymer physical mixtures of different composition using DSC and calculate the χ values using Equation 8.2, (ii) fit the interrelated χ, $T_{\text{m}}^{\text{mix}}$ values with Equation 8.3 in order to estimate A and B, and (iii) extrapolate the fitted empirical χ, T relationship in Equation 8.4 to predict the drug−polymer miscibility curve.

8.4 Results and discussion

8.4.1 Demonstration of the original method including confidence assessment

For good measure, the method proposed by Lin and Huang is initially demonstrated. In order to do this, the data used in the original work was adapted. The melting point depression measurements, however, were not tabulated and therefore, the data had to be adapted by graphical inspection. The data basis for the current study can be found in Tables 8.1 and 8.2. As the method did not include an uncertainty analysis, great emphasis has been put on assessing the confidence of the prediction. In the mathematical procedure by Lin and Huang the first step i) involves finding χ by Equation 8.2 from the experimental melting point depression data in Table 8.2. Here Lin and Huang calculated χ from the average value of $T_{\text{m}}^{\text{mix}}$ at each composition. This averaging operation will discard some of the variability in the data and in the current case the consequences thereof are severe as will be elaborated later.

Table 8.1: Physical properties adapted from Lin and Huang.

Component	M_w (g/mol)	ρ (g/cm^3)	ΔH_m (J/g)
Felodipine	384.26	1.28	78.5[a]
Poly (acrylic acid)	1,800	1.27	-

[a]Data reported in the literature.

Table 8.2: Melting point depression data (T_m^{mix}) for different drug−polymer compositions (ϕ_{drug}) and the interrelated average χ values adapted from Lin and Huang (values for T_m^{mix} are mean ± SD, n = 2).

ϕ_{drug}	T_m^{mix} (°C)	Average χ
1.00	144.66 ± 0.32	-
0.85	143.20 ± 0.40	0.6241
0.80	142.79 ± 0.62	0.6678
0.75	142.25 ± 0.10	0.6493
0.70	141.73 ± 0.64	0.6589
0.65	141.43 ± 0.50	0.7160
0.60	141.00 ± 0.60	0.7459

The next step in the procedure, step ii), is to fit the interrelated χ, T_m^{mix} values with Equation 8.3 in order to estimate A and B and enable extrapolation of χ to any temperature. Here, Lin and Huang made another routine mathematical operation to obtain a simple linear regression by inverting the 1st-axis before fitting the equation to the experimental data, given by $x=1/T_m^{mix}$. This procedure is historically one of the most used mathematical operations in non-linear regression analysis, referred to as "transformation to linearity,"[177] and the drawbacks of this will also be elaborated later. For now however, we will disregard the consequences of the two mathematical operations described above and use the unverified assumptions of Lin and Huang for statistical inference. Fitting the mean values of T_m^{mix} from Table 8.2 with the procedure proposed by Lin and Huang, the least-square estimates obtained were given by $\chi = -18.790 + 8084\,\frac{1}{T_m^{mix}}$. This implies that the estimates reported in the original work $\chi = -18.843 + 8105\,\frac{1}{T_m^{mix}}$ were reproduced with a good approximation in this work, thus validating the values adapted from graphical inspection. In addition to the least-square estimate the confidence intervals for the coefficients should always be calculated when performing a regression analysis.

Consequently, the 95% approximate Wald confidence interval for the expected response at x_0 is[178]:

$$x_0^T\hat{\theta} \pm s\sqrt{x_0^T\left(X^T X\right)^{-1}x_0}\,t\left(N-P;\alpha/2\right) \tag{8.5}$$

where $\hat{\theta}=\left(\hat{A},\hat{B}\right)^T$ is the estimate of the parameters, $x_0=(1,1/T_{\mathrm{m}}{}^{\mathrm{mix}})^T$ is the level at which the prediction is desired, N is the number of observations, $P = 2$ is the number of predictor variables, X is a $N \times P$ matrix of the regressor variables, $s = \sqrt{\frac{SSR}{N-P}}$ is the estimate of the sample standard deviation, SSR is the sum of squared residuals and $t(N - P; \alpha/2)$ is the $\alpha/2$ quantile in the t distribution with $N - P$ degrees of freedom.

The 95% confidence intervals for the coefficients were given as $A = [-34.378, -3.202]$ and $B = [1611\ \mathrm{K}, 14557\ \mathrm{K}]$ and the least-square estimate including the 95% confidence interval as given by Equation 8.5 is shown in Figure 8.1.

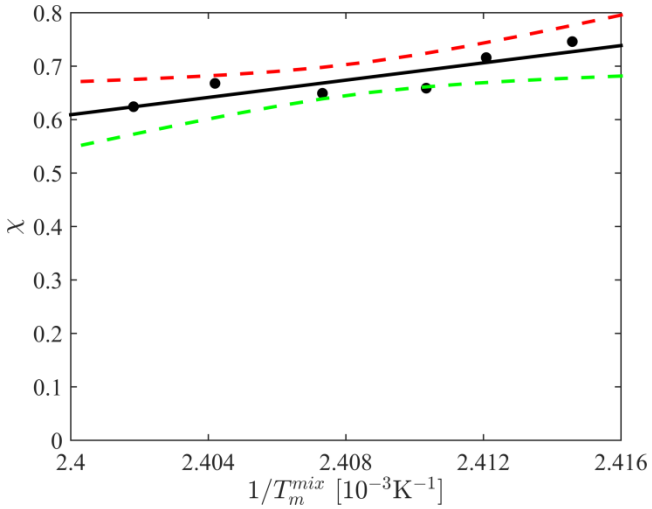

Figure 8.1: Linear fit of χ as a function of $1/T_{\mathrm{m}}{}^{\mathrm{mix}}$ based on Equation 8.2 to estimate A and B (from mean $T_{\mathrm{m}}{}^{\mathrm{mix}}$ values) as illustrated by Lin *et al.* including the 95% confidence interval.

In order to predict the miscibility and confidence interval at other temperatures (e.g. room temperature), Equation 8.3 needs to be extrapolated. In this context, it is obvious that the further the extrapolation is made from the empirical data, the more vulnerable the prediction will be. This is evident from Figure 8.2, where the influence of extrapolation on the least-square estimate for χ including the approximate 95% confidence interval is illustrated. Particularly at temperatures of practical relevance (e.g., 20 °C), the extrapolation resulted in relatively large confidence intervals which will affect the confidence of the miscibility curve.

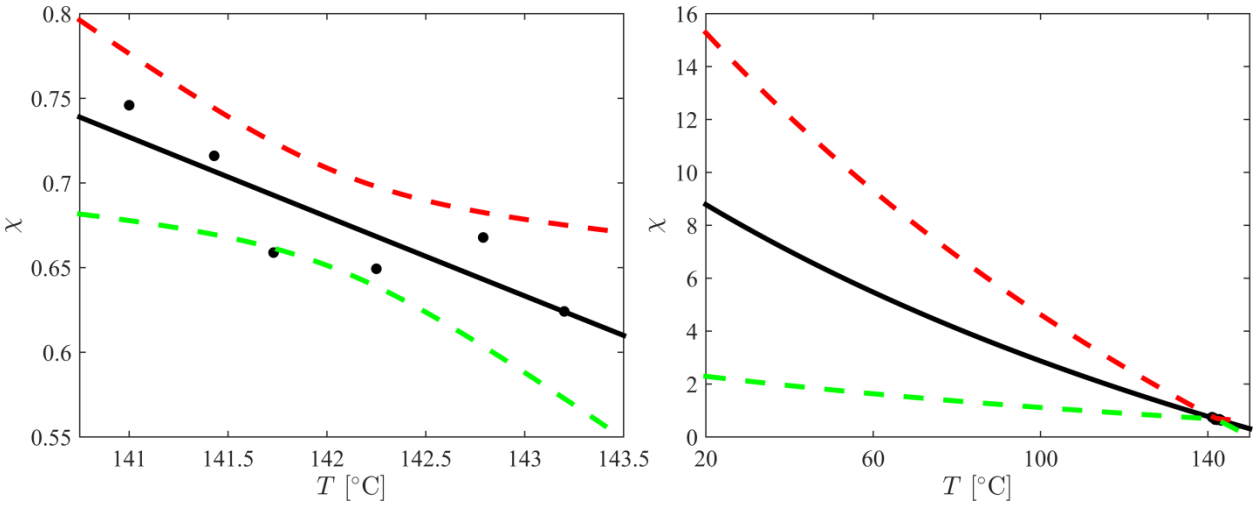

Figure 8.2: The least-square estimate of $\chi = A + \frac{B}{T_m^{mix}}$ including the 95% confidence intervals as a function of temperature in (left) the measurement range and (right) extrapolated to 20 °C. Note that the 1st-axis is now displayed on the normal temperature scale as opposed to Figure 8.1.

To demonstrate this, the fitted empirical χ, T relationship was extrapolated using Equation 8.4 to predict the drug–polymer miscibility curve as shown in Figure 8.3. It is seen that the large confidence intervals for the χ prediction (shown in Figure 8.2) was not directly translated into a wide confidence interval of the predicted miscibility at 20 °C. However, the measurements were subject to some additional error which was disregarded in the original work as mentioned previously. Consequently, in order to better reflect how the standard deviations of T_m^{mix} influenced the prediction of a future observation of the miscibility, a Monte Carlo simulation was conducted as shown Figure 8.4. The procedure proposed by Lin and Huang was simulated 1000 times using the mean and standard deviations of T_m^{mix} shown in Table 8.2. Even though the Monte Carlo simulation of the miscibility curves were seen to cover all possible values of ϕ_{drug}, only 453 of the 1000 simulations fell into the defined space (0 K to T_m^0). This means that the inclusion of the inherent uncertainty of the T_m^{mix} measurements resulted in an indefinite prediction interval where only the lower limit of the 95% prediction interval of the miscibility curve could be identified. Consequently, the central estimate becomes extremely vague and does not tell much about the miscibility curve, which could not have been predicted in advance. This could indicate that the DSC is not currently at a stage where the melting point can be determined with sufficient precision to predict the drug–polymer miscibility curve with any statistical significance. However, it is important to emphasize that the legitimacy of this provisional assessment relies on the assumptions made by Lin and Huang to be valid.

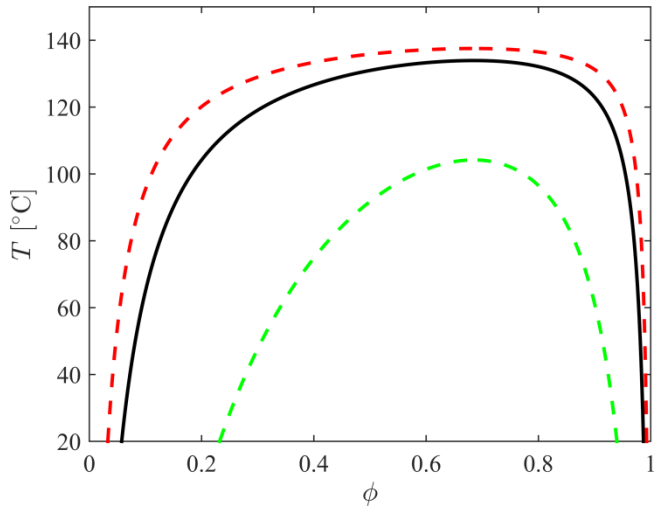

Figure 8.3: Drug−polymer miscibility curve for the felodipine−PAA system based on Equation 8.4 including the 95% confidence interval.

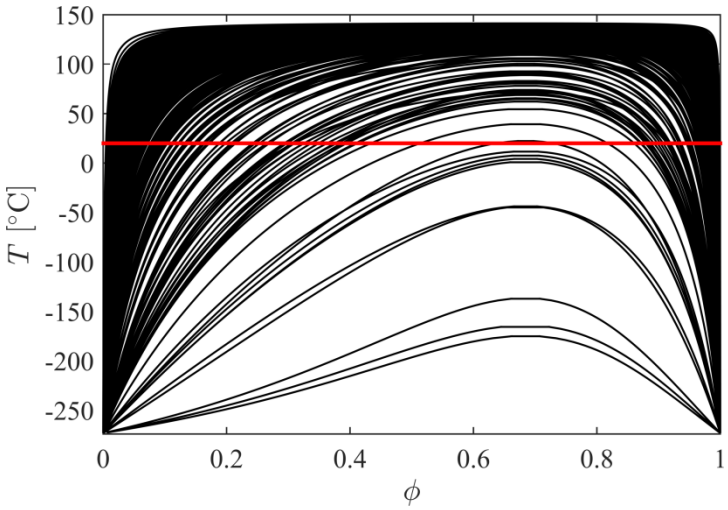

Figure 8.4: Monte Carlo simulations (453 runs of 1000) of the miscibility curve based on the data from Table 8.2 including the standard deviations. The red line indicates 20 °C.

8.4.2 Assessment of the underlying statistical assumptions

As the underlying statistical assumptions of the procedure have not yet been assessed, the prediction has limited credibility. In order to make such an assessment, the raw data from Lin and Huang was required. In the original work, the average values from two replicate experiments were used to fit Equation 8.3. Therefore, it was possible to deduce the values of the raw data from the standard deviations of the average data. Remarkably, when repeating the mathematical procedure proposed by Lin and Huang with the raw data (i.e., without the averaging treatment),

the B value becomes negative and the least-square estimate is given by $\chi = 30.830 - 12520\,\frac{1}{T_{\mathrm{m}}^{\mathrm{mix}}}$.

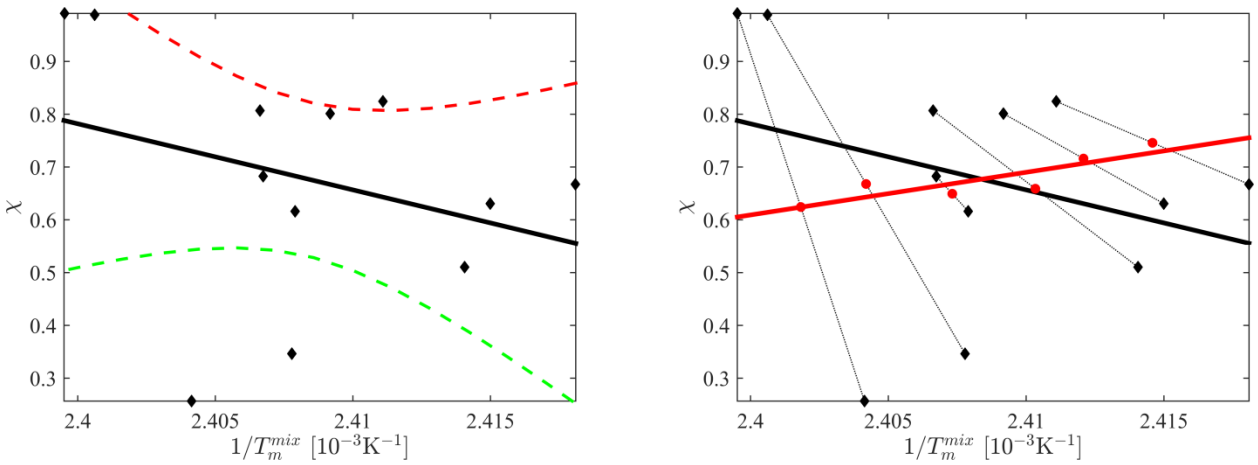

Figure 8.5: (Illustration of left) The least-square estimate of $\chi = A + \frac{B}{T_{\mathrm{m}}^{\mathrm{mix}}}$ including the 95% confidence intervals fitted to the raw data and (right) comparison of the fit to the raw data (black line) and the mean values (red line). The interrelated values (ϕ_{drug}) are connected by dotted lines.

In Figure 8.5, the difference between fitting to the raw data and mean values is illustrated. Note that the χ prediction is increasingly sensitive toward experimental uncertainty as $T_{\mathrm{m}}^{\mathrm{mix}}$ approaches T_{m}^{0} as stated previously. At a first glance, the discrepancy between the fit to the raw data and mean values was surprising. There was, however, nothing erroneous in the fits as can be inspected from Figure 8.5 (right), where both the raw data and the mean values are shown together with the two best fitted lines. This discrepancy is in fact known to be a result of the routine mathematical operation "transformation to linearity" as outlined below. As previously described, the least-square estimator is optimal in a statistical sense, as it is unbiased and has the lowest variance (among the group of unbiased estimators). However, the optimality is based on several assumptions; here, we will only address the main assumptions that are violated resulting in the bias shown in Figure 8.5. The least-square estimate can be found by minimizing a proper objective function and the implicit objective function used in the mathematical procedure by Lin and Huang is defined by the sum-of-square of the residuals of χ:

$$SSR\left(T_{\mathrm{m}}^{\mathrm{mix}}(i); A, B\right) = \sum_{\text{all } i} \left(\chi(i)^{\mathrm{measurement}} - \chi(i)^{\mathrm{model}}\right)^2 \tag{8.6}$$

where $\chi(i)^{\text{measurement}}$ is the measurement of the interaction parameter, $\chi(i)^{\text{model}}$ is the model of the interaction parameter, and $SSR(T_{\text{m}}{}^{\text{mix}}(\text{i}); A, B)$ are the sum-of-square of the residuals, which is a function of the parameters A and B, and i is an index variable for the level of $T_{\text{m}}{}^{\text{mix}}(i)$ where the measurements were conducted.

The model of the measurement was given by $\chi(i)^{\text{model}} = A + \frac{B}{T_{\text{m}}^{\text{mix}}(i)}$, which has two parameters, A and B, and one predictor variable, $T_{\text{m}}{}^{\text{mix}}(i)$. By this definition of the objective function, Lin and Huang implicitly assumed that the predictor variable $T_{\text{m}}{}^{\text{mix}}(i)$ is free of noise. However, the experimentally measured quantity is the melting temperature and not χ. Therefore, it is the melting temperature, which in the first place is subject to experimental noise. As the value of $\chi(i)^{\text{measurement}}$ associated with each value of $T_{\text{m}}{}^{\text{mix}}(i)$ is calculated from the Flory−Huggins equation, it is clear that $\chi(i)^{\text{measurement}}$ also will be subject to noise. Thus, the variance of the predictor variable $\frac{1}{T_{\text{m}}^{\text{mix}}}$ cannot be neglected and the residuals are highly correlated and therefore, the regression function $\chi = A + \frac{B}{T_{\text{m}}^{\text{mix}}}$ is no longer deterministic, but stochastic. This means that the assumptions of the regression analysis are violated[178], resulting in biased predictions. A more productive opportunity is to derive an objective function which results in the unbiased, minimum variance properties of the least-square estimator. Consequently, using melting point depression measurements the variable subject to experimental noise is $T_{\text{m}}{}^{\text{mix}}$ and thus, the least-squares estimate (best fit) should be defined as the minimum sum-of-squares of the residuals of $T_{\text{m}}{}^{\text{mix}}$ i.e.:

$$SSR(\phi_{\text{d}}(i); A, B) = \sum_{\text{all } i} \left(T_{\text{m}}^{\text{mix}}(i)^{\text{measurement}} - T_{\text{m}}^{\text{mix}}(i)^{\text{model}} \right)^2 \tag{8.7}$$

where the regression function $T_{\text{m}}{}^{\text{mix}}(i)^{\text{model}}$ can be found by inserting the empirical relation for $\chi = A + \frac{B}{T_{\text{m}}^{\text{mix}}}$ into Equation 8.2, and solving for $T_{\text{m}}{}^{\text{mix}}$:

$$T_{\text{m}}^{\text{mix}}(i)^{\text{model}} = \frac{B \cdot \left(1 - \phi_{\text{drug}}(i)\right)^2 + \frac{\Delta H_{\text{m}}}{R}}{-A \cdot \left(1 - \phi_{\text{drug}}(i)\right)^2 - \ln\left(\phi_{\text{drug}}(i)\right) - \left(1 - \frac{1}{m}\right)\left(1 - \phi_{\text{drug}}(i)\right) + \frac{1}{T_{\text{m}}^0}\frac{\Delta H_{\text{m}}}{R}} \tag{8.8}$$

Application of Equation 8.8 would result in more sound miscibility prediction from a statistical point of view. In addition to the statistical assumption discussed above, the physical assumptions for the model to allow an extrapolation are crucial and in order to truly believe in the predictions, the underlying physical assumptions (e.g., the temperature dependence of χ) need to be assessed. However, this is far beyond the scope of this work and will have to be elaborated in detail in future work.

8.5 Conclusions

In this study, a statistical analysis of a method proposed by Lin and Huang to predict drug−polymer miscibility from melting point depression measurements was performed. The concerns raised by Lin and Huang in the original work turned out to be justified. Using the mathematical procedure and raw data from Lin and Huang, the predicted miscibility curve could not be trusted with statistical confidence. This could indicate that the DSC is not currently at a stage where the melting point can be determined with sufficient precision to predict the drug−polymer miscibility. Furthermore, a comparison of the fit to the mean values and the fit to the raw data resulted in two qualitative contradictive conclusions, which indicates that the mathematical procedure is biased because of the operation "transformation to linearity." Consequently, the statistical inference based on the mathematical procedure is problematic and may foster uncritical and misguiding interpretations. From a statistical perspective, the potential of DSC measurements to make miscibility predictions should instead be examined by deriving an objective function, which results in the unbiased, minimum variance properties of the least-square estimator. However, even though this objective function will provide more sound miscibility predictions from a statistical point of view, arguments in favor of the underlying physical assumptions (e.g., the temperature dependence of χ) needs to be put forward in order to truly believe in the predictions.

Chapter 9

A promising new method to estimate drug–polymer solubility at room temperature

9.1 Abstract

The established methods to predict drug–polymer solubility at room temperature either rely on extrapolation over a long temperature range or are limited by the availability of a liquid analogue of the polymer. To overcome these issues, this work investigated a new methodology where the drug–polymer solubility is estimated from the solubility of the drug in a solution of the polymer at room temperature using the shake-flask method. Thus, the new polymer in solution method does not rely on temperature extrapolations and only requires the polymer and a solvent, in which the polymer is soluble, that does not affect the molecular structure of the drug and polymer relative to that in the solid state. Consequently, as this method has the potential to provide fast and precise estimates of drug–polymer solubility at room temperature, we encourage the scientific community to further investigate this principle both fundamentally and practically.

9.2 Introduction

On account of increasing focus on the physical stability of amorphous solid dispersions, several experimental methods to predict the solubility of drugs in polymers at room temperature have been proposed[39,80,83,95,179,180]. As most pharmaceutically relevant drugs and polymers are solid or highly viscous at room temperature, measuring the drug solubility under these conditions is not feasible[48], and therefore, the methods are based on equilibrium thermodynamics at elevated temperature and subsequent extrapolation to room temperature. Most of the methods are based on differential scanning calorimetry (DSC) measurements and is time consuming due to slow dissolution or crystallization kinetics of the drug into or from the polymer. As a consequence, predictions from these methods are associated with a degree of uncertainty, the extent of which depends on several factors including the precision of the measurements, the validity of the assumptions underlying the proposed model (e.g., the Flory-Huggins model), and the magnitude of the temperature extrapolation[155]. To overcome these issues, a method to estimate the solubility of drugs in polymers, based on the solubility of the drug in a liquid analogue and/or monomer of the polymer at room temperature, was proposed by Marsac et al.[89]. A key assumption underlying this method is that the interactions between the drug and analogue and/or monomer in the liquid state are similar to the interactions between the drug and polymer in the solid state[89,91]. However, as the method requires a liquid analogue/monomer of the polymer, it is not applicable to all polymers, and furthermore, it does not account for the fundamental chemical and physical differences between monomers and polymers. In contrast to the covalently bound monomers in a

polymer chain, liquid monomers have relatively unrestricted intermolecular movement, which allows for interactions with the drug molecules without steric hindrance, and therefore, the method tends to overestimate the solubility of drugs in polymers[181].

Under the premise of similar interactions in the solid and liquid state, this study investigated the possibility of estimating the drug–polymer solubility from the solubility of the drug in a polymer solution at room temperature rather than in a liquid analogue and/or monomer. This approach appears feasible if the solvent does not influence the molecular structure of the drug and polymer relative to that in the solid state (e.g., through protonation/deprotonation) or the interactions between the drug and polymer. Consequently, we hypothesize that the solubility of a drug in a polymer can be derived from the increase of drug solubility as a function polymer concentration in a solvent by considering the solvent as an inert component. Compared to the existing methods, this new polymer in solution method does not require extrapolations over long temperature ranges and may therefore provide faster and more precise solubility estimates. The potential of this method was investigated using chloramphenicol (CAP), celecoxib (CCX), and paracetamol (PCM) as model drugs, polyvinylpyrrolidone (PVP), polyvinyl acetate (PVA), and polyvinyl caprolactam-polyvinyl acetate-polyethylene glycol *graft* copolymer (Soluplus®, SOL) as polymers, and methanol and ethanol as solvents. To verify the solubility estimates from the new polymer in solution method, the results were compared with predictions from an established method based on melting point depression determinations[83].

9.3 Materials and methods

9.3.1 Materials

CCX (M_w = 381.37 g/mol) was purchased from AK Scientific, Inc. (Union City, CA, USA). PCM (M_w = 151.17 g/mol), CAP (M_w = 323.13 g/mol), methanol (>99.9%), and ethanol (~96%) were purchased from Sigma-Aldrich Co. (St. Louis, MO, USA). Kollidon® 17 PF (PVP, M_w = 10,000 g/mol) and Soluplus® (SOL, M_w = 118,000 g/mol) were kindly supplied by BASF (Ludwigshafen, Germany), and PVA (M_w = 40,000 g/mol) was purchased from VWR Chemicals (Leuven, Belgium).

9.3.2 Thermal analysis

The melting temperature (T_m, onset) of the pure materials and physical mixtures was determined using DSC. The analyses were performed using a Q2000 DSC from TA Instruments Inc. (New Castle, DE). Sample powders (2–3 mg) were packed into Tzero aluminum hermetic pans with a perforated lid and scanned at 1 °C/min from 60−180 °C under 50 mL/min dry nitrogen gas purge. The instrument was calibrated for enthalpy and temperature using indium as a standard and the heat capacity was calibrated using a sapphire standard. The melting temperature (T_m,

onset), melting enthalpy (ΔH_m), and glass transition temperature (T_g, inflection) were determined using the Universal Analysis 2000 (version 4.5A) software.

9.3.3 Quantitative analysis

A reversed phase HPLC method was developed for quantification of CAP, CCX, and PCM. The HPLC system consisted of an L-7100 pump, an L-7200 auto sampler, a T-6000 column oven, an L-7400 UV-detector, and a D-7000 Interface all from Merck-Hitachi LaChrom (Tokyo, Japan). A total of 25 µL of was injected into a reverse phase X-Bridge C-18 column (4.6 × 150 mm, 3.5 µm) from Waters (Milford, MA, USA) for the separation. The mobile phase consisted of methanol and 20 mM ammonium phosphate buffer (65:35 v/v) adjusted to pH 2.35 ± 0.05 with phosphoric acid and was eluted at a flow rate of 1.0 mL/min. The effluent was monitored at 280 nm, 235 nm, and 250 nm and retention times of 2.0 min, 6.2 min, and 1.6 min for CAP, CCX, and PCM, respectively.

9.3.4 Established method (melting point depression)

If the dissolution of a crystalline drug into an amorphous polymer is favored by the thermodynamics of mixing, the melting point of the drug will be depressed. According to the Flory-Huggins model, it is possible to relate the magnitude of this melting point depression to the solubility of the crystalline drug in the polymer[83,85]:

$$\frac{\Delta H_m}{R}\cdot\left(\frac{1}{T_m}-\frac{1}{T}\right)=\ln\left(v_{drug}\right)+\left(1-\frac{1}{\lambda}\right)\cdot\left(1-v_{drug}\right)+\chi\cdot\left(1-v_{drug}\right)^2 \qquad (9.1)$$

where ΔH_m and T_m are the enthalpy of fusion and melting temperature for the pure drug, respectively, R is the gas constant, λ is the molar volume ratio of the polymer and drug, χ is the Flory-Huggins interaction parameter, and T is the melting temperature (onset) at a given volume fraction of drug (v_{drug}). To obtain the solubility of the drug in the polymer at room temperature, the melting points at different drug fractions were determined at elevated temperatures, fitted to Equation 9.1 and extrapolated to 25 °C. Therefore, physical mixtures of crystalline drug and polymer of known composition were prepared by gentle milling using a mortar and pestle. The exact drug fraction after the milling procedure was determined using HPLC, and the samples were stored in air-tight vessels at room temperature until use. The melting points of the different physical mixtures were determined at a heating rate of 1 °C/min using the DSC. For a more detailed description of the theoretical background and experimental protocol of the method, the interested reader is referred to Marsac et al.[83].

9.3.5 New method (polymer in solution)

In this study, we hypothesize that the drug–polymer solubility may also be derived from the increase of drug solubility as a function of polymer concentration in an inert solvent (slope of the linear regression). The solubilities of the drugs in the pure solvents and polymer solutions were determined using the shake-flask method. Polymer solutions of known concentration (10–40% w/v) were prepared by dissolving the polymer in the solvent (methanol or ethanol). An excess of crystalline drug was added to a capped glass tube containing 1 mL of the pure solvent or the polymer solution and rotated at 5 rpm using a mechanical rotor from Heto Lab Equipment (Birkerod, Denmark). The suspensions were rotated at 25 ± 1 °C for 1 week to ensure that equilibrium was reached. Thereafter, the samples were filtered using 0.2 μm polytetrafluroethene hydrophobic syringe filters from Merck Millipore Ltd. (Darmstadt, Germany) and diluted with methanol to appropriate concentrations. The diluted samples were quantified using the HPLC method described previously.

9.3.5 Statistical analysis

The Flory-Huggins model (Eq. 1) was used to describe the measurements obtained by the melting point depression method. The optimal fit with χ as an adjustable parameter was found by regression analysis, and the 95% prediction interval was obtained by extrapolation to 25 °C as previously described by Knopp et al.[155]. The data from the polymer in solution method, proposed in this work, were analyzed by linear regression, that is $X_{\text{drug}} = a \cdot X_{\text{polymer}} + b$, where X_{drug} is the solubility of the drug in the polymer solution, X_{polymer} is the concentration of the polymer in the solvent, and b is the solubility of the drug in the pure solvent. The mean drug–polymer solubility estimate in the solid state $\hat{X}_{\text{drug}}^{\text{solid}}$ was found by the slope of the regression (a). As the solubility of the drug in the pure solvent (b) is also subject to uncertainty both a and b should be used as fitting parameters, and thus, the prediction interval for this estimate was found by $\hat{X}_{\text{drug}}^{\text{solid}} \pm t_{0.025,N-2} \cdot (\sigma_{\text{a}} + 2\sigma_{\text{b}}) \cdot \sqrt{1+1/N}$, where σ_{a} and σ_{b} are the standard deviations of the 2 fitting parameters (assumed to be independent), $t_{0.025,N-2}$ is the 2.5% quantile in the t-distribution and N is the number of measurements.

9.4 Results and discussion

To illustrate the basic principle behind the polymer in solution method, the increase of CCX solubility as a function of PVP concentration in methanol and ethanol is shown in Figure 9.1. As can be seen, the solubility of CCX in ethanol and methanol increased linearly with increasing PVP concentration. Furthermore, the slopes of the 2 regressions were almost identical, which means that the increase in solubility of CCX in a solution of PVP was probably independent on the solvent and thus indicates that the assumptions underlying the method were met in this case. To confirm that this trend observed for CCX in PVP solutions was not an isolated incident, the

validity of the new polymer in solution method was investigated using a range of different drugs, polymers, and solvents and compared with solubility predictions from the established method based on melting point depression. The predicted drug–polymer solubility obtained from the melting point depression method and the estimated drug–polymer solubility obtained from the new polymer in solution method using methanol and ethanol as solvents for all drug–polymer systems at 25 °C, including the prediction intervals, are presented in Table 1 and illustrated in Figure 9.2. The raw data from both methods, along with the experimental physical and thermodynamic values used to predict the drug–polymer solubility from the melting point depression method, can be found in Appendix B.

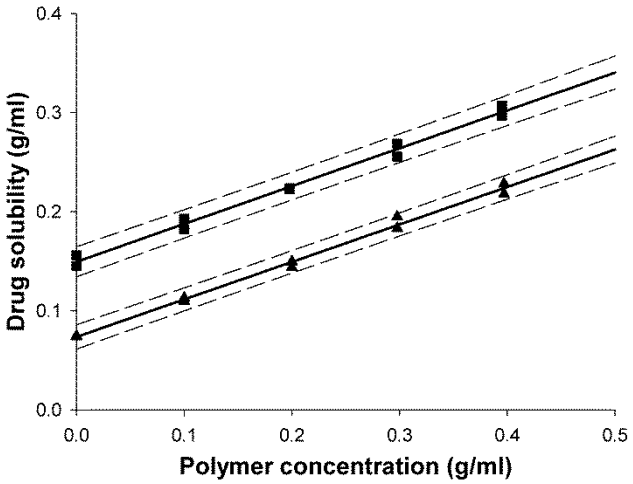

Figure 9.1: Illustration of the basic principle behind the new polymer in solution method. The increase in CCX solubility is plotted as a function of PVP concentration in methanol (■) and ethanol (▲) at 25 °C. The solid line is the best linear fit and the dotted lines are the (non-linear) prediction intervals. Data points represent raw data (n = 2).

Table 9.1: Predicted solubilities from the melting point depression method and the estimated solubilities from the new polymer in solution method in methanol and ethanol. Values represent mean drug–polymer solubility (w/w) at 25 °C with the prediction intervals in parentheses.

	CAP:PVP	CAP:PVA	CAP:SOL	CCX:PVP	CCX:PVA	CCX:SOL	PCM:PVP	PCM:PVA	PCM:SOL
Melting point depression	0.40 (0.29-0.48)	0.04 (0.02-0.06)	0.14 (0.07-0.22)	0.43 (0.34-0.49)	0.08 (0.02-0.18)	0.25 (0.10-0.36)	0.29 (0.14-0.39)	0.01 (0.01-0.02)	0.04 (0.01-0.09)
Polymer in methanol	0.39 (0.32-0.46)	0.06 (0.03-0.10)	0.14 (0.04-0.23)	0.38 (0.35-0.41)	0.13 (0.07-0.20)	0.23 (0.20-0.27)	0.17 (0.15-0.18)	0.01 (0.00-0.03)	0.10 (0.08-0.13)
Polymer in ethanol	0.40 (0.37-0.44)	0.05 (0.02-0.07)	0.11 (0.07-0.15)	0.38 (0.35-0.40)	0.16 (0.15-0.18)	0.23 (0.19-0.26)	0.19 (0.16-0.23)	0.01 (0.00-0.03)	0.09 (0.07-0.11)

These results show that the linear increase in drug solubility with increasing polymer concentration observed for the CCX in PVP solutions was observed for all systems under investigation. Furthermore, a *t*-test revealed that the mean drug–polymer solubility estimates from the methanol and ethanol solutions were not significantly different ($p > 0.05$). As the solvents do not influence the molecular structure of the drugs or polymers compared to that in the solid state, it is rational to assume that the solvents were inert in this context. The increase in drug solubility with increasing polymer concentration was therefore more likely a reflection of other factors, such as interactions between the drug and polymer. By assuming that the interactions between the drug and polymer in the liquid (dissolved) state were similar to the interactions between the drug and polymer in the solid state, the solubility of the drug in the polymer in the solid state could be estimated from the solubility of the drug in a polymer solution. Consequently, if the solvent is inert, it is expected that the increase in drug solubility with increasing polymer concentration will be linear for any given drug–polymer combination.

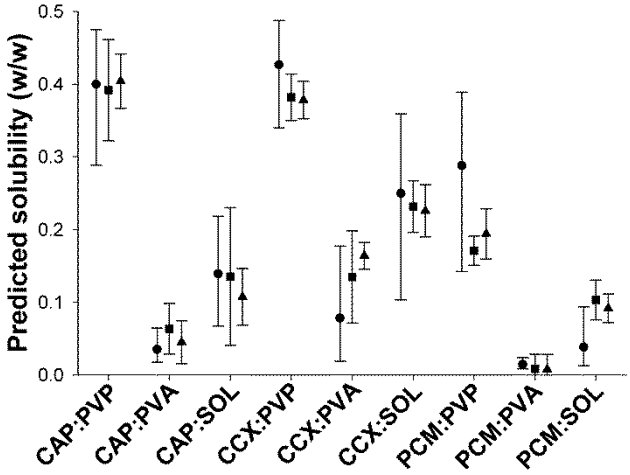

Figure 9.2: Comparison of the solubility predictions for all investigated drug–polymer systems obtained from the melting point depression method (●) with the solubility estimates obtained from the new polymer in solution method using methanol (■) and ethanol (▲) as solvents. Data points represent mean drug–polymer solubility (w/w) at 25 °C including the prediction intervals.

As demonstrated in Table 9.1 and Figure 9.2, only 2 of the 18 mean estimates (PCM:PVA in ethanol and PCM:SOL in methanol) from the new polymer in solution method was not within the prediction interval from the melting point depression method. In addition, half of the prediction intervals (9 of 18) from the new polymer in solution method were equivalent to the prediction intervals from the melting point depression method (i.e., the prediction interval from the new polymer in solution method was within the prediction interval from the melting point depression method), and most of the prediction intervals (13 of 18) were narrower than the prediction intervals from the melting point depression method. This indicates that the new polymer in solution method provides more precise solubility estimates, which is probably

because it is based on measurements made at room temperature and thus, does not rely on extrapolation from data obtained at elevated temperature. Based on these findings, we feel that it is reasonable to propose that the 2 different methods to predict drug–polymer solubility provide equivalent results, at least for the systems investigated in this study. In theory, the new polymer in solution method can be applied to all drugs that are stable in solutions and polymers that can be dissolved (preferably >100 mg/mL) by any given solvent that does not influence the molecular structure of the drug and polymer or the interactions between the drug and polymer compared to that in the solid state. Compared to the melting point depression method, it seems that the new polymer in solution method provides faster and more precise estimates, because of its simplicity the method, if refined, has the potential to enable high-throughput screening of polymers suitable for amorphous solid dispersions or glass solutions (e.g., using a 96 well-plate setup). Therefore, we encourage the scientific community to investigate and challenge this principle, both fundamentally and practically, to identify the advantages of the method and define its limitations.

9.5 Conclusion

With the introduction of the new polymer in solution method in this study, the issues associated with the established methods to predict the drug–polymer solubility at room temperature may be overcome. The method is based on the solubility of a drug in a polymer solution, and thus, does not rely on temperature extrapolations and only requires the polymer and a solvent in which the polymer is soluble. Unlike the melting point depression method, the new polymer in solution method does not require advanced equipment or complex nonlinear data treatment, and as it is based on the simple shake-flask method and HPLC quantification, it can be implemented in most laboratory setups. If refined, the method could enable high-throughput screening of polymers suitable for amorphous solid dispersions or glass solutions, which would significantly reduce the time to obtain drug–polymer solubility estimates compared to the existing thermal methods. Consequently, we believe that this method has potential to provide fast and precise estimates of drug–polymer solubility at room temperature.

Chapter 10

Influence of polymer molecular weight on *in vitro* dissolution behavior and *in vivo* performance of celecoxib:PVP amorphous solid dispersions

10.1 Abstract

In this study, the influence of the molecular weight of polyvinylpyrrolidone (PVP) on the non-sink *in vitro* dissolution and *in vivo* performance of celecoxib (CCX):PVP amorphous solid dispersions were investigated. The dissolution rate of CCX from the amorphous solid dispersions increased with decreasing PVP molecular weight and crystallization inhibition was increased with increasing molecular weight of PVP, but reached a maximum for PVP K30. This suggested that the crystallization inhibition was not proportional with molecular weight of the polymer, but rather there was an optimal molecular weight where the crystallization inhibition was strongest. Consistent with the findings from the non-sink *in vitro* dissolution tests, the amorphous solid dispersions with the highest molecular weight PVPs (K30 and K60) resulted in significantly higher *in vivo* bioavailability (AUC_{0-24h}) compared with pure amorphous and crystalline CCX. A linear relationship between the *in vitro* and *in vivo* parameter AUC_{0-24h} indicated that the simple non-sink *in vitro* dissolution method used in this study could be used to predict the *in vivo* performance of amorphous solid dispersion with good precision, which enabled a ranking between the different formulations. In conclusion, the findings of this study demonstrated that the *in vitro* and *in vivo* performance of CCX:PVP amorphous solid dispersions were significantly controlled by the molecular weight of the polymer.

10.2 Introduction

Oral delivery remains the preferred route for drug administration, mainly due to improved patient compliance and convenience[1,182]. An increasing number of new drug candidates are, however, poorly water-soluble and exhibit low and variable oral bioavailability. Therefore, formulation strategies to overcome this issue currently constitute one of the biggest challenges for the pharmaceutical industry[4,183,184]. After oral administration, a drug undergoes a dissolution process in the gastro-intestinal fluids to become available for absorption. For poorly water-soluble drugs with high permeability this process has been identified as the rate-limiting step for absorption and is thus, responsible for their low oral bioavailability[3,7,185]. Consequently, by improving the dissolution profile of these drugs it is possible to enhance their bioavailability[3,5]. Different supersaturating drug delivery systems have been identified to improve dissolution rate and enhance bioavailability by transiently increasing the intraluminal drug solubility[4,18,186]. One

approach that is getting increasingly popular is the use of amorphous solid dispersions due to their broad applicability for a broad range of poorly water-soluble drugs[11]. Amorphous solid dispersions can be defined as a molecular mixture of amorphous drug in a polymeric amorphous carrier, which present a drug release profile that is driven by the polymer properties[11,74]. Besides inducing supersaturation, polymers have also been shown to stabilize amorphous drugs during storage and inhibit recrystallization of the supersaturated drug[10,11,154]. This generation of a supersaturated state and subsequent inhibition of precipitation has been referred to as the "spring and parachute" effect[18,103] and the magnitude of this effect is highly dependent on the type and molecular weight of the polymer[10].

The polymer polyvinylpyrrolidone (PVP) is among the most commonly used carriers for amorphous solid dispersions due to its universal solubility in both hydrophobic and hydrophilic solvents and favorable thermoplastic characteristics. This makes it suitable for both solvent evaporation techniques such as spray drying as well as hot-melt extrusion[10,130,187]. A literature survey reveals that amorphous solid dispersions with PVP generally exhibit increased dissolution rate and higher apparent drug solubility in aqueous solution when compared to the crystalline drug compound[137,138]. PVP has also been shown to have significant inhibitory effects on the crystallization of drugs both in solution and in the solid state[111,188]. In addition, the dissolution rate decreases with increasing molecular weight of PVP[133,135,189] due to an increase in viscosity of the stagnant diffusion layer during the dissolution process[134]. Besides the polymer properties, the dissolution profile of an amorphous solid dispersion is also dependent on the physicochemical properties of the drug and the stability of its amorphous form[16]. Furthermore, specific intermolecular interactions between the drug and polymer may also affect the dissolution rate and nucleation/crystallization from the supersaturated state[18,190]. In pharmaceutical drug development, traditional dissolution testing is one of the most important tools used to evaluate the biopharmaceutical performance of a formulation[191]. This also applies to supersaturating drug delivery systems; however, the selection of appropriate dissolution conditions is crucial for evaluation of these formulations[16]. The polymer selection process for amorphous solid dispersions is often ranked according to their dissolution profile with fast dissolution being considered a desirable endpoint[105]. However, as the precipitation rate is dependent on the degree of supersaturation, rapid dissolution could generate a driving force for precipitation, which means that the fastest dissolving system will not necessarily show the best performance. Therefore, non-sink dissolution conditions are essential when evaluating the ability of a polymer to induce supersaturation and crystallization inhibition to enable a rational comparison of different polymers[36,105]. Despite the increasing interest in amorphous solid dispersions, the influence of the molecular weight of the polymer on the non-sink *in vitro* dissolution behavior and *in vivo* performance has to the best of our knowledge not been investigated. Therefore, the aims of the present study were to determine the effect of molecular weight of PVP (K12, 17, 25, 30, and 60) on the dissolution rate, degree of supersaturation and bioavailability of amorphous solid dispersions using the poorly water-soluble drug celecoxib (CCX) as a model compound and, if possible, to establish an *in vitro−in vivo* correlation.

CCX is a cyclooxygenase-2 selective nonsteroidal anti-inflammatory drug[192] that despite its high gastrointestinal permeability, exhibits poor oral bioavailability attributed to its low aqueous solubility (<5 μg/mL)[193,194] and is consequently classified as a class II compound in the biopharmaceutics classification system (BCS)[195]. It is a hydrophobic (log *P* = 3.5), moderately weak acid with a pK_a of 11.1[168], and therefore the solubility of CCX is not affected significantly by the physiological pH changes in the gastrointestinal tract. However, other elements in the *in vivo* environment (e.g. surfactants and lipids) play a significant role in the dissolution of CCX[195]. This is reflected by the solubility of CCX in different biorelevant media, which have been reported to be 2.3, 101.5, 46.2 and 103.3 μg/mL in fasted and fed state simulated gastric fluid, and fasted and fed state simulated intestinal fluid (FaSSIF and FeSSIF), respectively[33]. In a study on the food effect of CCX, the bioavailability after administration in dogs on a high fat diet was approximately 2.5 times higher than in fasted dogs[193]. This is in agreement with the solubility difference between fasted and fed state simulated fluids[33] and indicates that the largest effect of an amorphous solid dispersion is likely to be observed in the fasted state. Finally, previous studies have shown that amorphous solid dispersions of CCX can increase the bioavailability and dissolution rate *in vitro* compared to crystalline CCX[196-199].

10.3 Experimental section

10.3.1 Materials

Celecoxib (M_w = 381.37 g/mol) was purchased from Astatech, Inc. (Bristol, PA, USA). Ibuprofen (M_w = 206.29), Kollidon® 12 PF (PVP K12, M_w = 2000−3000 g/mol), Kollidon® 17 PF (PVP K17, M_w = 7000−11,000 g/mol), Kollidon® 25 (PVP K25, M_w = 28,000−34,000 g/mol), and Kollidon® 30 (PVP K30, M_w = 44,000–54,000 g/mol) were kindly supplied by BASF (Ludwigshafen, Germany). Polyvinylpyrrolidone PVP360 (PVP K60, M_w = 360,000 g/mol), sodium chloride (≥99%), methanol (≥99.9%), acetonitrile (≥99.9%) and ammonium dihydrogen phosphate were purchased from Sigma-Aldrich (St. Louis, MO, USA). Disodium hydrogen phosphate (≥99.5%), hydrogen chloride, monopotassium phosphate (99.5−100.5%), phosphoric acid (85%), sodium hydroxide pellets (≥99%) and sodium dihydrogen phosphate monohydrate were purchased from Merck (Darmstadt, Germany). SIF™ Powder instant biorelevant medium was purchased from Phares AG (Muttenz, Switzerland). The chemicals used were of analytical grade and all materials were used as received. The water used was obtained from a Millipore purification system (Billerica, MA, USA).

10.3.2 Preparation of solid dispersions

The CCX:PVP amorphous solid dispersions and amorphous CCX were prepared by melt-quenching. Drug and polymer were weighed (25:75 w/w), ground and mixed thoroughly using a mortar and pestle. The physical mixture was then spread evenly on aluminum foil covered with 50.8 mm PTFE (Teflon) extruded film tape mm from 3M (St. Paul, MN, USA) and placed in an

APT.line™ model ED electrical furnace from Binder GmbH (Tuttlingen, Germany) at 168 °C. After 2 min, the mixture was cooled at room temperature by removing it from the furnace, pulverized using a mortar and pestle and sieved with a 0.4 mm sieve. To ensure the homogeneity of the amorphous solid dispersion, this procedure was repeated and the solid state properties of the resulting powder were confirmed before being stored in air-tight vessels until use.

10.3.3 Solid state characterization

The solid-state properties of the pure materials and amorphous solid dispersions were analyzed using X-ray powder diffraction (XRPD). The analyses were conducted using an X'Pert PRO MRD diffractometer from PANalytical (Almelo, the Netherlands) equipped with a TCU 100 temperature control unit and an X'Celerator detector using nickel-filtered Cu Kα radiation (λ = 1.5406 Å) with an output voltage of 45 kV and an output current of 40 mA. Sample powders (1−2 mg) were compressed on zero background Si-plates and measured over the angular range 3−40 °2θ at a scan rate of 1.20 °2θ/min.

10.3.4 Thermal analysis

The thermal properties of the pure materials and amorphous solid dispersions were analyzed using differential scanning calorimetry (DSC). The analyses were performed using a Q2000 DSC from TA Instruments Inc. (New Castle, DE, USA). Sample powders (2−3 mg) were packed into Tzero aluminum hermetic pans with a perforated lid and scanned at 5 °C/min from 20−200 °C under 50 mL/min pure nitrogen gas purge. The instrument was calibrated for enthalpy and temperature using indium as a standard.

10.3.5 Preparation of dissolution medium

Fasted state simulated intestinal fluid (FaSSIF) was utilized as dissolution medium in order to predict *in vivo* dissolution. For the preparation of 1000 mL FaSSIF, 2.240 g of SIF powder was weighed into a 1000 mL volumetric flask and dissolved in approximately 500 mL of phosphate buffer pH 6.5 (0.420 g of NaOH, 3.954 g of NaH_2PO_4 monohydrate and 6.286 g of NaCl to 1000 mL adjusted to pH 6.5 with 1M HCl or 1M NaOH). The mixture was stirred until an opalescent solution was obtained after which the volume was adjusted to 1000 mL with phosphate buffer pH 6.5. The FaSSIF was then stirred for an additional 2 h, degassed and used within 24 h of preparation.

10.3.6 In vitro dissolution testing

Non-sink *in vitro* dissolution studies were performed according to the USP Dissolution Apparatus 2 – Paddle method using a VK7010 dissolution tester integrated with a VK650A

heater/circulator, from VanKel Technology Group (Cary, NC, USA). The *in vitro* dissolution profiles of crystalline CCX, amorphous CCX and amorphous solid dispersions of CCX in PVP were determined in 500 mL of FaSSIF at 37 ± 0.5 °C using a stirring rate of 100 rpm and a dose corresponding to 400 mg CCX, resulting in non-sink conditions and a potential 23.6-fold supersaturation (saturation solubility 33.9 μg/mL). 300 mL FaSSIF were placed in each dissolution vessel and preheated to 37 ± 0.5 °C and the remaining FaSSIF was heated to 37 ± 0.5 °C in an APT.line^{TM} model ED electrical furnace from Binder GmbH (Tuttlingen, Germany). Immediately before initiation of the dissolution experiment, the powders were dispersed by hand in 200 mL of preheated FaSSIF and added to the vessels at 0 min to yield a total volume of 500 mL. Aliquots of 2 mL were withdrawn at 1, 5, 10, 15, 20, 30, 45, 60, 90, 120, 180, 240, 360, and 1440 min and filtered through 0.22 μm PTFE hydrophilic membrane Q-Max syringe filters from Frisenette ApS (Knebel, Denmark). Of the filtered sample, 1 mL was diluted immediately with 1 mL mobile phase (methanol:20 mM ammonium phosphate buffer pH 2.35 65:35 v/v) to avoid crystallization of the supersaturated solution prior to analysis. The CCX was subsequently quantified using high-performance liquid chromatography (HPLC).

10.3.7 In vivo study in rats

The procedure for the *in vivo* study was approved by the Animal Welfare Committee appointed by the Danish Ministry of Food, Agriculture and Fisheries. All animal procedures were carried out in compliance with Danish laws regulating the experiments in animals as well as EC Directive 2010/63/EU and NIH guidelines for the care and use of laboratory animals. Male Sprague-Dawley rats weighing between 286 and 336 g on the day of the experiment were purchased from Charles River Laboratories (Sulzfeld, Germany) and acclimatized for a minimum of 5 days prior to the experiment. To avoid interactions with lipid components in food all rats were fasted 16−20 h prior to the study and until 12 h after dosing but allowed free access to water at all times. Immediately before administration, the powders were dispersed in FaSSIF using a magnetic stirrer. A total of 42 animals divided into 7 groups was included in the study (CCX crystalline, CCX amorphous, CCX:PVP K12, CCX:PVP K17, CCX:PVP K25, CCX:PVP K30, CCX:PVP K60), each consisted of 6 animals and dosed with 100 mg/kg body weight of CCX by oral gavage. After administration, blood samples of approximately 100 μL were collected from the tail vein at time points 0.5, 1, 2, 3, 4, 6, 8, 10, 12 and 24 h after dosing and transferred to ethylenediaminetetraacetic acid (EDTA)-coated tubes to prevent coagulation. The blood samples were centrifuged for 10 min at 3600×g in a Heraeus Multifuge 1 SR from Thermo Scientific Inc. (Hanau, Germany) and plasma was collected into labelled plastic tubes and stored at – 80 °C until analysis. Before quantification, 20 μL of plasma samples was added to 20 μL of 0.1 mg/mL ibuprofen in acetonitrile (internal standard). This mixture was vortex-mixed with 100 μL acetonitrile to precipitate the proteins and then centrifuged for 10 min at 16,060×g in a Heraeus Labofuge 400 centrifuge from Thermo Scientific Inc. (Hanau, Germany) and the supernatant was transferred to vials and CCX was quantified using HPLC.

10.3.8 Quantitative analysis

A reversed phase HPLC method was developed for quantification of CCX in the *in vitro* and *in vivo* studies. The HPLC system consisted of an L-7100 pump, an L-7200 auto sampler, a T-6000 column oven, an L-7400 UV-detector and a D-7000 Interface all from Merck-Hitachi LaChrom (Tokyo, Japan). A reverse phase X-Bridge C-18 column (4.6 × 150 mm, 3.5 μm) from Waters (Milford, MA, USA) was used for the separation and the mobile phase consisted of methanol and 20 mM ammonium phosphate buffer (65:35 v/v) adjusted to pH 2.35 ± 0.05 with phosphoric acid. The mobile phase was eluted at a flow rate of 1.0 mL/min and the effluent was monitored at 254 nm after a retention time of 6.1 min. The assay was linear for CCX in the concentration range of 50–100,000 ng/mL in both the stock solution and from plasma. The linear correlation coefficients for the calibration curve were greater than 0.99 and intra- and inter-assay variabilities were below 1.7%. Using the extraction procedure specified above, the recoveries of CCX were higher than 97.4%, and therefore the procedure was considered suitable for the assay of CCX in plasma.

10.3.9 Statistical analysis

The primary pharmacokinetic parameters area under the plasma concentration-time curve (AUC), maximum plasma concentration (C_{max}) and time to reach C_{max} (t_{max}) were obtained by non-compartmental analysis of the plasma data. An analysis of variance (ANOVA) and Tukey's post hoc test were performed for untransformed data for the pharmacokinetic parameters C_{max} and AUC_{0-24h} using SigmaPlot 11.0 from Systat Software, Inc. (Chicago, IL, USA). The values of t_{max} were analyzed using the Mann−Whitney U-test for the paired samples. A statistical p-value < 0.05 was considered significant.

10.4 Results and discussion

10.4.1 Preparation and physical characterization of the formulations

For the preparation of the amorphous solid dispersions and amorphous CCX a melt-quenching procedure was applied to imitate a melt extrusion process. After melt-quenching and pulverizing, the resulting powders were sieved in order to ensure similar particle sizes and thereby limit the effect of particle size on the dissolution behavior. The thermal decomposition of CCX and PVP starts around 185 °C and 250 °C, respectively[171,200], which is below the melt-quenching temperature of 168 °C ensuring thermal stability during processing. After the preparation, all the formulations showed a diffuse halo with no Bragg peaks in the XRPD diffractograms and only one glass transition temperature in the DSC thermograms (data not shown). This implies that the produced formulations were fully amorphous and homogenously mixed at a molecular level (glass solutions), and that the melt-quenching procedure applied in this study was applicable for the preparation of CCX:PVP amorphous solid dispersions. The drug:polymer weight ratio for all

the amorphous solid dispersions was fixed at 25:75 w/w as this has previously been found to have favorable dissolution behavior compared to lower PVP ratios[201]. Higher PVP ratios might have resulted in further improvement of the dissolution behavior, but would have limited practical relevance due to the low drug load. Furthermore, a study on the solid drug–polymer solubility showed that the solubility of CCX in PVP was not influenced by the molecular weight of PVP[150], and therefore cannot account for any potential differences in the dissolution profiles.

10.4.2 In vitro dissolution testing

The dissolution profiles after non-sink *in vitro* dissolution of crystalline CCX, amorphous CCX and CCX:PVP amorphous solid dispersions are shown in Figure 10.1. The initial dissolution rate (0–1 min) was examined and revealed that the release rates from amorphous CCX and the amorphous solid dispersions were considerably higher than that of the crystalline CCX. As can be seen from Table 10.1, there was a 27-fold increase in the initial dissolution rate for amorphous CCX compared to crystalline CCX. Furthermore, the amorphous solid dispersions also showed a higher initial dissolution rate than crystalline CCX, with a decreasing dissolution rate with increasing molecular weight of PVP (from a 12-fold increase for CCX:PVP K12 to a 3-fold increase for CCX:PVP K60). This is in accordance with a previous study that showed that the dissolution rate of pure PVP was inversely proportional with the molecular weight of PVP, which was probably due to increased viscosity and hydrophobicity of higher molecular weight PVPs, and hence decreased wettability of the matrices[74,134]. This is also in line with the time to reach the maximum CCX concentration, which were inversely proportional to the dissolution rate, with amorphous CCX having reached maximum concentration already after 1 min. As expected, the time to reach maximum concentration for the amorphous solid dispersions increased with increasing molecular weight of PVP from 12 min for CCX:PVP K12 to 45 min for CCX:PVP K30 and CCX:PVP K60.

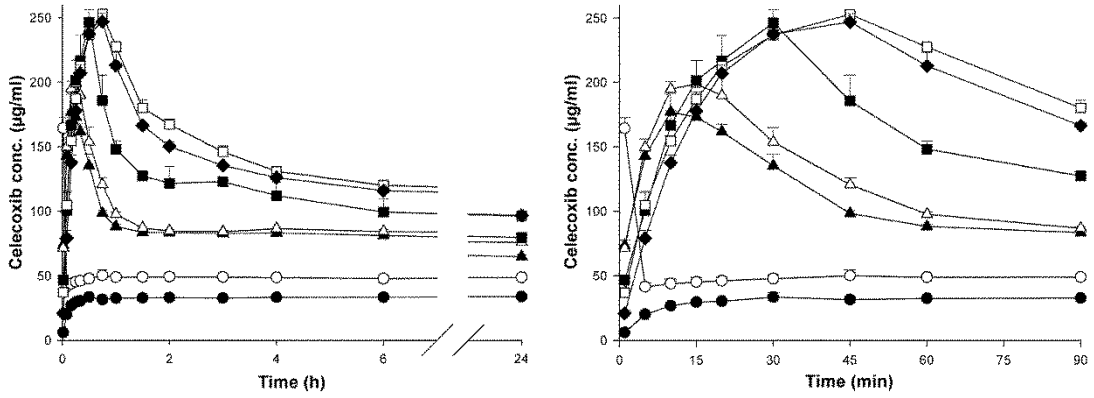

Figure 10.1: Concentration-time profiles after non-sink *in vitro* dissolution of crystalline CCX (●), amorphous CCX (○) and amorphous solid dispersions of CCX in PVP (K12: ▲, K17: Δ, K25: ■, K30: □, K60: ♦) in FaSSIF at a dose corresponding to 0.8 mg/mL or a total of 400 mg of celecoxib from left: 0–24 h and right: 0–90 min. Values represent mean celecoxib concentration ± SD (n = 3).

Table 10.1: Non-sink *in vitro* dissolution parameters of various formulations (values are mean ± SD, *n* = 3).

Formulation	AUC_{0-24h} (mg min mL^{-1})	Maximum concentration (µg mL^{-1})	Time to reach maximum concentration (min)	Initial dissolution rate (µg mL^{-1} min^{-1})
Crystalline CCX	48.1 ± 0.8	33.8 ± 0.9	1080 ± 624	6.0 ± 0.7
Amorphous CCX	69.9 ± 0.4	164.4 ± 8.4	1 ± 0	164.4 ± 8.4
CCX:PVP K12	111.4 ± 2.1	177.4 ± 1.4	12 ± 3	73.6 ± 4.0
CCX:PVP K17	121.0 ± 5.2	202.5 ± 11.7	13 ± 3	71.2 ± 2.9
CCX:PVP K25	142.6 ± 7.3	246.3 ± 10.2	30 ± 0	48.5 ± 3.1
CCX:PVP K30	173.2 ± 1.8	252.8 ± 1.5	45 ± 0	37.1 ± 7.5
CCX:PVP K60	168.0 ± 2.3	247.0 ± 6.4	45 ± 0	20.8 ± 2.3

Initially, amorphous CCX induced a 5-fold supersaturation compared to the equilibrium solubility of CCX in FaSSIF. However, after 5 min of dissolution, the supersaturated CCX had recrystallized to reach a concentration just above the equilibrium solubility. Therefore, the ability of PVP to inhibit crystallization of CCX from the supersaturated state can be partly observed from the maximum concentration achieved, as this (for the supersaturating formulations) defines the concentration where the PVP could no longer inhibit the recrystallization of the supersaturated CCX. Generally, the apparent solubility of CCX in the amorphous solid dispersions was increased compared to crystalline CCX indicating that the solvent-mediated crystallization of CCX was delayed by PVP[198]. Furthermore, it seems that the polymers are capable of maintaining a supersaturation until a certain CCX concentration, where the drug crystallized spontaneously, and therefore it is rational to assume that crystallization inhibition is correlated with the maximum concentration. The maximum concentration was 5-fold for CCX:PVP K12 and increased with increasing molecular weight of PVP to 7-fold for CCX:PVP K30, compared to crystalline CCX. However, the maximum drug concentration for CCX:PVP K60 was not higher than for CCX:PVP K30, which could indicate that crystallization inhibition reached a plateau. This is in accordance with the findings reported by Khougaz et al.[202], who investigated the effect of molecular weight of PVP on the ability to inhibit crystallization of another BCS class II compound (MK-0591). In this study, the authors found that crystallization inhibition increased with increasing PVP molecular weight, but molecular weights higher than for PVP K30 did not inhibit crystallization further (K90 = K30 > K17 > K12)[202]. Another study across compounds reported that PVP K30 exhibited increased crystallization inhibition compared to PVP K90, which suggests that viscosity and hydrophobicity of PVP (cf. molecular weight) may not be a major controlling factor in crystallization inhibition of the polymer[189]. Rather, it is likely that other factors such as molecular interactions between the drug and polymer could be responsible for the nucleation and crystal growth inhibition[107] as indicated by strong hydrogen bond interactions between the $–NH_2$ group of CCX and the –C=O groups of PVP[154]. According

to Guzmán et al.[103], the dissolution profile of amorphous solid dispersions is essentially governed by two factors: generation and stabilization of a supersaturated solution. This is popularly referred to as the "spring and parachute effect"[18,103] and basically suggests that the performance of amorphous solid dispersions is determined by the dissolution rate and crystallization inhibition of the polymer. Consequently, in order to evaluate the influence of PVP molecular weight on the overall performance of the amorphous solid dispersions *in vitro*, the area under the dissolution concentration–time curve (AUC_{0-24h}) was calculated as this value represents a combination of these two effects. From Table 10.1 it can be seen that the AUC_{0-24h} of the different formulations was proportional to the maximum concentration and ranked CCX:PVP K30 > CCX:PVP K60 > CCX:PVP K25 > CCX:PVP K17 > CCX:PVP K12 > amorphous CCX > crystalline CCX.

Even though the low molecular weight PVPs led to the highest dissolution rates of CCX, they were not able to inhibit crystallization to the same extent as the higher molecular weight PVPs, and therefore the AUC_{0-24h} of the amorphous solid dispersions with low molecular weight PVPs was lower. A statistical analysis of the data similar to that described in Section 10.3.9 revealed that the dissolution profiles (AUC_{0-24h}) for all the different formulations were significantly different (data not shown). This indicates that for PVP there may be a molecular weight where the balance between the dissolution rate enhancing and precipitation inhibiting factors is optimal and emphasizes that for amorphous solid dispersions the dissolution profile was driven by the polymer properties[11,74]. Ultimately, this means that in theory the release of drugs from amorphous solid dispersions can possibly be controlled simply by changing the molecular weight of the polymer. However, even though the molecular weight of PVP K30 was optimal for CCX in this study, it may well be drug dependent, which would have to be confirmed in future work.

10.4.3 In vivo study in rats

To assess whether the *in vitro* dissolution parameters could be used to predict *in vivo* performance, a pharmacokinetic study was performed in rats. As mentioned above, previous work showed that CCX is subject to significant food effects due to physiological changes in the gastrointestinal tract[33,193]. Consequently, differences in absorption may disappear upon food intake, and therefore the study was performed with fasted rats for increased differentiation. The mean plasma concentration–time profiles following a single oral administration of each formulation are shown in Figure 10.2. Immediately prior to administration the formulations were suspended in FaSSIF in order to prevent lumping of the polymer particles, which could delay or even prevent drug release. The maximum plasma concentration (C_{max}) of CCX, time to reach C_{max} (t_{max}) and area under the plasma concentration–time curve (AUC_{0-24h}) are provided in Table 10.2.

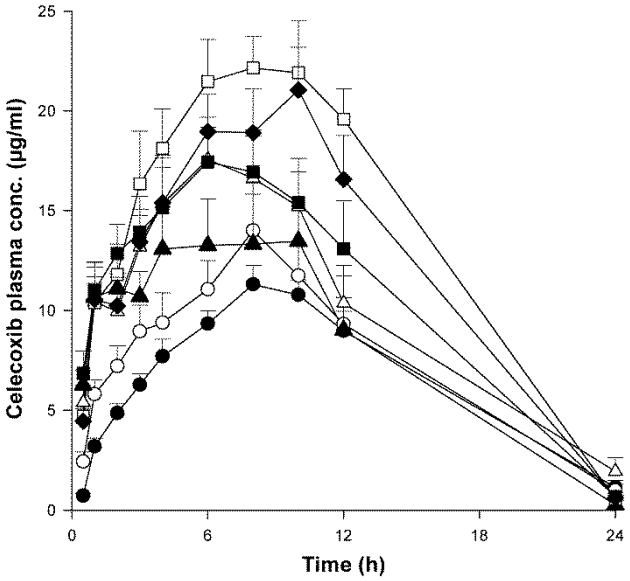

Figure 10.2: Plasma concentration-time profiles in fasted rats after oral administration of crystalline CCX (●), amorphous CCX (○) and amorphous solid dispersions of CCX in PVP (K12: ▲, K17: Δ, K25: ■, K30: □, K60: ♦) at a dose corresponding to 100 mg/kg rat. Values represent mean celecoxib plasma concentration ± SEM (n = 6).

Table 10.2: Pharmacokinetic parameters of the various formulations (values are mean ± SD, n = 6).

Formulation	AUC_{0-24h} (µg h mL^{-1})	C_{max} (µg mL^{-1})	t_{max} (h)
Crystalline CCX	158.0 ± 27.9	11.7 ± 2.0	8.7 ± 1.0 [e]
Amorphous CCX	180.5 ± 45.4	14.5 ± 4.4	7.7 ± 2.0
CCX:PVP K12	197.4 ± 103.3	14.5 ± 7.4	7.7 ± 2.3
CCX:PVP K17	239.6 ± 67.4	18.9 ± 4.7	6.7 ± 2.1
CCX:PVP K25	256.4 ± 87.5	19.2 ± 5.3	6.0 ± 2.2
CCX:PVP K30	336.9 ± 62.6 [a,b,c]	25.4 ± 6.1 [a,b,c]	7.8 ± 3.1
CCX:PVP K60	294.4 ± 77.1 [a]	21.6 ± 4.8 [a]	9.7 ± 2.0 [d,e]

Significantly different at $p < 0.05$: [a] vs. crystalline CCX; [b] vs. amorphous CCX; [c] vs. CCX:PVP K12; [d] vs. CCX:PVP K17; [e] vs. CCX:PVP K25

Compared to the *in vitro* dissolution study, the dose of 100 mg/kg rat probably resulted in higher drug concentrations, at least initially, due to the relatively low water volume in the gastrointestinal tract of rats[203]. As a higher degree of supersaturation would increase the driving force for crystallization, the formulations probably behaved differently *in vivo* than *in vitro*. Nevertheless, it was still assumed that the formulation capable of maintaining supersaturation for longest at a given dose was also able to maintain it for longest at a higher dose and thus, the ranking between the different formulations (with regards to AUC) was expected to be the same regardless of dose. The t_{max} varied from an average of 6.0−9.7 h for CCX:PVP K25 and

CCX:PVP K60, respectively. This is higher than the combined transit time in the stomach and small intestine in rats (approximately 4 h), suggesting that CCX is also absorbed in the large intestine, which was also confirmed by a previous study[37]. In contrast to the *in vitro* data, there was no correlation between the t_{max} and the molecular weight of PVP *in vivo*. Nevertheless, CCX:PVP K60 had a significantly higher t_{max} than both CCX:PVP K17 and CCX:PVP K25, and crystalline CCX had a higher t_{max} than CCX:PVP K25, which seen in isolation was in accordance with the observations made in the *in vitro* dissolution experiment. This suggested that that the dissolution rate *in vivo* was also affected to some extent by the molecular weight of PVP even though this could merely be an artifact due to the unusual peak at 12 h for the average plasma profile for CCX:PVP K60, the data suggested. However, the differences observed in t_{max} for the amorphous solid dispersions between *in vitro* and *in vivo* indicate that the majority of the drug absorption did not commence until after the formulations had recrystallized. This may be a reflection of drug reaching the previously mentioned critical concentration where the polymer can no longer maintain the supersaturation, causing the drug to crystallize spontaneously before the drug has passed to the small intestine. Based on this assumption, it is likely that amorphous solid dispersions containing polymers with a slower dissolution rate and/or increased crystallization inhibition will result in higher bioavailability.

Consistent with the findings from the non-sink *in vitro* dissolution tests, the amorphous solid dispersions resulted in higher bioavailability compared with pure amorphous and crystalline CCX as reflected by both C_{max} and $AUC_{0–24h}$ values. Furthermore, as can be seen in Table 10.2, the ranking of C_{max} for the different formulations was proportional to the $AUC_{0–24h}$ and ranked CCX:PVP K30 > CCX:PVP K60 > CCX:PVP K25 > CCX:PVP K17 > CCX:PVP K12 > amorphous CCX > crystalline CCX, which correlated well with the results from the *in vitro* tests. Both the C_{max} and $AUC_{0–24h}$ for CCX:PVP K30 were significantly different from crystalline CCX, amorphous CCX and CCX:PVP K12, and CCX:PVP K60 was significantly different from crystalline CCX. Consequently, as predicted from the non-sink *in vitro* dissolution tests, the *in vivo* study in rats confirmed that the amorphous solid dispersions had a higher bioavailability than the crystalline CCX. Therefore, the increased bioavailability of CCX in the presence of PVP appears to be linked to the increase in dissolution rate and apparent solubility compared to that of crystalline CCX. Furthermore, in accordance with expectations based on the results from the *in vitro* test, the molecular weight of PVP had a significant influence on the *in vivo* performance of CCX:PVP amorphous solid dispersions. Interestingly, both C_{max} and $AUC_{0–24h}$ for CCX:PVP K30 were higher than for CCX:PVP K60 (although not statistically significant), which was again in accordance with the results from the *in vitro* tests. Based on the previous considerations this emphasizes that for amorphous solid dispersions a fast dissolving formulation will not necessarily show the best *in vivo* performance whereas a more controlled dissolution in some cases might be more beneficial[105].

10.4.4 In vitro-in vivo correlation

In order to establish a relationship between the *in vitro* dissolution parameters and the *in vivo* pharmacokinetic parameters, the C_{max} and $AUC_{0–24h}$ values obtained from the *in vitro* tests and *in vivo* study were subjected to linear regression analysis and the correlation coefficient (r) was calculated. The correlation between the $AUC_{0–24h}$ values obtained from the *in vitro* tests and *in vivo* study is shown in Figure 10.3.

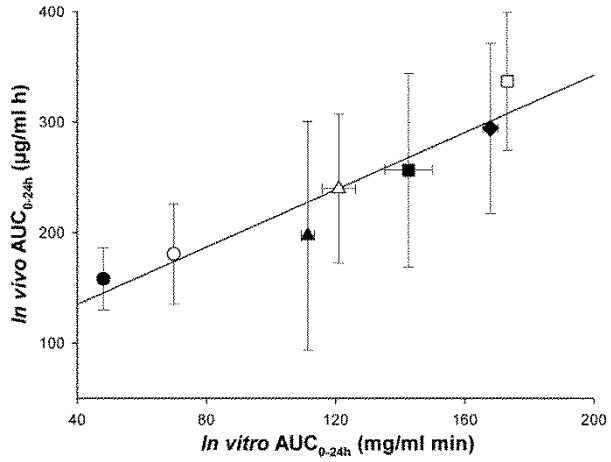

Figure 10.3: Relationships between the *in vitro* and *in vivo* parameter $AUC_{0–24h}$ for crystalline CCX (●), amorphous CCX (○) and amorphous solid dispersions of CCX in PVP (K12: ▲, K17: Δ, K25: ■, K30: □, K60: ♦). Values for *in vitro* represent mean $AUC_{0–24h}$ ± SD (n = 3) and values for *in vivo* represent mean $AUC_{0–24h}$ ± SD (n = 6). The linear regression of the data points is plotted by a solid line (r^2 = 0.913).

It should be noted that there are significant differences between the physiology of the rat and human and also in the composition of the gastrointestinal fluids. As the FaSSIF used in this study is simulating the human gastrointestinal fluid it may not be representative of rat gastrointestinal fluid with regard to e.g. pH and bile concentration, which could give rise to discrepancies with regard to the predictively of the *in vitro* method[203]. Nevertheless, the linear regression analysis between the *in vitro* $AUC_{0–24h}$ and *in vivo* $AUC_{0–24h}$ in this study showed a good correlation. Even though the ranking of the C_{max} values was comparable between the *in vitro* and *in vivo* data, no linear correlation could be demonstrated for this parameter. Furthermore, there was no correlation between the initial dissolution rate *in vitro* and the bioavailability *in vivo*, which indicates that the absorption of CCX was solubility-limited rather than dissolution rate-limited. The established correlation between *in vitro* and *in vivo* parameters indicates that non-sink *in vitro* dissolution of amorphous solid dispersions could be used to predict the *in vivo* performance. In fact, based on these findings, simple non-sink *in vitro* dissolution in FaSSIF might be as predictive or maybe even more predictive than other more complex *in vitro* methods such as multimedia/multi-compartment dissolution[100], dissolution-membrane permeation[101] or dynamic dialysis[102] that have also been proposed to predict *in vivo* performance of amorphous solid dispersions.

10.5 Conclusion

The present study demonstrated that the dissolution behavior and *in vivo* performance of amorphous solid dispersions of CCX in PVP were dependent on the molecular weight of PVP. For both *in vitro* and *in vivo*, the AUC_{0-24h} of the different amorphous solid dispersions increased with increasing molecular weight of PVP, except for CCX:PVP K60, which showed a lower AUC_{0-24h} than CCX:PVP K30. This was likely a consequence of disproportional crystallization inhibition relative to the molecular weight of PVP, indicating that there may be a molecular weight where the balance between the dissolution rate-enhancing and precipitation inhibiting factors was optimal. A linear relationship between the *in vitro* and *in vivo* AUC_{0-24h} implied the biopredictive power of the *in vitro* method, which confirmed that the absorption of CCX was solubility-limited. Consequently, although the *in vitro* method used in this study did not account for all events that could affect the *in vivo* fate of the drug, the data indicated that the simple non-sink *in vitro* dissolution method could be used to predict the *in vivo* performance of amorphous solid dispersion with good precision, which enables a ranking between the different formulations for a BCS class II compound. Furthermore, the findings of this study demonstrated that the *in vitro* and *in vivo* performances of CCX:PVP amorphous solid dispersions were significantly controlled by the molecular weight of the polymer.

Chapter 11

Influence of copolymer composition on *in vitro* and *in vivo* performance of celecoxib:PVP/VA amorphous solid dispersions

11.1 Abstract

Previous studies suggested that an amorphous solid dispersion with a copolymer consisting of both hydrophobic and hydrophilic monomers could improve the dissolution profile of a poorly water-soluble drug compared to the crystalline form. Therefore, this study investigated the influence of the copolymer composition of polyvinylpyrrolidone/vinyl acetate (PVP/VA) on the non-sink *in vitro* dissolution behavior and *in vivo* performance of celecoxib (CCX) amorphous solid dispersions. The study showed that the hydrophilic monomer vinylpyrrolidone (VP) was responsible for the generation of CCX supersaturation whereas the hydrophobic monomer vinyl acetate (VA) was responsible for the stabilization of the supersaturated solution. For CCX, there was an optimal copolymer composition around 50−60% VP content where further replacement of VP monomers with VA monomers did not have any biopharmaceutical advantages. A linear relationship was found between the *in vitro* AUC_{0-4h} and *in vivo* AUC_{0-24h} for the CCX:PVP/VA systems, indicating that the non-sink *in vitro* dissolution method applied in this study was useful in predicting the *in vivo* performance. These results indicated that when formulating a poorly water-soluble drug as an amorphous solid dispersion using a copolymer, the copolymer composition has a significant influence on the dissolution profile and *in vivo* performance. Thus, the dissolution profile of a drug can theoretically be tailored by changing the monomer ratio of a copolymer with respect to the required *in vivo* plasma–concentration profile. As this ratio is likely to be drug dependent, determining the optimal ratio between the hydrophilic (dissolution enhancing) and hydrophobic (crystallization inhibiting) monomers for a given drug is imperative.

11.2 Introduction

Development of formulation strategies to overcome the limited bioavailability associated with the increasing number of poorly water-soluble drug candidates is one of the most important challenges facing the pharmaceutical industry[5,204]. It is well known that the utilization of the amorphous form may increase the apparent solubility and dissolution rate of a drug as a consequence of increased internal free energy. However, due to the high internal free energy and molecular mobility, amorphous materials also tend to crystallize[12,13,124]. In order to circumvent crystallization and subsequent loss of the dissolution advantage, the amorphous drug can be dispersed in an amorphous polymer; a formulation strategy commonly referred to as an

amorphous solid dispersion[11,16]. Besides stabilizing the drug against crystallization in the solid state, the polymer can also further improve the dissolution profile through inhibition of the crystallization from the supersaturated solution generated upon dissolution[15,198].

The development of a successful amorphous solid dispersion is based on its dissolution performance after oral administration. Generally, the goal is to obtain a so-called spring and parachute dissolution profile[14]. This means that the drug should dissolve rapidly to reach a supersaturated concentration (spring effect) followed by crystallization inhibition in order to maintain the supersaturation long enough for the drug to be absorbed (parachute effect)[18,103]. Even though the underlying processes that govern the dissolution of amorphous solid dispersions are still not fully understood, the stabilization against crystallization is thought to be attributed to specific intermolecular interactions between the drug and polymer[125,205]. Under non-sink dissolution conditions, both the dissolution rates and supersaturation levels obtained from amorphous solid dispersions have been reported to be higher with water-soluble (hydrophilic) carriers compared to systems with water-insoluble (hydrophobic) carriers[206]. This interlinks well with the fact that the two most commonly used carriers for marketed amorphous solid dispersion are the hydrophilic polymers hydroxypropyl methylcellulose (HPMC) and polyvinylpyrrolidone (PVP)[14,37]. Even though hydrophilic polymers can provide a good "spring effect," the fast dissolution and high degree of supersaturation could also generate a driving force for crystallization[105]. Furthermore, studies have suggested that hydrophobicity is an important polymer property with respect to crystallization inhibition[108,206]. This means that the fastest dissolving system may not necessarily show the best *in vivo* performance, and, hence, that the choice of polymer(s) will have a great effect on the dissolution profile and bioavailability of the amorphous solid dispersion[15,105]. Consequently, in order to limit the crystallization upon dissolution of the drug from an amorphous solid dispersion, a hydrophobic polymer could be used in combination with a hydrophilic polymer (a so-called third generation solid dispersion)[53]. This opportunity was investigated by Xie and Taylor, who found that combining an effective crystallization inhibition polymer with a dissolution-enhancing polymer in an amorphous solid dispersion significantly improved the dissolution profile of the drug compared to any of the pure polymers[207].

Alternatively, a copolymer consisting of both hydrophobic and hydrophilic monomers could hypothetically improve both dissolution and delay crystallization of the supersaturated drug. In this case, finding the optimal ratio between the hydrophilic (dissolution enhancing) and hydrophobic (crystallization inhibiting) monomers would be the critical formulation parameter. Thus, it is possible that the dissolution profile of a drug from an amorphous solid dispersion can be tailored by changing the monomer ratio in a copolymer. Even though this hypothesis seems straightforward, the influence of the copolymer composition on the performance of amorphous solid dispersions has, to the best of our knowledge, not yet been investigated systematically. In addition, despite the great potential of amorphous solid dispersions, the number of published *in vivo* studies is still limited[37]. Therefore, the purpose of this study was to investigate the influence of copolymer composition on the non-sink *in vitro* dissolution behavior and *in vivo* performance

of an amorphous solid dispersion using celecoxib (CCX) as model drug and polyvinylpyrrolidone-co-vinyl acetate (PVP/VA) as copolymer. This copolymer consists of the hydrophilic monomer vinylpyrrolidone (VP) and the hydrophobic monomer vinyl acetate (VA) and is available in different monomer ratios: PVP/VA 335, PVP/VA 535, PVP/VA 635, and PVP/VA 735 (with 30, 50, 60, and 70% VP, respectively). The performance of the amorphous solid dispersions with the different copolymer ratios will be compared with that of the pure homopolymers PVP and polyvinyl acetate (PVA).

11.3 Methods and materials

11.3.1 Materials

Celecoxib (CCX, M_w = 381.37 g/mol) was purchased from Astatech Inc. (Bristol, PA, USA). Ibuprofen (M_w = 206.29 g/mol) and Kollidon® 30 (PVP K30, Mw = 44,000−54,000 g/mol) were purchased from BASF (Ludwigshafen, Germany). Methanol (≥99.9%), acetonitrile (≥99.9%), and ammonium dihydrogen phosphate were purchased from Sigma-Aldrich (St. Louis, MO, USA). Sodium chloride, disodium hydrogen phosphate, hydrogen chloride, monopotassium phosphate, phosphoric acid (85%), sodium dihydrogen phosphate monohydrate, and sodium hydroxide pellets were purchased from Merck (Darmstadt, Germany). SIF™ Powder instant biorelevant medium was purchased from Phares AG (Muttenz, Switzerland). Polyvinyl acetate (PVA, M_w = 35,000−45,000 g/mol) was purchased from VWR Chemicals (Pool, England), and polyvinylpyrrolidone/vinyl acetate (PVP/VA) copolymer E-335 (PVP/VA 335, M_w = 28,000 g/mol), PVP/VA copolymer E-535 (PVP/VA 535, M_w = 36,700 g/mol), PVP/VA copolymer E-635 (PVP/VA 635, M_w = 38,200 g/mol), and PVP/VA copolymer E-735 (PVP/VA 735, M_w = 56,700 g/mol) were kindly supplied by Ashland Chemical Co. (Columbus, OH, USA). PVA was received as pellets and was therefore pulverized using a Tube Mill control (at 10,000 rpm) from IKA® (Staufen, Germany) and sieved through a 0.4-mm sieve. The PVP/VA copolymers were sourced as 50% (w/w) ethanol solutions and converted to the solid form by spray drying. The solutions were diluted with ethanol to 5% (w/w) and processed using the B-290 Mini Spray Dryer from Büchi (Flawil, Switzerland). Air was drawn through the open-loop system with an aspirator rate at 100% and a temperature of 140 °C, and the pump speed was set to 30%, which resulted in an outlet temperature of approximately 80 °C[155].

11.3.2 Sample preparation

The amorphous solid dispersions and amorphous CCX were prepared by melt quenching. Drug and polymer were weighed (25:75 w/w) and mixed thoroughly using a mortar and pestle. The physical mixture was then spread evenly on aluminum foil covered with 50.8 mm PTFE (Teflon) extruded film tape mm from 3M (St. Paul, MN, USA) and placed in an APT.line™ model ED electrical furnace from Binder GmbH (Tuttlingen, Germany) at 168 °C for 2 min. The mixture was removed from the furnace, cooled to room temperature, and pulverized using a mortar and

pestle. This procedure was repeated once more for the amorphous solid dispersions. The resulting powders were sieved with a 0.4-mm sieve in order to screen out any large particles or agglomerates and stored in air-tight containers until use.

11.3.3 Solid state characterization

X-ray powder diffraction (XRPD) measurements were performed on an X'Pert PRO MRD diffractometer (PANalytical, Almelo, the Netherlands) equipped with a TCU 100 temperature control unit and an X'Celerator detector using nickel-filtered CuKα radiation (λ = 1.5406 Å) at 45 kV and 40 mA. Samples were placed on zero background (0-BG) Si plates and measured over the angular range 3−40 °2θ at a scanning rate of 1.20 °2θ/min. Results were analyzed using X'Pert Data Viewer (version 1.2) software.

11.3.4 Thermal analysis

Differential scanning calorimetry (DSC) thermograms were acquired using a DSC Q2000 calorimeter (TA Instruments Inc, New Castle, DE, USA). Sample powders (2−4 mg) were analyzed in Tzero Aluminium Hermetic pans with a perforated lid and scanned from −10 to 200 °C at a heating rate of 5 °C/min and purged with 50 mL/min pure nitrogen gas. Temperature and enthalpy of the DSC instrument were calibrated using indium as a standard. The melting temperature (T_m, onset) and glass transition temperatures (T_g, midpoint) were determined using the Universal Analysis 2000 (version 4.5A) software.

11.3.5 Preparation of fasted state simulated intestinal fluid

Fasted state simulated intestinal fluid (FaSSIF) was both utilized as dissolution medium for *in vitro* dissolution and as a suspension liquid for the *in vivo* studies. Phosphate buffer pH 6.5 was prepared in a 1000-mL volumetric flask, by dissolving 0.420 g sodium hydroxide, 3.954 g of sodium dihydrogen phosphate monohydrate, and 6.286 g sodium chloride in approximately 900 mL of demineralized water. The pH was then adjusted to 6.5 with 1 M sodium hydroxide or 1 M hydrogen chloride, and the buffer was diluted to 1000 mL with demineralized water. The FaSSIF was prepared by dissolving 2.240 g SIF^{TM} Powder in 500 mL phosphate buffer pH 6.5 and stirred on a magnetic stirrer until the powder was dissolved and an opalescent solution was obtained. The solution was then diluted to 1000 mL with phosphate buffer pH 6.5, stirred on a magnetic stirrer for a minimum of 2 h, and degassed before use. The FaSSIF was used within 24 h as specified by the supplier. The water used was from a Millipore purification system (Billerica, MA, USA).

11.3.6 In vitro studies

The non-sink *in vitro* dissolution studies were conducted at 37 ± 0.5 °C in 500 mL of FaSSIF in an USP type II apparatus (paddle method) operating at 100 rpm using a VK7010 dissolution tester integrated with a VK650A heater/circulator, both from VanKel Technology Group (Cary, NC, USA). A total of 300 mL of the freshly prepared and degassed FaSSIF was placed in each of the six round-bottomed vessels and heated to 37 ± 0.5 °C. The remaining 200 mL FaSSIF was heated to 37 ± 0.5 °C in a type B 8023 oven from Termaks (Bergen, Norway). In order to achieve non-sink conditions, formulation corresponding to 400 mg CCX (saturation solubility 34.1 μg/mL) was suspended in the preheated 200 mL FaSSIF and added to the vessel at 0 min. Aliquots of 2 mL were withdrawn at 1, 5, 10, 15, 20, 30, 45, 60, 90, 120, 180, 240, 360, and 1440 min and filtered using 0.22 μm PTFE hydrophilic membrane Q-Max syringe filters from Frisenette ApS (Knebel, Denmark). Of the filtered sample, 1 mL was diluted with 1 mL mobile phase in order to avoid crystallization and analyzed using high-performance liquid chromatography (HPLC, see below).

11.3.7 In vivo studies

Male Sprague-Dawley rats weighing in the range of 277–330 g at the day of the experiment were purchased from Charles River Laboratories (Sulzfeld, Germany). To avoid interactions with lipid components in food, all rats were fasted 16–20 h prior to the study and until 12 h after dosing. Water was available at all times. Immediately before oral dosing of 100 mg/kg body weight of CCX in a volume of 5 mL/kg, the formulations were suspended in FaSSIF using a magnetic stirrer. A total of 48 rats were randomly assigned to one of the following groups, each consisting of 6 animals: (i) crystalline CCX, (ii) amorphous CCX, (iii) amorphous solid dispersions (25:75 w/w) of CCX/PVA, (iv) CCX.PVP/VA 335, (v) CCX.PVP/VA 535, (vi) CCX.PVP/VA 635, CCX.PVP/VA 735, and (vii) CCX.PVP K30. Blood samples of 100–200 μL were collected at 0.5, 1, 2, 3, 4, 6, 8, 10, 12, and 24 h after administration by individual vein puncture and transferred to ethylenediaminetetraacetic acid (EDTA)-coated tubes to prevent coagulation. The blood samples were then centrifuged for 10 min at 3600×g with a Heraeus Multifuge 1 S-R from Thermo Scientific Inc. (Hanau, Germany). Plasma was subsequently transferred to labeled plastic tubes and stored at − 80 °C until analysis. After collection of the last sample, the animals were euthanized.

11.3.8 Analytical method

A HPLC method was used for the quantification of CCX in the samples from all the *in vitro* and *in vivo* studies. The HPLC system consisted of an L-7400 UV-detector, T-6000 column oven, L-7200 auto sampler, L-7100 pump, and D-7000 interface from Merck-Hitachi LaChrom (Tokyo, Japan). A reverse phase X-Bridge C-18 column (4.6×150 mm, 3.5 μm) from Waters (Milford, MA, USA) was used for the separation, and the mobile phase consisted of a methanol:20 mM

ammonium phosphate buffer (65:35 v/v) adjusted to pH 2.35 ± 0.05 with phosphoric acid. A total of 25 µL of sample was eluted at a flow rate of 1 mL/min, and the effluent was detected at a wavelength of 230 nm after approximately 7 min. A calibration standard concentration (100 µg/mL) was injected in between every 12 samples. The concentration of CCX was then calculated using the mean value of the peak areas obtained from the injected calibration standard concentration. The standard curve was linear over the range 0–500 µg/mL. The bioanalysis was conducted by adding 20 µL of 0.1 mg/mL ibuprofen dissolved in acetonitrile (internal standard) to 20 µL of plasma samples. This mixture was then vortex-mixed with 100 µL acetonitrile to precipitate the proteins and centrifuged for 10 min at 11,500 rpm in a Hereaeus Labofuge 400 (Thermo Scientific Inc., Germany). The supernatant was transferred to vials and analyzed by HPLC. Using this extraction procedure, the recovery of CCX was 95–98% for calibration standard concentrations with a lower quantification limit of 50 ng/mL CCX.

11.3.9 Statistical analysis

The primary pharmacokinetic parameters, area under the plasma concentration–time curve (AUC), maximum plasma concentration (C_{max}), and time to reach C_{max} (t_{max}) were obtained by non-compartmental analysis of the plasma data. An analysis of variance (ANOVA) followed by a Newman-Keuls post hoc test was performed for untransformed data in order to detect differences in the pharmacokinetic parameters C_{max} and $AUC_{0–24h}$ using SigmaPlot 11.0 from Systat Software, Inc. (Chicago, IL, USA). The values of t_{max} were analyzed using a Mann-Whitney rank sum test for the paired samples. A statistical p value < 0.05 was considered significant.

11.4 Results and discussion

11.4.1 Thermal stability and homogeneity of the formulations

In recent years, melt extrusion and spray drying have become the most common techniques for the preparation of amorphous solid dispersions[53]. As these techniques are complex and require relatively large amounts of drug and polymer, a simple melt-quenching procedure was applied in this study to imitate the melt extrusion process and to limit the time and compound consumption. Due to the relatively high temperature applied in melting techniques, it is possible that the drug or excipients may degrade during processing. However, as the thermal degradation of CCX, PVA, PVP/VA, and PVP starts well after the melt quenching temperature of 168 °C[171,200,208,209], the thermal stability of the amorphous solid dispersions was ensured during processing (confirmed by HPLC). After preparation, it was confirmed that all the formulations were completely amorphous, as evident from a diffuse halo with no Bragg peaks in the XRPD diffractogram, and homogenously mixed at a molecular level implied by only one glass transition temperature between that of the pure components in the DSC thermogram (data not shown). The

drug/polymer weight ratio was fixed at 25:75 w/w to investigate the effect of the composition of the copolymer on the *in vitro* behavior and *in vivo* performance rather than the drug/polymer ratio.

11.4.2 Effect of copolymer composition on drug dissolution at non-sink conditions

The dissolution profiles after non-sink *in vitro* dissolution of the different formulations in FaSSIF are shown in Figure 11.1 and parameters descriptive for the dissolution profile are presented in Table 11.1. As can be seen, the dissolution rates from amorphous CCX and CCX:PVP K30 were higher than for the other formulations. For the CCX:PVP/VA systems, the dissolution rate increased with increasing VP content. However, interestingly, the CCX:PVA system showed a lower dissolution rate than crystalline CCX. A previous study showed that the dissolution rates from sulfathiazole:PVP solid dispersions were highly depending on the molecular weight of the polymer[133]. However, as the molecular weight of the polymers and copolymers used in this study was kept relatively constant (28,000–56,700 g/mol), this effect is thought to be due to the composition of the (co)polymers.

Table 11.1: Non-sink *in vitro* dissolution parameters of various formulations (values are mean ± SD, *n* = 3).

Formulation	AUC_{0-24h} (mg min mL^{-1})	AUC_{0-4h} (mg min mL^{-1})	Maximum concentration (µg mL^{-1})	Time to reach maximum concentration (min)
Crystalline CCX	48.1 ± 0.8	7.6 ± 0.1	34.1 ± 0.4	[a]
Amorphous CCX	69.9 ± 0.4	11.9 ± 0.4	164.4 ± 8.4	1 ± 0
CCX:PVA	52.5 ± 2.2	6.0 ± 0.3	43.9 ± 3.3	[a]
CCX:PVP/VA 335	122.6 ± 0.9	13.5 ± 0.6	102.7 ± 3.5	[a]
CCX:PVP/VA 535	652.4 ± 13.9	54.1 ± 1.9	694.0 ± 47.6	[a]
CCX:PVP/VA 635	346.0 ± 1.5	49.9 ± 0.3	254.1 ± 1.0	[a]
CCX:PVP/VA 735	304.9 ± 5.7	51.5 ± 0.8	237.0 ± 7.5	260 ± 92
CCX:PVP K30	185.2 ± 1.9	44.2 ± 0.7	270.3 ± 1.6	45 ± 0

[a]Maxiumum at end of sampling period (1440 min)

Furthermore, other studies indicated that drug release from amorphous solid dispersions is dependent on the wettability of the polymer matrix and thus viscosity and solubility in the medium (hydrophilicity)[133,134]. The K value (viscosity in 1% w/v ethanol solution) for all the (co)polymers used in this study is around 30 (technical information, Ashland Chemical Co.). Assuming that the viscosity of the (co)polymers in FaSSIF is also equal, the effect of viscosity can be ignored, and hence, the increased dissolution rate may be isolated to the hydrophilicity of the (co)polymer. Therefore, the increasing dissolution rate is a function of copolymer composition as an increase in VP content will increase the overall hydrophilicity of the copolymer and thus the dissolution rate of the copolymer itself. These observations were all in accordance with a study by Sun and Lee, who suggested that for soluble (hydrophilic) polymers, the drug release mechanism is controlled by the dissolution of the drug, and for insoluble (hydrophobic) polymers, the drug release mechanism is controlled by the drug diffusion through the polymer matrix[206]. However, the fastest dissolving system will not necessarily show the best *in vivo* performance as rapid generation of a supersaturated solution could generate a driving force for crystallization. Therefore, non-sink dissolution conditions are essential to enable a rational comparison of different polymers[36,105].

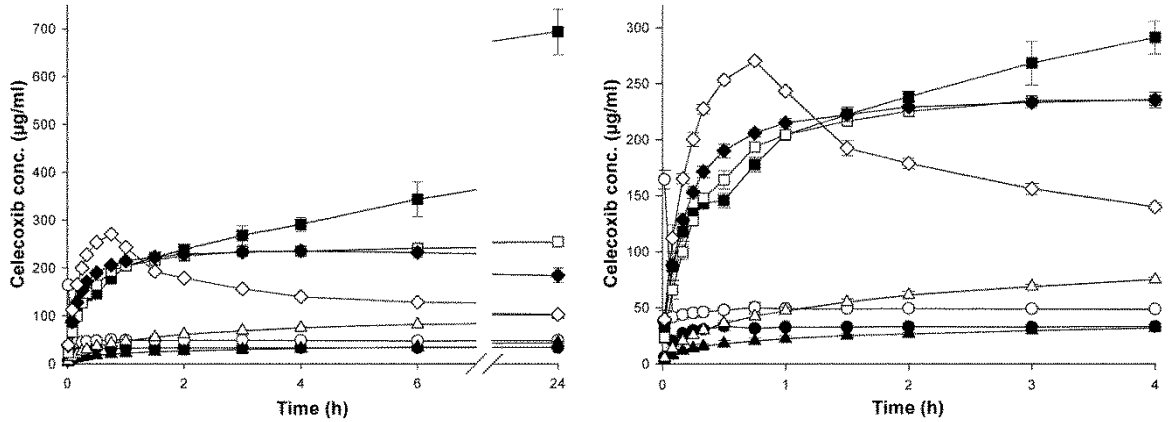

Figure 11.1: Dissolution profiles after non-sink *in vitro* dissolution of crystalline CCX (●), amorphous CCX (○) and amorphous solid dispersions of CCX in PVA (▲), PVP/VA 335 (Δ), PVP/VA 535 (■), PVP/VA 635 (□), PVP/VA 735 (♦), and PVP K30 (◊) in FaSSIF at a dose corresponding to 0.8 mg/mL or a total of 400 mg of CCX from left, 0–24 h, and right, 0–4 h. Values represent mean CCX concentration ± SD (n = 3).

As can be seen from Table 11.1, a direct correlation between the VP content and the maximum dissolution concentration was not observed. Even though the copolymers with the highest VP content offered the highest maximum concentration, there was no apparent correlation between the maximum drug concentration and copolymer composition (VP content). The maximum concentration for CCX:PVP/VA 635, CCX:PVP/VA 735, and CCX:PVP K30 was relatively similar (around 250 µg/mL), while CCX:PVP/VA 535 differed with a maximum concentration of almost 700 µg/mL (after 24 h)–more than twice as high as the formulation with the second highest concentration (CCX:PVP K30) and approximately 20 times higher than the equilibrium

solubility of crystalline CCX (~35 μg/mL). The true cause for this phenomenon is still unknown, but it is likely that the hydrophobic VA monomer plays an important role. This hypothesis is supported by observing the time to reach maximum concentration (Table 11.1), where it is evident that CCX:PVA, CCX:PVP/VA 335, CCX:PVP/VA 535, and CCX:PVP/VA 635 did not crystallize during non-sink dissolution whereas amorphous CCX, CCX:PVP/VA 735, and CCX:PVP K30 crystallized. The amorphicity and crystallinity of the undissolved material/precipitate after dissolution was also confirmed by XRPD (data not shown). Consequently, the amorphous solid dispersions with (co)polymers containing a high content of VA monomers (40−100%) inhibited crystallization, which indicates that the hydrophobic VA monomer could be responsible for this.

According to the "spring and parachute effect," the dissolution profile and thus overall performance of amorphous solid dispersions is essentially governed by two factors: generation and stabilization of a supersaturated solution[103]. Consequently, in order to enable a ranking in relation to the overall *in vitro* performance of the different formulations, the area under the dissolution concentration–time curve (AUC_{0-24h}) was calculated. Generally, it is recommended that the time frames used in *in vitro* studies are similar to those observed in biological systems when evaluating potential crystallization processes[36]. Accordingly, as the combined transit time in the stomach and small intestine in fasted rats has been reported to be approximately 4 h[203] and another *in vivo* study on CCX suspensions also using male Sprague-Dawley rats found that the t_{max} for CCX was around 4 h[210], the AUC_{0-4h} was also calculated. Even though the two different *in vitro* AUCs deviate on the specific ranking, they both show that the formulation with (co)polymers containing a high VP content (CCX:PVP/VA 535, CCX:PVP/VA 635, CCX:PVP/VA 735, CCX:PVP/VA K30) performed better than the formulations containing no or low VP content (crystalline CCX, amorphous CCX, CCX:PVA and CCX:PVP/VA 335). Furthermore, in both cases the copolymers with a high VP content (CCX:PVP/VA 535, CCX:PVP/VA 635, and CCX:PVP/VA 735) also showed higher AUCs than the pure PVP homopolymer (CCX:PVP K30).

Based on the results from this *in vitro* study, the copolymer composition has significant influence on the dissolution profile of CCX. In summary, the VP monomer appeared to be responsible for the generation of supersaturation (dissolution enhancement) and the VA monomer for the stabilization of the supersaturated solution (crystallization inhibition). The optimal copolymer composition for CCX was around 50−70% VP content; further replacement of VP monomers with VA monomers or vice versa did not have any advantage in relation to the overall *in vitro* performance. As this optimal copolymer composition is most likely drug dependent, it must be anticipated that for a drug that has a strong tendency to crystallize upon dissolution, a higher content of the stabilizing VA monomer is required compared to a drug with a lower tendency to crystallize and vice versa. This means that, in theory, the release of drugs from amorphous solid dispersions can be controlled simply by modifying the composition of a given copolymer. In order to assess if the copolymer composition also has an influence on the bioavailability, an *in vivo* study was performed.

11.4.3 Effect of copolymer composition on in vivo performance in rats

The mean plasma concentration–time profiles following oral administration of the different formulations are shown in Figure 11.2. The calculated pharmacokinetic parameters, maximum plasma concentration (C_{max}) of CCX, time to reach C_{max} (t_{max}), and area under the plasma concentration–time curve ($AUC_{0–24h}$) are provided in Table 11.2. As can be seen in Figure 11.2, the amorphous solid dispersions with (co)polymers containing a high VP content (CCX:PVP/VA 535, CCX:PVP/VA 635, CCX:PVP/VA 735, and CCX:PVP K30) resulted in a faster absorption of CCX (concentration in the first blood sample) than the (co)polymers containing no or low VP content (crystalline CCX, amorphous CCX, CCX:PVA and CCX:PVP/VA 335). This was also reflected in the C_{max}, where the same four (co)polymers with high VP content had statistically significant higher values than the other four formulations. Furthermore, all formulations had a significantly higher C_{max} than CCX:PVA, which was also in line with the observations from the *in vitro* dissolution study.

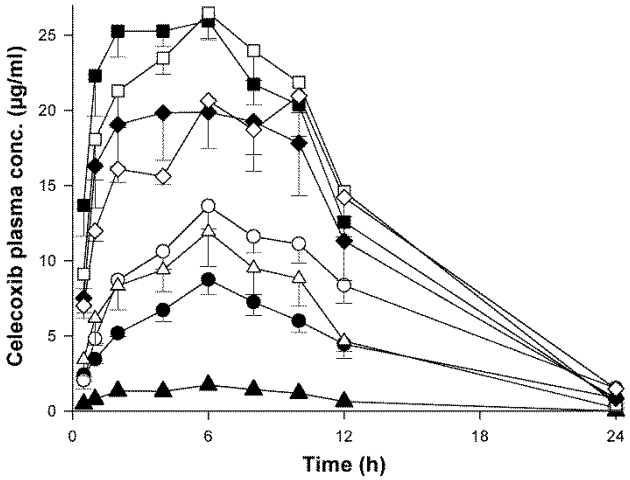

Figure 11.2: Plasma concentration-time profiles in rats after oral administrations of crystalline CCX (●), amorphous CCX (○), and amorphous solid dispersions of CCX in PVA (▲), PVP/VA 335 (Δ), PVP/VA 535 (■), PVP/VA 635 (□), PVP/VA 735 (♦), and PVP K30 (◊) at a dose corresponding to 100 mg/kg body weight of CCX. Values represent mean CCX plasma concentration ± SEM (n = 6).

The data also revealed that the $AUC_{0–24h}$ of the different formulations was proportional to the C_{max}, and thus, both parameters ranked the formulations CCX:PVP/VA 635 > CCX:PVP/VA 535 > CCX:PVP K30 > CCX:PVP/VA 735 > amorphous CCX > CCX:PVP/VA 335 > crystalline CCX > CCX:PVA. A statistical analysis of the data showed that the formulations with a (co)polymer containing a high VP content showed significantly higher C_{max} and $AUC_{0–24h}$ than the formulations containing no or low VP content (except $AUC_{0–24h}$ for CCX:PVP/VA 735 vs amorphous CCX). In agreement with the statistical differences observed for C_{max}, all formulations also had a significantly higher $AUC_{0–24h}$ than CCX:PVA. The reason for this is

most likely that the drug is never released from the polymeric matrix because the polymer itself is never dissolved (as seen *in vitro*). This emphasizes that not all amorphous solid dispersions can increase the bioavailability of a poorly water-soluble drug, but in some cases, the bioavailability can actually be reduced. For all the formulations, the t_{max} was approximately 6 h, and no significant difference could be found. Hence, the short time to reach maximum concentration *in vitro* for amorphous CCX and CCX:PVP K30, due to crystallization during dissolution, was not reflected *in vivo*. A potential explanation for this could be that CCX crystallized *in vivo* before reaching the site of absorption, and thus, the majority of drug absorption did not commence until after CCX had crystallized. For formulations that have a potential to crystallize before the site of absorption, even small variations in transit times could have a major influence on the bioavailability[36], and therefore, it must be expected that these formulations provide the most variable bioavailability (AUC_{0-24h}). This was in line with the observations in the present study on the four amorphous solid dispersions that provided a bioavailability (AUC_{0-24h}) significantly larger than crystalline CCX. The bioavailability for the crystallizing formulations CCX:PVP K30 and CCX:PVP/VA 735 varied by 26 and 42%, respectively, whereas the bioavailability for the non-crystallizing formulations CCX:PVP/VA 535 and CCX:PVP 635 only varied by 10 and 15%, respectively.

As predicted from the non-sink *in vitro* dissolution tests, the *in vivo* study in rats confirmed that, except for CCX:PVA, the amorphous solid dispersions had a higher bioavailability than crystalline CCX. In accordance with the observations from the *in vitro* study, two of the copolymers PVP/VA 535 and PVP/VA 635 performed better than the other formulations, and therefore, it seems as if that there is an optimum copolymer composition around 50−60% VP content. Compared to the pure PVP homopolymer, inclusion of a VA monomer in a PVP/VA copolymer can increase the overall performance of an amorphous solid dispersion and lower the variability in the bioavailability significantly because of its ability to inhibit the crystallization of CCX. The results of this study indicate that the copolymer composition (ratio between the hydrophilic monomer VP and hydrophobic monomer VA) has significant influence on the dissolution profile and *in vivo* performance of poorly water-soluble drugs. Furthermore, a recent study has also shown that the physical stability of the PVP/VA copolymer could be better than that of pure PVP due to an overall decrease of the hygroscopicity of the polymer[181]. This means that replacing the hydrophilic VP repeat units with hydrophobic VA repeat units will not only significantly inhibit the crystallization upon dissolution of the amorphous solid dispersion, but it may also improve the physical stability of the formulation during storage[81,163]. Consequently, knowledge about the optimum monomer ratio may be used advantageously in the future development of amorphous drug delivery systems as copolymers can theoretically be customized to “fit” any given drug.

Table 11.2: Pharmacokinetic parameters of various formulations (values are mean ± SD, *n* = 3).

Formulation	$AUC_{0-24\ h}$ (µg h mL^{-1})	C_{max} (µg mL^{-1})	t_{max} (h)
Crystalline CCX	105.1 ± 24.9 [c]	8.7 ± 2.5 [c]	6.3 ± 0.8
Amorphous CCX	178.8 ± 48.6 [a,c]	13.8 ± 3.7 [c]	5.7 ± 0.8
CCX:PVA	18.3 ± 9.8	1.8 ± 0.6	5.7 ± 2.7
CCX:PVP/VA 335	131.7 ± 59.1 [c]	12.0 ± 5.6 [c]	6.7 ± 1.6
CCX:PVP/VA 535	339.9 ± 34.8 [a,b,c,d]	28.5 ± 2.0 [a,b,c,d]	4.2 ± 2.9
CCX:PVP/VA 635	346.2 ± 51.0 [a,b,c,d]	28.7 ± 2.9 [a,b,c,d]	5.0 ± 2.4
CCX:PVP/VA 735	282.2 ± 118.6 [a,c,d]	22.9 ± 8.2 [a,b,c,d]	5.0 ± 2.1
CCX:PVP K30	296.5 ± 75.9 [a,b,c,d]	22.9 ± 6.0 [a,b,c,d]	7.3 ± 2.1

Significantly different at $p < 0.05$: [a] vs. crystalline CCX; [b] vs. amorphous CCX; [c] vs. CCX:PVA; [d] vs. CCX:PVP/VA 335; [e] vs. CCX:PVP/VA 535

11.4.4 In vitro-in vivo correlation

The ultimate goal when performing *in vitro* studies is to establish a method that can predict the clinical performance of a formulation (*in vivo* performance)[36]. Although the intraluminal behavior of amorphous solid dispersions still needs to be elucidated, the crystallization observed *in vitro* is also believed to occur *in vivo*. Therefore, in the case of supersaturating formulations, it is important that the *in vitro* dissolution behavior is evaluated in non-sink conditions to account for the effect of potential crystallization[105]. Another crucial element is the comparison of relevant *in vitro* parameters with *in vivo* pharmacokinetic parameters. Of these pharmacokinetic parameters, the most important relating to the overall performance (bioavailability) of a formulation is the AUC. However, comparing the data from Table 11.1 and Table 11.2, no correlation between C_{max} and maximum dissolution concentration or t_{max} and time to reach maximum dissolution concentration could be established. Furthermore, no correlation was found between *in vitro* AUC_{0-24h} and *in vivo* AUC_{0-24h}. Even though CCX is absorbed throughout the gastrointestinal tract, it is rational to assume that the majority of the dose is absorbed in the small intestine[193] as this constitutes more than 75% of the total length and 98% of the total surface volume of the gastrointestinal tract[211]. The transit times in the stomach, small intestine, and large intestine of rats have been reported to be 15−30 min, 3−4 h, and 10−11 h, respectively[203]. In comparison, the transit times in fasted humans have been reported to be 10−15 min (for liquids), 3−4 h, and 8−18 h, respectively[212]. The combined transit time in the stomach and small intestine of both fasted humans and rats is thus approximately 4 h, and therefore the *in vitro* AUC_{0-4h} might be more predictive than the AUC_{0-24h}. And in fact (CCX:PVA excluded), it was possible to establish an *in vitro-in vivo* correlation between *in vitro* AUC_{0-4h} with *in vivo* AUC_{0-24h} as illustrated in Figure 11.3.

The present study indicated that the *in vitro* non-sink dissolution method could be used to predict the *in vivo* performance of the formulations under investigation. However, it should be noted that the optimal *in vitro* time frame to predict *in vivo* performance could very well be drug dependent. Therefore, more investigations across compounds and (co)polymers need to be performed in order to confirm the predictive power of the non-sink dissolution method and the effect of copolymer composition on the *in vivo* performance in general.

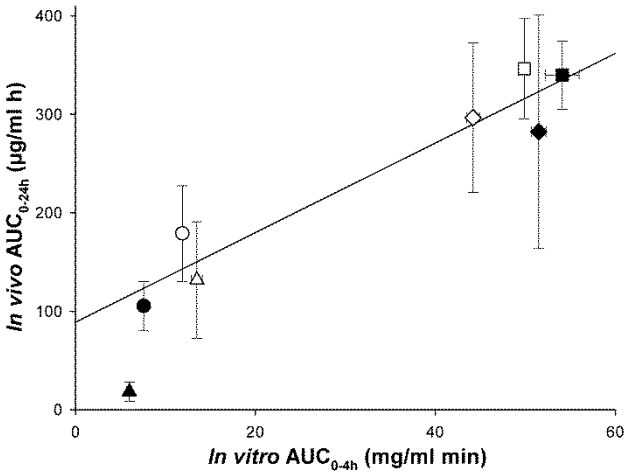

Figure 11.3: Relationships between *in vitro* $AUC_{0–4h}$ and *in vivo* $AUC_{0–24h}$ for crystalline CCX (●), amorphous CCX (○), and amorphous solid dispersions of CCX in PVA (▲), PVP/VA 335 (Δ), PVP/VA 535 (■), PVP/VA 635 (□), PVP/VA 735 (♦), and PVP K30 (◊). Values for *in vitro* represent mean $AUC_{0–4h}$ ± SD (n = 3) and values for *in vivo* represent mean $AUC_{0–24h}$ ± SD (n = 6). The linear regression of the data points (CCX:PVA excluded) is plotted by a solid line (r^2 = 0.923).

11.5 Conclusion

Amorphous solid dispersions of CCX in PVA, PVP, and PVP/VA of different copolymer compositions were successfully prepared by a melt-quenching procedure. Except for CCX:PVA, all formulations showed an increased dissolution rate and apparent solubility compared to crystalline CCX. This improved dissolution behavior was also reflected in an increase in oral bioavailability in rats, which indicates that the absorption of CCX was solubility and dissolution limited. The formulations with (co)polymers containing a high VP content displayed superior *in vitro* and *in vivo* performance compared to those containing no VP or low VP content. The amorphous solid dispersion using the copolymers PVP/VA 535 and PVP/VA 635 performed better than the pure homopolymers PVA and PVP, and therefore, it seems that there is an optimum copolymer composition around 50−60% VP content. Of the two monomers contained in the copolymer, the hydrophilic VP monomer appeared responsible for the generation of supersaturation (dissolution enhancement) whereas the hydrophobic VA monomer was responsible for the stabilization of the supersaturated solution (crystallization inhibition). Finally,

a correlation between *in vitro* AUC_{0-4h} and *in vivo* AUC_{0-24h} suggests that the *in vitro* non-sink dissolution method applied in this study could be used to predict *in vivo* performance.

The results of this study show that the implementation of the amorphous solid dispersion strategy holds great potential to increase the bioavailability of a poorly water-soluble drug if the right (co)polymeric carriers are chosen. The copolymer composition had significant influence on the dissolution profile and *in vivo* performance, which indicates that a copolymer consisting of a mix of hydrophobic and hydrophilic monomers, in theory, could improve both dissolution rate and delay crystallization of the supersaturated drug. Hence, it is possible that the dissolution profile can be tailored by changing the monomer ratio of a copolymer with respect to the required *in vivo* plasma–concentration profile. As this ratio is likely to be drug dependent, determining the optimal ratio between the hydrophilic (dissolution enhancing) and hydrophobic (crystallization inhibiting) monomers for a given drug is a critical formulation parameter when developing an amorphous solid dispersion with a copolymer such as PVP/VA as carrier.

Chapter 12

Effect of polymer type and drug dose on the *in vitro* and *in vivo* behavior of amorphous solid dispersions

12.1 Abstract

This study investigated the non-sink *in vitro* dissolution behavior and *in vivo* performance in rats of celecoxib (CCX) amorphous solid dispersions with polyvinyl acetate (PVA), polyvinylpyrrolidone (PVP) and hydroxypropyl methylcellulose (HPMC) at different drug doses. Both *in vitro* and *in vivo*, the amorphous solid dispersions with the hydrophilic polymers PVP and HPMC led to higher areas under both, the *in vitro* dissolution and the plasma concentration–time curves (AUC) compared to crystalline and amorphous CCX for all doses. In contrast, the amorphous solid dispersion with the hydrophobic polymer PVA showed a lower AUC both *in vitro* and *in vivo* than crystalline CCX. For crystalline CCX and CCX:PVA, the *in vitro* AUC was limited by the low solubility of the drug and the slow release of the drug from the hydrophobic polymer, respectively. For the supersaturating formulations; amorphous CCX, CCX:PVP and CCX:HPMC, the *in vitro* performance was mainly dependent on the dissolution rate and precipitation/crystallization inhibition of the polymer. As expected, the crystallization tendency increased with increasing dose, and therefore the *in vitro* AUCs did not increase proportionally with dose. Even though the *in vivo* AUC for all formulations increased with increasing dose, the relative bioavailability decreased significantly, indicating that the supersaturating formulations also crystallized *in vivo* and that the absorption of CCX was solubility-limited. These findings underline the importance of evaluating relevant *in vitro* doses, in order to rationally assess the performance of amorphous solid dispersions and avoid confusion in early *in vivo* studies.

12.2 Introduction

Oral delivery remains the most preferred route of administration for pharmaceutical products in spite of the natural barriers that exist in the gastrointestinal tract. This is mainly due to the advantages associated with oral drug delivery such as patient acceptability and compliance[1]. However, as an increasing number of new drug candidates have poor oral bioavailability due to low aqueous solubility; formulation strategies that overcome this solubility-limited bioavailability are needed[5,6]. Several strategies have already been proposed and amongst these, formulations containing the drug in the amorphous form are probably the most promising[7,8,18]. The internal free energy of the amorphous form is higher than that of the crystalline form and thus, upon dissolution of the drug this energy is released, leading to increased dissolution rate and apparent solubility. This may result in improved absorption and ultimately increased

bioavailability of an amorphous drug relative to its crystalline counterpart[11,13,173,213]. Despite the potential of amorphous solid dosage forms, the number of products on the market is still relatively limited[17]. This is mainly because the material is thermodynamically unstable and will eventually nucleate and crystallize, not only during storage, but potentially also from the supersaturation generated upon dissolution in the gastrointestinal tract[16,214]. In an attempt to overcome these stability issues, the drug can be molecularly dispersed in a polymer to form an amorphous solid dispersion as polymers have been shown to enhance the physical stability of amorphous drugs and in some cases also serve as a crystallization inhibitor from a supersaturated solution[9,10]. However, although the mechanisms underlying the physical stabilization abilities of polymers have been well studied and are believed to be attributed to e.g. reduced molecular mobility and specific molecular interactions[49,154,173,214], little is known about the mechanisms responsible for inhibiting crystallization of the supersaturation generated upon dissolution of amorphous solid dispersions[36,215].

Previous studies have shown that the choice of polymer(s) has significant influence on the dissolution behavior of amorphous solid dispersions[15,199,207,216,217]. Furthermore, as the driving force for crystallization is increased with an increasing degree of supersaturation, the dissolution behavior of amorphous solid dispersions both *in vitro* and *in vivo* will be highly dependent on the drug dose[15,18]. As sink conditions are unlikely to be found for poorly water-soluble drugs *in vivo*, this underlines the importance of applying non-sink conditions when evaluating the amorphous solid dispersions *in vitro*[105]. The aims of the current study were, therefore, to investigate the effect of dose on the non-sink *in vitro* dissolution behavior of the poorly water-soluble model drug celecoxib (CCX) in amorphous solid dispersions with polyvinyl acetate (PVA), polyvinylpyrrolidone (PVP) and hydroxypropyl methylcellulose (HPMC). Furthermore, the biopharmaceutical advantages of the amorphous solid dispersions over crystalline and amorphous CCX were also evaluated *in vivo* in rats at four different doses.

12.3 Experimental section

12.3.1 Materials

Celecoxib (CCX, M_w = 381.37 g/mol) was purchased from Matrix Scientific (Columbia, SC, USA). Ibuprofen (M_w = 206.29 g/mol) and Kollidon® 30 (PVP, M_w ~49,000 g/mol) were purchased from BASF (Ludwigshafen, Germany). Pharmacoat 603 (HPMC, M_w ~54,000 g/mol) was kindly supplied by Shin-Etsu (Wiesbaden, Germany) and polyvinylacetate (PVA, M_w ~ 40,000 g/mol) was purchased from VWR Chemicals (Leuven, Belgium). PVA was received as pellets and powdered using a Tube Mill control (at 10,000 rpm) from IKA® (Staufen, Germany) and sieved through a 0.4 mm sieve before use. Acetonitrile (≥99.9%), ammonium dihydrogen phosphate and methanol (≥99.9%) were purchased from Sigma-Aldrich (St. Louis, MO, USA). Sodium dihydrogen phosphate monohydrate (>99%), sodium chloride, hydrochloric acid (37–38%), phosphoric acid (85%), and sodium hydroxide (pellets, >99%) were purchased from

Merck (Darnmstadt, Germany) and SIF™ Powder instant biorelevant medium was purchased from Phares AG (Muttenz, Switzerland). Purified water was obtained from a Millipore Milli-Q Ultrapure Water purification system (Billerica, MA, USA).

12.3.2 Sample preparation

Amorphous CCX and amorphous solid dispersions were prepared by a melt quenching technique in batches of 10 g each. A drug:polymer physical mixture (25:75 w/w) was prepared and spread evenly on aluminum foil covered with PFTE tape from 3M (St. Paul, MN, USA). The powder mixture was heated to 168 °C (approximately 5 °C above the melting temperature of CCX) in an APT.line™ model ED oven from Binder GmbH (Tuttlingen, Germany). Subsequently, the mixture was cooled by removing it from the oven and pulverized using a mortar and pestle. This procedure was repeated in order to ensure homogeneity and the resulting powder was then sieved with a 0.3 mm sieve in order to screen out any large particles or agglomerates but keeping the fines. The coarse fraction was then pulverized and sieved once again to minimize waste and avoid dose variation. After sample preparation, the solid state and thermal properties of the different formulations were analyzed using X-ray powder diffraction (XRPD) and differential scanning calorimetry (DSC). A diffuse halo in combination with the absence of Bragg peaks in the XRPD diffractograms implied that the samples were amorphous and the presence of only one glass transition temperature, between that of the pure components, in the DSC thermograms indicated that the formulations were homogenously mixed (see Appendix C). The final formulations were stored in air-tight vessels until use.

12.3.3 Preparation of dissolution medium

Fasted state simulated intestinal fluid (FaSSIF) was used as biorelevant medium for *in vitro* dissolution and as a suspension liquid for the *in vivo* studies. For the preparation of 1000 mL of FaSSIF, phosphate buffer pH 6.5 was produced by dissolving 0.420 g of sodium hydroxide (pellets), 3.954 g of sodium dihydrogen phosphate monohydrate and 6.286 g of sodium chloride in about 900 mL of purified water. The pH was adjusted to 6.5 with either 1 M sodium hydroxide or 1 M hydrochloric acid and the volume was diluted to 1000 mL with purified water. In about 500 mL of the phosphate buffer pH 6.5, 2.240 g of SIF™ powder was added and placed on a magnetic stirrer until the powder was completely dissolved. Hereafter, the solution was diluted to 1000 mL with phosphate buffer pH 6.5 and allowed to stand under stirring for at least 2 h at room temperature until it became slightly opalescent. The FaSSIF was degassed and used within 24 h of preparation as recommended by the supplier.

12.3.4 In vitro dissolution

Non-sink dissolution studies were performed using the USP apparatus II – paddle method in a VK 7010 dissolution testing station with a VK650A heater/circulator from VanKel Technology Group (Cary, NC, USA). All *in vitro* dissolution studies were conducted in 500 mL of the biorelevant medium (FaSSIF) with a stirring speed at 100 rpm. Approximately 300 mL of the freshly prepared and degassed FaSSIF was placed in each vessel and heated to 37 ± 0.5 °C before start. The remaining 200 mL from each vessel were heated to 37 ± 0.5 °C in a heating oven. The formulations were dispersed in the 200 mL pre-heated FaSSIF and added to the vessels at 0 min. Aliquots of 2 mL were withdrawn and filtered using 0.22 μm PTFE hydrophilic membrane Q-Max syringe filters from Frisenette ApS (Knebel, Denmark) at times 1, 5, 10, 15, 20, 30, 45, 60, 90, 120, 180, 240, 360 and 1440 min. Of the filtrate, 1 mL was diluted with 1 mL mobile phase to avoid precipitation/crystallization before HPLC analyis (see below).

12.3.5 In vivo study

All animal experiments were approved by the local Animal Welfare Committee appointed by the Danish Ministry of Food, Agriculture and Fisheries and performed according to Danish laws regulating studies on animals, EC Directive 2010/63/EU and, National Institute of Health (NIH) guidelines for the Care and Use of Laboratory Animals. Male Sprague Dawley rats weighing between 278–350 g on the day of administration were purchased from Charles River Laboratories (Sulzfeld, Germany) and acclimatized for a minimum of 5 days prior to entering the experiment, where they were offered standard rodent food and carrots. All rats had free access to water, but to avoid food-effect, the rats were deprived of fodder 16–20 h before dosing until 12 h after dosing after which carrots were offered to the animals. Immediately before dosing, the formulations were suspended in FaSSIF on a magnetic stirrer. The animals were given five different formulations (crystalline CCX, amorphous CCX, CCX:PVA, CCX:PVP and CCX:HPMC), each dosed as suspensions corresponding to 12.5, 50, 100 and 200 mg/kg CCX in 5 mL/kg FaSSIF by oral gavage to six randomly assigned rats. After oral administration, blood samples of approximately 150 μL were taken at 0.5, 1, 2, 4, 6, 8, 10, 12 and 24 h after administration by individual tail vein puncture and transferred into ethylenediaminetetraacetic acid (EDTA)-coated tubes to prevent blood coagulation. The blood samples were then centrifuged for 10 min at 3600 rpm in a Heraeus Multifuge 1 S-R from Thermo Fisher Scientific Inc. (Waltham, MA, USA) and the plasma was transferred to individual plastic tubes and stored at – 80 °C until analyzed. The rats were euthanized after collection of the last sample.

12.3.6 High-performance liquid chromatography

Drug contents were quantified for CCX by reverse-phase high-performance liquid chromatography (HPLC) with an L-7400 UV-detector, T-6000 column oven, L-7200 auto sampler, L-7100 pump and D-7000 interface from Merck-Hitachi LaChrom (Tokyo, Japan). The

reverse-phase column used for separation was an X-Bridge C-18 column (150 × 4.6 mm, 3.5 µm) (Waters, MA, USA). The mobile phase consisted of methanol:20 µM ammonium phosphate buffer pH 2.35 (65:35, v/v), and the UV detector was set at 254 nm. The flow rate was maintained at 1.0 mL/min and 25 µL was injected, yielding a retention time of around 6.5 min. The standard curve was linear over the range 50 – 500,000 ng/mL with a correlation coefficient greater than 0.99 and intra- and inter-assay variability below 1.9%. The limit of detection (LOD) and limit of quantification (LOQ) was calculated to 3.8 ng/mL and 11.4 ng/mL, respectively.

Before quantification of the plasma samples 20 µL of plasma was added to individual Eppendorf tubes containing 20 µL of 0.1 mg/mL ibuprofen in acetonitrile (internal standard). This mixture was vortex-mixed with 100 µL acetonitrile to precipitate the proteins and then centrifuged for 10 min at 16,060 × g (11,500 rpm) in a Hereaeus Labofuge 400 centrifuge from Thermo Scientific Inc. (Hanau, Germany). The supernatant was transferred to vials and quantified for CCX using HPLC[218]. Using this extraction procedure, the recoveries of both CCX and internal standard (ibuprofen) were higher than 97.3%.

12.3.7 Statistical analysis

SigmaPlot version 11.0 from Systat Software Inc. (Chicago, IL, USA) was used for the statistical analysis. The pharmacokinetic parameters; area under the plasma concentration–time curve (AUC), maximum plasma concentration (C_{max}), and time to reach C_{max} (t_{max}) were obtained by non-compartmental analysis of the plasma data. A one-way analysis of variance (ANOVA) followed by a Student-Newman-Keuls (SNK) test was used to compare the untransformed data in order to identify statistical differences in the pharmacokinetic parameters C_{max} and $AUC_{0–24h}$. The values of t_{max} were analyzed using a Mann-Whitney rank sum test for the paired samples. A statistical p-value < 0.05 was considered significant.

12.4 Results and discussion

12.4.1 Effect of polymer type and drug dose on in vitro behavior

Non-sink dissolution of crystalline CCX, amorphous CCX and the different amorphous solid dispersions was conducted in 500 mL FaSSIF pH 6.5 using a USP apparatus II (paddle method). In order to study the effect of dose and polymer type, the drug:polymer weight ratio for the amorphous solid dispersions was fixed at 25:75 w/w as this has previously been identified as the optimal ratio in relation to dissolution behavior for CCX:HPMC and CCX:PVP amorphous solid dispersions compared to higher polymer ratios[201]. This means that when the drug dose is increased, the amount of polymer is increased accordingly.

The influence of drug dose on the dissolution profiles for all the formulations is shown in Figure 12.1 and *in vitro* parameters descriptive for the dissolution profiles are presented in Table 12.1. As can be seen in Table 12.1, the initial dissolution rate and maximum concentration generally

increased with increasing dose for all the formulations. The concentration for all doses of crystalline CCX reached a maximum of approximately 40 μg/mL, which was considered the equilibrium solubility of CCX in FaSSIF. Based on this, it is evident that amorphous CCX, CCX:PVP and CCX:HPMC reached supersaturated CCX concentrations for all doses. CCX:PVA, on the other hand, only reached supersaturation for the two highest doses during dissolution. The maximum CCX concentrations achieved for CCX:HPMC and CCX:PVP were ~5 times higher than CCX:PVA on average, with a maximum of ~6-fold and ~7-fold supersaturation, respectively. For all doses, the observed rank order of the maximum concentration for the amorphous solid dispersions was CCX:PVP > CCX:HPMC > CCX:PVA, which correlates well with the water-solubility (hydrophilicity) of the polymers and indicates that higher maximum concentrations can be achieved with more water-soluble polymers. In this context, however, it is important to emphasize that the dissolution profile of a supersaturating amorphous solid dispersion is controlled by two opposing processes i.e. the dissolution of the drug/polymer matrix and crystallization/precipitation of the supersaturated drug. As the driving force for crystallization increases with increasing degree of supersaturation, the formulation that reaches the highest maximum concentration will not necessarily show the best performance[105]. For the supersaturating formulations, the maximum concentration may be considered as a critical degree of supersaturation (that is formulation-specific), where the drug concentration exceeds the metastable limit of supersaturation, causing the drug to spontaneously crystallize. For CCX:PVA, CCX:PVP and CCX:HPMC, the maximum concentration increased with increasing dose. As previous studies have shown that the aqueous solubility of poorly water-soluble drugs can increase with increasing PVP and HPMC concentration[219,220], the increase in maximum concentration with increasing dose observed in this study may therefore, at least partly, be ascribed to the higher absolute concentration of the polymer in the dissolution medium. However, for amorphous CCX, the concentration reached a maximum of ~80 μg/mL for the two highest doses i.e. above the equilibrium solubility of CCX in FaSSIF, but lower than the amorphous solid dispersions with hydrophilic polymer (PVP and HPMC). This lower maximum concentration was probably a reflection of the pure amorphous CCX not containing any crystallization inhibiting and/or solubilizing polymer, and therefore CCX should in principle crystallize when the critical degree of supersaturation was reached regardless of dose. After 24 h of dissolution of amorphous CCX, the concentration for all the doses approached a so-called "amorphous solubility" that was 1.5-fold (~60 μg/mL) of the equilibrium solubility of crystalline CCX). The term "amorphous solubility" used in this context refers to a sustained metastable equilibrium that is higher than the true thermodynamic solubility[221].

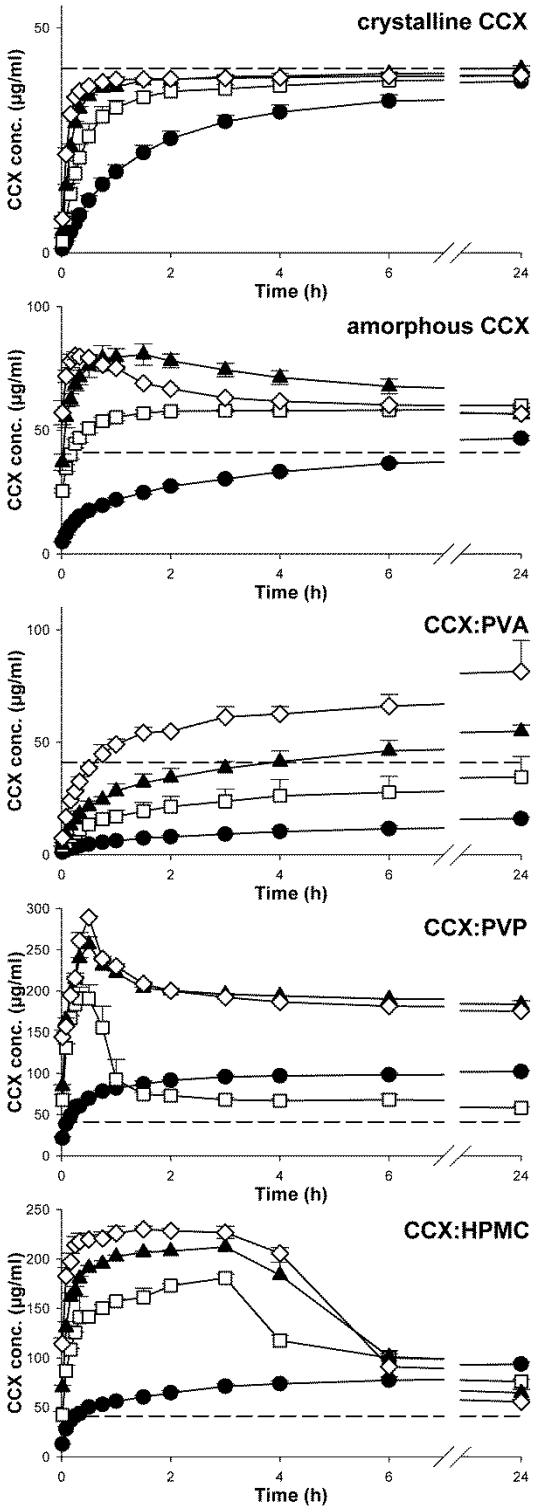

Figure 12.1: Dissolution profiles after non-sink *in vitro* dissolution of crystalline CCX and amorphous CCX, and amorphous solid dispersions of CCX:PVA, CCX:PVP and CCX:HPMC at a CCX dose of 50 mg (●), 200 mg (□), 400 mg (▲) and 800 mg (◊) in 500 mL FaSSIF. Note that the scale of the y-axis varies between the different subfigures. Values represent mean CCX concentration ± SD (n = 3). The dashed line indicates the equilibrium solubility of crystalline CCX in FaSSIF.

Table 12.1: *In vitro* parameters after non-sink dissolution of crystalline CCX, amorphous CCX, CCX:PVA, CCX:PVP and CCX:HPMC at different doses (values are mean ± SD, *n* = 3).

Dose (mg)	$AUC_{0\text{-}24h}$ (mg min mL^{-1})	$AUC_{0\text{-}4h}$ (mg min mL^{-1})	Maximum concentration (µg mL^{-1})	Initial dissolution rate (µg mL^{-1} min^{-1})	Time to reach maximum concentration (min)
Crystalline CCX					
50	48.1 ± 1.7	5.4 ± 0.3	38.1 ± 1.0	0.9 ± 0.1	[a]
200	54.3 ± 1.3	7.8 ± 0.3	39.4 ± 0.9	2.6 ± 0.8	[a]
400	57.2 ± 0.5	8.8 ± 0.1	41.0 ± 0.6	4.9 ± 0.5	[a]
800	56.2 ± 0.3	9.0 ± 0.1	39.5 ± 0.5	7.8 ± 0.6	[a]
Amorphous CCX					
50	55.2 ± 1.1	6.1 ± 0.2	46.7 ± 1.1	4.9 ± 0.2	[a]
200	84.0 ± 0.4	13.2 ± 0.2	60.1 ± 0.8	25.5 ± 0.9	[a]
400	93.3 ± 3.0	18.0 ± 0.7	80.6 ± 4.3	37.1 ± 3.3	90 ± 0
800	86.9 ± 1.2	16.4 ± 0.1	80.1 ± 1.6	57.1 ± 4.9	15 ± 0
CCX:PVA					
50	18.0 ± 1.4	1.8 ± 0.1	16.0 ± 0.8	1.1 ± 0.1	[a]
200	41.6 ± 10.6	4.8 ± 1.0	34.6 ± 9.1	3.8 ± 0.1	[a]
400	67.5 ± 5.3	7.7 ± 0.8	54.9 ± 2.8	4.4 ± 0.9	[a]
800	99.9 ± 10.9	12.5 ± 0.5	81.5 ± 13.8	7.4 ± 0.2	[a]
CCX:PVP					
50	140.2 ± 2.4	20.5 ± 0.2	102.0 ± 1.8	21.4 ± 2.1	[a]
200	98.6 ± 4.5	24.1 ± 1.6	193.1 ± 15.8	67.8 ± 6.8	15 ± 5
400	274.3 ± 3.0	49.2 ± 0.5	256.5 ± 9.0	84.5 ± 1.8	30 ± 0
800	264.7 ± 3.9	49.8 ± 0.5	289.0 ± 1.5	144.1 ± 8.5	30 ± 0
CCX:HPMC					
50	116.2 ± 1.9	14.8 ± 0.4	93.7 ± 2.2	12.9 ± 0.4	[a]
200	145.6 ± 1.6	37.3 ± 0.5	180.8 ± 4.1	42.3 ± 3.7	180 ± 0
400	154.0 ± 2.0	47.5 ± 1.0	212.5 ± 8.3	70.3 ± 2.2	140 ± 35
800	150.1 ± 5.2	52.9 ± 0.5	232.3 ± 1.0	114.2 ± 6.2	110 ± 62

[a]Maxiumum at end of sampling period (1440 min)

As the mechanism of drug release from amorphous solid dispersions is thought to be governed by the dissolution of the carrier[74], the dissolution rate of the drug is dependent of two processes i.e. the diffusion of solvent molecules into the polymer (swelling) followed by complete dispersion of the polymer in the solvent medium (dissolution). For some polymers, the swollen surface layer can delay or even counteract the dissolution process by diminution of the concentration gradient depending on the chemical structure, molecular weight and other physicochemical properties of the polymer[222]. As can be seen in Table 12.1, the initial dissolution rate for crystalline CCX and amorphous solid dispersion with the hydrophobic polymer PVA was almost equal for all doses. In contrast, amorphous CCX, and amorphous solid dispersions with the hydrophilic polymers HPMC and PVP showed a ~8-fold, ~15-fold and ~21-fold increase in the initial dissolution rate on average compared to crystalline CCX and CCX:PVA, respectively. The higher dissolution rate of the amorphous solid dispersion with PVP relative to HPMC (as PVP swells faster than HPMC) is in accordance with a previous study[223] and indicates that the release of CCX from the amorphous solid dispersions was indeed controlled by the dissolution rate of the polymer. Based on these findings it is reasonable to assume that amorphous solid dispersions with more hydrophilic (water-soluble) polymers will generally display higher dissolution rates. However, as described previously, a rapid dissolution will also create a higher driving force for crystallization and therefore, a more controlled dissolution rate might be a more attractive alternative[105]. This phenomenon becomes evident when comparing the time to reach maximum concentration that in practice indicates when the formulation starts to crystallize. As expected, crystalline CCX showed a maximum concentration at the end of the sampling period (1440 min). The same applied to CCX:PVA most likely because CCX was entrapped in the hydrophobic polymer matrix and therefore, never reached the aforementioned critical degree of supersaturation during the duration of the dissolution study. In contrast, for amorphous CCX, CCX:PVP and CCX:HPMC, the time to reach maximum concentration decreased with increasing dose (except CCX:PVP 200 mg). Furthermore, CCX:PVP crystallized faster than CCX:HPMC, which could either be a consequence of the lower dissolution rate of CCX:HPMC (as it tends to swell before it dissolves) compared to CCX:PVP or alternatively because HPMC is a better crystallization inhibitor than PVP. The latter is in accordance with the findings of Xie and Taylor[207] that studied the nucleation induction time of CCX in the presence of different polymers and reported that HPMC was more effective at maintaining supersaturation than PVP. Nevertheless, by observing the CCX concentrations after crystallization from both formulations, it is obvious that the concentrations after 1440 min were higher for CCX:PVP than CCX:HPMC (~180 μg/mL vs. ~60 μg/mL). Even though HPMC appeared to be a more effective crystallization inhibitor than PVP, the findings in the present study indicated that PVP was a more efficient solubilizer than HPMC and thus, the fast crystallization from CCX:PVP may not be critical for the performance of the formulation.

Consequently, in order to assess the overall performance of the formulations and potentially predict bioavailability, the area under the *in vitro* dissolution curve (AUC) from 0–24 h and 0–4 h was calculated. Based on these results, there is no apparent relationship between the dose and

$AUC_{0–24h}$ for any of the formulations except for CCX:PVA. Furthermore, a previous study has shown that the *in vitro* $AUC_{0–4h}$ was more predictive of the bioavailability than the *in vitro* $AUC_{0–24h}$, probably because the combined transit time in the stomach and small intestine in both humans and rats is approximately 4 h[199,203], and therefore the $AUC_{0–4h}$ was used to compare the different formulations. From Table 12.1 it can be seen that generally, the $AUC_{0–4h}$ increased with increasing dose and the different formulations were ranked CCX:PVP ≈ CCX:HPMC > amorphous CCX > crystalline CCX > CCX:PVA. Interestingly, the dissolution curves for the low doses of CCX:PVA were below those of crystalline CCX, which was also reflected in lower $AUC_{0–4h}$ values. Thus, based on this parameter, it was somewhat surprising to discover that the amorphous solid dispersion CCX:PVA was expected to perform worse than crystalline CCX *in vivo*. More expectedly, amorphous CCX, CCX:PVP and CCX:HPMC have higher $AUC_{0–4h}$ than crystalline CCX. However, it seems as if the $AUC_{0–4h}$ plateaus with increasing dose for all the formulations. In fact the $AUC_{0–4h}$ for amorphous CCX decreased when the dose was increased from 400 mg to 800 mg. This was most likely because the critical crystallization concentration was reached faster and thus, the drug crystallized accordingly to reach the "amorphous solubility".

12.4.2 Effect of polymer type and drug dose on in vivo behavior

To evaluate the influence of both dose and polymer type on the *in vivo* performance of amorphous solid dispersions, a pharmacokinetic study was performed in rats. In order to avoid any potential effect of formulation excipients such as binders, fillers, disintegrants or polymers (present in most solid dosage forms such as tablets and capsules) on the *in vivo* behavior, and thus isolate the effect of dose and polymer type, all the formulations were dosed as suspensions in FaSSIF by oral gavage. For example, a previous study showed that filling a supersaturating self-emulsifying drug delivery system (SEDDS) into HPMC capsules significantly improved both *in vitro* and *in vivo* AUC compared to the SEDDS alone because HPMC inhibited crystallization of the released drug and thus, maintained the supersaturation for longer[224].

The influence of drug dose on the plasma concentration-time curves for all the formulations is shown in Figure 12.2 and the pharmacokinetic data obtained from this study are summarized in Table 12.2. From Table 12.2 it can be seen that $AUC_{0–24h}$ and C_{max} increased with increasing dose and were ranked CCX:PVP ≈ CCX:HPMC > amorphous CCX > crystalline CCX > CCX:PVA for both parameters and for all doses, which was in line with the observations from the *in vitro* dissolution study. For the majority of the formulations, the increase in C_{max} with increasing dose was statistically significant, however, for crystalline CCX and CCX:PVA only the C_{max} from the lowest dose was found to be significantly lower than for the higher doses. The increase in $AUC_{0–24h}$ with increasing dose for the majority of the formulations was also significant, but for CCX:PVA, the $AUC_{0–24h}$ did not increase significantly with increasing dose. Similarly for crystalline CCX, only the $AUC_{0–24h}$ from the lowest dose was found to be significantly lower than for the higher doses. The *in vivo* study confirmed that the bioavailability

of the amorphous solid dispersions CCX:PVP and CCX:HPMC was significantly higher than the other formulations for all doses (with exception of 50 mg/kg CCX:PVP). Furthermore, all formulations including crystalline CCX performed significantly better than the same dose of CCX:PVA with regards to both $AUC_{0–24h}$ and C_{max}. As the drug in amorphous solid dispersions was molecularly dispersed in the polymer and PVA is poorly water-soluble, this observation was most likely because the release of CCX was limited by the dissolution of the hydrophobic polymer. Thus, the majority of the dose was probably not available for absorption as it did not dissolve in the gastrointestinal tract. The influence of dose on bioavailability of the different formulations was generally in accordance with the findings from the *in vitro* dissolution study and indicates that the absorption of CCX was solubility-limited rather than dissolution rate-limited.

On average, t_{max} for crystalline CCX, amorphous CCX, CCX:PVP and CCX:HPMC was ~6.5 h. Interestingly t_{max} for CCX:PVA was shorter on average than for all the other formulations (~5 h), suggesting that the drug was released earlier than in the other formulations, probably driven by an increased dissolution rate and/or solubility of PVA. This rationale is supported by a previous study that showed that the dissolution rate of PVA-coated pellets was faster at pH 1 than in pH 6.8[225]. Based on these findings it is obvious that not all amorphous solid dispersions will increase the bioavailability of poorly water-soluble drugs. Indeed, it is plausible that amorphous solid dispersions with hydrophobic polymers may generally perform worse than the pure crystalline drug because the formulation (polymeric matrix) will never fully dissolve. Nevertheless, as previous studies have indicated that hydrophobic polymers are good crystallization inhibitors it is possible that combining a hydrophobic polymer such as PVA with a hydrophilic polymer such as PVP may both increase the dissolution rate and prevent crystallization from the supersaturation[108]. However, this is out of the scope of the current study and will have to be investigated in detail in future work.

The bioavailability of a formulation is dependent on several factors including the rate and extent of dissolution and intestinal crystallization, permeability, gastric emptying and formulation design. Therefore, it can be difficult to predict the bioavailability based on *in vitro* dissolution profiles, especially when the interpretation of the dissolution curves is complicated by opposing dissolution and crystallization/precipitation kinetics. However, previous studies have shown that the simple *in vitro* method applied in this study was predictive of bioavailability of amorphous solid dispersions with CCX[199,218]. Since it is practically impossible to directly relate a dose *in vitro* with a dose *in vivo*, a classic *in vitro–in vivo* correlation analysis was not possible in this case. Therefore, instead of cross-comparing the different pharmacokinetic parameters, we have illustrated the effect of increasing dose on the *in vitro* $AUC_{0–4h}$ and *in vivo* $AUC_{0–24h}$ as a pharmacokinetic linearity plot in Figure 12.3. This analysis provides information about the dose-dependency of the formulations and allow for a comparison between the effect of dose and polymer type on the *in vitro* and *in vivo* performance, which ultimately enables a ranking between the different formulations.

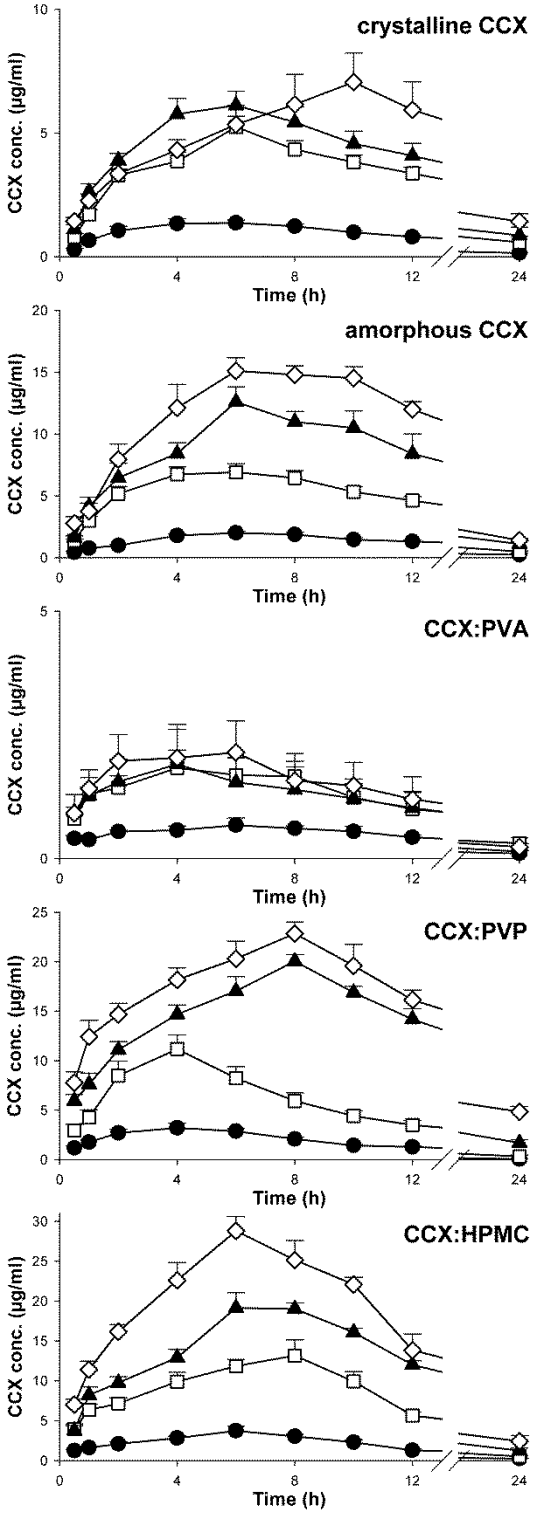

Figure 12.2: Plasma concentration profiles in rats after oral administrations of crystalline CCX and amorphous CCX, and amorphous solid dispersions of CCX:PVA, CCX:PVP and CCX:HPMC at a dose corresponding to 12.5 mg/kg (●), 50 mg/kg (□), 100 mg/kg (▲) and 200 mg/kg (◊) body weight of CCX. Note that the scale of the y-axis varies between the different subfigures. Values represent mean plasma concentration ± SEM (n = 6).

Table 12.2: Pharmacokinetic parameters of crystalline CCX, amorphous CCX, CCX:PVA, CCX:PVP and CCX:HPMC administered to rats at different doses (values are mean ± SD, *n* = 6).

Dose (mg/kg rat)	$AUC_{0\text{-}24\ h}$ (µg h mL^{-1})	C_{max} (µg mL^{-1})	t_{max} (h)
Crystalline CCX			
12.5	18.5 ± 3.4 $^{\gamma}$	1.5 ± 0.3 $^{\gamma}$	6.0 ± 1.8
50	68.2 ± 14.5 $^{a,\gamma}$	5.2 ± 1.1 $^{a,\gamma}$	6.0 ± 0.0
100	85.9 ± 16.0 $^{a,\gamma}$	7.2 ± 1.1 $^{a,\gamma}$	5.3 ± 1.6
200	103.2 ± 34.4 $^{a,\gamma}$	7.4 ± 3.2 $^{a,\gamma}$	8.7 ± 1.6 $^{a,b,c,\gamma}$
Amorphous CCX			
12.5	27.1 ± 5.9 $^{\alpha,\gamma}$	2.1 ± 0.4 $^{\alpha,\gamma}$	6.7 ± 1.0
50	96.8 ± 15.6 $^{a,\alpha,\gamma}$	7.4 ± 1.6 $^{a,\alpha,\gamma}$	5.0 ± 1.1
100	164.1 ± 43.9 $^{a,b,\alpha,\gamma}$	13.2 ± 3.3 $^{a,b,\alpha,\gamma}$	6.7 ± 1.6 $^{\gamma}$
200	221.5 ± 23.2 $^{a,b,c,\alpha,\gamma}$	16.4 ± 2.1 $^{a,b,\alpha,\gamma}$	7.3 ± 2.4
CCX:PVA			
12.5	9.7 ± 2.7	0.8 ± 0.3	5.8 ± 2.6
50	25.2 ± 13.9	2.2 ± 0.5 ^{a}	4.8 ± 2.4
100	23.8 ± 18.1	2.1 ± 1.5 ^{a}	3.7 ± 1.5
200	28.7 ± 22.6	2.4 ± 1.6 ^{a}	4.7 ± 2.4
CCX:PVP			
12.5	34.5 ± 6.6 $^{\alpha,\beta,\gamma}$	3.4 ± 1.0 $^{\alpha,\beta,\gamma}$	5.0 ± 2.1
50	103.4 ± 28.0 $^{a,\alpha,\gamma}$	11.3 ± 3.6 $^{a,\alpha,\beta,\gamma}$	4.7 ± 1.0
100	272.2 ± 31.8 $^{a,b,\alpha,\beta,\gamma}$	20.8 ± 2.3 $^{a,b,\alpha,\beta,\gamma}$	7.7 ± 0.8 $^{a,b,\alpha,\gamma}$
200	339.0 ± 41.9 $^{a,b,c,\alpha,\beta,\gamma}$	24.2 ± 4.3 $^{a,b,\alpha,\beta,\gamma}$	8.0 ± 1.3 $^{a,b,\gamma}$
CCX:HPMC			
12.5	39.4 ± 10.5 $^{\alpha,\beta,\gamma}$	3.8 ± 1.4 $^{\alpha,\beta,\gamma}$	6.0 ± 1.3
50	150.0 ± 28.3 $^{a,\alpha,\beta,\gamma,\delta}$	14.0 ± 4.2 $^{a,\alpha,\beta,\gamma}$	6.3 ± 1.5
100	248.6 ± 27.1 $^{a,b,\alpha,\beta,\gamma}$	19.7 ± 2.5 $^{a,b,\alpha,\beta,\gamma}$	7.3 ± 1.0 $^{\gamma}$
200	345.2 ± 45.5 $^{a,b,c,\alpha,\beta,\gamma}$	31.0 ± 5.1 $^{a,b,c,\alpha,\beta,\gamma,\delta}$	6.3 ± 1.5

Significantly larger at $p < 0.05$: ^{a} vs. same formulation 12.5 mg/kg; ^{b} vs. formulation 50 mg/kg; ^{c} vs. same formulation 100 mg/kg; $^{\alpha}$ vs. same dose crystalline CCX; $^{\beta}$ vs. same dose amorphous CCX; $^{\gamma}$ vs. same dose CCX:PVA; $^{\delta}$ vs. same dose CCX:PVP.

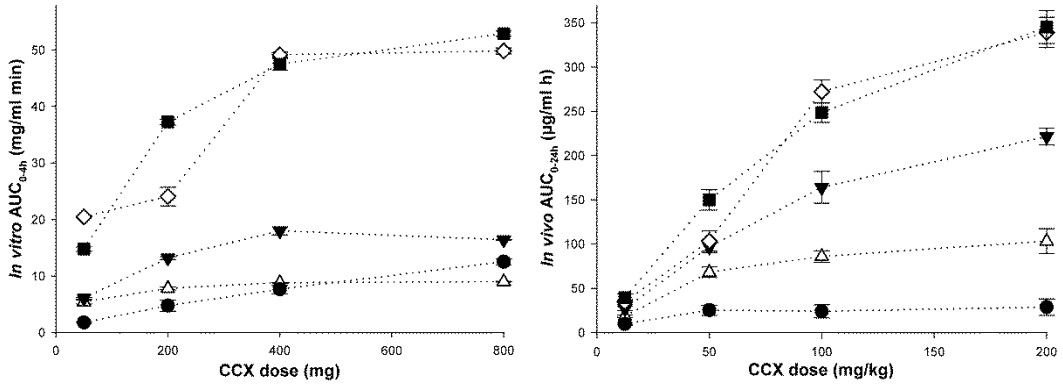

Figure 12.3: Pharmacokinetic linearity plot showing left) *in vitro* $AUC_{0\text{-}4h}$ vs. *in vitro* dose and right) *in vivo* $AUC_{0\text{-}24h}$ vs. *in vivo* dose for crystalline CCX (Δ), amorphous CCX (▼), CCX:PVA (●), CCX:PVP (◊) and CCX:HPMC (■). Values for *in vitro* represent mean $AUC_{0\text{-}4h}$ ± SD (n = 3) and values for *in vivo* represent mean $AUC_{0\text{-}24h}$ ± SEM (n = 6).

As can be seen in Figure 12.3, the formulations that performed better *in vitro* also perform better *in vivo*. Furthermore, the *in vitro* method enabled a ranking between the formulations under investigations for all doses, which indicates that it could be used to predict *in vivo* performance. Both *in vitro* and *in vivo*, no dose-linearity or proportionality could be established because the relative overall performance (AUC) increased in a non-linear fashion with increasing dose. For crystalline CCX and CCX:PVA, the relative *in vivo* bioavailability (compared to the bioavailability for 12.5 mg/kg CCX) was decreased with increasing dose to 35% and 18% for 200 mg/kg CCX, respectively. This means that with increasing dose, the fraction of drug being absorbed decreased, which was probably because the absorption was hampered by the limited solubility of CCX. For amorphous CCX, CCX:PVP and CCX:HPMC, even though the *in vivo* bioavailability increased significantly with increasing dose, the relative bioavailability also decreased with increasing dose to 51, 61 and 55% for 200 mg/kg CCX, respectively. This indicates that the fraction of CCX that crystallized increased with increasing dose, in accordance with the observations *in vitro*. However, based on the *in vitro* results (400 mg vs. 800 mg), it was expected that the relative *in vivo* bioavailability would plateau or even decrease with increasing dose. A similar behavior was found in the *in vivo* study, where lack of dose linarity was also observed. This indicates that, even though amorphous solid dispersions are a potent formulation strategy to increase the bioavailability of poorly water-soluble drugs, there seems to be a limitation to how much these formulations can increase exposure. These findings demonstrate the biopharmaceutical challenges when increasing dose for amorphous solid dispersions even when the drug:polymer ratio is fixed and underline the importance of selecting relevant *in vitro* variables in order to avoid confusion in early *in vivo* studies.

12.5 Conclusion

The results from this study showed that both the polymer type and drug dose significantly influenced the non-sink *in vitro* dissolution behavior and *in vivo* performance of amorphous solid dispersions. Compared to crystalline and amorphous CCX, the amorphous solid dispersions with PVP and HPMC improved the *in vitro* $AUC_{0–4h}$. Even though the formulations crystallized upon dissolution, the supersaturation generated was sustained long enough to significantly increase the *in vivo* $AUC_{0–24h}$ for all doses. In contrast, the amorphous solid dispersion with PVA did not improve the *in vitro* $AUC_{0–4h}$ compared to crystalline and amorphous CCX. The *in vivo* $AUC_{0–24h}$ for crystalline CCX was in fact significantly higher than for CCX:PVA, most likely because CCX was incorporated in the hydrophobic polymer and therefore, was not released from the undissolved polymer matrix. However, as CCX reached supersaturated concentrations at high doses of CCX:PVA upon dissolution and did not crystallize, it is possible that amorphous solid dispersions with a combination of hydrophilic and hydrophobic polymers may improve the performance compared to any of the polymers alone.

As the crystallization tendency increased with increasing dose, the *in vitro* $AUC_{0–4h}$ did not increase proportionally for all the formulations. Based on these results, it was expected that the *in vivo* study would not show dose-linearity or proportionality. The simple non-sink *in vitro* dissolution model applied in this study enabled a ranking of the five different formulations that was predictive of the *in vivo* performance. Even though the *in vivo* $AUC_{0–24h}$ of all the formulations increased with increasing dose, the relative bioavailability decreased significantly, confirming that absorption of CCX was solubility-limited. This suggests that the supersaturating formulations crystallized *in vivo* and that the fraction of CCX that crystallized increased with increasing dose, which was in accordance with the observations from the *in vitro* study. These findings underline the importance of selecting relevant *in vitro* variables (i.e. dose), in order to rationally asses the performance of amorphous solid dispersions and avoid confusion in early *in vivo* studies.

General discussion

In this chapter, a general discussion of the key findings of the present dissertation is given. The first part of the discussion will focus on the measurement of drug–polymer solubility as a predictive tool to ensure stability of amorphous solid dispersions over the entire product shelf-life, whereas the second part will focus on the identification of important *in vitro* parameters predictive of *in vivo* performance.

As introduced previously, several methods have been proposed to predict the drug–polymer solubility at room temperature based on extrapolation of data obtained at elevated temperatures using the Flory-Huggins model (Section 3.2). However, none of these methods assessed the predictive power of such extrapolations. Therefore, in order to enable a rational comparison of the solubility predictions based on these methods, the confidence of the extrapolation was evaluated through formal statistical analysis, considering both the inter-variability (reproducibility) and the intra-variability (fit to the Flory-Huggins model) of the measurements (Chapter 4). The introduction of a 95% prediction interval enabled a comparison of the influence of different preparation techniques (ball milling, film casting and spray drying) on the solubility predictions of IMC in PVP. The recrystallization method used is based on recrystallization from a supersaturated solution (*b*→*e* in Figure 3.2), and therefore an important prerequisite for this method is that a molecularly dispersed supersaturated amorphous solid dispersion can be prepared before the annealing stage. Even though all the different preparation techniques seemed to have produced homogenous supersaturated amorphous solid dispersions (indicated by a single T_g), the solubility prediction based on the mixture prepared by ball milling was lower than for those prepared by film casting and spray drying. As previous studies suggested that mixtures produced by ball milling are heterogeneous at the molecular level, the process involved in reaching equilibrium solubility from the ball milled mixture was most likely driven by dissolution (into an undersaturated solution) rather than by the intentional recrystallization (from a supersaturated solution). Hence, since the dissolution process is generally more time-consuming than recrystallization, due to lower molecular mobility, it was expected that equilibrium solubility for the ball milled mixture was not reached within the 2 h of annealing, and therefore the solubility was underestimated. This finding emphasizes that even though amorphous solid dispersions can be prepared using different methods, they will not necessarily be identical on a molecular level, and thus their physical properties may differ.

Having optimized the recrystallization method by introducing spray drying as the preparation technique for the supersaturated amorphous solid dispersions and increasing the annealing time to 3 h, the influence of polymer (PVP) molecular weight on the solubility of IMC was investigated (Chapter 5). A homopolymer such as PVP consists of a chain of identical monomeric repeat units, and thus the molecular weight is a measure of how many repeat units are present in the polymer chain. As the solubility between a drug and a polymer is most likely induced by intermolecular interactions between the functional groups of the drug and the repeat

unit (e.g. hydrogen bonding), the molecular weight of the polymer should in theory not influence the drug–polymer solubility. If any, the biggest difference in solubility is expected for low-molecular-weight polymers as the end groups potentially have different structures or properties than the other repeat units in the polymer chain. These theoretical considerations were all supported experimentally by the findings of this study where the solubility of IMC in PVP was not found to be significantly different between the molecular weights investigated (2,000−1,200,000 g/mol). Even though the findings indicated that solubility was indeed mainly governed by drug–polymer intermolecular interactions, and independent of the molecular weight of the polymer, the molecular weight of the polymer might still have an influence on the drug–polymer miscibility (Figure 3.1). This is because an increase in molecular weight would increase the T_g of the system (and decrease molecular mobility), and thus slow down the crystallization kinetics, which in turn would increase the physical stability.

Initially it was intended to include miscibility predictions in Chapter 5 along with the solubility predictions; however, as it was discovered that the confidence of the miscibility predictions were biased, it was necessary to assess the statistical assumptions of the method proposed by Lin and Huang to predict the drug–polymer miscibility (Chapter 8). The method is based on the melting point depression measurements using DSC and relies on the assumption that the Flory-Huggins interaction parameter χ is temperature dependent and decreases with increasing temperature. However, as for the methods to predict drug–polymer solubility, this method did not include a statistical assessment of the experimental uncertainty. Furthermore, it applies a routine mathematical operation known as "transformation to linearity", which has previously been shown to be subject to substantial bias. Using the mathematical procedure and raw data from the original method, it was found that the predicted miscibility curve could not be trusted at any reasonable level of statistical significance. This was mainly due to the bias associated with the "transformation to linearity" and because the miscibility (or more specifically the interaction parameter χ) is very sensitive towards experimental uncertainty. Therefore, even though the information gained from the method suggested by Lin and Huang may be valuable from an industrial perspective (especially if drug–polymer solubility is low); currently it seems that thermal properties cannot be determined with sufficient precision to enable reliable drug–polymer miscibility predictions. Furthermore, the temperature dependence of χ is depending on the method used to obtain the solubility data (unpublished findings). This is associated with how different methods approach the equilibrium solubility. For example, if equilibrium solubility is approached from a supersaturated solution e.g. using the recrystallization method, the solubility prediction will be slightly overestimated and χ will decrease (i.e. have higher negative values) with decreasing temperature. According to miscibility theory, this kind of temperature dependence of χ would mean that the miscibility curve does not exist and that the system is miscible in the entire composition and temperature range. Therefore, even though regression with a proper objective function would provide statistically sound and unbiased miscibility predictions, arguments in favor of the temperature dependence of χ need to be put forward to have any confidence in the predictions.

As the drug–polymer solubility was shown not to be influenced by the molecular weight of the polymer, drug–polymer solubility predictions can be compared despite slight differences in the molecular weight of polymers. Therefore, the influence of copolymer composition of PVP/VA (including pure PVP and PVA) on the solubility of CCX was investigated using the recrystallization method and compared with a prediction based on the liquid analogue solubility method (Chapter 7). The solubilities predicted using the liquid analogue solubility method increased linearly with increasing VP/VA ratio, which indicated that the VP repeat unit was responsible for inducing solubility. This was supported by the presence of strong hydrogen bonding between VP and CCX. However, interestingly, the predicted solubilities using the recrystallization method did not increase linearly with increasing VP ratio, but rather approached a solubility plateau. This difference in the solubility predictions between the recrystallization method and the liquid analogue solubility method is probably a consequence of the fundamental differences between monomers and polymers. In a liquid analogue, the molecules are relatively unrestricted which allows for intermolecular movement whereas in a solid polymer, the repeat units (monomers) are covalently bound in the polymeric chain. Therefore, if the molecular volume of the drug is larger than that of the repeat units, the drug will not be able to interact with all the repeat units in a polymer due to steric hindrance caused by already interacting drug molecules. As the liquid analogue solubility method does not take this into account (as it is theoretically possible for all drug molecules to interact with the monomer molecules in the liquid) it will tend to overestimate the drug–polymer solubility. Given that this steric hindrance hypothesis is true, the hydrophilic VP repeat units that do not interact with a drug molecule can in theory be replaced with hydrophobic VA repeat units without compromising drug–polymer solubility. Consequently, knowledge of the plateau effect may be used advantageously in the future development of amorphous solid dispersions as copolymers can theoretically be customized to fit any given drug with a ratio and sequence of repeat units and provide optimal drug–polymer solubility and physical stability.

The findings from the previous studies indicated that the choice of method to predict drug–polymer solubility will have an influence on the prediction. Therefore, a comparison of the most popular methods to predict drug–polymer solubility using five different model drugs and PVP/VA copolymers of different VP/VA ratio (including pure PVP and PVA) was carried out (Chapter 6). The methods included the recrystallization method, the liquid analogue solubility method, the melting point depression method and a variation of the melting point depression method (dissolution endpoint method) that uses the endpoint of melting rather than the onset. As expected, the solubility predictions varied considerably depending on the method used, but generally ranked the various drug–polymer systems in the same order. The recrystallization method and the melting point depression method provided similar solubility predictions that were significantly higher than the predictions based on the dissolution endpoint method. As the dissolution endpoint method relies on dissolution kinetics that is expected to be slower than the recrystallization kinetics (and the dissolution kinetics slow down when the concentration approaches equilibrium), an underestimation of the solubility prediction is reasonable to expect

as the equilibrium using this method cannot be measured at zero heating rate. Even though the liquid analogue solubility method overestimated the drug–polymer solubility (due to the steric hindrance hypothesis outlined above), if a drug is soluble in a liquid analogue it will most likely also be soluble in the polymer, and therefore this method can still provide valuable indications on drug–polymer solubility. Finally, the solubility measurements obtained using the recrystallization methods fitted the best to the Flory-Huggins model, which indicates that the method was superior to the others and might provide more precise solubility predictions.

The established methods proposed to predict drug–polymer solubility at room temperature are based on measurements at elevated temperatures in equilibrium thermodynamic conditions using DSC and subsequent extrapolation to room temperature. To overcome the uncertainty associated with this extrapolation, a new methodology to estimate drug–polymer solubility based on measurements at room temperature was proposed in this dissertation (Chapter 9). The method was similar to the liquid analogue solubility method, but instead of measuring the solubility of a drug in a liquid analogue, the new polymer in solution method measured the solubility of a drug in a polymer dissolved in a solvent at room temperature using the shake-flask approach (*a*→*e* in Figure 3.2). The idea behind this method was that, if the solvent is inert and does not influence the molecular structure of the drug and polymer in solution, then the interactions between the drug and polymer in the liquid (dissolved state) are similar to those in the solid state. If there are strong intermolecular interactions between the drug and polymer, the solubility of the drug will increase with increasing polymer concentration. Consequently, if the increase in drug solubility is linearly correlated to the increase in polymer concentration (which according to this theory it should be), the solubility of the drug in the polymer in the solid state can be derived from the slope of this function. The introduction of the new polymer in solution method has the potential to provide faster and more precise estimates than the established methods and thereby potentially save valuable time in early drug development. Furthermore, it overcomes issues related to the liquid analogue solubility method discussed above, and does not depend on the availability of a liquid analogue, as it directly applies the polymer intended as carrier in an amorphous solid dispersion.

Having contributed to the development of predictive tools to ensure the stability of amorphous solid dispersions, attention was shifted to another important aspect of amorphous solid dispersion development i.e. the identification of *in vitro* parameters predictive of *in vivo* performance. Initially, the influence of the molecular weight of PVP on the *in vitro* supersaturation behavior and *in vivo* performance in rats of amorphous solid dispersions using CCX as a model drug was investigated (Chapter 10). Previously it was shown that the molecular weight of PVP did not influence the solubility of CCX in PVP. However, as the release profile from an amorphous solid dispersion is driven by the properties of the polymer, the molecular weight of the polymer was expected to affect the pharmacokinetic profile. The dissolution rate of CCX was indeed found to decrease with increasing molecular weight of PVP. Nevertheless, as the low-molecular-weight polymers were not able to inhibit precipitation from the supersaturated solution to the same

extent as the high-molecular-weight PVP, the overall performance (*in vitro* AUC_{0-24h}) of the low-molecular-weight polymers was lower. These observations were also reflected in the *in vivo* study, where the amorphous solid dispersions prepared with the higher molecular weight PVPs (50,000−360,000 g/mol) showed higher bioavailability (*in vivo* AUC_{0-24h}) than those prepared with the low-molecular-weight PVPs (2,500−30,000 g/mol). A linear relationship between the *in vitro* AUC_{0-24h} and *in vivo* AUC_{0-24h} was found, indicating that the simple non-sink *in vitro* dissolution method applied in this study was biopredictive. Interestingly, the PVP that performed best both *in vitro* and *in vivo* was the one with the second highest molecular weight (50,000 g/mol), indicating that there is a molecular weight of any given polymer were the balance between dissolution rate-enhancing and precipitation inhibiting factors are optimal.

Besides the molecular weight, also the hydrophobicity of the polymer has been reported to influence precipitation inhibition. To study this in further detail, the influence of copolymer composition on PVP/VA (including pure PVP and PVA) on the *in vitro* and *in vivo* performance of amorphous solid dispersions was investigated (Chapter 11). Previous studies showed that the some of the hydrophilic VP repeat units in PVP can be replaced with VA repeat units without compromising the drug–polymer solubility (or intermolecular interactions). As VA is a hydrophobic repeat unit it will increase the overall hydrophobicity of the copolymer, which allow for direct comparison of the influence of the hydrophobicity of a polymer on the supersaturation behavior and biopharmaceutical performance. As expected, the dissolution rate of CCX decreased with increasing VA ratio (hydrophobicity) in the copolymer and in fact, the dissolution rate from CCX:PVA was slower than for crystalline CCX. Based on the dissolution profiles, it became evident that the hydrophilic VP repeat unit was responsible for the generation of the supersaturation and the hydrophobic VA repeat unit was responsible for maintaining the supersaturation through precipitation inhibition. Both *in vitro* and *in vivo*, the copolymer compositions with 50 and 60% VP repeat units performed better than the other amorphous solid dispersions, indicating that the balance between dissolution rate-enhancing and precipitation inhibiting factors for these copolymers were optimal. Thus, it seems that knowledge about the optimum monomer ratio may be used advantageously in the future development of amorphous drug delivery systems as copolymers can theoretically be customized to "fit" any given drug and improve not only the physical stability, but also the bioavailability of a formulation.

The biopharmaceutical performance of an amorphous solid dispersion is dependent on several factors including the rate and extent of dissolution and intestinal crystallization, permeability and gastric emptying, and therefore it is difficult to predict the bioavailability based on *in vitro* dissolution profiles. However, as the simple non-sink *in vitro* method had been shown to be predictive of bioavailability, the effect of drug dose on the non-sink *in vitro* dissolution behavior and the *in vivo* performance of CCX amorphous solid dispersions was studied. For this study the hydrophilic polymers PVP and HPMC and the hydrophobic polymer PVA were used (Chapter 12). As the driving force for crystallization increases with increasing degree of supersaturation, the dose was expected to influence both *in vitro* and *in vivo* performance significantly. Accordingly, even though the bioavailability increased, the relative bioavailability decreased

significantly with increasing dose, which indicates that the supersaturating formulations crystallized *in vivo* and that the fraction of CCX that crystallized increased with increasing dose. This was in line with the *in vitro* observations and underlines the importance of selecting relevant *in vitro* variables in order to rationally assess the performance of amorphous solid dispersions in order to avoid discrepancies with early *in vivo* studies. Even though three different polymers were used, the simple non-sink *in vitro* dissolution method still enabled a ranking between the different formulations *in vivo*. Furthermore, as the bioavailability from CCX:PVA was significantly lower than from crystalline CCX for all doses, it is obvious that not all amorphous solid dispersions (especially those using hydrophobic polymers) have the potential to increase the bioavailability of poorly water-soluble drugs. However, it is possible that amorphous solid dispersions using a combination of hydrophobic and hydrophilic polymers (e.g. HPMC/PVA) may improve the bioavailability compared to any of the pure polymers alone.

Future perspectives

Together with recent advances in academic and industrial research and an increased fundamental understanding of the thermodynamics of amorphous systems and glass solutions, this dissertation has demonstrated that amorphous solid dispersions present an exciting possibility for oral delivery of the increasing number of poorly water-soluble drugs. However, even though the number of commercially available amorphous solid dispersions has increased during the last decade, underlining its potential, more research is still needed in order for amorphous solid dispersions to become a routine formulation strategy in the pharmaceutical industry.

The main concerns regarding amorphous solid dispersions are associated with the inherent instability of the amorphous form and lack of understanding of the complex dissolution process. Based on the findings of this dissertation, the concept of drug-polymer solubility is now generally accepted and well-understood experimentally. The extrapolation of drug–polymer solubility measurements obtained at elevated temperatures to room temperature seems to be valid, but long-term stability studies to confirm the predicted solubility might still be necessary to substantiate this claim. However, as the current experimental methods are time-consuming, more focus on the development and optimization of faster methods is needed in order to enable a high-throughput screening of polymer carriers to prepare amorphous solid dispersions for a given drug. In this context, the polymer in solution method proposed in this dissertation, and the emergence of promising *in silico* methods such as PC-SAFT, seem to pave the way. Therefore, rather than developing more experimental methods to predict the drug–polymer solubility at room temperature based on DSC measurements, it is imperative that the validity of the new polymer in solution method (using more polymer and solvent combinations) is confirmed and that the current *in silico* methods are refined. Furthermore, as the solubility predictions are made under the assumption of dry conditions, the influence of water sorption (especially for hygroscopic polymers such as PVP) on the stability of amorphous solid dispersions will also have to be investigated in more detail.

Despite the possibility of dissolving a drug in a polymer, to ensure the thermodynamic stability of the system, it is estimated that the solubility of most drugs in polymeric matrices is low unless favorable interactions are formed. This calls for the development of methods to predict drug–polymer miscibility at room temperature. Attempts have been made, but it seems that, in order to truly believe miscibility predictions, arguments in favor of the underlying assumptions need to be put forward. Nevertheless, relying on the physical stability rather than the thermodynamic stability may not be necessary as the drug dose, and thus the drug–polymer ratio, is decreasing due to the increasing potency of new drug candidates. Finally, the prospective of combining hydrophilic and hydrophobic polymers, or even customized copolymers to obtain an optimal dissolution behavior and oral bioavailability of the drug, needs to be investigated further. Therefore, let this be an appeal to the polymer industry to revise their approach so that the properties of the excipient (polymer) may be tailored to fit the needs of a given drug.

Summary

The application of amorphous solid dosage forms is one of the most successful strategies to overcome the limited oral bioavailability of poorly soluble drugs. However, despite the increased interest in amorphous solid dispersions in academic and industrial research, the commercial application of this formulation strategy is still limited. This situation is mainly due to an insufficient understanding of the basic properties of amorphous solid dispersions such as their physical stability and the lack of predictive *in vitro* models. Therefore, the aim of the present dissertation was to contribute to the understanding and development of predictive tools for amorphous solid dispersions. The stability of an amorphous solid dispersion can only be fully ensured by dissolving the drug in the polymer below its equilibrium solubility (i.e. by forming a glass solution). Several methods to predict the drug–polymer solubility at room temperature have been proposed and the majority of these are based on data obtained at elevated temperature using DSC followed by extrapolation to room temperature using the Flory-Huggins model.

In order to enable a rational comparison of the solubility predictions, the confidence of the extrapolation by means of a prediction interval was introduced for the solubility curve through formal statistical analysis. This approach allowed for a range of interesting studies. Initially, the influence of polymer molecular weight and preparation method on the drug–polymer solubility was investigated. The solubility prediction based on mixtures prepared by ball milling was lower than for those prepared by film casting and spray drying, indicating that even though amorphous solid dispersions can be prepared using different methods, they will not necessarily be identical on a molecular level, and thus their physical properties may differ. In contrast, the drug–polymer solubility was found to be independent of the molecular weight of the polymer, which suggested that solubility is mainly governed by intermolecular interactions. As an increase in molecular weight would increase the T_g of the system, thus, decrease molecular mobility and slow down the crystallization kinetics, a higher molecular weight polymer should increase the drug–polymer miscibility. However, using a method proposed to predict drug–polymer miscibility, it was found that the predicted miscibility curve was not reliable at any reasonable level of statistical significance. Therefore, even though the information gained from the method may be valuable from an industrial perspective (especially if drug–polymer solubility is low); currently it seems that thermal properties cannot be determined with sufficient precision to enable reliable drug–polymer miscibility predictions. In a copolymer consisting of a hydrophilic and a hydrophobic repeat unit, the hydrophilic repeat unit was found to be responsible for inducing solubility of the drug in the polymer. However, interestingly, the predicted solubilities did not increase linearly with increasing hydrophilic repeat unit ratio, but rather approached a solubility plateau. Therefore, it seems that if the molecular volume of the drug is larger than that of the repeat units, the drug will not be able to interact with all the repeat units in a polymer due to steric hindrance caused by already interacting drug molecules. Given that this hypothesis is true, the hydrophilic VP repeat units that do not interact with a drug molecule can in theory be replaced with hydrophobic VA repeat units without compromising drug–polymer solubility. The findings from

the initial studies including a large comparative study confirmed that the choice of method to predict drug–polymer solubility will have an influence on the prediction. In order to overcome the uncertainty associated with the temperature extrapolation performed in the established methods, a new methodology to estimate drug–polymer solubility was developed. The method is based on the solubility of a drug in a polymer dissolved in an inert solvent at room temperature using a shake-flask approach. Hence, this new method has the potential to provide faster and possibly more precise solubility estimates than the established methods, which can save valuable time in the early drug development phase.

In addition to contributing to the understanding of the stability of amorphous solid dispersions, different polymer properties responsible for improving both *in vitro* and *in vivo* performance were also identified in this dissertation. Initially, the influence of the molecular weight of the polymer on the *in vitro* supersaturation behavior and *in vivo* performance of amorphous solid dispersions was investigated. The dissolution rate was found to decrease with increasing molecular weight of the polymer due to increased viscosity and hydrophobicity. Nevertheless, as the low-molecular-weight polymers were not able to inhibit precipitation from the supersaturated solution to the same extent as the high-molecular-weight polymers, the overall performance of the low-molecular-weight polymers was lower. Interestingly, the molecular weight that performed best both *in vitro* and *in vivo* was not the highest nor the lowest, which indicates that there is a molecular weight of the polymer where the balance between dissolution rate-enhancing and precipitation inhibiting factors are optimal.

Besides the molecular weight, also the hydrophobicity of the polymer was expected to have an influence on precipitation inhibition. To study this, the influence of copolymer composition on the *in vitro* and *in vivo* performance of amorphous solid dispersions was investigated. Both *in vitro* and *in vivo*, the copolymer compositions with 50 and 60% hydrophobic repeat units performed better than the other amorphous solid dispersions, indicating that the balance between dissolution rate-enhancing and precipitation inhibiting factors are optimal for these copolymer compositions. Interestingly, these copolymer compositions also provided the best physical stability, although the correlation between these two findings remains unclear at this stage. Finally, the effect of drug dose on the non-sink *in vitro* dissolution behavior and the *in vivo* performance of CCX amorphous solid dispersions were studied. As the driving force for crystallization increased with increasing degree of supersaturation, the dose significantly influenced both *in vitro* and *in vivo* performance. Even though the bioavailability increased, the relative bioavailability decreased significantly with increasing dose, which indicates that the supersaturating formulations crystallized *in vivo* and that the fraction of CCX that crystallized increased with increasing dose. In conclusion, this dissertation has contributed to the understanding of the thermodynamics behind amorphous solid dispersions and demonstrated that this formulation strategy presents an exciting possibility for oral delivery of poorly water-soluble drugs.

References

1. Sastry, S. V.; Nyshadham, J. R.; Fix, J. A. Recent technological advances in oral drug delivery - a review. *Pharm. Sci. Technol. Today* **2000,** *3* (4), 138-145.

2. Artursson, P.; Karlsson, J. Correlation between oral drug absorption in humans and apparent drug permeability coefficients in human intestinal epithelial (Caco-2) cells. *Biochem. Biophys. Res. Commun.* **1991,** *175* (3), 880-885.

3. Amidon, G. L.; Lennernas, H.; Shah, V. P.; Crison, J. R. A theoretical basis for a biopharmaceutic drug classification: the correlation of in vitro drug product dissolution and in vivo bioavailability. *Pharm. Res.* **1995,** *12* (3), 413-420.

4. Pouton, C. W. Formulation of poorly water-soluble drugs for oral administration: physicochemical and physiological issues and the lipid formulation classification system. *Eur. J. Pharm. Sci.* **2006,** *29* (3-4), 278-287.

5. Stegemann, S.; Leveiller, F.; Franchi, D.; de, J. H.; Linden, H. When poor solubility becomes an issue: from early stage to proof of concept. *Eur. J. Pharm. Sci.* **2007,** *31* (5), 249-261.

6. Lipp, R. The Innovator pipeline: bioavailability challenges and advanced oral drug delivery opportunities. *Am. Pharm. Rev.* **2013,** *16* (3), 14-16.

7. Fahr, A.; Liu, X. Drug delivery strategies for poorly water-soluble drugs. *Expert Opin. Drug Deliv.* **2007,** *4* (4), 403-416.

8. Kawabata, Y.; Wada, K.; Nakatani, M.; Yamada, S.; Onoue, S. Formulation design for poorly water-soluble drugs based on biopharmaceutics classification system: basic approaches and practical applications. *Int. J. Pharm.* **2011,** *420* (1), 1-10.

9. Serajuddin, A. T. Solid dispersion of poorly water-soluble drugs: early promises, subsequent problems, and recent breakthroughs. *J. Pharm. Sci.* **1999,** *88* (10), 1058-1066.

10. Leuner, C.; Dressman, J. Improving drug solubility for oral delivery using solid dispersions. *Eur. J. Pharm. Biopharm.* **2000,** *50* (1), 47-60.

11. Vasconcelos, T.; Sarmento, B.; Costa, P. Solid dispersions as strategy to improve oral bioavailability of poor water soluble drugs. *Drug Discov. Today* **2007,** *12* (23-24), 1068-1075.

12. Hancock, B. C.; Zografi, G. Characteristics and significance of the amorphous state in pharmaceutical systems. *J. Pharm. Sci.* **1997,** *86* (1), 1-12.

13. Murdande, S. B.; Pikal, M. J.; Shanker, R. M.; Bogner, R. H. Solubility advantage of amorphous pharmaceuticals: I. A thermodynamic analysis. *J. Pharm. Sci.* **2010,** *99* (3), 1254-1264.

14. Huang, Y.; Wei-Guo, D. Fundamental aspects of solid dispersion technology for poorly soluble drugs. *Acta Pharm. Sin. B* **2014,** *4* (1), 18-25.

15. Konno, H.; Handa, T.; Alonzo, D. E.; Taylor, L. S. Effect of polymer type on the dissolution profile of amorphous solid dispersions containing felodipine. *Eur. J. Pharm. Biopharm.* **2008,** *70* (2), 493-499.

16. Alonzo, D. E.; Zhang, G. G.; Zhou, D.; Gao, Y.; Taylor, L. S. Understanding the behavior of amorphous pharmaceutical systems during dissolution. *Pharm. Res.* **2010,** *27* (4), 608-618.

17. Van den Mooter, G. The use of amorphous solid dispersions: a formulation strategy to overcome poor solubility and dissolution rate. *Drug Discov. Today Technol.* **2012,** *9* (2), 79-85.

18. Brouwers, J.; Brewster, M. E.; Augustijns, P. Supersaturating drug delivery systems: the answer to solubility-limited oral bioavailability? *J. Pharm. Sci.* **2009,** *98* (8), 2549-2572.

19. Liu, H.; Taylor, L. S.; Edgar, K. J. The role of polymers in oral bioavailability enhancement; a review. *Polymer* **2015,** *77*, 399-415.

20. Rumondor, A. C.; Dhareshwar, S. S.; Kesisoglou, F. Amorphous solid dispersions or prodrugs: complementary strategies to increase drug absorption. *J. Pharm. Sci.* **2016**.

21. Babu, N. J.; Nangia, A. Solubility advantage of amorphous drugs and pharmaceutical cocrystals. *Cryst. Growth Des.* **2011,** *11* (7), 2662-2679.

22. Kostewicz, E. S.; Abrahamsson, B.; Brewster, M.; Brouwers, J.; Butler, J.; Carlert, S.; Dickinson, P. A.; Dressman, J.; Holm, R.; Klein, S.; Mann, J.; McAllister, M.; Minekus, M.; Muenster, U.; Mullertz, A.; Verwei, M.; Vertzoni, M.; Weitschies, W.; Augustijns, P. In vitro models for the prediction of in vivo performance of oral dosage forms. *Eur. J. Pharm. Sci.* **2014,** *57*, 342-366.

23. Butler, J. M.; Dressman, J. B. The developability classification system: application of biopharmaceutics concepts to formulation development. *J. Pharm. Sci.* **2010,** *99* (12), 4940-4954.

24. Dahan, A.; Miller, J. M.; Amidon, G. L. Prediction of solubility and permeability class membership: provisional BCS classification of the world's top oral drugs. *AAPS J.* **2009,** *11* (4), 740-746.

25. FDA *Waiver of in vivo bioavailability and bioequivalence studies for immediate-release solid oral dosage forms based on a biopharmaceutics classification system;* Food and Drug Administration: Rockville, MD, 2015.

26. Wu, C. Y.; Benet, L. Z. Predicting drug disposition via application of BCS: transport/absorption/elimination interplay and development of a biopharmaceutics drug disposition classification system. *Pharm. Res.* **2005,** *22* (1), 11-23.

27. Alzghoul, A.; Alhalaweh, A.; Mahlin, D.; Bergstrom, C. A. Experimental and computational prediction of glass transition temperature of drugs. *J. Chem. Inf. Model.* **2014,** *54* (12), 3396-3403.

28. Nalamachu, S.; Wortmann, R. Role of indomethacin in acute pain and inflammation management: a review of the literature. *Postgrad. Med.* **2014,** *126* (4), 92-97.

29. Gupta, P.; Chawla, G.; Bansal, A. K. Physical stability and solubility advantage from amorphous celecoxib: the role of thermodynamic quantities and molecular mobility. *Mol. Pharm.* **2004,** *1* (6), 406-413.

30. Benet, L. Z.; Broccatelli, F.; Oprea, T. I. BDDCS applied to over 900 drugs. *AAPS J.* **2011,** *13* (4), 519-547.

31. Sprunk, A.; Page, S.; Kleinebudde, P. Influence of process parameters and equipment on dry foam formulation properties using indomethacin as model drug. *Int. J. Pharm.* **2013,** *455* (1-2), 189-196.

32. Nandakishore, R.; Yalavarthi, P. R.; Kiran, Y. R.; Rajapranathi, M. Selective cyclooxygenase inhibitors: current status. *Curr. Drug Discov. Technol.* **2014,** *11* (2), 127-132.

33. Shono, Y.; Jantratid, E.; Janssen, N.; Kesisoglou, F.; Mao, Y.; Vertzoni, M.; Reppas, C.; Dressman, J. B. Prediction of food effects on the absorption of celecoxib based on biorelevant dissolution testing coupled with physiologically based pharmacokinetic modeling. *Eur. J. Pharm. Biopharm.* **2009,** *73* (1), 107-114.

34. Callister, W. D.; Rethwisch, D. G. *Materials science and engineering: an introduction;* 9th ed.; John Wiley & Sons: New York, 2007.

35. Chiou, W. L.; Riegelman, S. Pharmaceutical applications of solid dispersion systems. *J. Pharm. Sci.* **1971,** *60* (9), 1281-1302.

36. Newman, A.; Knipp, G.; Zografi, G. Assessing the performance of amorphous solid dispersions. *J. Pharm. Sci.* **2012,** *101* (4), 1355-1377.

37. Shah, N.; Sandhu, H.; Choi, D. S.; Chokshi, H.; Malick, A. W. *Amorphous solid dispersions: theory and practice;* Springer: New York, 2014.

38. Baird, J. A.; Taylor, L. S. Evaluation of amorphous solid dispersion properties using thermal analysis techniques. *Adv. Drug Deliv. Rev.* **2012,** *64* (5), 396-421.

39. Amharar, Y.; Curtin, V.; Gallagher, K. H.; Healy, A. M. Solubility of crystalline organic compounds in high and low molecular weight amorphous matrices above and below the glass transition by zero enthalpy extrapolation. *Int. J. Pharm.* **2014,** *472* (1-2), 241-247.

40. Baghel, S.; Cathcart, H.; O'Reilly, N. J. Polymeric amorphous solid dispersions: a review of amorphization, crystallization, stabilization, solid-state characterization, and aqueous solubilization of biopharmaceutical classification system class II drugs. *J. Pharm. Sci.* **2016**.

41. Yu, L. Amorphous pharmaceutical solids: preparation, characterization and stabilization. *Adv. Drug Deliver. Rev.* **2001,** *48* (1), 27-42.

42. Vippagunta, S. R.; Wang, Z.; Hornung, S.; Krill, S. L. Factors affecting the formation of eutectic solid dispersions and their dissolution behavior. *J. Pharm. Sci.* **2007,** *96* (2), 294-304.

43. Janssens, S.; Van den Mooter, G. Review: physical chemistry of solid dispersions. *J. Pharm. Pharmacol.* **2009,** *61* (12), 1571-1586.

44. Ford, J. L. The current status of solid dispersions. *Pharm. Acta Helv.* **1986,** *61* (3), 69-88.

45. Khachaturyan, A. G. Ordering in substitutional and interstitial solid solutions. *Prog. Mater. Sci.* **1978,** *22* (1), 1-150.

46. van Drooge, D. J.; Hinrichs, W. L.; Visser, M. R.; Frijlink, H. W. Characterization of the molecular distribution of drugs in glassy solid dispersions at the nano-meter scale, using differential scanning calorimetry and gravimetric water vapour sorption techniques. *Int. J. Pharm.* **2006,** *310* (1-2), 220-229.

47. Vasanthavada, M.; Tong, W. Q.; Joshi, Y.; Kislalioglu, M. S. Phase behavior of amorphous molecular dispersions I: determination of the degree and mechanism of solid solubility. *Pharm. Res.* **2004,** *21* (9), 1598-1606.

48. Tao, J.; Sun, Y.; Zhang, G. G.; Yu, L. Solubility of small-molecule crystals in polymers: D-mannitol in PVP, indomethacin in PVP/VA, and nifedipine in PVP/VA. *Pharm. Res.* **2009,** *26* (4), 855-864.

49. Qian, F.; Huang, J.; Hussain, M. A. Drug-polymer solubility and miscibility: stability consideration and practical challenges in amorphous solid dispersion development. *J. Pharm. Sci.* **2010,** *99* (7), 2941-2947.

50. Sekiguchi, K.; Obi, N. Studies on absorption of eutectic mixture. I. A comparison of the behavior of eutectic mixture of sulfathiazole and that of ordinary sulfathiazole in man. *Chem. Pharm. Bull.* **1961,** *9* (11), 866-872.

51. Kanig, J. L. Properties of fused mannitol in compressed tablets. *J. Pharm. Sci.* **1964,** *53* (2), 188-192.

52. Goldberg, A. H.; Gibaldi, M.; Kanig, J. L. Increasing dissolution rates and gastrointestinal absorption of drugs via solid solutions and eutectic mixtures. I. Theoretical considerations and discussion of the literature. *J. Pharm. Sci.* **1965,** *54* (8), 1145-1148.

53. Vo, C. L. N.; Park, C.; Lee, B. J. Current trends and future perspectives of solid dispersions containing poorly water-soluble drugs. *Eur. J. Pharm. Biopharm.* **2013,** *85* (3, Part B), 799-813.

54. Takayama, K.; Nagai, T. Application of interpolymer complexation of polyvinylpyrrolidone/carboxyvinyl polymer to control of drug release. *Chem. Pharm. Bull.* **1987,** *35* (12), 4921-4927.

55. Serajuddin, A. T.; Sheen, P. C.; Augustine, M. A. Improved dissolution of a poorly water-soluble drug from solid dispersions in polyethylene glycol: polysorbate 80 mixtures. *J. Pharm. Sci.* **1990,** *79* (5), 463-464.

56. Alshahrani, S. M.; Lu, W.; Park, J. B.; Morott, J. T.; Alsulays, B. B.; Majumdar, S.; Langley, N.; Kolter, K.; Gryczke, A.; Repka, M. A. Stability-enhanced hot-melt extruded amorphous solid dispersions via combinations of Soluplus® and HPMCAS-HF. *AAPS PharmSciTech.* **2015,** *16* (4), 824-834.

57. Allen, L. V. *An Introduction to Pharmacy;* 22nd ed.; Pharmaceutical Press: London, 2013.

58. Williams, H. D.; Trevaskis, N. L.; Charman, S. A.; Shanker, R. M.; Charman, W. N.; Pouton, C. W.; Porter, C. J. Strategies to address low drug solubility in discovery and development. *Pharmacol. Rev.* **2013,** *65* (1), 315-499.

59. Martins, R. M.; Siqueira, S.; Freitas, L. A. P. Spray congealing of pharmaceuticals: study on production of solid dispersions using Box-Behnken design. *Dry. Technol.* **2012,** *30* (9), 935-945.

60. Crowley, M. M.; Zhang, F.; Repka, M. A.; Thumma, S.; Upadhye, S. B.; Battu, S. K.; McGinity, J. W.; Martin, C. Pharmaceutical applications of hot-melt extrusion: part I. *Drug Dev. Ind. Pharm.* **2007,** *33* (9), 909-926.

61. Smithey, D.; Gao, P.; Taylor, L. S. Amorphous solid dispersions: an enabling formulation technology for oral delivery of poorly water soluble drugs. *AAPS Newsmagazine* **2013,** *16* (1), 11-14.

62. Paudel, A.; Worku, Z. A.; Meeus, J.; Guns, S.; Van den Mooter, G. Manufacturing of solid dispersions of poorly water soluble drugs by spray drying: formulation and process considerations. *Int. J. Pharm.* **2013,** *453* (1), 253-284.

63. Vasconcelos, T.; Marques, S.; das, N. J.; Sarmento, B. Amorphous solid dispersions: rational selection of a manufacturing process. *Adv. Drug Deliv. Rev.* **2016,** *100*, 85-101.

64. Teagarden, D. L.; Baker, D. S. Practical aspects of lyophilization using non-aqueous co-solvent systems. *Eur. J. Pharm. Sci.* **2002,** *15* (2), 115-133.

65. Girotra, P.; Singh, S. K.; Nagpal, K. Supercritical fluid technology: a promising approach in pharmaceutical research. *Pharm. Dev. Technol.* **2013,** *18* (1), 22-38.

66. Shah, N.; Sandhu, H.; Phuapradit, W.; Pinal, R.; Iyer, R.; Albano, A.; Chatterji, A.; Anand, S.; Choi, D. S.; Tang, K.; Tian, H.; Chokshi, H.; Singhal, D.; Malick, W. Development of novel microprecipitated bulk powder (MBP) technology for manufacturing stable amorphous formulations of poorly soluble drugs. *Int. J. Pharm.* **2012,** *438* (1-2), 53-60.

67. Shah, N.; Iyer, R. M.; Mair, H. J.; Choi, D. S.; Tian, H.; Diodone, R.; Fahnrich, K.; Pabst-Ravot, A.; Tang, K.; Scheubel, E.; Grippo, J. F.; Moreira, S. A.; Go, Z.; Mouskountakis, J.; Louie, T.; Ibrahim, P. N.; Sandhu, H.; Rubia, L.; Chokshi, H.; Singhal, D.; Malick, W. Improved human bioavailability of vemurafenib, a practically insoluble drug, using an amorphous

polymer-stabilized solid dispersion prepared by a solvent-controlled coprecipitation process. *J. Pharm. Sci.* **2013,** *102* (3), 967-981.

68. Loh, Z. H.; Samanta, A. K.; Heng, P. W. S. Overview of milling techniques for improving the solubility of poorly water-soluble drugs. *Asian J. Pharm. Sci.* **2015,** *10* (4), 255-274.

69. Descamps, M.; Willart, J. F.; Dudognon, E.; Caron, V. Transformation of pharmaceutical compounds upon milling and comilling: the role of Tg. *J. Pharm. Sci.* **2007,** *96* (5), 1398-1407.

70. Patterson, J. E.; James, M. B.; Forster, A. H.; Lancaster, R. W.; Butler, J. M.; Rades, T. Preparation of glass solutions of three poorly water soluble drugs by spray drying, melt extrusion and ball milling. *Int. J. Pharm.* **2007,** *336* (1), 22-34.

71. Adrjanowicz, K.; Kaminski, K.; Grzybowska, K.; Hawelek, L.; Paluch, M.; Gruszka, I.; Zakowiecki, D.; Sawicki, W.; Lepek, P.; Kamysz, W.; Guzik, L. Effect of cryogrinding on chemical stability of the sparingly water-soluble drug furosemide. *Pharm. Res.* **2011,** *28* (12), 3220-3236.

72. Yonemochi, E.; Inoue, Y.; Buckton, G.; Moffat, A.; Oguchi, T.; Yamamoto, K. Differences in crystallization behavior between quenched and ground amorphous ursodeoxycholic acid. *Pharm. Res.* **1999,** *16* (6), 835-840.

73. Karmwar, P.; Graeser, K.; Gordon, K. C.; Strachan, C. J.; Rades, T. Investigation of properties and recrystallisation behaviour of amorphous indomethacin samples prepared by different methods. *Int. J. Pharm.* **2011,** *417* (1-2), 94-100.

74. Craig, D. Q. The mechanisms of drug release from solid dispersions in water-soluble polymers. *Int. J. Pharm.* **2002,** *231* (2), 131-144.

75. Guo, Z.; Lu, M.; Li, Y.; Pang, H.; Lin, L.; Liu, X.; Wu, C. The utilization of drug-polymer interactions for improving the chemical stability of hot-melt extruded solid dispersions. *J. Pharm. Pharmacol.* **2014,** *66* (2), 285-296.

76. Li, J.; Zhao, J.; Tao, L.; Wang, J.; Waknis, V.; Pan, D.; Hubert, M.; Raghavan, K.; Patel, J. The effect of polymeric excipients on the physical properties and performance of amorphous dispersions: part I, free volume and glass transition. *Pharm. Res.* **2015,** *32* (2), 500-515.

77. Graeser, K. A.; Patterson, J. E.; Zeitler, J. A.; Gordon, K. C.; Rades, T. Correlating thermodynamic and kinetic parameters with amorphous stability. *Eur. J. Pharm. Sci.* **2009,** *37* (3-4), 492-498.

78. Hancock, B. C.; Shamblin, S. L.; Zografi, G. Molecular mobility of amorphous pharmaceutical solids below their glass transition temperatures. *Pharm. Res.* **1995,** *12* (6), 799-806.

79. Ghebremeskel, A. N.; Vemavarapu, C.; Lodaya, M. Use of surfactants as plasticizers in preparing solid dispersions of poorly soluble API: selection of polymer-surfactant combinations using solubility parameters and testing the processability. *Int. J. Pharm.* **2007,** *328* (2), 119-129.

80. Sun, Y.; Tao, J.; Zhang, G. G.; Yu, L. Solubilities of crystalline drugs in polymers: an improved analytical method and comparison of solubilities of indomethacin and nifedipine in PVP, PVP/VA, and PVAc. *J. Pharm. Sci.* **2010,** *99* (9), 4023-4031.

81. Prudic, A.; Kleetz, T.; Korf, M.; Ji, Y.; Sadowski, G. Influence of copolymer composition on the phase behavior of solid dispersions. *Mol. Pharm.* **2014,** *11* (11), 4189-4198.

82. Lin, D.; Huang, Y. A thermal analysis method to predict the complete phase diagram of drug-polymer solid dispersions. *Int. J. Pharm.* **2010,** *399* (1), 109-115.

83. Marsac, P. J.; Shamblin, S. L.; Taylor, L. S. Theoretical and practical approaches for prediction of drug-polymer miscibility and solubility. *Pharm. Res.* **2006,** *23* (10), 2417-2426.

84. Potter, R. W.; Clynne, M. A.; Brown, D. L. Freezing point depression of aqueous sodium chloride solutions. *Econ. Geol.* **1978,** *73* (2), 284-285.

85. Flory, P. J. *Principles of polymer chemistry;* Cornell University Press: Ithica, NY, 1953.

86. Hoei, Y.; Yamaura, K.; Matsuzawa, S. A lattice treatment of crystalline solvent-amorphous polymer mixtures on melting point depression. *J. Phys. Chem.* **1992,** *96* (26), 10584-10586.

87. Pajula, K.; Taskinen, M.; Lehto, V. P.; Ketolainen, J.; Korhonen, O. Predicting the formation and stability of amorphous small molecule binary mixtures from computationally determined Flory-Huggins interaction parameter and phase diagram. *Mol. Pharm.* **2010,** *7* (3), 795-804.

88. Mohan, R.; Lorenz, H.; Myerson, A. S. Solubility measurement using differential scanning calorimetry. *J. Ind. Eng. Chem.* **2002,** *41* (19), 4854-4862.

89. Marsac, P. J.; Li, T.; Taylor, L. S. Estimation of drug-polymer miscibility and solubility in amorphous solid dispersions using experimentally determined interaction parameters. *Pharm. Res.* **2009,** *26* (1), 139-151.

90. Tian, Y.; Caron, V.; Jones, D. S.; Healy, A. M.; Andrews, G. P. Using Flory-Huggins phase diagrams as a pre-formulation tool for the production of amorphous solid dispersions: a comparison between hot-melt extrusion and spray drying. *J. Pharm. Pharmacol.* **2014,** *66* (2), 256-274.

91. Paudel, A.; Van, H. J.; Van den Mooter, G. Theoretical and experimental investigation on the solid solubility and miscibility of naproxen in poly(vinylpyrrolidone). *Mol. Pharm.* **2010,** *7* (4), 1133-1148.

92. Caron, V.; Tajber, L.; Corrigan, O. I.; Healy, A. M. A comparison of spray drying and milling in the production of amorphous dispersions of sulfathiazole/polyvinylpyrrolidone and sulfadimidine/polyvinylpyrrolidone. *Mol. Pharm.* **2011,** *8* (2), 532-542.

93. Zhao, Y.; Inbar, P.; Chokshi, H. P.; Malick, A. W.; Choi, D. S. Prediction of the thermal phase diagram of amorphous solid dispersions by Flory-Huggins theory. *J. Pharm. Sci.* **2011,** *100* (8), 3196-3207.

94. Donnely, C.; Tian, Y.; Potter, C.; Jones, D. S.; Andrews, G. P. Probing the effects of experimental conditions on the character of drug-polymer phase diagrams constructed using Flory-Huggins theory. *Pharm. Res.* **2015,** *32* (1), 167-179.

95. Mahieu, A.; Willart, J. F.; Dudognon, E.; Danede, F.; Descamps, M. A new protocol to determine the solubility of drugs into polymer matrixes. *Mol. Pharm.* **2013,** *10* (2), 560-566.

96. Gordon, J. M.; Taylor, J. S. Ideal copolymers and the second-order transitions of synthetic rubbers. I. Non-crystalline copolymers. *J. App. Chem.* **1952,** *2* (9), 493-500.

97. Theeuwes, F.; Hussain, A.; Higuchi, T. Quantitative analytical method for determination of drugs dispersed in polymers using differential scanning calorimetry. *J. Pharm. Sci.* **1974,** *63* (3), 427-429.

98. Gramaglia, D.; Conway, B. R.; Kett, V. L.; Malcolm, R. K.; Batchelor, H. K. High speed DSC (hyper-DSC) as a tool to measure the solubility of a drug within a solid or semi-solid matrix. *Int. J. Pharm.* **2005,** *301* (1-2), 1-5.

99. Galia, E.; Nicolaides, E.; Horter, D.; Lobenberg, R.; Reppas, C.; Dressman, J. B. Evaluation of various dissolution media for predicting in vivo performance of class I and II drugs. *Pharm. Res.* **1998,** *15* (5), 698-705.

100. Dickinson, P. A.; Abu, R. R.; Ashworth, L.; Barker, R. A.; Burke, W. M.; Patterson, C. M.; Stainforth, N.; Yasin, M. An investigation into the utility of a multi-compartmental, dynamic, system of the upper gastrointestinal tract to support formulation development and establish bioequivalence of poorly soluble drugs. *AAPS J.* **2012,** *14* (2), 196-205.

101. Bevernage, J.; Brouwers, J.; Annaert, P.; Augustijns, P. Drug precipitation-permeation interplay: supersaturation in an absorptive environment. *Eur. J. Pharm. Biopharm.* **2012,** *82* (2), 424-428.

102. Alonzo, D. E.; Raina, S.; Zhou, D.; Gao, Y.; Zhang, G. G. Z.; Taylor, L. S. Characterizing the impact of hydroxypropylmethyl cellulose on the growth and nucleation kinetics of felodipine from supersaturated solutions. *Cryst. Growth Des.* **2012,** *12* (3), 1538-1547.

103. Guzman, H. R.; Tawa, M.; Zhang, Z.; Ratanabanangkoon, P.; Shaw, P.; Gardner, C. R.; Chen, H.; Moreau, J. P.; Almarsson, O.; Remenar, J. F. Combined use of crystalline salt forms and precipitation inhibitors to improve oral absorption of celecoxib from solid oral formulations. *J. Pharm. Sci.* **2007,** *96* (10), 2686-2702.

104. He, Y.; Ho, C. Amorphous solid dispersions: utilization and challenges in drug discovery and development. *J. Pharm. Sci.* **2015,** *104* (10), 3237-3258.

105. Augustijns, P.; Brewster, M. E. Supersaturating drug delivery systems: fast is not necessarily good enough. *J. Pharm. Sci.* **2012,** *101* (1), 7-9.

106. Xu, S.; Dai, W. G. Drug precipitation inhibitors in supersaturable formulations. *Int. J. Pharm.* **2013,** *453* (1), 36-43.

107. Raghavan, S. L.; Trividic, A.; Davis, A. F.; Hadgraft, J. Crystallization of hydrocortisone acetate: influence of polymers. *Int. J. Pharm.* **2001,** *212* (2), 213-221.

108. Ilevbare, G. A.; Liu, H.; Edgar, K. J.; Taylor, L. S. Understanding polymer properties important for crystal growth inhibition-impact of chemically diverse polymers on solution crystal growth of ritonavir. *Cryst. Growth Des.* **2012,** *12* (6), 3133-3143.

109. DiNunzio, J. C.; Brough, C.; Hughey, J. R.; Miller, D. A.; Williams, R. O.; McGinity, J. W. Fusion production of solid dispersions containing a heat-sensitive active ingredient by hot melt extrusion and Kinetisol® dispersing. *Eur. J. Pharm. Biopharm.* **2010,** *74* (2), 340-351.

110. Valizadeh, H.; Zakeri-Milani, P.; Barzegar-Jalali, M.; Mohammadi, G.; Danesh-Bahreini, M. A.; Adibkia, K.; Nokhodchi, A. Preparation and characterization of solid dispersions of piroxicam with hydrophilic carriers. *Drug Dev. Ind. Pharm.* **2007,** *33* (1), 45-56.

111. Crowley, K. J.; Zografi, G. The effect of low concentrations of molecularly dispersed poly(vinylpyrrolidone) on indomethacin crystallization from the amorphous state. *Pharm. Res.* **2003,** *20* (9), 1417-1422.

112. Friedrich, H.; Nada, A.; Bodmeier, R. Solid state and dissolution rate characterization of co-ground mixtures of nifedipine and hydrophilic carriers. *Drug Dev. Ind. Pharm.* **2005,** *31* (8), 719-728.

113. Shanbhag, A.; Rabel, S.; Nauka, E.; Casadevall, G.; Shivanand, P.; Eichenbaum, G.; Mansky, P. Method for screening of solid dispersion formulations of low-solubility compounds-miniaturization and automation of solvent casting and dissolution testing. *Int. J. Pharm.* **2008,** *351* (1-2), 209-218.

114. Kistenmacher, T. J.; Marsh, R. E. Crystal and molecular structure of an antiinflammatory agent, indomethacin, 1-(p-chlorobenzoyl)-5-methoxy-2-methylindole-3-acetic acid. *J. Am. Chem. Soc.* **1972,** *94* (4), 1340-1345.

115. Ke, P.; Hasegawa, S.; Al-Obaidi, H.; Buckton, G. Investigation of preparation methods on surface/bulk structural relaxation and glass fragility of amorphous solid dispersions. *Int. J. Pharm.* **2012,** *422* (1-2), 170-178.

116. Yoshioka, M.; Hancock, B. C.; Zografi, G. Crystallization of indomethacin from the amorphous state below and above its glass transition temperature. *J. Pharm. Sci.* **1994,** *83* (12), 1700-1705.

117. Timko, R. J.; Lordi, N. G. Thermal analysis studies of glass dispersion systems. *Drug Dev. Ind. Pharm.* **1984,** *10* (3), 425-451.

118. Matsumoto, T.; Zografi, G. Physical properties of solid molecular dispersions of indomethacin with poly(vinylpyrrolidone) and poly(vinylpyrrolidone-co-vinyl-acetate) in relation to indomethacin crystallization. *Pharm. Res.* **1999,** *16* (11), 1722-1728.

119. Rodriguez-Hornedo, N.; Murphy, D. Significance of controlling crystallization mechanisms and kinetics in pharmaceutical systems. *J. Pharm. Sci.* **1999,** *88* (7), 651-660.

120. Barton, A. F. M. *Handbook of polymer-liquid interaction parameters and solubility parameters;* CRC Press: Boca Raton, FL, 1990.

121. Forster, A.; Hempenstall, J.; Rades, T. Characterization of glass solutions of poorly water-soluble drugs produced by melt extrusion with hydrophilic amorphous polymers. *J. Pharm. Pharmacol.* **2001,** *53* (3), 303-315.

122. Surana, R.; Pyne, A.; Suryanarayanan, R. Effect of preparation method on physical properties of amorphous trehalose. *Pharm. Res.* **2004,** *21* (7), 1167-1176.

123. Qian, F.; Huang, J.; Zhu, Q.; Haddadin, R.; Gawel, J.; Garmise, R.; Hussain, M. Is a distinctive single Tg a reliable indicator for the homogeneity of amorphous solid dispersion? *Int. J. Pharm.* **2010,** *395* (1-2), 232-235.

124. Laitinen, R.; Lobmann, K.; Strachan, C. J.; Grohganz, H.; Rades, T. Emerging trends in the stabilization of amorphous drugs. *Int. J. Pharm.* **2013,** *453* (1), 65-79.

125. Taylor, L. S.; Zografi, G. Spectroscopic characterization of interactions between PVP and indomethacin in amorphous molecular dispersions. *Pharm. Res.* **1997,** *14* (12), 1691-1698.

126. Rumondor, A. C.; Ivanisevic, I.; Bates, S.; Alonzo, D. E.; Taylor, L. S. Evaluation of drug-polymer miscibility in amorphous solid dispersion systems. *Pharm. Res.* **2009,** *26* (11), 2523-2534.

127. Thakral, S.; Thakral, N. K. Prediction of drug-polymer miscibility through the use of solubility parameter based Flory-Huggins interaction parameter and the experimental validation: PEG as model polymer. *J. Pharm. Sci.* **2013,** *102* (7), 2254-2263.

128. Martin, J. R.; Johnson, J. F.; Cooper, A. R. Mechanical properties of polymers: the influence of molecular weight and molecular weight distribution. *J. Macromol. Sci. Polymer Rev.* **1972,** *8* (1), 57-199.

129. Nunes, R. W.; Martin, J. R.; Johnson, J. F. Influence of molecular weight and molecular weight distribution on mechanical properties of polymers. *Polym. Eng. Sci.* **1982,** *22* (4), 205-228.

130. Sethia, S.; Squillante, E. Solid dispersion of carbamazepine in PVP K30 by conventional solvent evaporation and supercritical methods. *Int. J. Pharm.* **2004,** *272* (1-2), 1-10.

131. Folttmann, H.; Quadir, A. Polyvinylpyrrolidone (PVP) - one of the most widely used excipients in pharmaceuticals: an overview. *Drug. Deliv. Technol.* **2008,** *8* (6).

132. Walking, W. D. Povidone. In *Handbook of pharmaceutical excipients*, Wade, A., Weller, P. J., Eds.; American Pharmaceutical Association/The Pharmaceutical Press: Washington DC/London, 1994; pp 392-399.

133. Simonelli, A. P.; Mehta, S. C.; Higuchi, W. I. Dissolution rates of high energy polyvinylpyrrolidone (PVP)-sulfathiazole coprecipitates. *J. Pharm. Sci.* **1969,** *58* (5), 538-549.

134. Hilton, J. E.; Summers, M. P. The effect of wetting agents on the dissolution of indomethacin solid dispersion systems. *Int. J. Pharm.* **1986,** *31*, 157-164.

135. Jachowicz, R. Dissolution rates of partially water-soluble drugs from solid dispersion systems. II. phenytoin. *Int. J. Pharm.* **1987,** *35*, 7-12.

136. Doherty, C.; York, P. Mechanisms of dissolution of furosemide/PVP solid dispersions. *Int. J. Pharm.* **1987,** *34* (3), 197-205.

137. Torrado, S.; Torrado, S.; Torrado, J. J.; Cadorniga, R. Preparation, dissolution and chracterization of albendazole solid dispersions. *Int. J. Pharm.* **1996,** *140* (2), 247-250.

138. Van den Mooter, G.; Augustijns, P.; Kinget, R. Physico-chemical characterization of solid dispersions of temazepam with polyethyl glycol 6000 and PVP K30. *Int. J. Pharm.* **1998,** *164* (1-2), 67-80.

139. Knopp, M. M.; Olesen, N. E.; Holm, P.; Löbmann, K.; Holm, R.; Langguth, P.; Rades, T. Evaluation of drug-polymer solubility curves through formal statistical analysis: comparison of preparation techniques. *J. Pharm. Sci.* **2015,** *104* (1), 44-51.

140. Otsuka, M.; Kato, F.; Matsuda, Y. Determination of indomethacin polymorphic contents by chemometric near-infrared spectroscopy and conventional powder X-ray diffractometry. *Analyst* **2001,** *126* (9), 1578-1582.

141. Xiang, T. X.; Anderson, B. D. Molecular dynamics simulation of amorphous indomethacin-poly(vinylpyrrolidone) glasses: solubility and hydrogen bonding interactions. *J. Pharm. Sci.* **2013,** *102* (3), 876-891.

142. Haaf, F.; Sanner, A.; Straub, F. Polymers of N-vinylpyrrolidone: synthesis, characterization and uses. *Polym. J.* **1985,** *17* (1), 143-152.

143. Van den Mooter, G.; Wuyts, M.; Blaton, N.; Busson, R.; Grobet, P.; Augustijns, P.; Kinget, R. Physical stabilisation of amorphous ketoconazole in solid dispersions with polyvinylpyrrolidone K25. *Eur. J. Pharm. Sci.* **2001,** *12* (3), 261-269.

144. Grohganz, H.; Priemel, P. A.; Lobmann, K.; Nielsen, L. H.; Laitinen, R.; Mullertz, A.; Van den Mooter, G.; Rades, T. Refining stability and dissolution rate of amorphous drug formulations. *Expert. Opin. Drug Deliv.* **2014,** *11* (6), 977-989.

145. Tian, Y.; Booth, J.; Meehan, E.; Jones, D. S.; Li, S.; Andrews, G. P. Construction of drug-polymer thermodynamic phase diagrams using Flory-Huggins interaction theory: identifying the relevance of temperature and drug weight fraction to phase separation within solid dispersions. *Mol. Pharm.* **2012,** *10* (1), 236-248.

146. Xie, X. L.; Li, R. K. Y.; Tjong, S. C.; Tang, C. Y. Flory-Huggins interaction parameters of LCP/thermoplastic blends measured by DSC analysis. *J. Therm. Anal. Calorim.* **2002,** *70* (2), 541-548.

147. Koningsveld, R.; Stockmayer, W. H.; Nies, E. *Polymer phase diagrams: a textbook;* Oxford University Press: 2001.

148. Lu, J.; Shah, S.; Jo, S.; Majumdar, S.; Gryczke, A.; Kolter, K.; Langley, N.; Repka, M. A. Investigation of phase diagrams and physical stability of drug-polymer solid dispersions. *Pharm. Dev. Technol.* **2015,** *20* (1), 105-117.

149. Nishi, T.; Wang, T. T. Melting point depression and kinetic effects of cooling on crystallization in poly (vinylidene fluoride)-poly (methyl metracrylate) mixtures. *Macromolecules* **1975,** *8* (6), 909-915.

150. Knopp, M. M.; Olesen, N. E.; Holm, P.; Langguth, P.; Holm, R.; Rades, T. Influence of polymer molecular weight on drug-polymer solubility: a comparison between experimentally determined solubility in PVP and prediction derived from solubility in monomer. *J. Pharm. Sci.* **2015,** *104* (9), 2905-2912.

151. Cook, R. D. Detection of influential observation in linear regression. *Technometrics* **1977,** 15-18.

152. Pinal, R. Entropy of mixing and the glass transition of amorphous mixtures. *Entropy* **2008,** *10* (3), 207-223.

153. Greenhalgh, D. J.; Williams, A. C.; Timmins, P.; York, P. Solubility parameters as predictors of miscibility in solid dispersions. *J. Pharm. Sci.* **1999,** *88* (11), 1182-1190.

154. Gupta, P.; Thilagavathi, R.; Chakraborti, A. K.; Bansal, A. K. Role of molecular interaction in stability of celecoxib-PVP amorphous systems. *Mol. Pharm.* **2005,** *2* (5), 384-391.

155. Knopp, M. M.; Tajber, L.; Tian, Y.; Olesen, N. E.; Jones, D. S.; Kozyra, A.; Löbmann, K.; Paluch, K.; Brennan, C. M.; Holm, R.; Healy, A. M.; Andrews, G. P.; Rades, T. Comparative study of different methods for the prediction of drug-polymer solubility. *Mol. Pharm.* **2015,** *12* (9), 3408-3419.

156. Gordon, J. M.; Rouse, G. B.; Gibbs, J. H.; Risen Jr, W. M. The composition dependence of glass transition properties. *J. Chem. Phys.* **1977,** *66* (11), 4971-4976.

157. Nair, R.; Nyamweya, N.; Gonen, S.; Martinez-Miranda, L. J.; Hoag, S. W. Influence of various drugs on the glass transition temperature of poly(vinylpyrrolidone): a thermodynamic and spectroscopic investigation. *Int. J. Pharm.* **2001,** *225* (1-2), 83-96.

158. Konno, H.; Taylor, L. S. Influence of different polymers on the crystallization tendency of molecularly dispersed amorphous felodipine. *J. Pharm. Sci.* **2006,** *95* (12), 2692-2705.

159. Kestur, U. S.; Taylor, L. S. Role of polymer chemistry in influencing crystal growth rates from amorphous felodipine. *Cryst. Eng. Comm.* **2010,** *12* (8), 2390-2397.

160. Blasi, P.; D'Souza, S. S.; Selmin, F.; DeLuca, P. P. Plasticizing effect of water on poly(lactide-co-glycolide). *J. Control. Release* **2005,** *108* (1), 1-9.

161. Aaltonen, J.; Rades, T. Towards physicorelevant dissolution testing: the importance of solid-state analysis in dissolution. *Dissolut. Technol.* **2009,** *16*, 47-54.

162. Oksanen, C. A.; Zografi, G. The relationship between the glass transition temperature and water vapor absorption by poly(vinylpyrrolidone). *Pharm. Res.* **1990,** *7* (6), 654-657.

163. Taylor, L. S.; Langkilde, F. W.; Zografi, G. Fourier transform Raman spectroscopic study of the interaction of water vapor with amorphous polymers. *J. Pharm. Sci.* **2001,** *90* (7), 888-901.

164. Sariban, A.; Binder, K. Critical properties of the Flory-Huggins lattice model of polymer mixtures. *J. Chem. Phys.* **1987,** *86* (10), 5859-5873.

165. Couchman, P. R.; Karasz, F. E. A classical thermodynamic discussion of the effect of composition on glass-transition temperatures. *Macromolecules* **1978,** *11* (1), 117-119.

166. Lu, G. W.; Hawley, M.; Smith, M.; Geiger, B. M.; Pfund, W. Characterization of a novel polymorphic form of celecoxib. *J. Pharm. Sci.* **2006,** *95* (2), 305-317.

167. Struik, L. C. E. The mechanical and physical ageing of semicrystalline polymers. *Polymer* **1987,** *28* (9), 1521-1533.

168. Chawla, G.; Gupta, P.; Thilagavathi, R.; Chakraborti, A. K.; Bansal, A. K. Characterization of solid-state forms of celecoxib. *Eur. J. Pharm. Sci.* **2003,** *20* (3), 305-317.

169. Du, Y. K.; Yang, P.; Mou, Z. G.; Hua, N. P.; Jiang, L. Thermal decomposition behaviors of PVP coated on platinum nanoparticles. *J. Appl. Polym. Sci.* **2006,** *99* (1), 23-26.

170. Holland, B. J.; Hay, J. N. The thermal degradation of poly (vinyl acetate) measured by thermal analysis-Fourier transform infrared spectroscopy. *Polymer* **2002,** *43* (8), 2207-2211.

171. Sovizi, M. Thermal behavior of drugs: investigation on decomposition kinetic of naproxen and celecoxib. *J. Therm. Anal. Calorim.* **2010,** *102* (1), 285-289.

172. Painter, P. C.; Coleman, M. M. *Fundamentals of polymer science: an introductory text;* Technomic Publishing Company Inc: Lancaster, PA, 1997.

173. Bhugra, C.; Pikal, M. J. Role of thermodynamic, molecular, and kinetic factors in crystallization from the amorphous state. *J. Pharm. Sci.* **2008,** *97* (4), 1329-1349.

174. Olabisi, O. Interpretations of polymer-polymer miscibility. *J. Chem. Edu.* **1981,** *58* (11), 944-950.

175. Keen, J. M.; Martin, C.; Machado, A.; Sandhu, H.; McGinity, J. W.; DiNunzio, J. C. Investigation of process temperature and screw speed on properties of a pharmaceutical solid dispersion using corotating and counter-rotating twin-screw extruders. *J. Pharm. Pharmacol* **2014,** *66* (2), 204-217.

176. Rubinstein, M.; Colby, R. *Polymer physics;* Oxford University Press: New York, NY, 2003.

177. Motulsky, H.; Christopoulos, A. *Fitting models to biological data using linear and nonlinear regression: a practical guide to curve fitting;* Oxford University Press: New York, NY, 2004.

178. Bates, D. M.; Watts, D. G. *Nonlinear regression analysis and its applications;* John Wiley & Sons: Hoboken, NY, 1988.

179. Bellantone, R. A.; Patel, P.; Sandhu, H.; Choi, D. S.; Singhal, D.; Chokshi, H.; Malick, A. W.; Shah, N. A method to predict the equilibrium solubility of drugs in solid polymers near room temperature using thermal analysis. *J. Pharm. Sci.* **2012,** *101* (12), 4549-4558.

180. Kyerematen, S. O.; Pudlas, M.; Woehrle, G. H. A fast and reliable empirical approach for estimating solubility of crystalline drugs in polymers for hot melt extrusion formulations. *J. Pharm. Sci.* **2014,** *103* (9), 2847-2858.

181. Rask, M. B.; Knopp, M. M.; Olesen, N. E.; Holm, R.; Rades, T. Influence of PVP/VA copolymer composition on drug-polymer solubility. *Eur. J. Pharm. Sci.* **2016,** *85*, 10-17.

182. Mignani, S.; El, K. S.; Bousmina, M.; Majoral, J. P. Expand classical drug administration ways by emerging routes using dendrimer drug delivery systems: a concise overview. *Adv. Drug Deliv. Rev.* **2013,** *65* (10), 1316-1330.

183. Lipinski, C. A. Drug-like properties and the causes of poor solubility and poor permeability. *J. Pharmacol. Toxicol.* **2000,** *44* (1), 235-249.

184. Gupta, S.; Kesarla, R.; Omri, A. Formulation strategies to improve the bioavailability of poorly absorbed drugs with special emphasis on self-emulsifying systems. *ISRN. Pharm* **2013,** *2013*, 848043.

185. Hörter, D.; Dressman, J. B. Influence of physicochemical properties on dissolution of drugs in the gastrointestinal tract. *Adv. Drug Deliv. Rev.* **2001,** *46* (1-3), 75-87.

186. Gao, P.; Shi, Y. Characterization of supersaturatable formulations for improved absorption of poorly soluble drugs. *AAPS J.* **2012,** *14* (4), 703-713.

187. Breitenbach, J. Melt extrusion: from process to drug delivery technology. *Eur. J. Pharm. Biopharm.* **2002,** *54* (2), 107-117.

188. Trasi, N. S.; Oucherif, K. A.; Litster, J. D.; Taylor, L. S. Evaluating the influence of polymers on nucleation and growth in supersaturated solutions of acetaminophen. *Cryst. Eng. Comm.* **2015,** *17* (6), 1242-1248.

189. Sekikawa, H.; Nakano, M.; Arita, T. Inhibitory effect of polyvinylpyrrolidone on the crystallization of drugs. *Chem. Pharm. Bull.* **1978,** *26* (1), 118-126.

190. Anwar, J.; Boateng, P. K.; Tamaki, R.; Odedra, S. Mode of action and design rules for additives that modulate crystal nucleation. *Angew. Chem. Int. Ed Engl.* **2009,** *48* (9), 1596-1600.

191. Cohen, J. L.; Hubert, B. B.; Leeson, L. J.; Rhodes, C. T.; Robinson, J. R.; Roseman, T. J.; Shefter, E. The development of USP dissolution and drug release standards. *Pharm. Res.* **1990,** *7* (10), 983-987.

192. Davies, N. M.; McLachlan, A. J.; Day, R. O.; Williams, K. M. Clinical pharmacokinetics and pharmacodynamics of celecoxib. *Clin. Pharmacokinet.* **2000,** *38* (3), 225-242.

193. Paulson, S. K.; Vaughn, M. B.; Jessen, S. M.; Lawal, Y.; Gresk, C. J.; Yan, B.; Maziasz, T. J.; Cook, C. S.; Karim, A. Pharmacokinetics of celecoxib after oral administration in dogs and humans: effect of food and site of absorption. *J. Pharmacol. Exp. Ther.* **2001,** *297* (2), 638-645.

194. Subramanian, N.; Ray, S.; Ghosal, S. K.; Bhadra, R.; Moulik, S. P. Formulation design of self-microemulsifying drug delivery systems for improved oral bioavailability of celecoxib. *Biol. Pharm. Bull.* **2004,** *27* (12), 1993-1999.

195. Tsume, Y.; Mudie, D. M.; Langguth, P.; Amidon, G. E.; Amidon, G. L. The biopharmaceutics classification system: subclasses for in vivo predictive dissolution (IPD) methodology and IVIVC. *Eur. J. Pharm. Sci.* **2014,** *57*, 152-163.

196. Nagarsenker, M. S.; Joshi, M. S. Celecoxib-cyclodextrin systems: characterization and evaluation of in vitro and in vivo advantage. *Drug Dev. Ind. Pharm.* **2005,** *31* (2), 169-178.

197. Andrews, G. P.; Abu-Diak, O.; Kusmanto, F.; Hornsby, P.; Hui, Z.; Jones, D. S. Physicochemical characterization and drug-release properties of celecoxib hot-melt extruded glass solutions. *J. Pharm. Pharmacol.* **2010,** *62* (11), 1580-1590.

198. Gupta, P.; Kakumanu, V. K.; Bansal, A. K. Stability and solubility of celecoxib-PVP amorphous dispersions: a molecular perspective. *Pharm. Res.* **2004,** *21* (10), 1762-1769.

199. Knopp, M. M.; Nguyen, J. H.; Mu, H.; Langguth, P.; Rades, T.; Holm, R. Influence of copolymer composition on in vitro and in vivo performance of celecoxib-PVP/VA amorphous solid dispersions. *AAPS. J.* **2016,** *18* (2), 416-423.

200. Silva, M. F.; Da Silva, C. A.; Fogo, F. C.; Pineda, E. A. G.; Hechenleitner, A. A. W. Thermal and FTIR study of polyvinylpyrrolidone/lignin blends. *J. Therm. Anal. Calorim.* **2005,** *79* (2), 367-370.

201. Lee, J. H.; Kim, M. J.; Yoon, H.; Shim, C. R.; Ko, H. A.; Cho, S. A.; Lee, D.; Khang, G. Enhanced dissolution rate of celecoxib using PVP and/or HPMC-based solid dispersions prepared by spray drying method. *J. Pharm. Investig.* **2013,** *43* (3), 205-213.

202. Khougaz, K.; Clas, S. D. Crystallization inhibition in solid dispersions of MK-0591 and poly(vinylpyrrolidone) polymers. *J. Pharm. Sci.* **2000,** *89* (10), 1325-1334.

203. Sjögren, E.; Abrahamsson, B.; Augustijns, P.; Becker, D.; Bolger, M. B.; Brewster, M.; Brouwers, J.; Flanagan, T.; Harwood, M.; Heinen, C.; Holm, R.; Juretschke, H. P.; Kubbinga, M.; Lindahl, A.; Lukacova, V.; Munster, U.; Neuhoff, S.; Nguyen, M. A.; Peer, A.; Reppas, C.; Hodjegan, A. R.; Tannergren, C.; Weitschies, W.; Wilson, C.; Zane, P.; Lennernas, H.; Langguth, P. In vivo methods for drug absorption - comparative physiologies, model selection, correlations with in vitro methods (IVIVC), and applications for formulation/API/excipient characterization including food effects. *Eur. J. Pharm. Sci.* **2014,** *57*, 99-151.

204. Lipinski, C. A.; Lombardo, F.; Dominy, B. W.; Feeney, P. J. Experimental and computational approaches to estimate solubility and permeability in drug discovery and development settings. *Adv. Drug Deliv. Rev.* **2001,** *46* (1-3), 3-26.

205. Miyazaki, T.; Yoshioka, S.; Aso, Y.; Kojima, S. Ability of polyvinylpyrrolidone and polyacrylic acid to inhibit the crystallization of amorphous acetaminophen. *J. Pharm. Sci.* **2004,** *93* (11), 2710-2717.

206. Sun, D. D.; Lee, P. I. Probing the mechanisms of drug release from amorphous solid dispersions in medium-soluble and medium-insoluble carriers. *J. Control. Release* **2015,** *211*, 85-93.

207. Xie, T.; Taylor, L. S. Dissolution performance of high drug loading celecoxib amorphous solid dispersions formulated with polymer combinations. *Pharm. Res.* **2016,** *33* (3), 739-750.

208. Ballistreri, A.; Foti, S.; Montaudo, G.; Scamporrino, E. Evolution of aromatic compounds in the thermal decomposition of vinyl polymers. *J. Polymer Sci. Polymer Chem. Ed.* **1980,** *18* (4), 1147-1153.

209. Zaccaron, C. M.; Oliveira, R. V. B.; Guiotoku, M.; Pires, A. T. N.; Soldi, V. Blends of hydroxypropyl methylcellulose and poly(1-vinylpyrrolidone-co-vinyl acetate): miscibility and thermal stability. *Polym. Degrad. Stab.* **2005,** *90* (1), 21-27.

210. Song, W. H.; Yeom, D. W.; Lee, D. H.; Lee, K. M.; Yoo, H. J.; Chae, B. R.; Song, S. H.; Choi, Y. W. In situ intestinal permeability and in vivo oral bioavailability of celecoxib in supersaturating self-emulsifying drug delivery system. *Arch. Pharm. Res.* **2014,** *37* (5), 626-635.

211. Fadda, H. M.; Sousa, T.; Carlsson, A. S.; Abrahamsson, B.; Williams, J. G.; Kumar, D.; Basit, A. W. Drug solubility in luminal fluids from different regions of the small and large intestine of humans. *Mol. Pharm.* **2010,** *7* (5), 1527-1532.

212. Davis, S. S.; Hardy, J. G.; Fara, J. W. Transit of pharmaceutical dosage forms through the small intestine. *Gut* **1986,** *27* (8), 886-892.

213. Hancock, B. C.; Parks, M. What is the true solubility advantage for amorphous pharmaceuticals? *Pharm. Res.* **2000,** *17* (4), 397-404.

214. Zhou, D.; Zhang, G. G.; Law, D.; Grant, D. J.; Schmitt, E. A. Physical stability of amorphous pharmaceuticals: importance of configurational thermodynamic quantities and molecular mobility. *J. Pharm. Sci.* **2002,** *91* (8), 1863-1872.

215. Alonzo, D. E.; Gao, Y.; Zhou, D.; Mo, H.; Zhang, G. G.; Taylor, L. S. Dissolution and precipitation behavior of amorphous solid dispersions. *J. Pharm. Sci.* **2011,** *100* (8), 3316-3331.

216. Abu-Diak, O. A.; Jones, D. S.; Andrews, G. P. An investigation into the dissolution properties of celecoxib melt extrudates: understanding the role of polymer type and concentration in stabilizing supersaturated drug concentrations. *Mol. Pharm.* **2011,** *8* (4), 1362-1371.

217. Jackson, M. J.; Kestur, U. S.; Hussain, M. A.; Taylor, L. S. Dissolution of danazol amorphous solid dispersions: supersaturation and phase behavior as a function of drug loading and polymer type. *Mol. Pharm.* **2016,** *13* (1), 223-231.

218. Knopp, M. M.; Nguyen, J. H.; Becker, C.; Francke, N. M.; Jorgensen, E. B.; Holm, P.; Holm, R.; Mu, H.; Rades, T.; Langguth, P. Influence of polymer molecular weight on in vitro dissolution behavior and in vivo performance of celecoxib:PVP amorphous solid dispersions. *Eur. J. Pharm. Biopharm.* **2016,** *101*, 145-151.

219. Loftsson, T.; Fridriksdóttir, H.; Gudmundsdóttir, T. K. The effect of water-soluble polymers on aqueous solubility of drugs. *Int. J. Pharm.* **1996,** *127* (2), 293-296.

220. Suzuki, H.; Sunada, H. Influence of water-soluble polymers on the dissolution of nifedipine solid dispersions with combined carriers. *Chem. Pharm. Bull. (Tokyo)* **1998,** *46* (3), 482-487.

221. Murdande, S. B.; Pikal, M. J.; Shanker, R. M.; Bogner, R. H. Aqueous solubility of crystalline and amorphous drugs: challenges in measurement. *Pharm. Dev. Technol.* **2011,** *16* (3), 187-200.

222. Harland, R. S.; Gazzaniga, A.; Sangalli, M. E.; Colombo, P.; Peppas, N. A. Drug/polymer matrix swelling and dissolution. *Pharm. Res.* **1988,** *5* (8), 488-494.

223. Karavas, E.; Georgarakis, E.; Bikiaris, D. Application of PVP/HPMC miscible blends with enhanced mucoadhesive properties for adjusting drug release in predictable pulsatile chronotherapeutics. *Eur. J. Pharm. Biopharm.* **2006,** *64* (1), 115-126.

224. Gao, P.; Morozowich, W. Development of supersaturatable self-emulsifying drug delivery system formulations for improving the oral absorption of poorly soluble drugs. *Expert. Opin. Drug Deliv.* **2006,** *3* (1), 97-110.

225. Dashevsky, A.; Kolter, K.; Bodmeier, R. pH-independent release of a basic drug from pellets coated with the extended release polymer dispersion Kollicoat SR 30 D and the enteric polymer dispersion Kollicoat MAE 30 DP. *Eur. J. Pharm. Biopharm.* **2004,** *58* (1), 45-49.

Appendix A

Statement of the Flory-Huggins model

The Flory-Huggins model can be derived from statistical thermodynamics based on the lattice theory of solution. The model considers a binary solution of a solvent (the drug) and a solute (the polymer). It is assumed that the polymer is much larger than the drug molecules. The Flory-Huggins expression for the Gibbs free energy of mixing is given by

$$\Delta G_{\text{mix}} = RT\left(n_{\text{imc}} \ln v_{\text{pvp}} + n_{\text{pvp}} \ln v_{\text{imc}} + \chi n_{\text{imc}} v_{\text{imc}}\right) \tag{A.1}$$

where χ is the Flory-Huggins interaction parameter, n is the number of molecules and v_{pvp} and v_{imc} are volume fractions given by

$$v_{\text{pvp}} = \frac{\dfrac{x_{\text{imc}}}{\rho_{\text{imc}}}}{\dfrac{x_{\text{imc}}}{\rho_{\text{imc}}} + \dfrac{1 - x_{\text{imc}}}{\rho_{\text{pvp}}}}, \; v_{\text{imc}} = 1 - v_{\text{pvp}} \tag{A.2}$$

Flory-Huggins expression for a_{imc}

The chemical potential of the solvent μ_{imc} in the solution, relative to its chemical potential $\mu^0{}_{\text{imc}}$ in the pure liquid, is obtained by differentiating the free energy in Equation A.1 with respect to the number of solvent molecules n_{imc} (bearing in mind that v_{pvp} and v_{imc} are functions of n_{imc}):

$$\begin{aligned} \ln a_{\text{imc}} &= \frac{\rho_{\text{imc}} - \rho^0_{\text{imc}}}{RT} = \frac{\partial \Delta G_{\text{mix}}}{\Delta n_{\text{imc}}} = \frac{\left(n_{\text{imc}} \ln v_{\text{pvp}} + n_{\text{pvp}} \ln v_{\text{imc}} + \chi n_{\text{imc}} n_{\text{pvp}}\right)}{\partial n_{\text{imc}}} \\ &= \ln\left(1 - v_{\text{imc}}\right) + \left(1 - \frac{1}{\lambda}\right) v_{\text{imc}} + \chi v^2_{\text{imc}} \end{aligned} \tag{A.3}$$

where λ is the molar volume ratio of the polymer to the drug.

Relating a_{imc} to the annealing temperature

The activity of drug a_{imc} in a polymer can be calculated from measurements of the glass transition temperature $T_{\text{g(imc)}}$. By integration of Gibbs-Helmholtz equation it can be shown that:

$$\ln a_{\text{imc}} = \frac{\Delta H_{\text{m}}}{R}\left(\frac{1}{T_{\text{m}}} - \frac{1}{T_{\text{anneal}}}\right) \tag{A.4}$$

where T_{anneal} is the temperature at which the solubility of the drug is measured, T_m is the melting temperature and ΔH_m is the the enthalpy of fusion. Combining Equations A.3 and A.4, we get:

$$\ln(1-v_{imc})+\left(1-\frac{1}{\lambda}\right)v_{imc}+\chi v_{imc}^2=\frac{\Delta H_m}{R}\left(\frac{1}{T_m}-\frac{1}{T_{anneal}}\right) \quad \text{(A.5)}$$

Formulation of the regression problem

Equation A.5 has a single fitting-parameter χ which is linear. The temperature at which the sample was annealed T_{anneal}, is in practice free of experimental error. On the other hand, v_{imc} is calculated from the Gordon-Taylor equation from measurements of $T_{g(Ximc)}$. As $T_{g(Ximc)}$ can only be measured with noise, v_{imc} will be subject to this noise. Therefore, the regression problem must be formulated as an error-in-variable model:

$$T_{anneal}^{-1}=g(v_{imc}+noise;\chi) \quad \text{(A.6)}$$

With the residuals defined as $r(i) = v_{imc}(i) - v\hat{}_{imc}(i)$. As the model function g is non-linear in v_{imc} and thereby not invertible this is the only way to formulate the regression problem. If the regression problem if formulated as done by Mahieu et al. 2012 the estimate of χ will be biased:

$$T_{anneal}^{-1}=f(v_{imc};\chi)+noise \quad \text{(A7)}$$

The 95% prediction interval for a future observation at 20 °C

As the regression problem only have 1 parameter, the uncertainty in this parameter directly translates into the uncertainty in the prediction for the observations. That is:

$$Var[g(v_{imc}+noise;\hat{\chi})]=g(v_{imc}+noise;Var(\hat{\chi})) \quad \text{(A.8)}$$

We therefore only need to calculate the uncertainty in χ to get the intervals. The 95% prediction interval for a future observation at T_{anneal} = 20 °C can be found by solving Equation A.9 with respect to v_{imc}:

$$g\left(v_{imc};\chi\pm t_{\alpha/2}(n-k)s_n\sqrt{1+\frac{1}{n}}\right)=\frac{1}{293.15K} \quad \text{(A.9)}$$

Fitting results

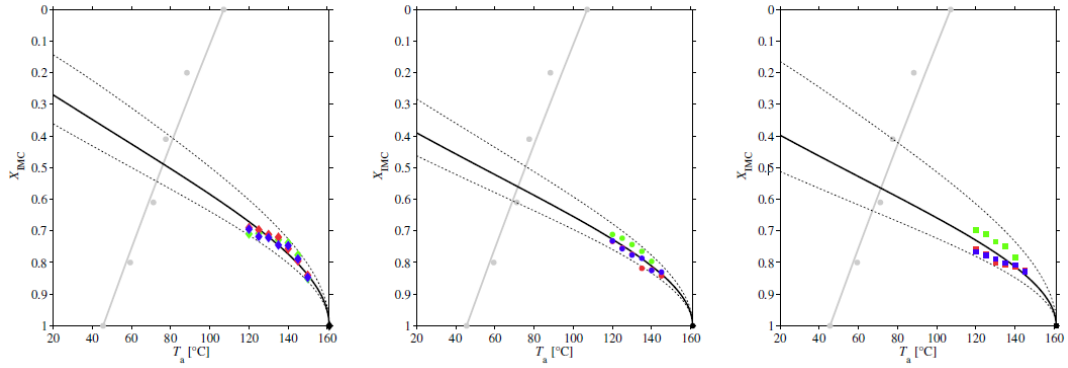

	Parameter	Estimate	Standard error
Ball milling	χ_{bm}	-8.3	0.3
Spray drying	χ_{sd}	-12.1	0.4
Film casting	χ_{fc}	-12.4	0.7

Measurements

Ball milling			
T_{anneal}	$T_g(X_{imc})$	$T_g(X_{imc})$	$T_g(X_{imc})$
°C	°C	°C	°C
150	54.3	54.9	54.5
145	58.7	57.6	58.0
140	61.0	59.9	60.5
135	61.6	62.1	60.6
130	62.2	62.6	62.0
125	62.8	63.5	62.2
120	62.7	63.9	63.6

Spray drying			
T_{anneal}	$T_g(X_{imc})$	$T_g(X_{imc})$	$T_g(X_{imc})$
°C	°C	°C	°C
145	55.2	54.8	55.5
140	57.5	55.9	55.8
135	59.4	56.2	58.1
130	60.7	58.8	58.7
125	61.9	60.0	59.9
120	62.6	61.3	61.4

Film casting			
T_{anneal}	$T_g(X_{imc})$	$T_g(X_{imc})$	$T_g(X_{imc})$
°C	°C	°C	°C
145	55.8	55.8	55.6
140	58.2	56.6	56.8
135	60.4	56.8	57.2
130	61.2	57.3	58.0
125	62.7	58.8	58.6
120	63.5	59.8	59.3

Appendix B

Table B.1: Experimental physical and thermodynamic values measured by DSC and density measured by helium pycnometry (values are mean ± s.d., *n* = 3).

Material	M_w (g/mol)	Density (g/cm^3)	T_g (°C)	ΔH_m (J/g)	T_m (°C)
CAP	323.13	1.50 ± 0.00	29.5 ± 0.3	106.2 ± 2.3	150.27 ± 0.11
CCX	381.37	1.41 ± 0.00	56.8 ± 0.1	96.3 ± 0.3	162.27 ± 0.04
PCM	151.17	1.29 ± 0.00	23.3 ± 0.2	181.9 ± 1.2	169.02 ± 0.01
PVP	10,000	1.18 ± 0.00	118.8 ± 0.8	-	-
PVA	40,000	1.18 ± 0.00	37.4 ± 0.4	-	-
SOL	118,000	1.14 ± 0.00	68.7 ± 2.1	-	-

Table B.2: Raw data from the new polymer in solution method in methanol (values are mean drug solubility ± SD, *n* = 2).

	CAP:PVP	**CAP:PVA**	**CAP:SOL**	**CCX:PVP**	**CCX:PVA**	**CCX:SOL**	**PCM:PVP**	**PCM:PVA**	**PCM:SOL**
$C_{polymer}$ (g/ml)	C_{drug} (g/ml)	C_{drug} (g/ml)	C_{drug} (g/ml)	C_{drug} (g/ml)	C_{drug} (g/ml)	C_{drug} (g/ml)	C_{drug} (g/ml)	C_{drug} (g/ml)	C_{drug} (g/ml)
0.00	0.248 ± 0.008	0.248 ± 0.008	0.248 ± 0.008	0.150 ± 0.008	0.150 ± 0.008	0.150 ± 0.008	0.130 ± 0.005	0.130 ± 0.005	0.130 ± 0.005
0.10	0.288 ± 0.007	0.257 ± 0.012	0.255 ± 0.047	0.188 ± 0.007	0.163 ± 0.011	0.181 ± 0.004	0.149 ± 0.001	0.130 ± 0.001	0.145 ± 0.001
0.20	0.332 ± 0.007	0.261 ± 0.002	0.277 ± 0.04	0.223 ± 0.001	0.168 ± 0.004	0.204 ± 0.003	0.164 ± 0.002	0.131 ± 0.002	0.147 ± 0.006
0.30	0.362 ± 0.030	0.266 ± 0.007	0.286 ± 0.04	0.262 ± 0.009	0.194 ± 0.006	0.217 ± 0.001	0.186 ± 0.005	0.132 ± 0.009	0.157 ± 0.002
0.40	0.404 ± 0.009	0.275 ± 0.008	0.300 ± 0.006	0.302 ± 0.007	-	0.248 ± 0.010	0.195 ± 0.001	0.133 ± 0.001	0.175 ± 0.003

Table B.3: Raw data from the new polymer in solution method in ethanol (values are mean drug solubility ± SD, *n* = 2).

	CAP:PVP	CAP:PVA	CAP:SOL	CCX:PVP	CCX:PVA	CCX:SOL	PCM:PVP	PCM:PVA	PCM:SOL
$C_{polymer}$ (g/ml)	C_{drug} (g/ml)	C_{drug} (g/ml)	C_{drug} (g/ml)	C_{drug} (g/ml)	C_{drug} (g/ml)	C_{drug} (g/ml)	C_{drug} (g/ml)	C_{drug} (g/ml)	C_{drug} (g/ml)
0.00	0.201 ± 0.008	0.201 ± 0.008	0.201 ± 0.008	0.074 ± 0.001	0.074 ± 0.001	0.074 ± 0.001	0.149 ± 0.004	0.149 ± 0.004	0.149 ± 0.004
0.10	0.237 ± 0.012	0.201 ± 0.005	0.210 ± 0.016	0.111 ± 0.003	0.094 ± 0.004	0.99 ± 0.001	0.176 ± 0.001	0.150 ± 0.001	0.159 ± 0.006
0.20	0.281 ± 0.005	0.209 ± 0.002	0.221 ± 0.001	0.147 ± 0.004	0.108 ± 0.001	0.131 ± 0.006	0.198 ± 0.005	0.148 ± 0.001	0.167 ± 0.007
0.30	0.323 ± 0.003	0.213 ± 0.003	0.232 ± 0.001	0.189 ± 0.008	0.124 ± 0.005	0.145 ± 0.004	0.214 ± 0.009	0.152 ± 0.004	0.175 ± 0.002
0.40	0.359 ± 0.009	0.217 ± 0.011	0.243 ± 0.009	0.223 ± 0.007	0.141 ± 0.004	0.163 ± 0.010	0.226 ± 0.001	-	0.186 ± 0.001

Table B.4: Raw data from the melting point depression method (values are mean melting temperature ± SD, *n* = 3).

	CAP:PVP	CAP:PVA	CAP:SOL	CCX:PVP	CCX:PVA	CCX:SOL	PCM:PVP	PCM:PVA	PCM:SOL
X_{drug} (w/w)	T_m (°C)	T_m (°C)	T_m (°C)	T_m (°C)	T_m (°C)	T_m (°C)	T_m (°C)	T_m (°C)	T_m (°C)
0.95	-	-	-	159.00 ± 0.15	-	-	-	-	-
0.90	144.53 ± 1.15	148.53 ± 0.46	147.16 ± 0.26	153.45 ± 0.74	-	-	166.10 ± 0.49	168.46 ± 0.05	168.07 ± 0.02
0.85	138.71 ± 0.17	147.16 ± 0.18	143.37 ± 0.35	141.49 ± 0.89	160.04 ± 0.37	154.87 ± 0.55	161.76 ± 1.10	167.96 ± 0.06	167.28 ± 0.05
0.8	130.78 ± 0.40	144.29 ± 0.34	139.53 ± 0.15	126.65 ± 0.40	154.29 ± 0.25	146.26 ± 1.06	155.90 ± 1.02	167.98 ± 0.16	165.75 ± 0.31
0.75	119.23 ± 2.15	140.11 ± 0.34	131.32 ± 0.13	-	148.95 ± 0.14	137.41 ± 0.39	148.91 ± 0.57	166.77 ± 0.35	163.09 ± 0.49
0.70	95.52 ± 0.36	135.55 ± 0.38	123. 58 ± 0.64	-	142.13 ± 0.43	118.63 ± 0.49	139.56 ± 0.75	164.71 ± 0.84	158.13 ± 0.55
0.65	-	130.57 ± 0.52	109.62 ± 1.96	-	137.69 ± 0.76	-	131.55 ± 0.29	161.14 ± 0.86	152.12 ± 0.84
0.60	-	-	-	-	131.43 ± 0.47	-	-	157.81 ± 0.80	144.75 ± 1.14
0.55	-	-	-	-	-	-	-	150.98 ± 2.52	134.08 ± 1.62

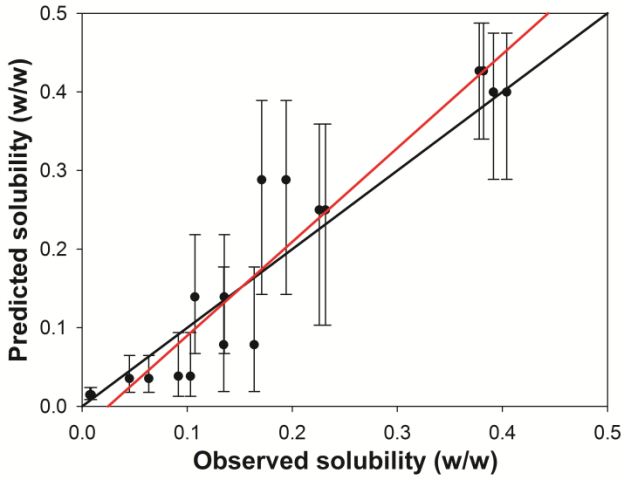

Figure B.1: Plot of predicted vs observed solubility including diagonal (black line) and the best fit obtained from total least-squares regression analysis (red line, y = 1.1938x – 0.0295). The predicted solubility is given as the mean prediction from the melting point depression method including error bars corresponding to the asymmetrical 95% prediction intervals and the observed solubility is given as the mean solubility determined from the new polymer in solution method. The horizontal error bars (confidence intervals from the new polymer in solution method) were left out for graphical reasons.

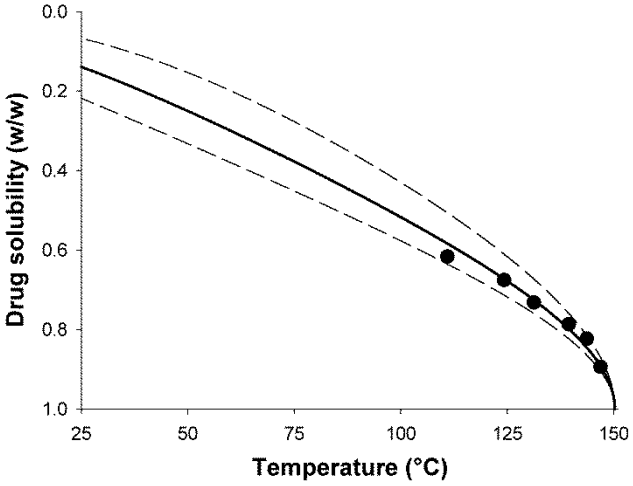

Figure B.2: Representative equilibrium solubility curve of CAP in SOL as a function of temperature from the melting point depression method. The solubility curve has been extrapolated to 25 °C by fitting with the Flory-Huggins model (solid line) including the prediction interval (dotted lines). Data points represent (depressed) melting points and are illustrated as averages (n = 3).

Appendix C

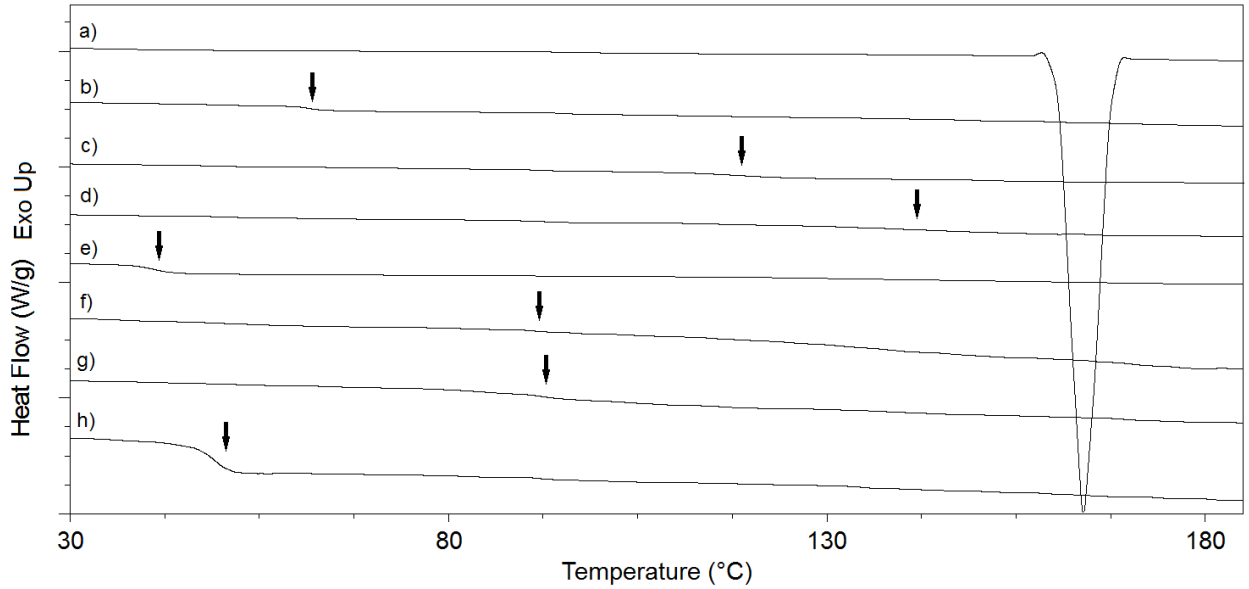

Figure C.1: Differential scanning calorimetry thermograms of a) crystalline CCX, b) amorphous CCX, c) PVP, d) HPMC, e) PVA, and amorphous solid dispersions of f) CCX:PVP (25:75), g) CCX:HPMC (25:75), and h) CCX:PVA (25:75). The arrows indicate the location of the single glass transition temperature (T_g).

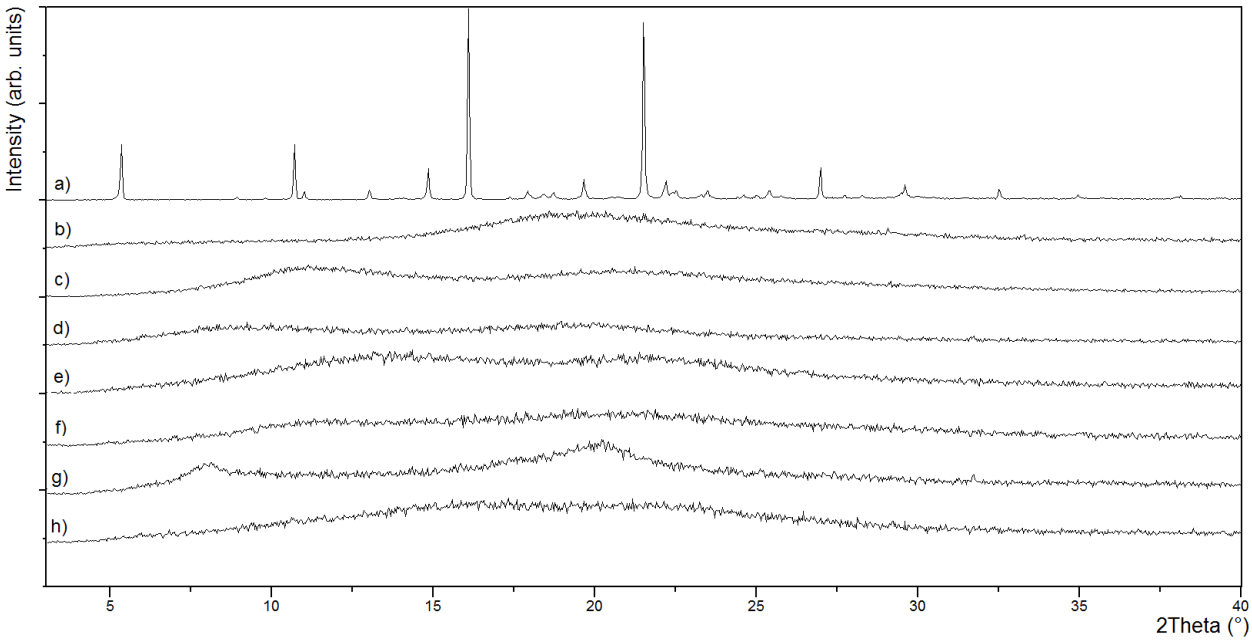

Figure C.2: X-ray powder diffraction patterns of a) crystalline CCX, b) amorphous CCX, c) PVP, d) HPMC, e) PVA, and amorphous solid dispersions of f) CCX:PVP (25:75), g) CCX:HPMC (25:75), and h) CCX:PVA (25:75).

List of publications

The present dissertation entitled “Development of predictive tools for amorphous solid dosage forms” is submitted to Johannes Gutenberg Universität Mainz to achieve a PhD in Pharmacy. The dissertation is based on the following publications (with permission from the publishers):

1) **Knopp, M. M.**, Olesen, N. E., Holm, P., Löbmann, K., Holm, R., Langguth, P., & Rades, T. (2015). Evaluation of drug–polymer solubility curves through formal statistical analysis: Comparison of preparation techniques. *Journal of Pharmaceutical Sciences*, *104*(1), 44−51.

2) **Knopp, M. M.**, Olesen, N. E., Holm, P., Langguth, P., Holm, R., & Rades, T. (2015). Influence of polymer molecular weight on drug–polymer solubility: a comparison between experimentally determined solubility in PVP and prediction derived from solubility in monomer. *Journal of Pharmaceutical Sciences*, *104*(9), 2905−2912.

3) **Knopp, M. M.**, Tajber, L., Tian, Y., Olesen, N. E., Jones, D. S., Kozyra, A., Löbmann, K., Paluch, K., Brennan, C. M., Holm, R., Healy, A. M., Andrews, G. A., & Rades, T. (2015). Comparative study of different methods for the prediction of drug–polymer solubility. *Molecular Pharmaceutics*, *12*(9), 3408−3419.

4) Rask, M. B., **Knopp, M. M.** (co-first author), Olesen, N. E., Holm, R., & Rades, T. (2016). Influence of PVP/VA copolymer composition on drug–polymer solubility. *European Journal of Pharmaceutical Sciences*, *85*, 10−17.

5) **Knopp, M. M.**, Olesen, N. E., Huang, Y., Holm, R., & Rades, T. (2015). Statistical analysis of a method to predict drug–polymer miscibility. *Journal of Pharmaceutical Sciences* (in press).

6) **Knopp, M. M.**, Gannon, N., Porsch, I., Rask, M. B., Olesen, N. E., Langguth, P., Holm, R., & Rades, T. (2016). A promising new method to estimate drug–polymer solubility at room temperature. *Journal of Pharmaceutical Sciences*, *105*(9), 2621-2624.

7) **Knopp, M. M.**, Nguyen, J. H., Becker, C., Francke, N. M., Jørgensen, E. B., Holm, P., Holm, R., Mu, H., Rades, T., & Langguth, P. (2016). Influence of polymer molecular weight on *in vitro* dissolution behavior and *in vivo* performance of celecoxib:PVP amorphous solid dispersions. *European Journal of Pharmaceutics and Biopharmaceutics*, *101*, 145−151.

8) **Knopp, M. M.**, Nguyen, J. H., Mu, H., Langguth, P., Rades, T., & Holm, R. (2016). Influence of copolymer composition on *in vitro* and *in vivo* performance of celecoxib-PVP/VA amorphous solid dispersions. *The AAPS Journal*, *18*(2), 416−423.

9) **Knopp, M. M.**, Chourak, N., Khan, F., Wendelboe, J., Langguth, P., Rades, T., & Holm, R. (2016). Effect of polymer type and drug dose on the *in vitro* and *in vivo* behavior of amorphous solid dispersions. *European Journal of Pharmaceutics and Biopharmaceutics*, *105*, 106-114.

Curriculum vitae